TEMPORAL AND SPATIAL SCALING OF COUPLED HYDROLOGICAL AND BIOGEOCHEMICAL PROCESSES IN RIVER BASINS

BY

SHENG YE

DISSERTATION

Submitted in partial fulfillment of the requirements
for the degree of Doctor of Philosophy in Geography
in the Graduate College of the
University of Illinois at Urbana-Champaign, 2014

Urbana, Illinois

Doctoral Committee:

Professor Murugesu Sivapalan, Chair and Director of Research
Professor Bruce L. Rhoads
Professor Shaowen Wang
Professor Jennifer L. Tank, University of Notre Dame
Assistant Professor Nandita B. Basu, University of Waterloo

Abstract

The goal of this dissertation is to understand nutrient delivery processes in river networks, including the processes and factors controlling both the flow generation and nutrient retention mechanisms. An analysis framework that synthesizes the bottom-up and top-down approaches is implemented in this dissertation to explore these questions. In the top-down approach, empirical data from several catchments within the continental United States is analyzed to generate patterns across gradients of scale, climate, and topography to guide the study of the underlying mechanisms as well as to serve as the inspiration to generate hypotheses regarding possible explanations of the empirical observations. In the bottom-up approach, models are developed based on the understanding gained in through the data analysis to test hypotheses and to discover previously hidden relationships and laws which could further facilitate future data collection, data analysis and model development.

The dissertation is separated into two parts governing the two major perspectives that underpin nutrient transport and transformation processes in river networks: hydrology and biogeochemistry. Part one focuses on how soil moisture and the dominant hydrological processes change across a climate gradient, the factors governing these spatio-temporal patterns, and in particular, the effects of climate (i.e. aridity, seasonality). Analysis of the flow regime curves reveals the dominant runoff generation processes in catchments across the continental United States and is used in the model development that follows. The study of flow recession curves also reveals insights for the future modeling of the storage-discharge relationship governing subsurface stormflow. These studies demonstrate the overall influence of climate (i.e. seasonality and aridity) on the various hydrologic processes through long-term co-evolution of climate, soils, vegetation and topography.

With the understanding gained of the processes related to the movement of water, the carrier and controller of nutrients, the second part of the dissertation looks at the nutrient delivery and uptake processes across the river network: the influence of spatial scale on these processes, and the effects of temporal variability of flow inherited from climate. Empirical relationships between several nutrient uptake metrics and the flow condition and nutrient concentration level

are derived from field measurements and are incorporated into a coupled hydrology and biogeochemistry model to simulate the nutrient uptake processes across river networks, from the small headwater streams all the way to big rivers. The effect of hydrologic variability inherited from climate on nutrient uptake is then examined. The studies highlighted the contribution of big rivers downstream to overall nutrient uptake and also have emphasized the important role of flow variability on nutrient retention.

The results arising from this dissertation research have helped to significantly improve our understanding of nutrient transport and transformation processes across river networks, which could prove extremely useful to government agencies and community organizations on the effective use of land use management and water quality regulation to alleviate water quality problems in rivers and in receiving waters such as the Gulf of Mexico. On the other hand, this work has demonstrated the feasibility and power of the study framework that combines both the bottom-up and top-down approaches to the study of complex environmental problems, and could be adopted in future studies involving hydrologic and/or biogeochemical processes.

For Mom and Dad

Acknowledgements

It isn't until now, sitting at my desk writing this, that I finally feel the end of my PhD. I owe a debt of thanks to many people, since it is their generous help along the way that has led me here. First and foremost, I must present my sincere gratitude to my advisor Prof. Sivapalan, who introduced me to academia and guided me through the tough exploration period at the beginning to find my own place. It's his passion for research that inspired me, and his vision and knowledge of hydrology that has supported me. The great opportunities he gave me to work with different people expanded the breadth of my knowledge. I couldn't have come to the position I am now without an insightful, patient, supportive advisor like Siva.

I also really appreciate all the mentors I met along the way for their instruction and support all these years: Bruce Rhoads, whose patience, kindness and generous support brought me into the physical geography area from my first year of graduate school; Shaowen Wang, who greatly broadened my knowledge of GIS and the advantage of the support of GIS; Nandita Basu, who guided me into biogeochemistry and clarified my understanding with questions and explanations; Jennifer Tank, whose rich experience and knowledge in stream ecology substantially extended and deepened my understanding of nutrient spiraling; Praveen Kumar, whose questions and inputs always inspire me with a thinking pattern different from Siva.

I gained significant amount of help from my fellow colleagues as, some of whom are already outstanding young faculty members: Hongyi Li for his instructions in modeling and research; Sally Thompson and Ciaran Harman for their mentor-like advice and guidance; Tim Covino for his generous and insightful support in my first paper; Kaiyu Guan, a great life-time friend; all the people I worked with, specifically Mary Yaeger, Evan Coopersmith, Stefano Zarnado, Sopan Patil, and AJ Reisinger; Jennifer Wilson, Susan Etter, and Matthew Cohn for taking care of the bureaucratic things; and my friends who make life here interesting: Jun Wan, Yanli Zhao, Tianying Jiang, Xiao Zhang, Xiao Bao and many others.

Thanks to the Hydrologic Synthesis Summer School, the recession curve work funded by Pacific Northwest National Lab and the Big River project for the opportunities in research.

In the end, I shall dedicate all my appreciations to my dearest parents. It's their unconditional support and love that has brought me here. Knowing that whatever happens they are always there for me makes me strong and brave to confront anything in my life.

Table of Contents

List of Tables

List of Figures

Chapter 1

Introduction

1.1 Motivation for the Study

Oxygen depletion in receiving waters such as rivers, lakes, estuaries and coastal areas is a worldwide environmental problem. Excess nutrient loading from landscapes to these aquatic systems is one of the key factors that contribute to eutrophication (Viney *et al.*, 2000). Excess nutrients stimulate phytoplankton growth, which then blocks sunlight, depletes dissolved oxygen needed for their decomposition, and in this way it threatens the survival of fishes, reduces aquatic species diversity, leading to overall water quality degradation. One prominent example is the development of the hypoxic zone in the Gulf of Mexico, which is also known as the "dead zone", and the consequent threats to aquatic life (Rabalais *et al.*, 2002). The overloading of nutrients in the Gulf of Mexico is sourced to the Mississippi and Atchafalaya Rivers (Dunn, 1996), parts of which drain through the agricultural areas in the US Midwest (i.e., the so-called Corn Belt region) where more than 65% of the land is put to agriculture. Tile drainage construction in the Midwest, which helped to drain out the soil water quickly, also enhances nitrogen loss in the landscape through rapid subsurface flow. The shortened channels, stabilized river banks and levee constructions in aid of agricultural use designed for rapid drainage also contributed rapid nutrient transport in the rivers and have prevented absorption and removal by the alluvial soils in rivers and in river banks (Abernethy and Turner, 1987). Assuming a soil layer of one meter thickness with 2% organic matter, the current nutrient (carbon, nitrogen and phosphorous) yield of the Mississippi River Basin caused by the agricultural land use change is less than 0.1% of the soil nutrient storage. Therefore, any further land use change in this area (i.e., biofuel crop harvest), even a small one, could have a significant impact on water quality in the Mississippi river and in the Gulf of Mexico (Turner and Rabalais, 2003).

To solve the eutrophication problems in the aquatic environment, it is essential to understand how nutrients added for agriculture eventually ending up in the ocean (or other receiving waters) after being transported through river networks and transformed along the way through biogeochemical reactions (Bencala and Walters, 1983; Dodds *et al.*, 2002; Donner *et al.*,

2002; Alexander *et al.*, 2009; Claessens and Tague, 2009; Claessens *et al.*, 2009; Mulholland *et al.*, 2010). Besides the nutrient, being the carrier of nutrients (especially in the case of dissolved nutrients) as water is, its dynamics is intimately connected to the dynamics of nutrient transport and transformation processes from points in the landscape where nutrients are added as fertilizer and going all the way to the receiving waters through a multiplicity of flow pathways. The accompanying biogeochemical, geomorphological, and ecological processes in the river network, all exhibit considerable heterogeneity, and enormous process complexity arising from the process interactions and feedbacks. To understand these processes and process interactions and to provide scientific guidance for management actions aimed at alleviating the eutrophication problems in the receiving waters, we need fundamental knowledge of water flows and nutrient transport and reaction processes from the hillslopes to the estuaries through river network, as well as predictive tools (i.e. models) built based on such understanding.

This dissertation is aimed to exploring dissolved nutrient cycling at the catchment scale in general, and in particular it is concerned with understanding how and why the magnitudes of nutrient retention and export might vary with the increasing size of catchment s under different climatic and landscape characteristics, and how they would be impacted by temporal variability of streamflow generation processes, and the particular role of seasonality of climate. This introduction chapter presents the analysis framework that is adopted in this dissertation to address this problem. Each chapter of the dissertation can be seen as a piece of a jigsaw puzzle; taken together they try to answer the questions in a more holistic manner. The adopted framework will be applied in each of the chapter, and serves as an overall guide to the study. In this introductory chapter, the contents are organized as follows: Section 2 provides a background to nutrient transformation and transport at the catchment scale and the challenges faced in this area; Section 3 will present the overall study framework as a combination of both bottom-up and top-down approaches applied across places; Section 4 discusses the advantages and supports gained from GIS tools and platform; the Section 5 presents the general outlines of the specific research that will be presented in the various chapters of this dissertation.

1.2 Scientific Background

1.2.1 Catchment runoff generation mechanisms

Soluble nutrients such as nitrates, are chemically transformed, dissolved in soil water, and retained with soil water storage, and then delivered to the river network along with runoff, especially subsurface runoff. Water being the solvent of dissolved nutrients water cycling is closely connected to nutrient cycling, both physically and also interactively. The cycling of dissolved nutrients exhibits major differences with that of particulate nutrients such as phosphorus, which is transported by fast, surface runoff pathways. Different runoff generation mechanisms impact nutrient transformation and transport in different ways: surface runoff, characterized by short and fast flow pathways tends to carry phosphorus along with the sediment but less nitrogen, whereas subsurface flow has much longer pathways and travel times and therefore carries more nitrogen in dissolved form, but carries less phosphorus.

The total amount of runoff generated during and between rainfall events and the partitioning of the runoff between surface and subsurface components is a result of the combined effects of climate, soils, topography and vegetation cover. In this way, the hydrologic regime, i.e., reflecting the dominant runoff generation processes, can impact the magnitude and timing of nutrient transport and transformation processes. Therefore, the understanding of dominant hydrological processes, their temporal variability during and between precipitation events, and how these vary across gradients of climate and landscape characteristics (e.g., soils and geology) are a prerequisite for the conduct of nutrient studies, including model development, especially if the goal is to develop theories and models that work everywhere.

Historically, several key runoff signatures extracted from runoff observations are used to quantify different aspects of temporal runoff variability and to characterize the dominant hydrologic processes operating in a catchment. Examples include the flow duration curve (FDC), the regime curve (RC), and the recession curve (RC). FDC presents observed daily streamflow magnitude as a function of the occurrence frequency (instead of as time series). RC describes the mean seasonal variation of streamflow. RCs measure the flow recession profile at the end of individual storm events. Each signature describes a different aspect of a catchment's streamflow behavior, and in this way reveals different aspects of the interactions of climate variability with

the landscape, the different pathways and residence times of water, and in this way helps to decipher the relative roles of climate and landscape characteristics. These are discussed in detail in the next sections.

Flow duration curve and regime curve

The flow duration curve (FDC), is a frequency-based manifestation of the filtering of daily precipitation variability by runoff generation and movement along the multiplicity of flow pathways that water follows within a catchment. In effect, the shape of the FDC acts as bridge between the fast, slow and intermediate runoff processes, and in this way it helps to identify the dominant processes operative within the catchment (Yaeger *et al.*, 2012). As a classical signature in the realm of hydrology, FDC has been studied for a long time graphically (Ward and Robinson, 1990; Vogel and Fennessey, 1994, 1995) or stochastically (Castellarin *et al.*, 2004; Iacobellis, 2008) by fitting to appropriate statistical distributions with optimal parameters. Although widely used and studied for predicting flood or drought magnitude and frequency, not much work has been done on exploring the climatic and landscape controls on the shape of the FDC (Yokoo and Sivapalan, 2011). In view of the role of runoff variability in governing the variability of nutrient cycling processes, the understanding of the physical controls of the FDC in a fundamental way has become critical.

There has been recent progress in the development of process based models to connect the dynamics of runoff variability to the variability in climate variables (Botter *et al.*, 2007, 2009; Muneepeerakul *et al.*, 2010). These early studies were built on the assumption that rainfall arrives as a Poisson process (identically and independently distributed events), without the explicit carryover of soil moisture storage between events and, in particular, between seasons. Although these simplifying assumptions enable insightful analytical solutions to the problem, the non-inclusion of the carryover between different seasons precludes their adoption in situations where the seasonality of precipitation and solar energy (or potential evaporation), such as California which has a Mediterranean climate, or Florida which experiences tropical cyclones on a seasonal basis.

Yokoo and Sivapalan (2011) recently proposed a new process-based framework to the study of FDCs, but without the assumption of Poisson storm arrivals. Instead of the Poisson

storm arrivals, observed actual precipitation data or synthetic precipitation series that preserve both the inherent randomness and seasonal variability in precipitation and potential evaporation were used as climate forcing to a physically based hydrologic model to derive the FDCs. Importantly, the carryover of soil moisture between events and between seasons is enabled because of the use of a continuous simulation model. The numerical simulations with the hydrological model under different combinations of climate and landscape characteristics enabled Yokoo and Sivapalan (2011) to partition FDC into three parts: the upper limb, middle part, and the lower limb, corresponding to fast flow, slow flow and evaporation, respectively. It turned out that the middle limb of the FDC, serving as the bridge between the high/fast and low/slow flows at either ends of the FDC, can be represented by the regime curves (i.e., mean seasonal variability of flow), which reflects the strength of seasonality of streamflow in the catchment. This not only confirmed the importance of seasonality in governing the shape of FDCs, but also showed that understanding of the physical controls of the regime curve can assist in achieving the same regarding the FDC.

Streamflow recession curve

The recession curve (RC) (Brutsaert and Nieber, 1977) is one of the most widely used signatures that provide insights into (slow) subsurface flow generation processes (Tague and Grant, 2004). RC measures how river streamflow recedes at the end of a storm event, and is thus a measure of the drainage characteristics of a catchment, i.e., the net effects of the behaviors of the population of hillslopes (of various sizes and shapes) that constitute the catchment, and independent of the event characteristics. For convenience, the recession behavior of catchments is usually expressed in terms of the so-called recession-slope curve, the relationship between streamflow itself (i.e., Q) and its rate of decline (i.e., -dQ/dt), in terms of the following power-law relationship:

$$-\frac{dQ}{dt} = \alpha Q^{\beta} \qquad (1)$$

which is often found to remain invariant and thus represents a unique signature of the catchment response. The coefficient α and exponent β in Equation (1) can be directly estimated from observed recession curves by curve fitting, and reflect the net effects of climatic and catchment characteristics (e.g., soils, topography, and network structure).

One of the ways to decipher the physical meaning or controls of the parameters α and β is through recourse to the fundamental equations governing saturated-unsaturated subsurface flow (i.e., Richards equation), based on application of Darcy's law. Application of such physically based models to understand the controls on recession curve parameters must accommodate the considerable heterogeneity of both soil properties (e.g., soil depth, porosity and hydraulic conductivity) and topography (e.g., slope, shape). Approximations to Richards' equation in the case of saturated flow in shallow subsurface homogeneous and unconfined aquifers, such as the Boussinesq equation, have been used in the past in a theoretical way to explore the effects of soils and topography on the shape of the recession curves. These theoretical studies suggest that the shapes of the recession curves are strongly related to the hydraulic conductivity and its vertical and horizontal heterogeneity (Rupp and Selker, 2005; Rupp and Selker, 2006; Harman et al., 2009). Other studies have studied the effects of landscape geomorphologic structure on the shapes of the recession curves (Biswal and Marani, 2010; Lyon and Troch, 2010). Due to the many simplifying assumptions and lack of data, most of the pioneering studies have been largely theoretical, and only applicable at the scale of individual hillslopes; only a few studies have looked at implementation and validation of the so-derived equations in real catchments (Harman et al., 2009; Lyon and Troch, 2010). In fact, very few studies have looked at the up-scaling of hillslope recession behavior all the way to the scale of a whole catchment, incorporating the significant heterogeneity of both soil properties and topographic variables that exist amongst the population of hillslopes constituting the catchment (Ali et al., 2013).

The above theoretical approach, based on the Richards equation, involving either approximate analytical solutions or numerical simulations at the hillslope scale and up-scaling to catchment scale, can yield results that are physically consistent. Yet, their applicability in actual catchments is hampered by our inability to fully characterize the heterogeneity of soils and topography present in actual catchments. Some of the organized heterogeneity can be observed and mapped, and yet there is much other heterogeneity and complexity that are hidden and are harder to measure and map. Examples include networks of macro-pores and other preferred pathways, the flows through which are difficult to characterize in terms of the Richards equation.

On the other hand, empirical relationships extracted directly from observed recession curves are much more realistic in terms of revealing the net emergent effects of the full range of heterogeneity and organization that is present within a catchment. However, they remain empirical and are not physics based, which makes it difficult to interpret them physically and to extrapolate from gauged to ungauged sites. One solution is to undertake a reconciliation or synthesis of the outcomes of both the empirical (i.e., top-down) and theoretical (i.e., bottom-up) approaches, and in this way develop relationships that may be valid across a range of climates and locations, and yet are physically meaningful. This will be discussed later in the methodology section.

1.2.2 Nutrient retention and transport in river network

Once the dissolved nutrient arrives in the stream from adjacent hillslopes, it is transported into receiving waters such as lakes, estuaries and oceans through the river network. Nutrient release experiments have been conducted in streams to measure the nutrient retention rate. Most of the nutrient release experiments are carried out in headwaters during low flows (Tank et al., 2008). The hydrologic condition can be considered as being at steady state during low flows, and the retention efficiency can be expected to be the highest in these headwaters. Besides, nutrient release experiments are typically more tractable in such small headwater streams than in larger rivers or during times of high discharge (Hall *et al.*, 2009).

Measurement results show that a large part of nutrient retention occurs in the transient storage (TS) zone (Runkel and Bencala, 1995), which refers to the region with water flow pathways for which the velocity is much smaller than that in the main channel (MC). Examples include surface water “dead zones” such as pools, off-channel storages such as floodplains, the hyporheic zone, and other flow non-uniformities where the velocity is much smaller than that in the MC. On the modeling side, consistent with the reach scale observations, the nutrient transformation and transport in the TS and MC zones are usually described by a one-dimensional transport model with inflow and transient storage (i.e., OTIS) in time and space (Runkel, 1998). Field measurements of solute concentrations and loads are used within this formulation to characterize reach-scale hydrologic and biogeochemical processes and their parameterizations.

There are two major challenges in extrapolating what can be learned from such steady-state, small reach scale studies to make predictions at the whole catchment scale and over the annual timescale: (i) considerable heterogeneity in the size, shape of the set of reaches that constitute the river network, and (ii) the accommodation of the effects of within-year variability of runoff and nutrient inputs from hillslopes (e.g., within-even and between-event variability as well as that of seasonality). Distributed modeling studies have now called attention to the issue of network effects, the effects of increasing spatial scale, and the effects of the dynamics of within-year hydrologic variability on nutrient transport in river networks at the river basin scale (Wollheim *et al.,* 2006; Tank *et al.,* 2008; Helton *et al.,* 2011; Ye *et al.,* 2012). For example, despite the relatively low retention efficiency compared to the efficiency in small headwater streams, big streams behave not just as pipes, as is often assumed, and instead, due to the long travel times, they may contribute a much larger amount of nutrient retention or removal than previously assumed. A similar situation arises during high flows, compared to during low flows (Ye *et al.,* 2012). The steady state assumption is no longer valid at annual timescales, and the impact of within-year (within-event, between-event and between-season) hydrological variability on nutrient retention and delivery has to be taken into account as well.

The importance of the scaling issue and the impact of temporal hydrologic variability on nutrient retention have been confirmed both by observations, analysis of observed data, and through numerical simulations (Basu *et al.,* 2010; Basu *et al.,* 2011a, b). For example, the nutrient release experiments of Tank *et al. (*2008) in the Upper Snake River, Wyoming, a medium size pristine river, indicated a surprisingly high biotic demand for nitrate and ammonium. Long term data from even larger river basins with intense anthropogenic activities (Mississippi-Atchafalaya River basin and Baltic Sea Drainage Basin) reveal a chemostatic pattern, where the concentration of nitrogen and phosphorous are invariant at annual scale and the total-N and total-P loads are dominated by total streamflow (Basu *et al.,* 2010). The importance of hydrologic variability has also been highlighted during an experiment conducted in a mountain stream (Hall *et al.,* 2009) that suggested that biological demand for nitrate was much higher than expected during floods and that reach scale nutrient uptake during low flows and spring floods were indeed similar. This can potentially be attributed to the presence of a large hyporheic zone (i.e., increased extent of the hyporheic zone during flood events) relative to the size of the drainage area. The impact of the temporal organization of storm events (i.e.,

within year hydrological variability) have also been reproduced in the numerical simulations. The simulation results of Basu *et al.* (2011a) indicated that, in "flashy" streams with high flow events distributed less uniformly, less nutrient is processed in the stream, with most of the nutrients being exported out of the basin, whereas when the flow events are distributed uniformly, a larger amount of nutrients stays in channel which helps further in-stream processing, thus reducing export. Particularly for larger river basins with strong human influences, the variability of nutrient load is dominantly controlled by within-year streamflow variability because of the big nutrient storage in soil from fertilizer application (Basu *et al.,* 2011b).

Although the OTIS model (Runkel et al., 1998) provides an excellent description of the nutrient retention and transport processes in a channel reach, including the factors that influence these processes, it is meant to be applicable for a single reach. To characterize how nutrient transport and transformation processes evolve in the downstream direction, including in a river network, and how they impact retention and delivery at the catchment scale, we need catchment or network scale models that can accommodate distributed loading from the hillslopes that organized around the network, and transport and transformation along the river channel network itself.

Several biogeochemical models are in wide use to predict nutrient transport at a range of spatial scales (e.g., Smith *et al.,* 1997; Donner *et al.,* 2002; Mulholland et al., 2002; Seitzinger et al., 2002, Wollheim et al., 2006, 2008; Alexander et al., 2009). Many of these models use observed data to predict nutrient transport as a function of hydrologic variables (i.e., stream depth, travel time). These empirical relationships are then applied at the catchment scale to obtain estimates of annual nutrient export (Smith *et al.,* 1997). Other models have applied the one-dimensional advection-dispersion equation with effective parameters to capture reach scale nutrient cycling processes for each month, expressing a bulk retention coefficient k_e as a function of nutrient concentration, flow depth and water temperature (e.g., Alexander *et al.,* 2009). Many of these models have assumed steady flow conditions, and although they capture the impact of seasonal variability on nutrient transport, they are unable to make predictions under highly variable flow conditions that occur during flood events, as well as seasonally over the year, or in space (e.g., across the river network), a notable exception being the work by Wollheim (*et al.* 2008).

1.3 Study framework: a combination of two worldviews and approaches

Questions similar to "how do nutrients get transported within a catchment" that we have asked here have been raised and studied, albeit in different contexts, throughout human history: what does this world look like and why is it the way it is. Traditionally in hydrology, we answer this kind of how and why questions in a Newtonian way (Sivapalan et al., 2011): we study problems of small spatial extent, explore the associated physical processes in the laboratory or in the field to develop governing equations (i.e. Richards equation, Saint Venant equations, etc.), from where we then up-scale to the larger scales (i.e. larger catchment scale, regional scale, global scale, etc.) at which predictions are required. The resulting process based models are often developed and calibrated in catchments that have considerable historical data available, and validated in other catchments over different time periods. The strength of this approach is that the physical meaning of both the processes and the parameters are easily interpreted. However, these equations are developed in the laboratory or in the field under somewhat ideal conditions or assumptions, and when applied to real (larger) catchments they need to be characterized with a large number of parameters that may not be easy to acquire in reality. If the system is too complex, with many processes operating over different time scales, some of which not even recognized beforehand, then in spite of obtaining good fits to observed data during calibration, such models may not be able to capture the actual processes occurring in these catchments. This characterization and application process would be even harder when we bring the biological and biogeochemical processes to account for nutrient transformation and transport.

An alternative view to address these questions follows the Darwinian way: this embraces the heterogeneity within and among these catchments and the different histories followed by each catchment, by studying emergent patterns and comparisons among catchments simultaneously to generate generalizable understanding and predictive capability. As we look around, we appreciate how beautiful this ever-changing nature is. Unlike some of the modern architecture, nature never bores us: lives change from sunrise to sunset, and everything is different from place to place, there are no two same leaves on this planet. This endless variation constitutes spectacular landscapes, but also increases the difficulties for us to understand the underlying mechanisms and essential functions. Each catchment is different from the others with unique climate, topography, ecosystem, etc. Consider the mechanisms underlying the whole seen

as white light, the characteristics of each catchment are like different kinds of prism or filter: only part of the solar spectrum is represented in these filters, these are the dominant processes or influencing factors we see in each catchment. For example, a Midwestern tile drained catchment filters out most of the subsurface flow generation processes leaving mainly the tile drainage and creates a nutrient enriched aquatic ecosystem; on the other hand a high attitude low vegetation snow dominated catchment in Idaho could screen out most of the flow generation processes to emphasize the snowmelt and thus maintain a pristine low nutrient river.

Therefore, what we see in an individual catchment under the Newtonian view is just a combination of some parts of the spectrum. However well we can model the catchment, we can only understand what is left from the filters, not the whole spectrum. On the other hand the Darwinian view could provide us the resources we can put together to make up the whole solar spectrum. Both approaches have advantages and disadvantages. To understand the natural system, we need a synthesis of both Newtonian and Darwinian views to identify each process as the wavelength in the range but without missing the whole pattern of the spectrum. Since the goal of this study is to develop generalizable understanding of nitrogen cycling at river basin scale, and over annual and longer timescales, we will emphasize slightly more on the Darwinian approach in this study but the Newtonian view is also used. All of the studies proposed here will be carried out under the framework of the synthesis of both Newtonian and Darwinian approaches with different preferences on either worldview depending on the specific topic. The Darwinian approach will involve using empirical data analysis to first identify and extract emergent patterns or signatures, and then to use process based models of appropriate complexity to interpret these emergent patterns, and in this way to help make general statements about climate and landscape controls on nutrient retention and delivery at the river basin scale.

1.3.1 Top-down approach: Learning from data

The MOPEX dataset (Duan et al., 2006) will be used for empirical analysis of dominant hydrological processes as well as the factors controlling slow flow generation. Daily precipitation (P), temperature (T), and potential evaporation (PET) time series are used as climate inputs, while daily flow data are used to generate the regime curves (RCs), which are 50-year averages of streamflow for each day of the year in 197 catchments with more than 50-years

data. Regime curves derived here are used for model development, calibration and comparative performance assessment in later work.

For the parameterization of the storage-discharge relationship, recession curves will be the runoff signature used to derive the underlying relationship and to study the influence of catchment characteristics on that relationship. Daily flow data from 428 MOPEX catchments with over 10-years of record will be used to derive parameterizations of the recession curves, which can be used to estimate the coefficient and exponent of a power-law type storage-discharge relationship. The aridity index (PET/P) and the topographic slope data from the MOPEX dataset, drainage density estimates extracted from the National Hydrography Dataset (NHD) (http://nhd.usgs.gov/) and soil properties from the USGS SSURGO dataset (http://soils.usda.gov/survey/geography/ssurgo/) in 50 selected MOPEX catchment will be used to describe climatic, topographic characteristics.

Flow and nutrient (nitrate, ammonium and phosphorous) data from pulse experiments in fifteen western and Midwestern rivers with discharges > 10,000L (provided by Dr. Jennifer Tank of the University of Notre Dame and the Big River team) will also be used to parameterize the nutrient spiraling model at the river network scale to study the nutrient spiraling in the river network across a range of land use, hydrologic dynamics and biological activity.

1.3.2 Bottom-up approach: Model interpretation

With the understanding gained from the data analysis, we then build hydrological and biogeochemical models to help interpret the patterns we have obtained from the empirical studies. To explore the dominant flow generation processes, we start with a simple two-stage bucket model; incorporate additional processes we hypothesize would be able to fill the gap when parameterization of current model is not able to generate reasonable results. The parameters are calibrated automatically via the Markov Chain Monte Carlo (MCMC) algorithm, a tool designed to search a multi-dimensional parameter space more efficiently than brute force. The performance of the various models for each catchment, containing differing numbers of parameters, are compared with the use of the Akaike Information Criterion (AIC), which assesses the marginal value of each new parameter added to address the relative differences in complexity.

Once the nutrient enters channel with flow, a dynamic hydrologic network model, coupled with a transient storage zone solute transport model, will then be used to simulate dissolved nutrient (i.e. nitrate, nitrite, phosphate, etc.) retention processes during transient flow events at the channel network scale. Flow will be routed in each river reach via the river network, and the nutrient exchange between the main channel and the transient storage zone will also be taken into account.

1.4 GIS support

With the capability of spatial (geographically referenced) data manipulation and presentation, GIS is essential to the whole work as prerequisite tool for model and data analysis and as an important platform for model presentation and future development.

The modeling units are delineated based on the Digital Elevation Model (DEM) by the GIS software and the river networks are also extracted from the DEM by the same platform. These are the prerequisites to the hydrological and biogeochemical modeling. Moreover, spatial information such as topography and soil property characteristics are also collected, calculated, and organized with GIS tools. For example, the soil property characteristics were aggregated from the spatial data set from USGS soil survey.

Besides pre-processing of data, once the whole coupled hydrologic and biogeochemical model is completed, it could be incorporated into GISolve, a framework that can be used to solve computationally intensive and associated problems in GIS and spatial analysis (Wang, 2010). As a synthesis of cyberinfrastructure (which integrates distributed information and communication technologies), GIS and spatial analysis, this framework (GISolve) could provide data management, high performance computing and spatial information visualization online. Once the coupled model is incorporated into the platform, researchers from the world could run the model for their study areas online using the computing resources behind the platform and visualize the simulated flow and nitrogen results. With further developments and enhancements expected in the future, scientists everywhere could be directly involved in further model improvement through this platform utilizing their process understanding and knowledge about particular places to make the model more sophisticated and more widely applicable.

1.5 Outline of this dissertation

The proposed framework is broad and could be used to study a range of problems. The work presented here is an application of this framework to nutrient transformation and transport at the catchment scale. Each chapter focuses on different parts of the nutrient transport questions and is explored under this synthesis framework with an emphasis on one or both of the world views. The major objectives are the following two questions:

1. How will soil moisture and dominant hydrological processes change across a climate gradient, what are the controlling factors governing these processes, and in particular, what are the effects of climate, i.e. aridity, seasonality?
2. How do the nutrients get retained and delivered across river network, what is the spatial scaling influence on these processes, and what are the effects of temporal variability in flow that is inherited from climate?

To answer these two questions, we divide the work into two parts, the water and the nutrient for each question, respectively. The first part focuses on the question how soil moisture and dominant hydrological processes change across a climate gradient, and in particular, what the effects of climate seasonality are? Since the nutrient delivery is intimately connected to soil water storage, runoff generation mechanisms, and flow variability in the river network, the knowledge of hydrological processes is a prerequisite to understanding of nitrogen cycling processes. Due to the significant influence of seasonality of runoff generation processes, this study will mainly focus on the impact of seasonality on nitrogen retention and transport under different hydrological conditions. Chapters 2 and 3 explore the process controls underpinning regional patterns of variations of streamflow regime behavior across the continental United States. Chapter 2 applies a two-stage bucket model which is systematically enhanced through addition of new processes on the basis of model performance assessment in relation to observations in the MOPEX catchments to determine the dominant processes for each catchment. Chapter 3 is aimed at deriving regionalized parameterizations of the storage-discharge relationship relating to subsurface stormflow from a top-down empirical data analysis of streamflow recession curves for the same catchments studied in Chapter 2.

With the understanding of water movement, the second part is about how nutrient retention and delivery across a river network are affected by climate seasonality and other catchment characteristics. Chapter 4 uses a dynamic hydrologic network model, coupled with a transient storage zone solute transport model, to simulate dissolved nutrient retention processes during transient flow events at the channel network scale in an idealized river network. In Chapter 5, the theoretical model developed in Chapter 4 is modified based on the field measurement data of 15 Big Rivers in Midwestern and Western United States, and is applied to these 15 catchments to examine the spatial patterns of nutrient uptake within the catchment (small streams vs. big rivers) and how it varies across catchments and across solutes. Chapter 6 is a repeat of Chapter 4 with the model improvements obtained in Chapter 5 with observational support.

Finally Chapter 7 is the concluding chapter which summaries the major findings from this dissertation and outlines future opportunities for extensions of this work, as well as potential other applications of the adopted study framework.

References

Abernethy Y. and R. E. Turner, (1987). US forested wetlands: 1940–1980. *BioScience* 37: 721–727.

Alexander, R. B., J. K. Böhlke, E. W. Boyer, M. B. David, J. W. Harvey, P. J. Mulholland, S.P. Seitzinger, C. R. Tobias, C. Tonitto, and W. M. Wollheim (2009), Dynamic modeling of nitrogen losses in river networks unravels the coupled effects of hydrological and biogeochemical processes, *Biogeochemistry, 93*, 91-116.

Ali, M., S. Ye, H.-Y Li, M-Y Huang, L.-Y. R. Leung, S.-W. Wang and M. Sivapalan (2013). Subsurface stormflow parameterization for land surface models, 1. Derivation from regional analysis of streamflow recession curves. Submitted to *J. Hydrol*.

Basu, N. B. et al. (2010), Nutrient loads exported from managed catchments reveal emergent biogeochemical stationarity, *Geophys. Res. Lett.*, 37, L23404, doi:10.1029/2010GL045168.

Basu, N. B., P. S. C. Rao, S. E. Thompson, N. V. Loukinova, S. D. Donner, S. Ye, and M. Sivapalan (2011a), Spatiotemporal averaging of in-stream solute removal dynamics, Water Resour. Res., 47, W00J06, doi:10.1029/2010WR010196.

Basu, N. B., S. E. Thompson, and P. S. C. Rao (2011b), Hydrologic and biogeochemical functioning of intensively managed catchments: A synthesis of top-down analyses, *Water Resour. Res.*, 47, W00J15, doi:10.1029/2011WR010800.

Bencala, K. E., and R. A. Walters (1983), Simulation of solute transport in a mountain pool-and riffle stream: a transient storage model, *Water Resour. Res., 19(3)*, 718-724.

Biswal B. and M. Marani (2010), Geomorphological origin of recession curves, Geophys. Res. Lett., 37, L24403, doi:10.1029/2010GL045415.

Botter, G., A. Porporato, I. Rodriguez-Iturbe, and A. Rinaldo, (2007), Basin-scale soil moisture dynamics and the probabilistic characterization of carrier hydrologic flows: Slow, leaching-prone components of the hydrologic response, *Water Resour. Res.*, 43, W02417, doi:10.1029/2006WR005043.

Botter, G., A. Porporato, I. Rodriguez-Iturbe, and A. Rinaldo (2009), Nonlinear storage-discharge relations and catchment streamflow regimes, *Water Resour. Res.*, 45, W10427, doi:10.1029/2008WR007658.

Brutsaert, W., and J. L. Nieber (1977), Regionalized drought flow hydrographs from a mature glaciated plateau, *Water Resour. Res.*, 13(3), 637–644.

Castellarin, A., R. M. Vogel, and A. Brath (2004), A stochastic index flow model of flow duration curves, *Water Resour. Res.*, 40, W03104, doi:10.1029/2003WR002524.

Claessens, L. and C. L. Tague (2009), Transport-based method for estimating in-stream nitrogen uptake at ambient concentration from nutrient addition experiments, *Limnol. Oceanogr.: Methods, 7,* 811-822.

Claessens, L., C. L. Tague, P. M. Groffman and J. M. Melack (2009), Longitudinal assessment of the effect of concentration on stream N uptake rates in an urbanizing watershed, *Biogeochemistry,* doi: 10.1007/s10533-009-9376-y.

Dodds, W. K., A. J. Lopez, W. B. Bowden, S. Gregory, N. B. Grimm, S. K. Hamilton, A. E. Hershey, E. Marti, W. H. McDowell, J. L, Meyer, D. Morrall, P. J. Mulholland, B. J. Peterson, J. L. Tank, H. M. Valett, J. R. Webster and W. M. Wollheim (2002), N uptake as a function of concentration in streams, *J. N. Am. Benthol. Soc., 21(2),* 206-220.

Donner, S. D., M. T. Coe, J. D. Lenters, T. E. Twine and J. A. Foley (2002), Modeling the impact of hydrological changes on nitrate transport in the Mississippi river basin from 1955 to 1994, *Global Biogeochemical Cycles, 16(3),* 1043, 10.1029/2001GB001396.

Duan, Q., J. Schaake, V. Andreassian, S. W. Franks, H. V. Gupta, Y. M. Gusev, F. Habets, A. Hall, L. Hay, T. Hogue, M. Huang, G. Leavesley, X. Liang, O. N. Nasonova, J. Noilhan, L. Oudin, S. Sorooshian, T. Wagener, and E. F. Wood (2006), Model Parameter Estimation Experiment (MOPEX): Overview and Summary of the Second and Third Workshop Results. J. Hydrol., 320, 3-17, doi:10.1016/j.jhydrol.2005.07.031.

Dunn, D. D. (1996), Trends in nutrient inflows to the Gulf of Mexico from streams draining the conterminous United States 1972-1993. *US Geol. Surv., Water-Res. Invest. Rep.,* 96-4113. Austin, TX: US Geol. Surv. 60 pp.

Harman, C. J., M. Sivapalan, and P. Kumar (2009), Power law catchment-scale recessions arising from heterogeneous linear small-scale dynamics, Water Resour. Res., 45, W09404, doi:10.1029/2008WR007392.

Hall, R. O. Jr, M. A. Baker, C. D. Arp, and B. J. Koch (2009), Hydrologic control of nitrogen removal, storage, and export in a mountain stream, *Limnol. Oceanogr., 54(6),* 2128-2142.

Iacobellis, V. (2008), Probabilistic model for the estimation of T year flow duration curves, *Water Resour. Res.,* 44, W02413, doi:10.1029/2006WR005400.

Lyon, S. W., and P. A. Troch (2010), Development and application of a catchment similarity index for subsurface flow, Water Resour. Res., 46, W03511, doi:10.1029/2009WR008500.

Mulholland, P. J., J. L. Tank, J. R. Webster, W. B. Bowden, W. K. Dodds, S. V. Gregory, N. B. Grimm, S. K. Hamilton, S. L. Johnson, E. Marti, W. H. McDowell, J. L. Merriam, J. L. Meyer, B. Muneepeerakul, R., S. Azaele, G. Botter, A. Rinaldo, and I. Rodriguez-Iturbe (2010), Daily streamflow analysis based on a two scaled gamma pulse model, *Water Resour. Res*., 46, W11546, doi:10.1029/2010WR009286.

Muneepeerakul, R., S. Azaele, G. Botter, A. Rinaldo, and I. Rodriguez-Iturbe (2010), Daily streamflow analysis based on a two scaled gamma pulse model, *Water Resour. Res*., 46, W11546, doi:10.1029/2010WR009286.

Rabalais, N. N., R. E. Turner and W. J. Wiseman, Jr. (2002), Gulf of Mexico hypoxia, aka "the dead zone", *Annu. Rev. Ecol. Syst., 33,* 235-263.

Runkel, R. L. and K. E. Bencala (1995), *Transport of Reacting Solutes in Rivers and Streams,* Chapter 5: in V. P. Singh (editor), *Environmental Hydrology,* Kluwer Academic Publishers, Dordrecht, The Netherlands, p. 137-164.

Runkel, R. L. (1998), *One Dimensional Transport with Inflow and Storage (OTIS): A Solute Transport Model for Streams and Rivers*. U.S. Geological Survey Water Resources Investigation Report No. 98–4018, http://co.water.usgs.gov/otis.

Rupp, D., and J. S. Selker (2005), Drainage of a horizontal Boussinesq aquifer with a power law hydraulic conductivity profile, *Water Resour. Res.,* 41, W11422, doi:10.1029/2005WR004241.

Rupp, D. E., and J. S. Selker (2006), On the use of the Boussinesq equation for interpreting recession hydrographs from sloping aquifers, *Water Resour. Res.,* 42, W12421, doi:10.1029/2006WR005080.

Seitzinger, S. P., R. V. Styles, E. W. Boyer, R. B. Alexander, G. Billen, R. W. Howarth, B. Mayer and N. V. Breemen (2002), Nitrogen retention in rivers: model development and application to watersheds in the northeastern U.S.A., *Biogeochemistry, 57/58*: 199–237, 2002.

Sivapalan, M., S. E. Thompson, C. J. Harman, N. B. Basu, and P. Kumar (2011), Water cycle dynamics in a changing environment: Improving predictability through synthesis, *Water Resour. Res.*, 47, W00J01, doi:10.1029/2011WR011377.

Smith, R. A., G. E. Schwarz and R. B. Alexander (1997), Regional interpretation of water quality monitoring data, *Water Resour. Res., 33 (12),* 2781-2798.

Tague, C., and G. Grant (2004), A geological framework for interpreting the low-flow regimes of Cascade streams, Willamette River Basin, Oregon, *Water Resour. Res.,* 40, W04303, doi:10.1029/2003WR002629.

Tank, J. L., E. J. Rosi-Marshall, M. A. Baker and R. O. Hall, Jr. (2008), Are rivers just big streams? A pulse method to quantify nitrogen demand in a large river, *Ecology, 89(10),* 2935-2945.

Turner, R. E., and N. N. Rabalais (2003), Linking landscape and water quality in the Mississippi river basin for 200 years, *BioSicence*, 53(6), 563-572.

Viney, N.R., M. Sivapalan, D. Deeley (2000), A conceptual model of nutrient mobilization and transport applicable at large catchment scales, *J. Hydrol.*, 240, 23-44

Vogel, R. M. and N. M. Fennessey (1994), Flow-duration curves I: New interpretation and confidence intervals, *J. Water Resour. Plan. Manag.*, 120(4), 485–504.

Vogel, R. M. and N. M. Fennessey (1995), Flow-duration curves II: A Review of applications in water resources planning, *Water Resour. Bullet*., 31(6), 1029–1039.

Wang, S. (2010), A CyberGIS framework for the synthesis of cyber infrastructure, GIS and spatial analysis, *Annals of the Association of American Geographers*.

Ward, R. C. and M. Robinson (1990), Principles of Hydrology, 3rd edition, McGraw-Hill, Maidenhead, Berkshire, England.

Wollheim, W. M., C. J. Vörösmarty, B. J. Peterson, S. P. Seitzinger, C. S. Hopkinson (2006), Relationship between river size and nutrient removal, *Geophys. Res. Lett., 33*, L06410, doi:10.1029/2006GL025845.

Wollheim, W. M., B. J. Peterson, S. M. Thomas, C. H. Hopkinson and C. J. Vorosmarty (2008), Dynamics of N removal over annual time periods in a suburban river network, *J. Geophys. Res. -Biogeosciences*, 113, G03038.

Yaeger, M., E. Coopersmith, S. Ye, L. Chang, and M. Sivapalan (2012), Exploring the physical controls of regional patterns of Flow Duration Curves: 4. A synthesis of empirical analysis, process modeling and catchment classification, *Hydrol. Earth Syst. Sci.*, 16, 4483-4498.

Ye, S., T. P. Covino, M. Sivapalan, N. B. Basu, H.-Y. Li, and S.-W. Wang (2012), Dissolved nutrient retention dynamics in river networks: A modeling investigation of transient flows and scale effects, *Water Resour. Res.*, 48, W00J17, doi:10.1029/ 2011WR010508.

Yokoo, Y. and M. Sivapalan (2011), Towards reconstruction of the flow duration curve: development of a conceptual framework with a physical basis, *Hydrol. Earth Syst. Sci.*, 15, 2805–2819, doi:10.5194/hess-15-2805-2011.

Part I: Climate and Hydrology

Chapter 2

Exploring the physical controls of regional patterns of Flow Duration Curves: Role of seasonality, the regime curve, and associated process controls

Abstract[1]

The goal of this paper is to explore the process controls underpinning regional patterns of variations of streamflow regime behavior, i.e., the mean seasonal variation of streamflow within the year, across the continental United States. The ultimate motivation is to use the resulting process understanding to generate insights into the physical controls of another signature of streamflow variability, namely the flow duration curve (FDC). The construction of the FDC removes the time dependence of flows. Thus in order to better understand the physical controls in regions that exhibit strong seasonal dependence, the regime curve (RC), which is closely connected to the FDC, is studied in this paper and later linked back to the FDC. To achieve these aims a top-down modeling approach is adopted; we start with a simple two-stage bucket model, which is systematically enhanced through addition of new processes on the basis of model performance assessment in relation to observations, using rainfall-runoff data from 197 United States catchments belonging to the MOPEX dataset. Exploration of dominant processes and the determination of required model complexity are carried out through model-based sensitivity analyses, guided by a performance metric. Results indicated systematic regional trends in dominant processes: snowmelt was a key process control in cold mountainous catchments in the north and north-west, whereas snowmelt and vegetation cover dynamics were key controls in the north-east; seasonal vegetation cover dynamics (phenology and interception) were important along the Appalachian mountain range in the east. A simple two-bucket model (with no other additions) was found to be adequate in warm humid catchments along the west coast and in the south-east, with both regions exhibiting strong seasonality, whereas much more complex models are needed in the dry south and southwest. Agricultural catchments in the mid-west were found to be difficult to predict with the use of simple lumped models, due to the strong influence of human activities. Overall, these process controls arose from general east-west (seasonality) and

north-south (aridity, temperature) trends in climate (with some exceptions), compounded by complex dynamics of vegetation cover and to a less extent by landscape factors (soils, geology and topography).

[1]This work has been submitted for publication to Hydrology and Earth System Sciences as: Ye, S., M. Yeger, E. Coopersmith, L. Cheng, and M. Sivapalan, Exploring the physical controls of regional patterns of flow duration curves – Part 2: Role of seasonality, the regime curve, and associated process controls. All figures, tables and data were created by Sheng Ye unless otherwise indicated.

2.1 Introduction

This is the second paper of a 4-part series (the others being Cheng et al., 2012; Coopersmith et al., 2012; and Yaeger et al., 2012) that attempt to understand the physical controls on regional patterns of variations of signatures of streamflow variability, with a particular focus on the Flow Duration Curve (FDC). Instead of directly exploring the FDC, a key frequency-based signature of daily streamflow variability, as in the first paper (Cheng et al., 2012), we will approach it from a different perspective, exploring regional patterns of another signature of streamflow variability, the regime curve (RC), which denotes the mean seasonal variation streamflow. This is motivated by a previous modeling study in hypothetical catchments by Yokoo and Sivapalan (2011), which suggested that the regime curve contains valuable information on the middle part of the FDC, serving as the bridge between the high and low flows at either ends of the FDC, and that understanding the physical controls of the regime curve can assist in achieving the same regarding the FDC. An empirical study of the FDCs of 197 catchments across the United States presented by Cheng et al. (2012), as part of the present study, has provided empirical support to these model predictions.

Motivated by the findings of Yokoo and Sivapalan (2011) and Cheng et al. (2012), the goal of this study is to explore the process controls of regime behavior, i.e., seasonal variation of streamflow, through a comparative study of 197 catchments located across the continental United States, covering a range of climates and physiographic properties, and belonging to the MOPEX dataset. This is essentially a data-based study, assisted by process-based modeling. Instead of applying an existing model to all 197 catchments, the analysis involves systematic model development and assessment of model predictions and performance in comparison to observed data. This downward or top-down approach to model development (Klemeš, 1983; Jothityangkoon et al., 2001; Farmer et al., 2003; Sivapalan et al., 2003; Bai et al., 2009; Thompson et al., 2011) commenced with the development of a simple two-bucket model (hereafter referred to as the "base model"). This model was initially applied to all 197 catchments, and its performance assessed. Guided by alternative hypotheses regarding the reasons for the poor fits against regime curves estimated from observed streamflow data, the model was enhanced step by step through addition of new processes initially left out of the base

model. Model development was continued until the model performance could not be improved any longer. The complete model was then utilized in sensitivity studies to (a) decipher the dominant process controls on the regime curve, and (b) the minimum complexity of models (i.e., the mix of processes required) needed to achieve a satisfactory fit to the empirical regime curves. In this way it is hoped to develop an understanding of the process controls of the regime curves across the continental United States, and also the main climatic and landscape factors that contribute to the regional patterns of the process controls underpinning the regime curves.

The work presented in this paper is an exercise in comparative hydrology (Falkenmark and Chapman, 1989; Sivapalan, 2009), where the goal is to develop generalizable understanding through comparative analysis of rainfall-runoff data in catchments located along a climatic or other gradient. Instead of studying one catchment in considerable detail, the focus is on the use of simpler models to discover features or process controls that are similar or different amongst a population of catchments (Sivapalan et al., 2011). Finally, the assessment of catchment response is with respect to holistic signatures of catchment response (e.g., flow duration curves, regime curve, flood frequency curve etc.) and not in terms of detailed process descriptions. This Darwinian (Harte, 2002; Sivapalan et al., 2011) and functional (Black, 1997; Sivapalan, 2005; McDonnell et al., 2007; Wagener et al., 2007; Sawicz et al., 2011) approach to comparative data analysis and modeling is in contrast with much of the past research in catchment hydrology modeling, which has focused on developing predictive understanding in individual catchments on the basis of models based on individual processes or internal descriptions (Dooge, 1986). Such bottom-up approaches have been hampered by the inability to map the heterogeneity of subsurface pathways and process complexity. Extrapolation to and prediction of catchment responses across different places and a range of scales has remained a challenging problem. A synthesis of these two top-down and bottom-up approaches is possibly the key to developing new understanding and new theories of hydrologic responses at catchment scales. The present study is a step in this direction.

The paper begins with information on the data used in the study and the methodology used to achieve its aims, which is presented next in Sect. 2. This section presents in particular the outlines of the downward approach to model development adopted in the paper, and procedures for model calibration and model performance assessment. Section 3 presents an illustration of the

model development exercise, using the results from 9 selected example catchments. This is followed, in Sect. 4, by a comparative assessment of model performance to determine (a) the dominant process control of the regime curve for the entire population of catchments, (b) the minimum model complexity required to achieve satisfactory predictions of the regime curves, and (c) the manifestations of these process controls on the shapes of the FDCs. The results are summarized in the form of a schematic diagram. Section 5 summarizes the main conclusions of the study and recommendations for further research.

2.2 Data and Methodology

2.2.1 Data

This is a study in comparative hydrology and uses data from 197 catchments located across the continental United States belonging to the MOPEX dataset and spanning a variety of climates and physiographic regions, with over 50 years of continuous daily climatic and flow data. Daily precipitation (*P*), temperature (*T*), and potential evaporation (*PET*) time series are used as climate inputs, while the daily flow data are used to generate regime curves (RCs), 50-year averages of streamflow for each day of the year, which are used for model development, calibration and comparative performance assessment. The *PET* was calculated based on the NOAA Pan Evaporation Atlas (NOAA, 1982), where it was estimated using Penman (1948)'s method, and the solar radiation required in the calculation was estimated from percent sunshine (Hamon et al., 1954). The mix of vegetation types for each catchment and the characteristic LAI (leaf area index) profiles for each vegetation type were obtained from the NASA Land Data Assimilation Systems (available at: http://ldas.gsfc.nasa.gov/nldas/NLDASmapveg.php). The composite LAI profile for each catchment, which is then used as input to the models, is calculated as the average of the monthly values for each vegetation type from the Mosaic vegetation dataset (University of Maryland (UMD) vegetation classification, with 14 classes in total), weighted by the area fraction of each vegetation type within the catchment.

Nine example catchments, chosen from this dataset and spread across the country, (from north to south, west to east, and dry to humid) are used to highlight the diversity of regime behaviors exhibited within the continental United States. Besides, they are also used to illustrate the systematic, downward approach to model development (Sivapalan et al., 2003) that is

eventually implemented in the 197 study catchments. They are selected based on both their locations and their classes within the Köppen climate classification map. Therefore, we can consider them representative of the climate conditions under the regional similarity assumption (Merz and Blöschl, 2004; Patil and Stieglitz, 2011), even though they are not wholly representative of the whole country. Figure 2.1 presents the empirical regime curves of the 9 selected catchments (estimated over the calendar year), which are located in the states of Washington (WA), Idaho (ID), New York (NY), California (CA), Missouri (MO), Georgia (GA), Texas (TX) and Florida (FL). Regime curves are presented for *P*, *PET*, and total streamflow (*Q*), as well as the fast flow (Q_f) and slow flow (Q_u) components of measured streamflow. The fast flow and slow flow components were obtained by the baseflow separation algorithm of Lyne and Hollick (1979),

$$Q_u(i) = aQ_u(i-1) + \frac{1-a}{2}(Q(i) + Q(i-1)) \qquad (1)$$

where *a* is the filter parameter, which was set to 0.925 (Brooks et al., 2011). Since the hydrologic partitioning is not strongly sensitive to baseflow separation methods, (Troch et al., 2009) we will use this easily implementable algorithm for the baseflow separation in this study. The RCs for *PET* show evident similarity with an almost sinusoidal variation with a uniform peak near the middle of the year, and also differences in amplitudes across the continent, exhibiting significant regional variations. For comparative purposes, the aridity index (AI), which is the ratio of annual *PET* to annual precipitation, is also noted in Figure 2.1.

Individually, catchments near the east coast (NY, GA, FL) are relatively humid with AI<1. In the north-east, e.g., NY, precipitation tends to remain constant throughout the year without much seasonality. In the south-east, rainfall seasonality increases north to south (GA, FL), with FL exhibiting strong precipitation seasonality that is almost in-phase with *PET*, due in part to the influence of the hurricane season. Consequently, while within-year variability of flows tends to decrease as we move from north to south along the east coast, the timing of peak flow shifts from March in NY to September in FL. As we move east to west in the north (NY, ID, WA), seasonality of precipitation increases, indeed becoming out of phase with *PET* (note ID and WA, which exhibit strong out-of-phase seasonality). NY and ID exhibit pronounced peak flows during spring not seen in the south, evidently due to snowmelt, whereas the catchment in

WA experiences bi-modal streamflow variability, during spring and again in winter. In the middle of the continent, the aridity index increases from the north (ID) to south (TX), with the seasonality of precipitation undergoing a significant transformation, culminating in a bi-modal distribution in TX (peaks in spring and again in autumn). In TX, because of high aridity, with $PET > P$ over the entire year, there is hardly any streamflow observed. Catchments on the west coast are very diverse, although they all display a precipitation seasonality that is out-of-phase with PET. The Washington catchment has flow peaks not only in winter but also in spring (likely arising from mountain snowmelt), whereas the catchment in Northern California remains humid, exhibiting high flows due to strong winter precipitation that coincides with low PET but without the spring flow peak caused by snowmelt. In Southern California, in spite of the fact that the climate is as dry as Texas, there is spring streamflow due to the out-of-phase seasonality between precipitation and PET. Overall, the variability captured in the 9 example catchments presented in Figure 2.1, provides a snapshot into the enormous spatio-temporal variability of climate and hydrology across the continental United States.

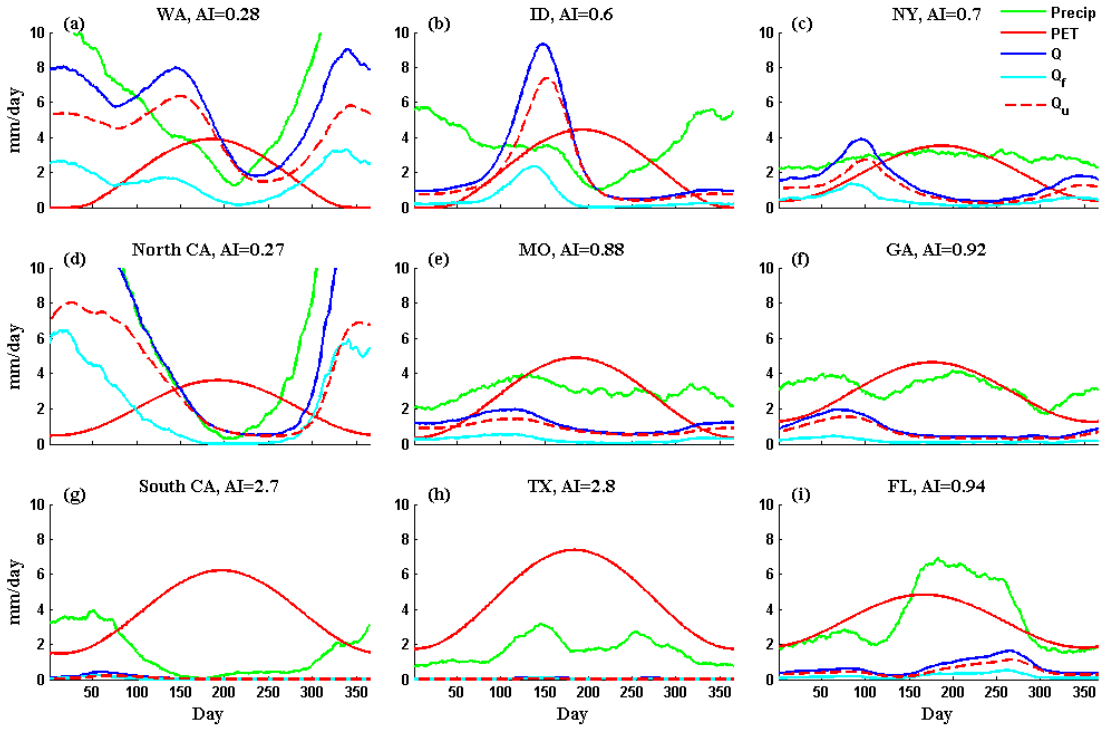

Figure 2.1: Observed regime curves of precipitation, PET, fast flow (Qf), slow flow (Qu) and total flow (Q) in the nine selected catchments across the country, AI is the Aridity Index (PET/P).

Figure 2.2 shows the corresponding FDCs of the nine selected catchments, which are plotted as the sorted 50-year daily streamflow against the frequency of occurrence. They indicate clear differences between the shapes of the FDCs of fast flow, Q_f (which show significant ephemerality in all cases), and those of slow flow, Q_u, and total flow, Q. On the other hand, for each catchment, the FDC of Q_u and Q show strong similarities to each other. In spite of this, there are regional differences between the FDCs, with the 9 catchments dividing into two groups, organized around the aridity index: TX and Southern CA exhibiting strong ephemerality of flows, and all of the remaining (more) humid catchments exhibiting similar FDCs, in spite of the strong differences in the timing of the within-year variability of climate and streamflow. In other words, much of the richness in the regime curves presented in Figure 2.1 is lost in the FDCs, due to the fact that the timing of flows is ignored in the construction of the FDCs.

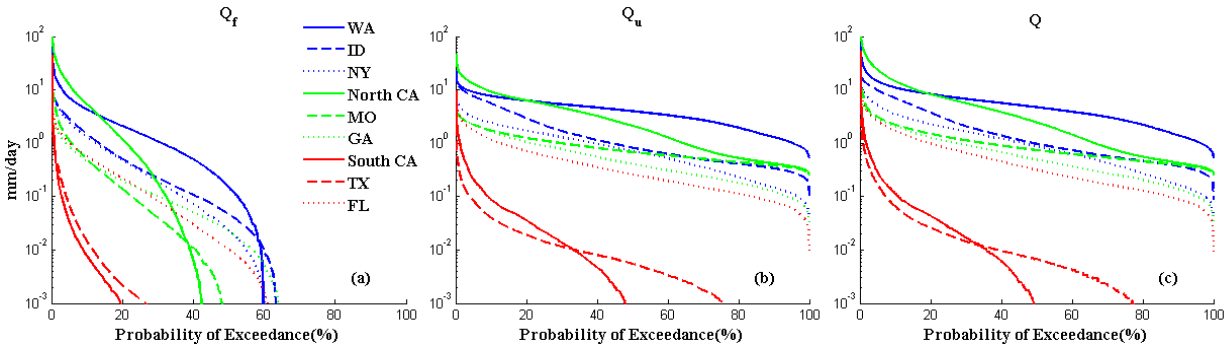

Figure 2.2: Observed flow duration curves of selected 9 catchments: (a) fast flow (Qf); (b) slow flow (Qu); (c) total flow (Q).

2.2.2 Downward Approach to Model development

We have already seen a glimpse into the enormous diversity of both regime behavior and FDCs, and the connections between the two. The main goal of this paper is the elucidation of the process controls underpinning regional patterns of variation of streamflow regime. To achieve this, we adopt a comparative modeling approach, using data from 197 catchments belonging to the MOPEX dataset, and representing strong gradients of climate (including aridity and seasonality), as well as soils, geology, topography and vegetation.

The model development follows the downward approach pioneered by Jothityangkoon et al. (2001) and Farmer et al. (2003), and later reviewed by Sivapalan et al. (2003). Model development commences with a simple two-stage bucket model, which we call the base model. We initially apply the base model to all the study catchments, and attempt to obtain the best possible fits to the empirically derived regime curves using an automatic calibration algorithm. Since our motivation is to explore the first order effects only, regime curves can provide sufficient information for this study. To keep it simple and robust, we use the regime curves estimated over the full length of record for the calibration. Being a simple model, it is not likely that the base model will be adequate in many catchments. In catchments where improved parameterization cannot improve the predictions, we incorporated additional processes that we hypothesized would be able to fill the gap between predictions and observed data. We then reapply the improved model to the study catchments, especially to catchments for which the previous model was found deficient, calibrate the parameters, assess the resulting improvements in model performance, and explore possible further improvements. We continue this process of model development until no further improvements can be obtained in model performance. Through this systematic assessment of model prediction, model updating, and model re-assessment, we used the model as a tool to explore the catchments' runoff characteristics. Note that the focus of the modeling is on comparative assessment across many catchments, and exploration of dominant process controls, and not on obtaining perfect fits to the observed streamflow hydrographs or quantifying model performances in detail for any given model or catchment.

The details of the base model, several model enhancements that were made to the base model as part of the downward approach outlined above, and the final complete model will be presented later in Sect. 3 together with the results of each improvement (Figure 2.3). We next describe the approach adopted for model calibration and parameter estimation, and methods used to carry out comparative assessment of model performance as a way to elucidate dominant process controls and the minimum complexity required to reproduce observed regime behavior.

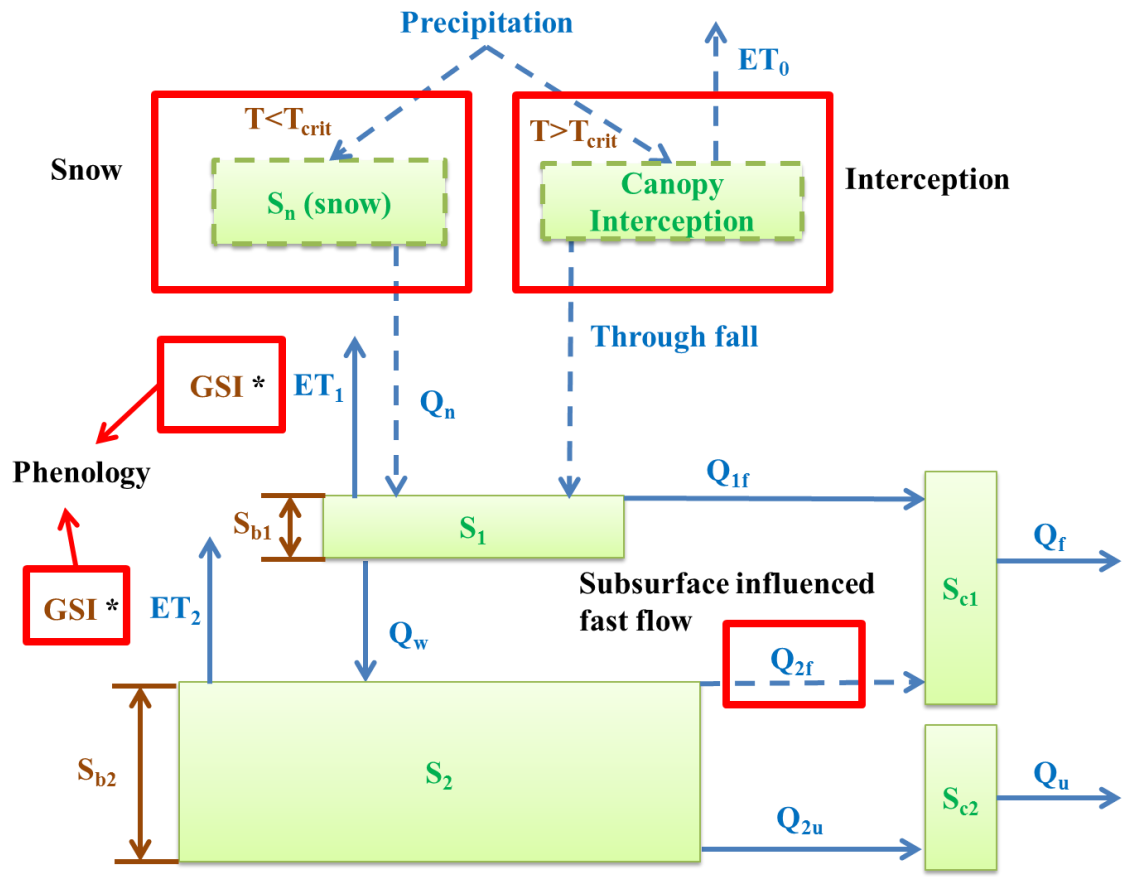

Figure 2.3: Structure of the complete model, reservoirs are represented in solid green boxes; green is used for state variables, blue for fluxes and brown for model parameters red boxes represents the added processes, and dashed lines denote the fluxes from these added processes.

2.2.3 Parameter Calibration and Model Performance Assessment

The distillation of dominant processes from these 197 catchments and the heterogeneous features that describe them is accomplished in four parts. First, we must determine which parameters are required – this was achieved, as described in Sect. 2.2, by sequentially increasing model complexity, adding new processes until the model's performance is adequate. Second, these parameters must be automatically calibrated for all the 197 catchments – this is done via the Markov Chain Monte Carlo (MCMC) algorithm, a tool designed to search a multidimensional parameter space more efficiently than brute force. Third, the model's performance must be assessed – this is done by a simple sum of squared errors between the observed and predicted regime curves. Finally, the performance of the various models for each catchment, containing differing number of parameters, must be compared, addressing the relative differences in

complexity. This last step is managed with the use of the Aikake Information Criterion (AIC) (Akaike, 1974), which assesses the marginal value of each new parameter added. This section will discuss the last three parts: parameter calibration, model performance assessment, and process selection.

2.2.3.1 Parameter Calibration and Validation

The measured total streamflow was separated into fast flow and slow flow through the application of the baseflow separation algorithm of Lyne and Hollick (1979), and regime curves of both flows were calculated for the purpose of model performance assessment. The full model (i.e. the base model with all modifications) was applied to all 197 MOPEX catchments to simulate the regime curves of both the fast and slow flow; explicit Euler was used to solve the model equations; and model parameters were estimated through automatic calibration, by comparing the predicted streamflow regime curves to those estimated from observed data.

We adapted the parameter estimation method from Harman et al. (2011), in what is called a naïve Bayesian model. Based on the fits obtained during model application, we assume that the errors associated with predicted fast flow and slow flow regime curves (Q_f, Q_u) are approximately normally distributed, i.e., $N[x|(\mu,\sigma^2)]$. We also assume Q_f and Q_u are normally distributed with their means as the values predicted by the model ($Q_f = f(P, PET, GSI, LAI, S_{b1}, t_w, \alpha, t_c)$, $Q_u = g(Q_w, PET, GSI, S_e, S_{b2}, t_u, t_c)$ with unknown variances (σ_f^2, σ_u^2). The likelihood function $L(X|\theta)$ of the observations $X = \{Q_{f1}, Q_{f2, \ldots,} Q_{fn}, Q_{u1}, Q_{u2, \ldots,} Q_{un}\}$, given the model $\theta = \{ S_{b1}, t_w, \alpha, t_c, S_e, S_{b2}, t_u, \sigma_f^2, \sigma_u^2\}$ with P, PET, GSI as input, can be calculated as follows:

$$L(X \mid \theta) = \left(\prod N(Q_{fi} \mid f(\mathrm{P,PET,GSI,LAI,S_{b1},t_w},\alpha,\mathrm{t_c}),\sigma_f^2)\right)\left(\prod N(Q_{ui} \mid f(\mathrm{Q_w,PET,GSI,S_e,S_{b2},t_u,t_c}),\sigma_f^2)\right) \quad (2)$$

The posterior likelihood function of the model based on the Bayes' theorem is then:

$$L(\theta \mid X) = \frac{L(X \mid \theta)L(\theta)}{L(X)}, \quad (3)$$

where $L(\theta)$ is the prior distribution; since we do not have definite information about the variables, it is set to unity as a uniform prior distribution. $L(X)$ is the probability of the observations,

although it is not necessary to evaluate it since the sampling method we use depends only on ratios of successive likelihoods, and so this term cancels.

We then employ the Metropolis algorithm (Metropolis et al., 1953; Kuczera and Parent, 1998) adapted from Harman et al. (2011) to sample the parameter space towards constructing the posterior distribution. The algorithm, a Markov Chain Monte Carlo (MCMC) technique, is able to sample the parameters efficiently in the vicinity of the maximum likelihood. Starting with an optimum based on previous model development, we calculate the likelihood value for each randomly selected set of parameters (θ_{i+1}) near the current parameter value (θ_i). The new parameter set is accepted if it leads to a larger likelihood value ($L(X|\theta_{i+1}) > L(X|\theta_i)$), i.e., it helps predict the streamflow regime better than the previous set, and then a new search starts from a new set (θ_{i+1}). However, there is the possibility that this set can lead to another local optimum. To reach the globally optimal parameter set, we accept the inadequate parameter set if the ratio of the likelihood values $L(X|\theta_{i+1})/L(X|\theta_i)$ is larger than a uniform random value between zero and one. We run this algorithm to search the next available parameter set that improves upon the largest likelihood and save the 500 samples in a chain. This algorithm is run twice to generate 1000 samples in total for each site. The parameter set with largest likelihood was selected as optimal for the full model.

Table 2.1: Overview of the estimated parameters for all the satisfactory catchments.

	S_{b1} (mm)	t_w (days)	α	S_e (mm)	t_u(days)	S_{b2} (mm)	t_c (days)
Minimum	0.001	0.013	0.000	0.037	1.548	4.184	0.073
Mean	0.069	0.189	0.274	49.756	187.987	326.358	1.538
Maximum	1.013	0.533	0.300	339.181	1301.191	879.561	9.659
SD	0.14	0.09	0.14	69.44	221.68	183.98	1.51
Median Rel. Error (%)	33.57	33.31	23.74	46.73	24.05	11.54	29.19

One of the advantages of a Bayesian framework is that we can estimate uncertainty (Bai et al., 2009; Harman et al., 2011): the upper and lower bounds are defined from the plot of

likelihood and parameter values. For each catchment, throughout the MCMC sampling, there is a chain of likelihood values which are added cumulatively from the smallest parameter value; the upper and lower bounds are then defined when the sum of the likelihood values just exceeds 95% and 5% of the total. The relative error is calculated as half of the range between the upper and lower bounds as a percentage of the parameter with the maximum likelihood value. Median relative error presented in Table 2.1 is the median of the uncertainty among the catchments.

Since our goal is not to deliver precise predictions of the streamflow time series, but rather to gain a general understanding of first order impacts of different processes on flow generation mechanisms along a climatic or other gradient, a qualitative validation, also called "scientific validation" (Biondi et al, 2012) suits our purpose better. Scientific validation can be used to identify integral processes for which the model should account, as well as to demonstrate the model's ability to adequately represent reality, since validation tests alone may not guard against an equi-final solution (Biondi et al, 2012). This is the essence of the downward approach to modeling, as outlined in Sect. 2.2, and it is this systematic model development procedure itself that helps to validate the importance of each remaining process. As a model could produce good results with a wide range of specific parameter values, to ensure that the model produces reasonable results with realistic parameters, the parameter set should be considered as a combined set (Freer et al., 1996). The Bayesian framework we used is able to find optimum parameter sets by giving greater weight to the better simulations. These parameter sets and predictions then can be chosen as more likely than others. In addition to the assessment of model hypotheses and parameters, a multi-criteria approach can also be used to verify model performance. In this work, we calibrate the parameters to optimize both the fast flow and slow flow simultaneously. This multi-objective check helps provide information regarding where individual subsystems or processes are significant in the catchments. For example, some processes may not affect the total discharge, but could influence the quantities of observed fast flow (Figure 2.6 and 2.7). A multi-objective calibration enables us to detect those improvements in model performance that negatively affect the global discharge but are beneficial for characterizing the fast flow component and detecting the main control processes.

2.2.3.2 Performance Assessment for the full model in all 197 catchments

Even with all modifications, the model is still relatively simple, and it is probable that even the full model may not be able to reproduce streamflow satisfactorily in catchments that have other, perhaps anthropogenic, factors dominating the flow generation mechanism. Therefore, after the calibration, we assessed the model performance for all 197 catchments and removed 45 catchments where the full model failed to generate adequate predictions. These were mostly located in the agricultural Mid-west, many of them known to be dominated by tile drains or irrigation.

Different catchments have distinct flow characteristics (i.e., the magnitude and the variability of the flow). To compare the performance among catchments, the model predictions are then assessed through the use of a performance indicator, the mean square error (MSE) estimated on the standardized flows (separately for both fast and slow flows) as follows:

$$MSE = \frac{\sum (SQ_{obs} - SQ_{sim})^2}{N} \tag{4}$$

where SQ_{obs} and SQ_{sim} are standardized flow value for observed and simulated flow, and N is the length of data. Both flows are standardized by the observed mean and standard deviation to remove the influence of the flow characteristic differences:

$$SQ = \frac{Q - mean\,(Q_{obs})}{std\,(Q_{obs})} \tag{5}$$

where Q represents the time series of flows (observed for SQ_{obs} or model-predicted for SQ_{sim}), Q_{obs} is the time series of observed flow, SQ_{obs} is the standardized observed flow, and SQ_{sim} is the standardized simulated flow, both SQ_{obs} and SQ_{sim} are represented by SQ in the equation as they are calculated in the same way. The summations in Eq. (4) and Eq. (5) are over 1-365 days, considering that we are dealing with the regime curve only.

2.2.3.3 Process selection for catchments with satisfactory prediction by full model

For the catchments classified as satisfactory, we assume the full model captures the dominant processes in those catchments. For each well-modeled catchment, we then performed

comparative assessments of the models using different combinations of the four modified processes identified through the model's development. The comparative assessment is carried out (a) to determine dominant processes that contributed most to the reproduction of the observed regime curves, and (b) the minimum model complexity (i.e., the number and type of model enhancements needed to be added to the base model to reproduce the observed regime curve).

The Akaike Information Criterion (AIC) is used to perform this comparative performance assessment (Akaike, 1974). The AIC is a statistical metric often used to measure the relative goodness of fit of models by generating a measure of information loss, and is used in model selection to choose the candidate model that minimizes information loss. Recently, it has also been used to assess needed model complexity to achieve the required quality of model predictions (Engelhardt, et al., 2012). The smaller the AIC value, the less information is lost, and the better the model. Assuming, for simplicity, a Gaussian distribution for the streamflow, we can estimate the AIC using the following expression:

$$AIC = \ln(Maximum\ Likelihood) + 2k = n \ln\left\{\sum (SQ_{obs} - SQ_{sim})^2\right\} + 2k \quad (6)$$

where n is the sample size (i.e., in this case 365 days as we resolve the regime curve on a daily basis) and k is the number of parameters used in each model.

The difference between the AIC of the model prediction after each model enhancement and the AIC of the base model prediction, i.e., $AIC_1 = AIC_0 - AIC_1$, is used as a measure of the improvement in model performance. Comparative assessments of the model performance after the addition of each process enhancement at the first level can be used to determine the dominant process, i.e. the one process that helps most to improve the prediction in comparison to that of the base model. Similarly, the required minimum model complexity is inferred also through the use of the AIC, when it can be determined that the addition of a particular process enhancement does not lead to significant improvement in model performance.

2.3 Illustrative Results: Progression of Model Development

In this section we present the detailed development and results of the model enhancement process, including the thought processes involved in making the model choices. In this

presentation, we focus on bringing out the process controls of the streamflow regime curve in qualitative terms, using some of the 9 catchments presented in Figure 2.1 and Figure 2.2 as examples.

2.3.1 Base model

Yokoo and Sivapalan (2011) suggested, in terms of reproducing the Flow Duration Curve, that a catchment's streamflow response can be partitioned into two different components: fast flow (e.g., surface streamflow processes whose variability directly reflects that of event precipitation), and slow flow (e.g., subsurface flow whose variability reflects the strong filtering of precipitation variability by flow pathways with significantly longer residence times, and is therefore reflected in the catchment's regime curve).

Guided by this thinking, we start with a nonlinear, six-parameter model operating as a two-stage filter, with two buckets arranged in series and simulating both fast flow and slow flow and their interactions (Figure 2.3). In the first stage, precipitation events are filtered nonlinearly into fast streamflow and soil wetting (infiltration to deeper soil). In the second stage, the infiltrated water is filtered (somewhat more linearly), governed by the competition between topographically-driven subsurface drainage and vegetation-driven evapotranspiration. In terms of streamflow generation, the first bucket is treated as an overflow bucket, whereas the second is treated initially as a leaky bucket (with no overflows). Each of the two filters (buckets) is assigned a storage capacity (i.e., S_{b1} and S_{b2}, respectively, although in the base model S_{b2} is not invoked) and associated characteristic response times (i.e., t_w and t_u, respectively). The second (deeper) bucket is also assigned a root zone storage capacity (i.e., S_e) that is used in the prediction of transpiration. Two more buckets are added to route the fast flow and slow flow components separately. In reality, once the fast flow and slow flow enter the channel, both flows are routed together. However, since we are not aiming to predict the hydrograph or peak flow precisely, but rather, to appropriately predict regime behavior, such a technique is acceptable for our purposes. Because the drainage area of these catchments varies from hundreds of square kilometers (10^2 km^2) to tens of thousands of square kilometers (10^4 km^2), these two routing buckets are used to introduce lag time for the flow and to attenuate the variability to obtain a smoother regime curve more closely resembling the observed regime curve. A sixth parameter (i.e., t_c) is used here to represent the lag times introduced by flow routing in the river network.

The water balance equations for the two storage buckets are as follows:

$$\frac{dS_1}{dt} = P - Q_{1f} - Q_w - ET_1 \quad (7)$$

$$\frac{dS_2}{dt} = Q_w - Q_{2u} - ET_2 \quad (8)$$

where S_1, S_2 are the water storage in the 1st stage and 2nd stage, P is the precipitation, $Q_{1f} = (S_1 - S_{b1})/\Delta t$, is saturation excess streamflow from the 1st bucket, $Q_w = S_1 / t_w$, is the wetting (infiltration) into the second bucket, $ET_1 = PET\ (S_1 / S_{b1})$, is evapotranspiration from the 1st bucket, $Q_{2u} = S_2 / t_u$, is the subsurface drainage from the 2nd bucket, $ET_2 = PET\ (S_2 / S_e)$, is evapotranspiration from the 2nd bucket. The water balance equations for the two stream routing buckets are as follows:

$$\frac{dS_{c_1}}{dt} = Q_{1f} - Q_f \quad (9)$$

$$\frac{dS_{c_2}}{dt} = Q_{2u} - Q_u \quad (10)$$

where S_{c1} is the water storage in the river network from the 1st bucket, $Q_f = S_{c1} / t_c$ is the fast flow at the catchment outlet after stream routing, S_{c2} is the water storage in the river network from the 2nd bucket, and $Q_u = S_{c2} / t_c$ is the slow flow at the catchment outlet after stream routing. The parameter t_c is the mean residence time – the catchment-scale-averaged time raindrops need to travel from hillslope to catchment outlet. It relates to the drainage area, river network structure, topographic gradient, etc.; however, in this paper we will estimate it through calibration. In spite of treating these runoff components separately because of their distinct generation mechanisms and flow paths, still they are routed together in the network once they enter river channels; thus we use the same mean residence time parameter for both fast flow and slow flow.

This base model works well in humid catchments that exhibit strong seasonality (Figure 2.4) such as those found in Northern CA, WA, and FL. In this case, there was little enhancement needed in spite of the fact that these are vegetated catchments. Since precipitation is a main driver of the model, it is reasonable to say that the model works well in catchments whose streamflow response follows a similar pattern as that of the precipitation.

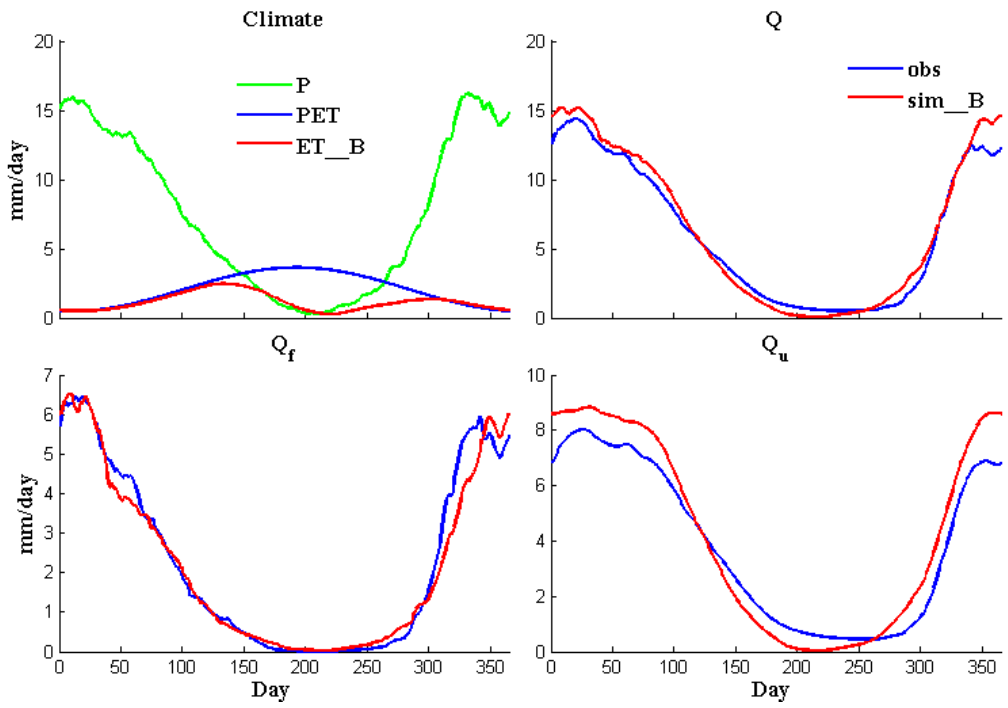

Figure 2.4: Comparison of regime curves of P, PET, ET, Q, Qf and Qu in a catchment in Northern CA between observation (blue line) and base model simulation (red line).

2.3.2 Modification 1: Snowmelt

The base model worked well in many humid catchments that exhibited strong seasonality (e.g., catchments in North CA and Florida, Figure 2.1). However, it failed in over half of the catchments, many of which were the northern, colder catchments. As seen in Figure 2.1, most of these catchments (e.g. WA, ID, NY), experience sharp peak flows in spring. Considering the temperatures at this time of the year, a plausible reason for this is snowmelt, especially in ID and NY. Winter precipitation at these latitudes, especially in mountainous regions, is typically in the form of snow which accumulates on the ground during winter months and remains there until spring when the temperatures increase and the snowpack melts. To improve the model further in these catchments, we incorporated a simple snowmelt component to the base model using the degree-day factor method (e.g., Eder et al, 2003), based on available mean daily air temperatures. The snowmelt component added to the model is as follows:

$$\frac{dS_n}{dt} = P_s - Q_n \tag{11}$$

$$\begin{cases} P_r = P, & T > T_{crit} \\ P_s = P, & T < T_{crit} \end{cases} \tag{12}$$

$$Q_n = \min\{H_{pos} ddf, S_n\}, \quad where \quad H_{pos} = \max\{T - T_{crit}, 0\} \tag{13}$$

where S_n is the storage in the snow pack, P_s is the precipitation in the form of snow, P_r is the precipitation in the form of rain, Q_n is the snowmelt, T_{crit} is the snow-rain transition temperature (assumed here as 0°C), *ddf* (1.5mm/day/K) is the degree day factor, and H_{pos} is the temperature excess over the critical temperature, used in combination with the degree-day factor, as a surrogate for the driving forces for snowmelt.

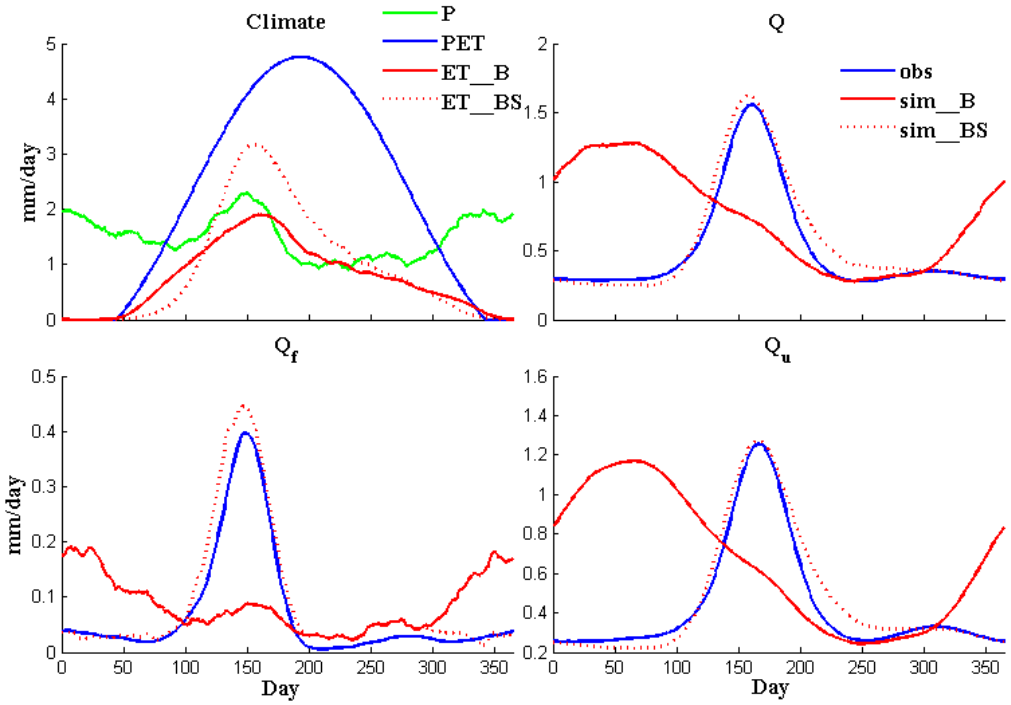

Figure 2.5: Comparison of regime curves of P, PET, ET, Q, Qf and Qu in a catchment in ID among observation (blue line), base model (B, red line) and base model with snowmelt component (BS, solid red line).

Figure 2.5 presents a comparison of the predictions of the base model with those of the enhanced model that included the snowmelt component for the catchment in Idaho. The results show that the enhanced model leads to a dramatic improvement in the ability to predict streamflow timing, duration and magnitude, even though the enhancements for snowmelt have

been rather parsimonious. On the other hand, the catchment in NY (we are not presenting a figure for the sake of brevity) required further modifications to reproduce the observed regime curves.

2.3.3 Modification 2: Subsurface influenced fast flow

With the incorporation of the snowmelt component, the model was able to capture the flow peak during late spring and early summer that was caused by snowmelt. It performed well in the northern mid-western mountainous catchments (e.g., ID, WY, *etc.*), but continued to under-estimate the fast flow during late winter and early spring, in the northeastern catchments (e.g. NY) where snowmelt was significant, and also southeastern (e.g. GA, VA) catchments, which exhibit low seasonality of precipitation and present little or no snowmelt impact. The rainfall during this period is similar to the rainfall experienced in summer but generates much larger streamflow and this non-linear rainfall-runoff response could be related to the high water-table (Lana-Renault et al., 2007; Li et al., 2011). These studies have shown that during the wet season, the hydrological response could be more dependent on the water table level than simply the precipitation characteristics (depth and intensity). Along with the influence of the rising water-table level, the dominant flow generation mechanism would then switch from infiltration excess to saturation excess. Analysis of internal dynamics based on model predictions (not presented here for brevity) showed that the under-estimation of fast flow during spring was accompanied by large amounts of water stored in the 2nd bucket, suggesting that water that otherwise would overflow to the river is being kept in storage due to the absence of an overflow mechanism in the second bucket. This may explain the under-estimation of fast flow during spring, when *PET* and *ET* are small.

As a result, an overflow mechanism that mimics a saturation excess induced fast flow (Q_{2f}) mechanism (albeit in a somewhat conceptual or qualitative manner) was introduced:

$$Q_{2f} = \frac{S_2 - S_{b2}}{\Delta t} \tag{14}$$

where Q_{2f} is the overflow from and S_{b2} is the threshold storage capacity of the second bucket.

To illustrate the impact of this process, we applied the model to a catchment with little snowmelt influence. Figure 2.6 presents a comparison of model predictions in GA between the base model (with snowmelt included) and an enhanced model that included the snowmelt and the

subsurface-influenced fast flow component. The results show that this enhancement indeed helped to increase fast flow during winter and early spring, but still over-estimated the fast flow during summer and fall seasons; the underestimation in slow flow was not improved. The improvement due to this component is less significant than the improvement due to the snowmelt component in the ID mountainous catchment because there, snowmelt is the dominant streamflow generation mechanism, and as such was able to transform both the timing and magnitude from precipitation to streamflow. In GA, other processes such as interception loss and phenology are all important in streamflow generation, and thus the streamflow regime curves follow the trend of precipitation regime curves, which has already been captured by the base model. The addition of these other processes helps to adjust the peak flows rather than alter both timing and magnitude of the streamflow dramatically, as snowmelt did in the ID catchment. However, this does not mean that subsurface-influenced fast flow is not important; as we will show in Sect. 3.5, the combination of all three processes does improve considerably the estimation of both streamflow timing and magnitude.

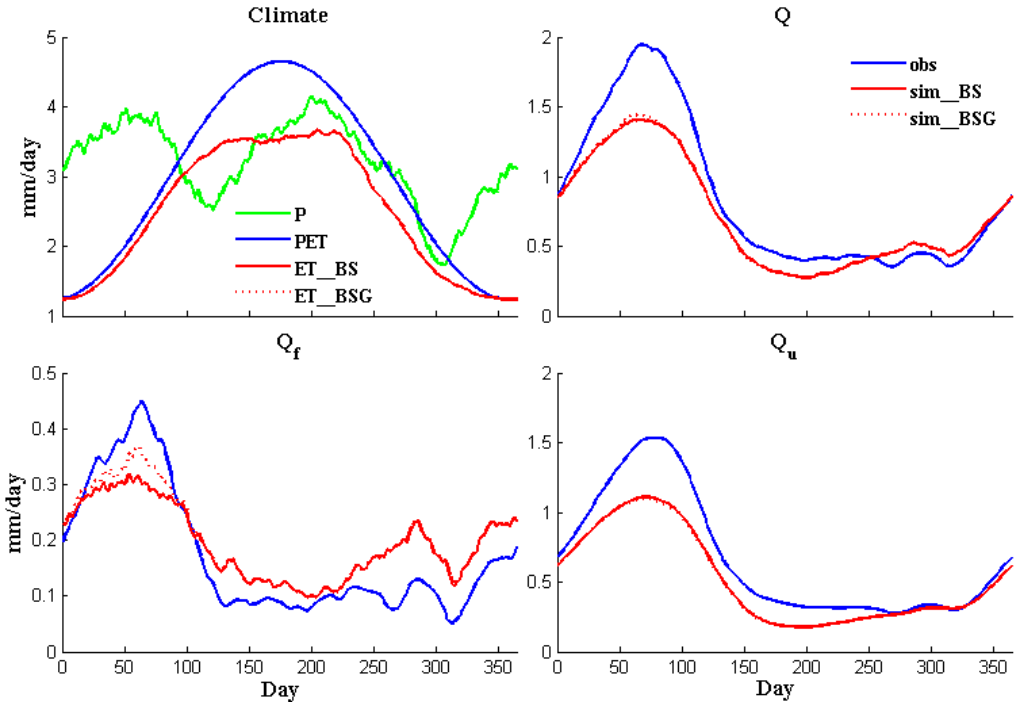

Figure 2.6: Comparison of regime curves of P, PET, ET, Q, Qf and Qu in a catchment in GA among observation (blue line), base model with snowmelt (BS, solid red line) and base model with snowmelt as well as subsurface-influenced fast flow component (BSG, red dotted line).

2.3.4 Modification 3: Interception Loss

Although the incorporation of the subsurface-influenced Q_f helped improve the fast flow prediction during late winter and early spring, we still tended to over-estimate the magnitude of Q_f for most of the year. This was especially evident in several humid catchments where seasonality of precipitation is not significant (e.g., no snow and precipitation is uniform throughout the year) and vegetation cover variability is the strongest controlling factor. In these catchments, Q_f tended to be over-estimated during the growing season (from late spring to fall) when vegetation cover begins to reach its maximum value. Since catchments on the east coast have dense vegetation cover; the overestimation of surface flow during the growing season and the underestimation during the non-growing season could be caused by the presence of vegetation. One of the effects of vegetation on the water cycle is canopy interception (Savenije, 2004). It has been shown that interception could have a significant impact on the water cycle (Beven, 2001; Savenije, 2004); evaporation from intercepted water may reach 35% of total rainfall in wet catchments and over 40% in dry areas (Calder, 1990). This influence can then affect the infiltration, antecedent soil moisture, and runoff generation (Keim, 2006). Given the high proportion of vegetation cover in these catchments, the interception mechanism should not have been ignored. Therefore, to reduce the overestimation of surface flow during the growing season, we added the interception loss component I, as follows:

$$I = \alpha P \frac{LAI}{LAI_{\max}} \tag{15}$$

where α is the fraction of precipitation that is intercepted (a model parameter, to be estimated by calibration), LAI is remotely sensed estimates of LAI, and LAI_{max} is the annual maximum of the LAI used to normalize the LAI time series.

Figure 2.7 shows the comparison of model predictions by the model enhanced with both the snowmelt and the subsurface-influenced fast flow component and a further enhanced one with snowmelt, subsurface-influenced fast flow, and interception loss. The results show that the incorporation of canopy interception helps reduce the fast flow magnitude throughout the year and increases the slow flow during winter and early spring slightly, but is still not able to capture the strong seasonality in the flow.

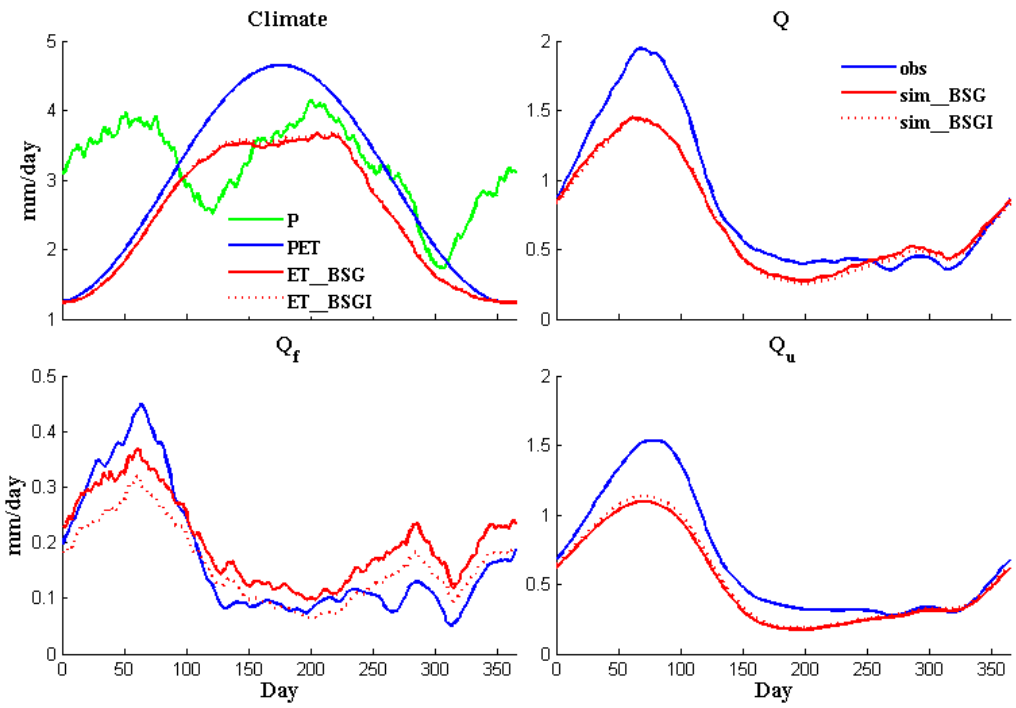

Figure 2.7: Comparison of regime curves of P, PET, ET, Q, Qf and Qu in a catchment in GA among observation (blue line), base model with snowmelt and subsurface-influenced fast flow component (BSG, solid red line) and base model with snowmelt, subsurface-influenced fast flow and interception loss component (BSGI, red dotted line).

2.3.5 Modification 4: Phenology

In several catchments where the intra-annual variability of precipitation is relatively small, seasonality of flow is nevertheless much stronger than that of precipitation. The incorporation of the interception loss reduced the fast flow magnitude without differentiation, but was not able to increase the seasonality in the flow; the model continued to underestimate the spring flow peak of both fast and slow flow components. This is even more pronounced in some semi-humid and humid catchments (e.g., GA, VA), where rainfall arrives year-round without significant seasonality, as illustrated by GA in Figure 2.1. We attribute this discrepancy to the growth cycle of vegetation and its impact on both interception and transpiration. Therefore we applied a correction to the PET data using a Growing Season Index (GSI) (Thompson et al., 2011) in order to improve the estimates of actual evapotranspiration and account for the effects of these plant

water-use patterns, i.e. phenology. The phenology-corrected *PET*, denoted as PET_c, is estimated as follows:

$$PET_c = PET \times GSI \tag{16}$$

$$GSI = \begin{cases} 0 & T < T_{\min} \\ \dfrac{T - T_{\min}}{T_{\max} - T_{\min}} & T_{\min} < T < T_{\max} \\ 1 & T > T_{\max} \end{cases} \tag{17}$$

where T_{min} and T_{max} were originally proposed as the minimum and maximum threshold soil temperatures of -2^{o}C and 5 ^{o}C (Jolly et al., 2005) to cover a large range of species, Here, we approximate them by air temperatures of -5^{o}C and 10 ^{o}C (Thompson et al., 2011) due to the non-availability of soil temperatures.

Figure 2.8 shows the comparison of the predictions by the base model with snowmelt, subsurface-influenced fast flow, and interception added to it and an enhanced model that incorporated phenology as well. The introduction of the Growing Season Index (GSI) affects the value of both Q_f and Q_u by increasing it substantially during winter and spring when transpiration from the vegetation is much smaller. This can also be seen in the simulated ET, where the ET for the model without phenology closely follows the PET during winter (since there is no restriction on water availability during this period), whereas ET for the enhanced model is much lower from November to April, thus increasing both the slow flow and fast flow substantially. With these three modifications, the model now performs well in these forested catchments. As a result, we reach the final and complete model resulting from the four different enhancements presented above (Figure 2.3), and the final water balance equations for the two complete hillslope buckets are shown below:

$$\frac{dS_1}{dt} = P_r - I + Q_n - Q_{1f} - Q_w - ET_1 \tag{18}$$

$$\frac{dS_2}{dt} = Q_w - Q_{2f} - Q_{2u} - ET_2 \tag{19}$$

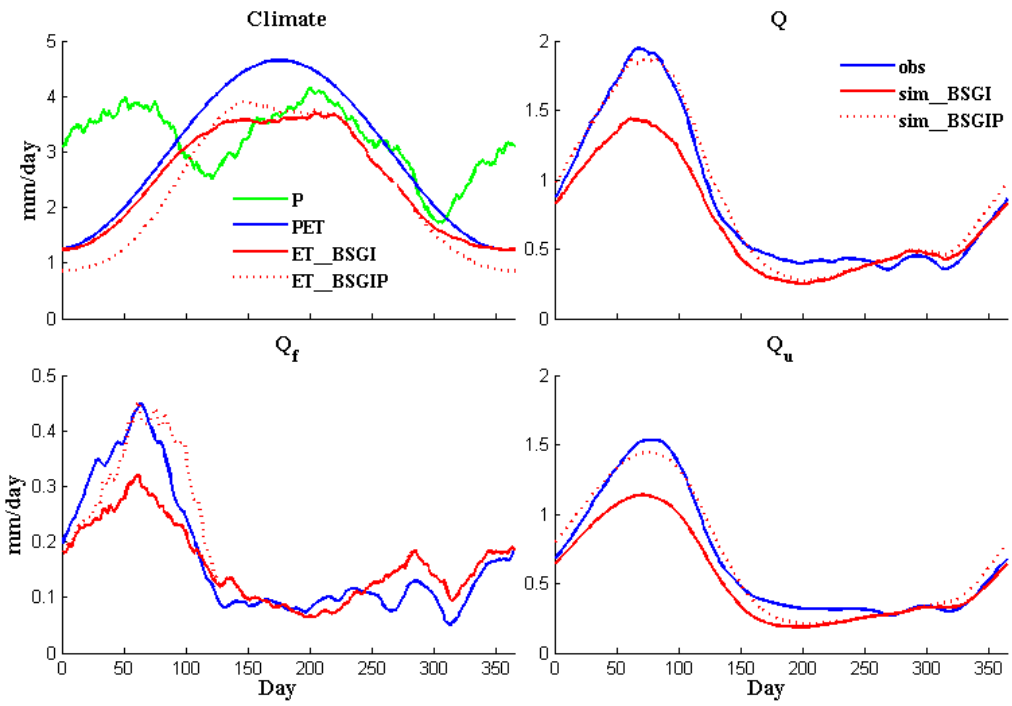

Figure 2.8: Comparison of regime curves of P, PET, ET, Q, Qf and Qu in a catchment in GA among observation (blue line), base model with snowmelt, subsurface-influenced fast flow and interception loss component (BSGI, solid red line) and the complete model (BSGIP, red dotted line).

2.4 Comparative model performance assessment

2.4.1 Performance of complete model across study catchments

The key aim of this paper is to use the complete model developed through the use of the downward approach above to explore (a) the dominant process controls that underpin the magnitude and timing of the regime curve, and (b) the minimum model complexity, in terms of the mix of processes, needed to reproduce the observed regime curves. Before we embark on this exploration, which is the subject matter of this section, we need to reassure ourselves that the complete model is sufficient for these purposes. For this reason we assessed the quality of model predictions on the basis of the MSE for normalized flows (see Eq. (4)). Simulation results with the full model showed that model simulations of the 50-year averaged fast flow and slow flow regime curves fitted the corresponding empirical regime curves well in the eastern and western

catchments, but failed in several mid-western catchments (e.g., Iowa) and also in extremely dry catchments in Oklahoma and Texas.

Catchments in the southwest (TX, OK) are very dry, with aridity indices exceeding 1.5. The primary vegetation cover is grassland, and rivers are ephemeral – there can be as few as just one flow event during the entire year. Catchment responses in these areas were found to be much more difficult to predict with the use of simple lumped models, compared to the humid, and more forested catchments in the east, or the highly seasonal catchments on the west coast. Another area where the complete model did not produce good predictions is in the Midwest (especially catchments in Iowa) where the dominant vegetation cover is agricultural and anthropogenic effects related to agricultural water extractions cannot be ignored. For example, in the Raccoon River catchment in Iowa, subsurface (i.e. tile) drainage is estimated to cover over 40% of the area (Zucker and Brown 1998). Additionally, there appears to be considerable human-induced water extraction (Hatfield et al., 2009). These human activities have significantly altered the hydrologic response, which our simple model is not yet able to address.

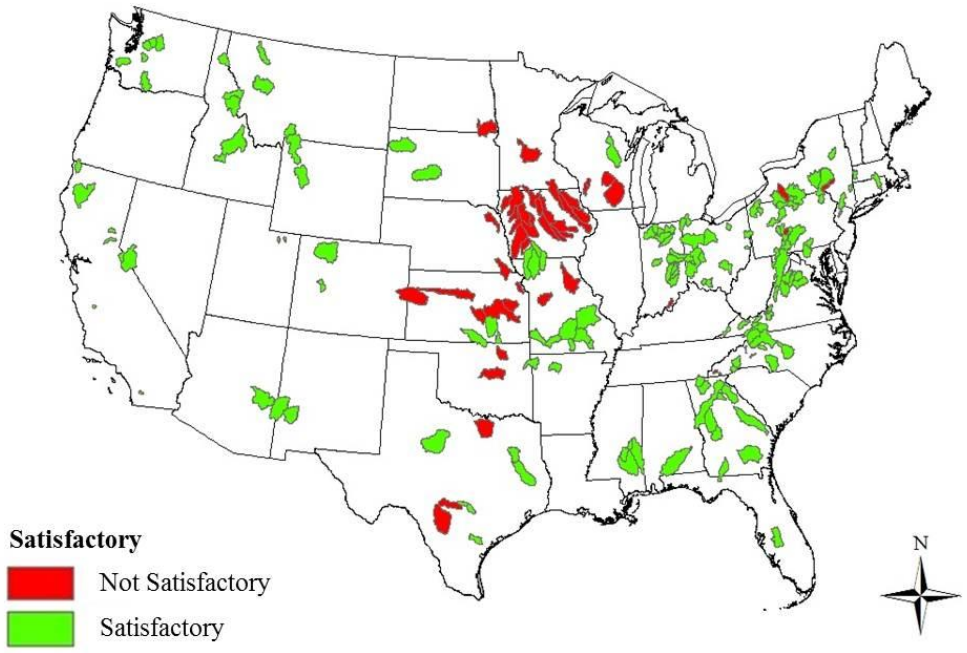

Figure 2.9: Spatial distribution of the goodness of the model prediction in 197 catchments

As a simple model, we would not expect that it could accommodate anthropogenic activities or very complex catchments; therefore, we need to eliminate these catchments where the model performs poorly. To ensure that the model captures the dynamics as well as the volume of the streamflow, we use MSE as our criterion. The decomposition of the MSE (or Nash-Sutcliffe efficiency) shows that the MSE consists of three components: the mean, variance and correlation coefficient (Gupta et al., 2009). However, as the error is scaled by the standard deviation, it can be problematic for comparisons amongst catchments. To avoid this, we standardized the flow before the MSE calculation. We selected the 90% of the catchments with the lowest MSE in fast flow, slow flow, and total flow separately and then obtained the intersection of these three sets to determine those catchments that had the lowest MSE in fast flow, slow flow, and total flow simulation. The resulting 152 catchments were then considered as "satisfactory" catchments, and the regional breakdown of the MOPEX catchments into "satisfactory" and "not satisfactory" is presented in Figure 2.9. Note that the "not satisfactory" catchments are left out from the analyses of comparative performance assessments presented next.

2.4.2 Regional distribution of model parameters

In the rest of the analysis we will focus on the catchments in which the complete model generated satisfactory regime curves for both fast flow and slow flow. Table 2.1 presents the overview of the parameters in all the "satisfactory" catchments: the mean, minimum, maximum, standard deviation and median relative error. The median relative error is the lowest, close to 10% (11.5%) for the 2nd bucket capacity (S_{b2}), around 20% for interception loss (α) and the subsurface flow drainage time scale (t_u), around 30% for the mean residence time associated with river network routing (t_c), the characteristic time scale of wetting (t_w) and the 1st bucket capacity (S_{b1}), and 46% for the root zone soil moisture capacity (S_e). Given the simplicity of the model and the large variations between catchments, this is deemed acceptable.

The average values of the key parameters are presented in Table 2.2 in detail for three catchment groups to give an impression of the regional distribution of these parameters: eastern US, central US, and western US. The eastern catchments are located near the east coast and within the Appalachian mountain region, while the western catchments are those located on the

west coast and in the Rocky Mountains area; the remainder of the catchments forms the central US group (after removal of catchments deemed "not satisfactory"). Nevertheless, these results should be considered as indicative only, given the conceptual nature of the models and the relative parsimony of model structures used.

Table 2.2: Mean value of 7 parameters for eastern, central and western catchments

		S_{b1} (mm)	t_w (days)	α	S_e (mm)	t_u (days)	S_{b2} (mm)	t_c (days)
East	**Mean**	0.065	0.218	0.306	36.846	120.260	281.858	1.469
	SD	0.158	0.078	0.128	49.540	64.644	163.704	1.268
	Median Rel. Error (%)	31.47	30.35	13.87	42.65	21.10	9.49	24.26
Center	**Mean**	0.068	0.140	0.221	78.007	323.567	350.640	1.763
	SD	0.098	0.084	0.147	101.615	282.408	160.895	2.049
	Median Rel. Error (%)	11.32	17.50	20.93	32.46	16.78	9.34	14.39
West	**Mean**	0.062	0.159	0.225	56.099	189.287	394.281	1.447
	SD	0.094	0.100	0.132	81.326	351.256	262.644	1.826
	Median Rel. Error (%)	29.19	23.86	20.34	51.94	29.30	7.71	27.28

Table 2.2 shows that interception loss as a fraction of precipitation (α), which has a significant impact on the water balance, especially on evaporation (Liu, 1997), lies in the 20-30% range. Generally, it is larger in the east coast where vegetation is dense, and smaller in the dry catchments in the west and south-west (e.g., Texas and Southern California). This is consistent with what would be expected: forests are believed to be able to intercept more rainfall than grasslands (Deguchi et al., 2006); while coniferous forests tend to retain more rainfall than broad-leaved forests (Marin et al., 2000). Average bucket storage capacities of the 1st (surface) bucket (e.g., S_{b1}) do not exhibit significant differences between the three regions. On the other hand, bucket capacities of the 2nd (subsurface) bucket (e.g., S_{b2}) show considerable variation: the mean value of S_{b2} in eastern U.S. catchments is comparatively smaller than those in the central US, which is smaller yet than those in the west, suggesting effectively deeper soils as we move towards the west and south-west. The root zone soil moisture capacity, S_e, is small in north-eastern catchments and in some southern mountainous catchments, reflecting the presence of thin soils and shallow-rooted trees. Root zone storage capacity turns out to be highest in central parts of the continent, reflecting deeper soils and deep rooted vegetation. This increasing trend of soil

moisture capacity from east to west may be related to climate seasonality (Samuel et al., 2008): in the eastern, humid catchments, where rainfall arrives throughout the year, the low moisture storage capacity and higher slopes help to drain this water quickly, leading to a smaller quantity of storage; in the center of the continent, with moderate seasonality and flat topography, the Midwestern catchments are usually characterized by deep soils and stronger soil moisture retention characteristics (Endres et al., 2001; McIsaac et al., 2010); near the west coast, due to the strong seasonality in P which is out of phase with PET, the soil moisture tends to accumulate during the wet season, leading to higher overall storage. The characteristic time scale of wetting (t_w) is longest in the east, smaller in the west, and smallest in the central US. This trend is opposite to that of the subsurface flow drainage time scale (t_u). This must reflect the effects of soil permeability and topographic slope, which show a similar regional pattern with respect to t_u. This is consistent with the findings of McGuire,et al. (2005) in seven catchments with diverse geologic and geomorphic conditions: instead of basin area, the residence time is strongly related to terrain indices representing flow path distance and gradient. The mean residence time associated with river network routing (t_c) is a function of topographic slope and drainage area: the larger the drainage area, the flatter the topography, the longer is the network residence time. In any case, the t_c values are much smaller than those of subsurface flow residence time, t_u. Since we are mainly concerned with the regime curve, the magnitudes of t_w and t_c are too small to have any impact on the streamflow regime curve, whereas the magnitude of t_u is highly critical.

2.4.3 Elucidation of dominant processes for fast flow and slow flow

Having completed the modeling of all 197 catchments, we then sought to identify which of the four process modifications we made to the base model contributed most to improving the model performance. This involved systematic sensitivity analyses with the model, where we run the base model with each one of the process enhancements, one by one, while maintaining all remaining model parameters at their previously calibrated values. For presentation purposes, we will denote the base model and the 4 subsequent additions by the names M0 to M4, where the numbers (1-4) refer to the number of processes added to the model. We then use the letters P, I, S, G to specify the added process, respectively as phenology, interception, snowmelt, or subsurface influenced fast flow. For example, M1P is a Level 1 model, i.e., the base model plus phenology, and M3PIS is a Level 3 model, with base model plus phenology, interception and snowmelt. We

estimated the AIC for the base model (AIC_0) and the AICs for each of four Level 1 models (AIC_{1P}, AIC_{1I}, AIC_{1S}, and AIC_{1G}), along with the corresponding reductions in AIC (ΔAIC_{1P}, ΔAIC_{1I}, ΔAIC_{1S}, and ΔAIC_{1G}). Based on assessments of model performance of the four Level 1 models (M1), the process addition that leads to the highest improvement in model performance (i.e., in relation to the base model) would then be deemed as the dominant process. For example, in the Idaho catchment (Figure 2.1 and Figure 2.5), ΔAIC_{1S} turned out to be largest, on the basis of which we could conclude that snowmelt is the dominant process in this catchment.

Note that if in a particular catchment, none of the processes contributed to a decrease in AIC through its addition to the base model, or if the reduction is too small (e.g., less than 3%), we would then consider the base model to be sufficient. The latter means that the magnitude of precipitation and its seasonality are the main or dominant controls on the regime curve, and the roles of vegetation, temperature and topography are second order effects, and thus can be left out in any initial model simulations.

Figure 2.10 presents the results of this assessment of dominant processes for the 152 satisfactory catchments, separately for fast flow and slow flow. For fast flow (Figure 2.10a), generally the dominant process in northern catchments is snowmelt due to the considerable amount of precipitation as snow (these catchments are circled and labeled as a, b, c, and d). Yet there are slight differences among them: the northwestern catchments (circles a, d) are mountainous catchments, and snowmelt is the only additional process needed. Moving east to the center of the continent, i.e. catchments in the Midwest such as in Indiana (circle b), catchments are much flatter and winter temperatures are higher than in the northwestern mountainous catchments. Snowmelt is no longer the only dominant process for these catchments, some are dominated by subsurface influenced fast flow, due to the fact that the soil in these places is silty clay loam with relatively smaller subsurface drainage rates, and consequently the water table could rise to the surface during parts of the year, generating saturation excess overland flow. On the other hand, on the east coast, the Appalachian catchments are covered with dense vegetation, and phenology is therefore dominant. The snow influence fades in the central and southern catchments, where vegetation impact increases (circles e, f, g). For the central catchments in Missouri (circle e), snow and vegetation impacts are equally important; in some of the northern catchments snowmelt helps to reduce AIC more and in others phenology and/or interception

reduces AIC more. Looking at the eastern forested catchments (circle f) where snow is rarely seen, phenology and interception are the most dominant processes in some of them, and in others, due to the small soil moisture storage capacity, subsurface driven fast flow appears to be important. Catchments in New Mexico and Arizona (circle g), even though they are arid, do contain woodland or wooded grassland coverage over 60% of the catchment areas, and given the dry climate, streamflow is extremely sensitive to vegetation effects. Southeastern catchments (circle h) are marked here as base model dominant. Although there is dense vegetation coverage in these catchments, seasonality in climate makes simulation much easier. The catchments in Florida experience a wet season from mid-summer to early fall (Figure 2.1(i)); they receive abundant rainfall that is caused by frequent convective activity as well as the occasional tropical storms similar to those experienced in monsoon Asia (Fernald and Purdum, 1998). The catchments in Georgia also display seasonality of precipitation; they receive heavy rainfall during winter and spring when the evapotransipiration rate is quite low, thus enhancing the seasonality observed in streamflow generation (Opsahl et al. 2007). The phenology influence is mitigated somewhat in these southern catchments since the duration of vegetation coverage is much longer than the Appalachian Mountain catchments.

When it comes to slow flow, spatial patterns of dominant processes are, for the most part, similar to those for fast flow: snowmelt dominates in northern catchments, replaced by vegetation effects in southern catchments. Snowmelt is the most dominant process in north-western catchments (catchments located within circles a, d, e.g., ID). As we move further east vegetation cover increases and phenology appears to be the dominant process in many northeastern catchments (circles b, c). Most of the catchments in the Mississippi River region (circle e) indicate phenology to be the dominant process given the considerable vegetation cover and intermediate rainfall. As in the case of fast flow, phenology is dominant in Arizona and New Mexico, and these otherwise dry catchments appear to be highly sensitive to vegetation effects (circle f). The dominant processes in southeastern catchments for slow flow generation appear to be more diverse than in the case of fast flow. In this case all four process additions are sufficiently involved in slow flow generation; their effects are of a similar order and not one process is most dominant.

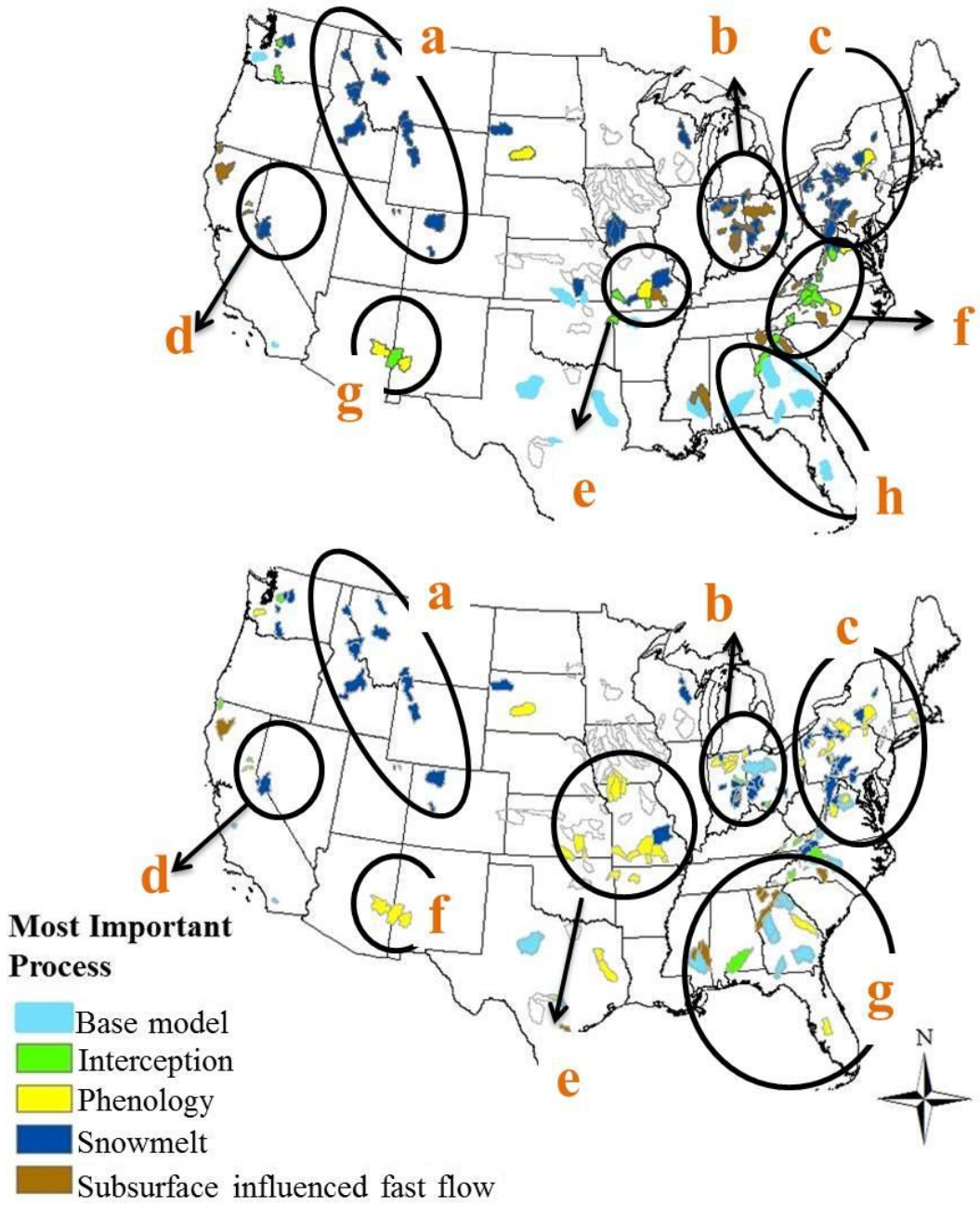

Figure 2.10: The most important process in catchments with effective model prediction: (a) fast flow, (b) slow flow. The circled areas represent regions of process similarity.

2.4.4 Minimum model complexity for reproduction of regime curves

Although the full model generated acceptable predictions of the streamflow regime for all "satisfactory" catchments, especially outside of the mid-west and south-west (see Figure 2.9), we

discovered in the previous section that the importance of each process addition was not the same everywhere. Some of the processes are never invoked (i.e. snowmelt in warm catchments) or could easily be left out in some of the catchments without loss of overall performance (i.e. phenology in southern catchments where the weather is always warm). In this section, we want to determine the minimum model complexity that can generate satisfactory predictions, including all processes that are deemed essential to reproduce the regime curve to reveal and concentrate on the most necessary processes in those catchments. In some catchments this is obvious; for example, snowmelt is clearly not needed in southern catchments. In many other catchments, this is not so self-evident, and we can only determine this through careful quantitative assessment.

Once again we use the AIC to measure model performance. However, this time we apply the optimized parameter sets for the full model repeatedly to the 15 possible model structures (including one Level 0 model (i.e., the base model), four Level 1 models, six combinations of Level 2 models, and four combinations of Level 3 models). In each case we estimate the AIC of the total flow predictions for each of the 15 models. Starting from the base model (M0), we compare the AIC at every modeling step with the AIC of the full model (AIC_4): if the AIC of the base model (AIC_0) is smaller than that of AIC_4, then we can say that the base model is adequate to generate satisfactory predictions. Otherwise, we continue to the Level 1 model (M1) and after comparing AIC_1 with AIC_4, if none of the M1 models can reduce AIC from AIC_4, we continue to the Level 2 models, and so on. This comparative assessment comes to an end when we arrive at model structure that produces the smallest AIC.

Since interception and phenology are both vegetation effects, to reduce the number of models for presentational purposes (i.e., to obtain a clearer picture), we combine interception and phenology into a single category of "vegetation effects". In this way half of the model classes are eliminated, with only 8 remaining model groups. Figure 2.11 presents the results of this analysis, displaying regional patterns of needed model complexity.

One can see in Figure 2.11 that the base model is sufficient for the west coast catchments as well as the southeastern catchments in Florida (circles a, i) where the climate is humid and seasonality is strong. Consistent with what was found in the case of the dominant process for fast and slow flows (Figure 2.10), snowmelt is again found to be important in many northern catchments (circles b, c, d, e). Most of the northwestern mountainous catchments (circle b) need

the base model plus snowmelt only, although some indicate the need to include vegetation effects and also subsurface-influenced fast flow (presumably reflecting the presence of thin soils and substantial vegetation cover). Moving further east, both snow and vegetation effects are found to be necessary (circles c, d). This is again consistent with the dominant processes identified for fast and slow flow (Figure 2.10), where both phenology and snow were seen to be equally important. On the east coast (circle e), not only vegetation and snow, but also subsurface induced fast flow are found to be necessary (reflecting the occurrence of saturation excess streamflow). In southern catchments (circles h, f, g), snow is obviously not needed, but vegetation effects and subsurface influenced fast flow must be accounted for. In North Carolina (circle g), vegetation effects are seen as the only addition needed, while both vegetation and subsurface influenced fast flow are found to be needed in Georgia and Missouri (circle f).

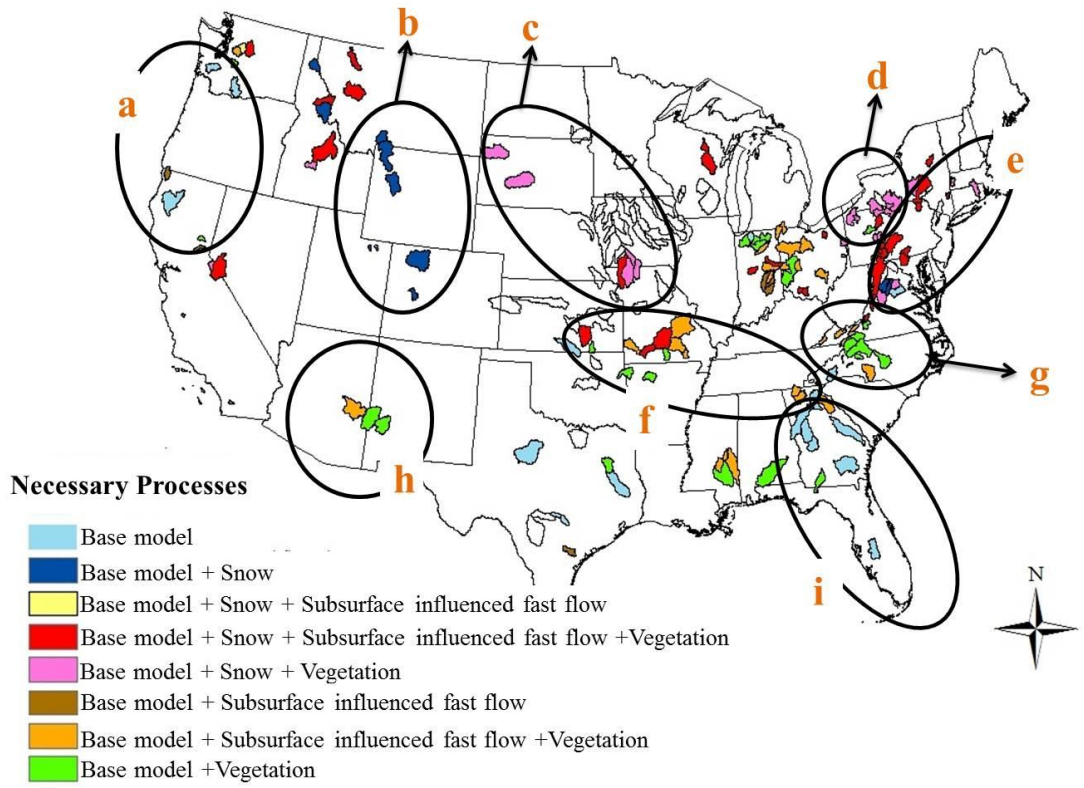

Figure 2.11: The needed process complexity for catchments that produced satisfactory simulation performance. The circled areas represent regions of process similarity.

2.4.5 Mapping the model process classes

The results from the model performance assessments presented in the previous sections, especially those presented in Figure 2.10 and Figure 2.11, can now be synthesized to develop broad classifications regarding dominant processes underpinning regional patterns of the variation of streamflow regimes across the continental United States. The results are presented in Figure 2.12, along with the cluster plot of the observed flow regime curves, to demonstrate this regional and functional hydrological similarity. Although these results must be looked at with some caution, considering that they are based on analysis of the 152 satisfactory catchments, the broad generalizations presented in Figure 2.12 can serve as the foundation or even motivation for further detailed data analyses and modeling investigations.

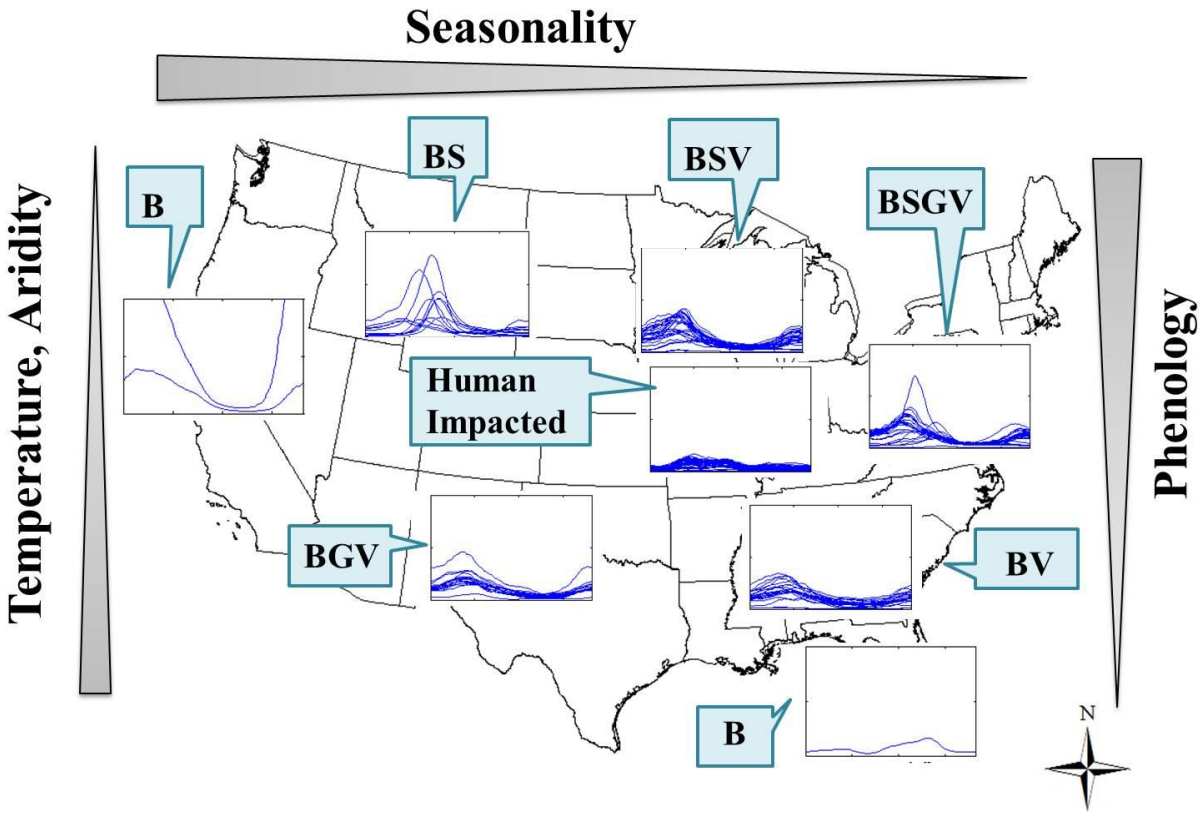

Figure 2.12: Conceptual map of the spatial distribution of the controlling processes and the regime curve clusters: "B" refer to the base model, "S" refers to snowmelt, "V" denotes vegetation impact (phenology and/or interception), "G" stands for subsurface influenced fast flow, and "Human impacted" means with strong anthropogenic activity impact.

The results shown in Figure 2.12 indicate, firstly, that the base model is sufficient to capture the regime curve in western and south-eastern catchments where seasonality dominates. In north-western mountainous catchments, such as in Idaho, the addition of snowmelt to the base model is sufficient to capture the shorter duration high flows occurring in late spring and early summer. Going west to east in the northern humid/cold regions, seasonality of precipitation decreases, vegetation cover becomes denser, and models must capture both snowmelt and vegetation effects, as well as the possibility of saturation excess overland flow. Moving north to south (in the east), the importance of snowmelt decreases, and only vegetation effects and saturation excess streamflow remain important. As one approaches Florida, once again the base model appears to be sufficient. As one moves east to west from Florida, catchments become drier, with much reduced streamflow, and prediction of regime behavior becomes increasingly difficult with simple lumped models, until one reaches Southern California, where again the base model appears sufficient due to the out-of-phase seasonality experienced there.

Figure 2.12 also summarizes the main drivers of the regional patterns of dominant processes and needed model complexity. In broad terms, seasonality increases east to west, while temperature and climate aridity increase north to south and phenology decreases north to south. There are exceptions to these trends as well. For example, the extreme south-east experiences strong seasonality, likely due in part to the influence of hurricanes as well as close proximity to two large bodies of water – the Gulf of Mexico and the Atlantic Ocean. Likewise, the north-west (e.g., Washington State) is warmer than would be expected for such northern latitudes. Additional features that are critical include the occurrence of precipitation as snow in northern latitudes, and vegetation cover dynamics (i.e., phenology) in the forested regions in the north-east and in the Appalachian region. The mid-west region proved difficult to model due to strong anthropogenic effects. One key factor that would be expected to have an impact on the regime behavior is topography, since it can potentially impact both subsurface drainage and saturation excess overland flow. However, this could not be conclusively assessed, due to the small number of catchments in key (e.g., mountainous) regions with which to carry out detailed comparative studies.

The flow regime curve clusters presented in Figure 2.12 suggest a regional and functional self-similarity, though with some variability due to the large numbers of catchments. Generally,

in western mountainous catchments with snowmelt dominance (BS), the flow regime curves tend to have a sharp peak in late spring and early summer. Moving east, the flow peak becomes wider and the duration much longer as vegetation effects and saturation excess flow comes into play (BSGV, BSV), but there is still an obvious rise in flow during spring. This rise disappears as we move south (BV) as the snow impact fades and the vegetation seasonal activity enhances the seasonality gently in the semi-humid and humid catchments. For the Midwestern catchments where the more sophisticated model is required (due to human impacts), the flow regime curves display more variance as well as a weak, dual-mode profile. The base model (B) performs well on the western coast and in Florida, but the flow profiles are completely different: in the west the flow is out of phase with potential evaporation while in the southeast it is in phase. Thus we can see that the seasonality of flow does share some similarity for catchments within the same model process class, and these model process classes do cluster geographically. However, there is still some variability in the flow regimes within a model process class, as illustrated by the western coast and the Florida catchments. A more detailed classification system, such as that developed by Coopersmith et al. (2012), may be needed to group catchments more accurately.

2.4.6 From Regime Curves to Flow Duration Curves

Our work on the regime curves was motivated ultimately by the quest to understand the physical and process controls of Flow Duration Curves (FDCs). We have already seen that the regime curve exhibits considerable variability across the continental United States. In order to illustrate the process controls on FDCs, we carried out model-based sensitivity analyses. Figure 2.13 presents the observed FDCs of total flow based on simulations with the complete model, as well as by four ”reduced” models in which one of the four processes from the complete model is removed, leaving only three processes. The parameter set, optimized for the full model, is applied to all five models.

We first compare the FDCs produced by the full model against those estimated from the observed record. Although the full model can predict the RCs reasonably well, the prediction of the FDC is not so good. This is to be expected since a model focused on predicting the regime curves only cannot be expected to predict well the high and low flows; therefore, the model needs to be further enhanced to achieve this.

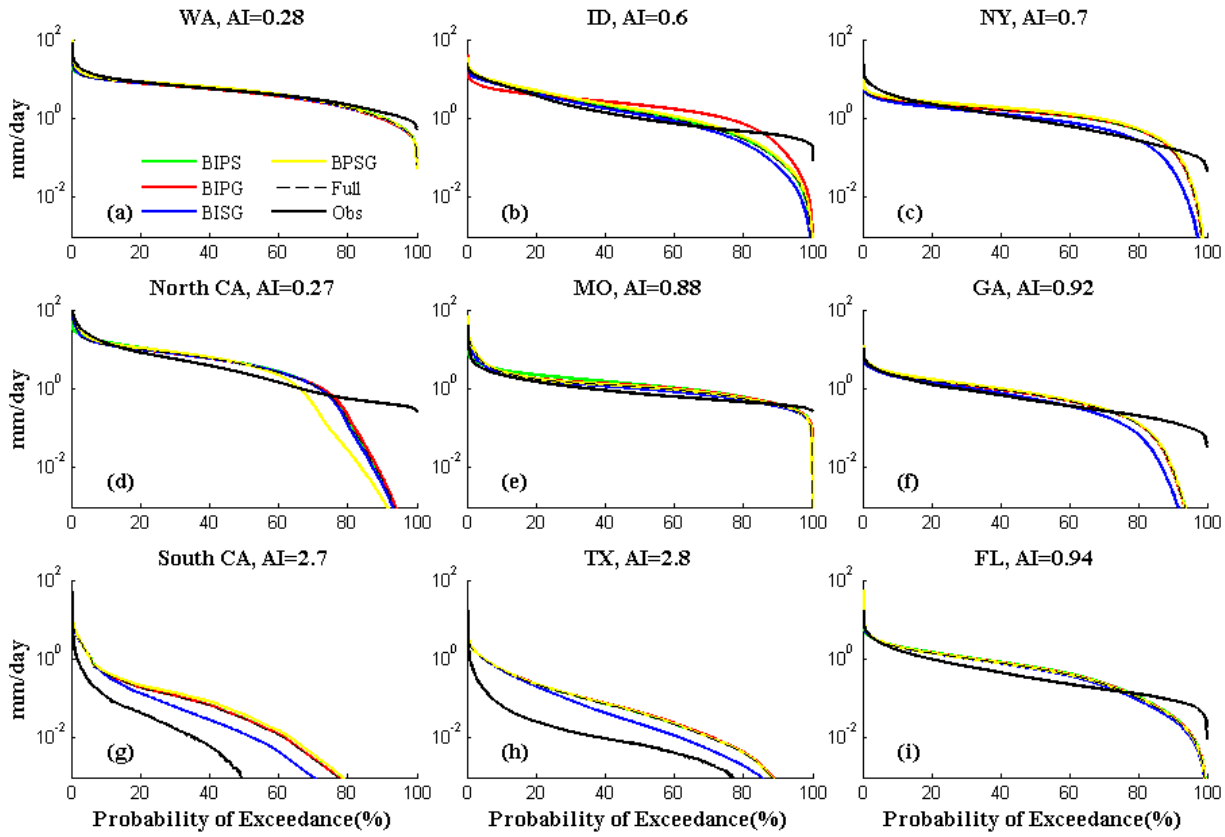

Figure 2.13: Flow duration curves of 9 selected catchments, B, I, P, S, G indicates the base model and four processes: interception, phenology, snowmelt, and subsurface influenced fast flow respectively. Thus, BIPS refers to the Level 3 model: base model with interception, phenology, and snowmelt.

The results also demonstrate that in some catchments (WA, MO, and FL) removal of a process does not have an obvious effect on the FDC. Conversely, for snowmelt dominated catchments such as the one in Idaho, the removal of snowmelt makes the FDC much flatter. This is consistent, given that snowmelt is the most important process addition in Idaho. On the other hand, in eastern catchments with dense vegetation cover (e.g., NY, GA), removal of phenology actually steepens the FDC. In dry catchments (Southern CA, TX), only the influence of phenology is recognizable, although we have learned from the regime curves that the other three processes are also important. Thus, differences in dominant processes can contribute to significant differences between the regime curves, which cannot be easily recognized in the

FDCs because of the strong influence of high flows and low flows. In general, because of the connection between the RC and the FDC, seasonality is present in the FDC, though not as obviously as in the RC, due to the loss of temporal information. While the time element is lost in the FDC, information on extreme values and frequencies, which are averaged out in the RC, is gained.

2.5 Discussion and Conclusions

The goal of this paper has been to identify the dominant processes underpinning streamflow regime behavior across the continental United States. For this reason, we analyzed rainfall-runoff data from 197 catchments belonging to the MOPEX dataset. The analyses involved a systematic process of model development following the downward approach (Sivapalan et al., 2003); starting with a simple base model, it is enhanced through the addition of key processes needed to reproduce the regime curve.

The resulting final (complete) model was then used to perform sensitivity studies to (a) decipher the most dominant process control, and (b) to determine the minimum model complexity needed to generate a satisfactory reproduction of the empirical regime curves. The sensitivity analyses were carried out in opposite directions. In one case, we started with the base model, and then increased model complexity by including additional processes one by one until we reached the final form of the model, all the while monitoring the improvement in model performance. In the other case, we start with the full model, and drop processes one by one until we arrive at the minimum model complexity needed to achieve satisfactory predictions.

The results revealed interesting regional patterns in the process controls of the regime curves across the continental United States, which is also related to Köppen's climate classification map. Snowmelt was found to be the most important process for modeling northwest catchments which falls in Köppen's snow steppe climate class (Dsa) for both fast and slow flows. However, it was not sufficient for slow flow prediction in cold, north-eastern catchments (the snow, fully humid, warm summer class (Dfb)), where the vegetation effects take over as most important due to the presence of significant forest cover. Vegetation effects and the role of rising water table are found to be significant for fast flow in the Appalachian and southern catchments. The requisite processes for modeling cold, mountainous forested catchments is

snowmelt; for cold, forested catchments near the east coast, however, they include both snowmelt and vegetation; the warm, humid catchments in the south-east with strong seasonality can be easily modeled with the simple base model (the warm temperate, fully humid, hot summer class (Cfa)), while the warm, very dry catchments in the south and south-west (Bsk: arid steppe cold arid) require much more complex models.

The reasons for the regional patterns of process controls of regime curves across the United States also became clear through these regional studies. The obvious reasons are seasonality (which increases east to west, with some exceptions), aridity (which increases north to south with some exceptions) as well as temperature (which increases north to south, again with exceptions due to effects of mountain topography, and proximity to oceans). As the seasonality increases from east to west, needed model complexity decreases (except in the mid-west due to human interferences); the same phenomenon is also observed as we go from south to north with the decrease in aridity; and importance of snowmelt increases from warm to cold catchments (south to north).

Despite the understanding gained regarding the process controls underpinning regional variations of regime curves, their impact on the shapes of FDCs has been found to be less strong. Two different processes that occur during different times of the year could have a significant effect on the shape of the regime curve, yet may not significantly affect the shape of the FDC. However, interesting regional patterns were seen in both the process controls on the regime curve determined here, and the empirically-determined parameters of the mixed gamma distribution as applied to the FDC determined in Cheng, et al. (2012). Sorting these catchments into classes may be a way to provide more explanatory power for these patterns and process controls, thus motivating the development of the classification scheme outlined in Coopersmith et al. (2012).

2.6 Acknowledgements

The work presented in this paper was carried out as part of the NSF-funded project ‘‘Water Cycle Dynamics in a Changing Environment: Advancing Hydrologic Science through Synthesis’’ (NSF grant EAR-0636043, M. Sivapalan, PI), and also the NSF project ‘‘Understanding the Hydrologic Implications of Landscape Structure and Climate—Toward a

Unifying Framework of Watershed Similarity'' (NSF Grant EAR-0635998, T. Wagener, PI). Special thanks are owed to Ciaran Harman and Sally Thompson for the support in the model development and to Matej Durcik of SAHRA (University of Arizona) for providing a version of the MOPEX dataset used in this study.

References

Akaike, H.: A new look at statistical model identification, IEEE T. Automat. Contr., AU-19, 716-722, 1974.

Bai, Y., Wagener, T., and Reed, P.: A top-down framework for watershed model evaluation and selection under uncertainty, *Environ. Modell. Softw*., 24(8), 901-916, doi:10.1016/j.envsoft.2008.12.012, 2009.

Beven, K. J.: Rainfall-runoff modelling, the primer. John Wiley & Sons: Chichester, UK, 2001.

Black, P. E.: Watershed Hydrology, 450 pp., CRC Press, Boca Raton, Fla, 1996.

Biondi, D., Freni, G., Iacobellis, V., Mascaro, G., Montanari, A.: Validation of hydrological models: Conceptual basis, methodological approaches and a proposal for a code of practice, *Phys. Chem. Earth*, 42-44, 70-76, doi:10.1016/j.pce.2011.07.037, 2012.

Brooks, P. D., Troch, P. A., Durcik, M., Gallo, E., and Schlegel, M.: Quantifying regional scale ecosystem response to changes in precipitation: Not all rain is created equal, *Water Resour. Res*., 47, W00J08, doi:10.1029/2010WR009762, 2011.

Calder, I. R..: Evaporation in the uplands. John Wiley & Sons: Chichester, UK, 1990.

Cheng, L., Yaeger, M., Coopersmith, E., Ye, Viglione, A. and Sivapalan, M.: Exploring the physical controls of regional patterns of Flow Duration Curves: 1. Insights from statistical analyses, *Hydrol. Earth Syst. Sci.*, 2012.

Coopersmith, E., Yaeger, M., Ye, S., Cheng, L. and Sivapalan, M.: Exploring the physical controls of regional patterns of Flow Duration Curves: 3. A catchment classification system based on seasonality and streamflow regime, *Hydrol. Earth Syst. Sci*., 2012.

Deguchi, A., Hattori, S., Park, H.: The influence of seasonal changes in canopy structure on interception loss: Application of the revised Gash model, *J. Hydrol*., 318, 80-102, 2006.

Dooge, J. C. I.: Looking for hydrologic laws, *Water Resour. Res*., 22(9): 46S–58S, 1986.

Eder, G., Sivapalan, M. and Nachtnebel, H. P.: Modelling water balances in an Alpine catchment through exploitation of emergent properties over changing time scales, *Hydrol. Process*., 17, 2125–2149, 2003.

Engelhardt, I., De Aguinaga, J. G., Mikat, H., Schuth, C., Lenz, O., and Liedl, R.: Complexity versus simplicity: an example of groundwater model ranking with the Akaike Information Criterion. *Hydrol. Earth Syst. Sci. Discuss*., 9, 9687-9714, 2012.

Falkenmark, M. and Chapman, T.: Comparative Hydrology: An Ecological Approach to Land and Water Resources, UNESCO, Paris. 310p, 1989.

Farmer, D., Sivapalan, M. and Jothityangkoon, C.: Climate, soil and vegetation controls upon the variability of water balance in temperate and semi-arid landscapes: Downward approach to hydrological prediction. *Water Resour. Res.*, 39(2), 1035, doi: 10.1029/2001WR000328, 2003.

Fernald, E. A. and Purdum, E. D.: Water Resources Atlas of Florida. Institute of Science and Public Affairs, Florida State University, Tallahassee, Florida. Atlas available at Marston Science Library, University of Florida, 1998.

Freer, J., Beven, K., and Ambroise, B.: Bayesian estimation of uncertainty in streamflow prediction and the value of data: An application of the GLUE approach, *Water Resour. Res.*, 32(7), 2161-2173, 1996.

Gupta, H. V., Kling, H., Yilmaz, K. K., and Martinez, F.: Decomposition of the mean squared error and NSE performance criteria: Implications from improving hydrological modeling, *J. Hydrol*., 377, 80-91, 2009.

Hamon, R. W., Weiss, L. L., and Wilson, W. T.: Insolation as an Empirical Function of Daily Sunshine Duration, *Monthly Weather Rev.*, 82 (6), 141-146, 1954.

Harman, C. J., Troch, P. A. and Sivapalan, M.: Functional model of water balance variability at the catchment scale: 2. Elasticity of fast and slow streamflow components to precipitation change in the continental United States, *Water Resour. Res.*, 47, W02523, doi:10.1029/2010WR009656, 2011.

Harte, J.: Toward a synthesis of the Newtonian and Darwinian worldviews, *Phys. Today*, 50 (10), 29– 34, 2002.

Hatfield, J.L., McMullen, L. D. and Jones, C. S.: Nitrate-nitrogen patterns in the Raccoon River Basin related to agricultural practices, *J. Soil Water Cons.*, 64, 190–199, doi: 10.2489/jswc.64.3.190, 2009.

Keim, R. F., Thromp-van Meerveld, H. J., McDonnell, J. J., A virtual experiment on the effects of evaporation and intensity smoothing by canopy interception on subsurface stormflow generation, *J. Hydrol.*, 327, 352-364, 2006.

Klemeš, V.: Conceptualization and scale in hydrology, *J. Hydrol*.,65, 1–23, 1983.

Jolly, W., Nemani, R. and Running, S.: A generalized bioclimatic index to predict foliar phenology in response to climate, *Global Change Biol.*, 11(4), 619–632, 2005.

Jothityangkoon, C., Sivapalan, M. and Farmer, D.: Process controls of water balance variability in a large semi-arid catchment: Downward approach to hydrological model development. *J. Hydrol*., 254(1-4), 174-198, 2001.

Kuczera, G., and Parent, E.: Monte Carlo assessment of parameter uncertainty in conceptual catchment models: The Metropolis algorithm, *J. Hydrol.*, 211(1– 4), 69– 85, doi:10.1016/S0022-1694(98) 00198-X, 1998.

Lana-Renault, N., Latron, J., Regues, D.: Stream response and water-table dynamics in a sub-Mediterranean research catchment (Central Pyrenees), *J. Hydrol.*, 347, 497-507, 2007.

Li, H., Sivapalan, M., Tian, F.: Comparative diagnostic analysis of streamflow generation processes in Oklahoma DMIP2 basins: The Blue River and the Illinois River, *J. Hydrol.*, 418-419, 90-109, doi: 10.1016/j.jhydrol.2010.08.005, 2011.

Liu, S.: A new model for the prediction of rainfall interception in forest canopies. *Ecol. Model.*, 99, 151–159, 1997.

Lyne, V., and Hollick, M.: Stochastic time-variable rainfall-runoff modelling, in Proceedings, Institute of Engineers Australia National Conference, Perth, 10-12 September 1979, Inst. Engrs., Canberra, Australia, ACT. Publ. 79/10: 89–93, 1979.

Marin, T.C., Bouten, W., Sevink, J.: Gross rainfall and its partitioning into throughfall, streamflow and evaporation of intercepted water in four forest ecosystems in western Amazonia. *J. Hydrol.*, 237, 40–57, 2000.

McDonnell, J. J., Sivapalan, M., Vaché, K., Dunn, S., Grant, G., Haggerty, R., Hinz, C., Hooper, R. P., Kirchner, J. W., Roderick, M. L., Selker, J. and Weiler, M.: Moving beyond heterogeneity and process complexity: A new vision for watershed hydrology. *Water Resour. Res.*, 43, W07301, doi: 10.1029/2006WR005467, 2007.

McGuire, K. J., McDonnell, J. J., Weiler, M., Kendall, C., McGlynn, B. L., Welker, J. M., and Seibert, J.: The role of topography on catchment-scale water residence time, *Water Resour. Res.*, 41, W05002, doi:10.1029/2004WR003657, 2005.

McIsaac, G. F., David, M. B., and Mitchell, C. A.: Miscanthus and switchgrass production in Central Illinois: impacts on hydrology and inorganic nitrogen leaching, *J. Environ. Qual*., 39, 1790-1799, 2010.

Merz, R. and Blöschl, G.: Regionalisation of catchment model parameters. *J. Hydrol.*, 287(1–4), 95–123, 2004.

Metropolis, N., Rosenbluth, A. W., Rosenbluth, M. N., Teller, A. H and Teller, E.: Equations of state calculations by fast computing machines, *J. Chem. Phys*., 21, 1087–1091, 1953.

NOAA Technical report NWS 33: Evaporation atlas for the contiguous 48 United States, Washington, D.C, 1982.

Opsahl, S. P., Chapal, S. E., Hicks, D. W., and Wheeler, C. K.: Evaluation of ground-water and surface-water exchanges using streamflow difference analyses, *J. Am. Water Resour. As*., 5, 1132-1141, 2007.

Patil, S. and Stieglitz, M.: Hydrologic similarity among catchments under variable flow conditions. *Hydrol. Earth Syst. Sci.*, 15, 989–997, 2011.

Penman, H. L.: Natural Evaporation from Open Water, Bare Soil and Grass, Proceedings of the Royal Society of London, Ser. A, Vol. 193, No. 1032, PP120-145 , April 1948.

Samuel, J. M., Sivapalan, M., and Struthers, I.: Diagnostic analysis of water balance variability: A comparative modeling study of catchments in Perth, Newcastle, and Darwin, Australia, *Water Resour. Res.*, 44, W06403, doi:10.1029/2007WR006694, 2008.

Savenije, H.H.G.: The importance of interception and why we should delete the term evapotranspiration, *Hydrol. Process*., 18, 1507–1512, 2004.

Sawicz, K., Wagener, T., Sivapalan, M., Troch, P. A. and Carrillo, G.: Catchment classification: Empirical analysis of hydrologic similarity based on catchment function in the Eastern USA, *Hydrol. Earth Syst. Sci.*, 15, 2895–2911, 2011.

Sivapalan, M., Blöschl, G., Zhang, L. and Vertessy, R.: Downward approach to hydrological prediction. *Hydrol. Process*., 17, 2101-2111, doi: 10.1002/hyp.1425, 2003.

Sivapalan, M.: Pattern, process and function: Elements of a new unified hydrologic theory at the catchment scale, in: Encyclopaedia of Hydrologic Sciences, 1(1), M. G. Anderson (Editor), Chap. 13, pp. 193-219, J. Wiley, Hoboken, N. J., 2005.

Sivapalan, M.: The secret to "doing better hydrological science": Change the question! *Hydrol. Process*., 23, 1391–1396, doi: 10.1002/hyp.7242, 2009.

Sivapalan, M., Thompson, S. E., Harman, C. J., Basu, N. B. and Kumar, P.: Water cycle dynamics in a changing environment: Improving predictability through synthesis. *Water Resour. Res.*, 47, W00J01, doi:10.1029/2011WR011377, 2011.

Thompson, S.E., Harman, C. J., Konings, A. G., Sivapalan, M., Neal, A. and Troch, P. A.: Comparative hydrology across Ameriux sites: the variable roles of climate, vegetation and groundwater, *Water. Resour. Res.*, W00J07, doi: 10.1029/2010WR009797, 2011.

Troch, P. A., Martinez, G. F., Pauwels, V. R. N., Durcik, M., Sivapalan, M., Harman, C., Brooks, P. D., Gupta, H., and Huxman, T.: Climate and vegetation water use efficiency at catchment scales, *Hydrol. Processes*, 23(16), 2409–2414, doi:10.1002/hyp.7358, 2009.

Wagener, T., Sivapalan, M., Troch, P. A. and Woods, R. A.: Catchment classification and hydrologic similarity. *Geog. Comp*., 1/4, 901-931, 10.1111/j.1749-8198.2007.00039.x, 2007.

Yaeger, M., Coopersmith, E., Ye, S., Chang, L. and Sivapalan, M.: Exploring the physical controls of regional patterns of Flow Duration Curves: 4. A synthesis of empirical analysis, process modeling and catchment classification, *Hydrol. Earth Syst. Sci.*, in review, 2012.

Yokoo, Y. and Sivapalan, M.: Toward construction of flow duration curves in ungauged basins: Flow duration curve separation and sensitivity to watershed characteristics, *Hydrol. Earth Syst. Sci.*, 15, 2805–2819, 2011.

Zucker L.A. and Brown, L. C.: Agricultural Drainage: Water Quality Impacts and Subsurface Drainage Studies in the Midwest. Ohio State University Extension Bulletin 871, the Ohio State University, Columbus, USA, 1998.

Chapter 3

Subsurface Stormflow Parameterization for Land Surface Models: Derivation from Regional Analysis of Streamflow Recession Curves

Abstract[1]

Subsurface stormflow is an important component of the rainfall-runoff response, especially in steep terrain. However; its contribution to total runoff is poorly represented in current generation of land surface models. The lack of physical basis of their common parameterizations precludes a priori estimation (i.e. without calibration), which is a major drawback for prediction in ungauged basins, or for use in global models. This paper is aimed at deriving regionalized parameterizations of the storage-discharge relationship relating to subsurface stormflow from a top-down empirical data analysis of streamflow recession curves extracted from 50 eastern United States catchments. Detailed regression analyses were performed between parameters of the empirical storage-discharge relationships and the controlling climate, soil and topographic characteristics. The regression analyses performed on empirical recession curves at catchment scale indicated that the coefficient of the power-law form storage-discharge relationship is closely related to the catchment hydrologic characteristics, which is consistent with the hydraulic theory derived mainly at hillslope scale. As for the exponent, besides the role of field scale soil hydraulic properties as suggested by hydraulic theory, it is found to be more strongly affected by climate (aridity) at the catchment scale. At a fundamental level these results point to the need for more detailed exploration of the co-dependence and co-evolution of climate, soil, vegetation and topography.

---

[1]This work has been submitted for publication to Journal of Hydrology as: Ye, S., H-Y. Li, M. Huang, M. Ali, G. Leng, L. R. Leung, S-W. Wang, and M. Sivapalan, Subsurface Stormflow Parameterization for Land Surface Models: Derivation from Regional Analysis of Streamflow Recession Curves. All figures, tables and data were created by Sheng Ye unless otherwise indicated.

3.1 Introduction

Land surface processes are an integral part of the Earth system. By regulating surface moisture and heat fluxes, land surface processes can provide important feedbacks to climate and influence the regional and global hydrologic cycle (e.g., Koster et al., 2004; Seneviratne et al., 2010). To improve predictions of future climate, it is crucial to understand and constrain uncertainty stemming from parameterizations used in land surface models (LSMs). Recently Hou et al. (2012) and Huang et al. (2013) used an uncertainty quantification framework to assess hydrologic parameter uncertainties in Version 4 of the Community Land Model (CLM4) (Lawrence et al. 2011). Applying their framework to 13 flux towers and 20 catchments across the U.S. spanning a wide range of climate and landscape characteristics, they found that the simulated land surface water and energy fluxes as well as runoff showed the largest sensitivity to parameters related to subsurface runoff generation (Niu et al., 2005; 2007). This highlights the need to improve subsurface runoff generation schemes in LSMs.

As shown by several previous studies, subsurface runoff generation can be parameterized using storage-discharge relationships of a power law form, which can capture the asymmetric response of subsurface hydrologic processes to floods and droughts (e.g., Eltahir and Yeh, 1999; Liang et al., 2003). Such parameterizations, including the TOPMODEL approach (Beven and Kirby, 1979, Beven et al. 1984; Beven, 1997) used in CLM4 and the ARNO model (Francini and Pacciani, 1991; Todini, 1996), are now widely used in LSMs (e.g., Liang et al., 1994; Huang and Liang, 2006; Warrach et al., 2002; Niu et al., 2005; 2007; Oleson et al., 2010; 2013; Ringeval et al., 2012), although each approach still suffers from limitations and can be further improved. Recent reviews on the advantages and disadvantages of these parameterizations can be found in Huang and Liang (2006), Huang et al. (2008), and Li et al. (2011). A particular challenge in applying these parameterizations in Earth system models is the limited availability of naturalized streamflow data for calibrating model parameters globally, and reducing the dependence of parameterizations on calibrations is a key requirement. This is the first of a two-part paper (the other being Ali et al., 2013) that aims towards developing improved parameterizations of shallow subsurface flow for land surface models such as CLM4, expressed in terms of the power-law form of a lumped storage-discharge relationship:

$$Q = aS^b \qquad (1)$$

where Q is subsurface flow and S is saturated subsurface storage, both at the catchment scale, and a and b are parameters that represent the effects of land surface heterogeneity (i.e., of both soil hydraulic properties and topography). Ideally, for subsurface flow to be predicted using Eq (1) without calibration (e.g., in ungauged basins or landscapes), the parameters a and b must be estimated *a priori* on the basis of measurable landscape characteristics. Such a parameterization of the subsurface flow must capture the effects of soil and landscape properties in a simple way, accounting for the effects of spatial heterogeneity without the need to resolve flows at smaller scales explicitly. This is the motivation for the work behind this paper. We have approached this estimation problem from two alternative perspectives: (i) empirical (top-down), and (ii) theoretical (bottom-up).

The theoretical (or bottom-up) approach (see accompanying paper by Ali et al., 2013) involves the use of numerical simulations that help to derive closure relations through application of detailed, distributed physically based hydrological models using appropriate boundary conditions and assumed forms of spatial variability of soil and topographic properties (Robinson and Sivapalan, 1995; Viney and Sivapalan, 2004). We categorize the spatial heterogeneities entering the problem here as (i) within hillslope, where the heterogeneity is assumed to relate to soil only, and topography is taken to be fixed, and (ii) between hillslopes, where the heterogeneity arising from topography is explicitly resolved, while the effects of within-hillslope heterogeneity of soil properties is parameterized from (i). The theoretical approach of Ali et al. (2013) is based on Richards equation based simulations at the hillslope scale, parameterizing the effects of within-hillslope heterogeneity and their subsequent up-scaling to the catchment scale, incorporating the effects of topographic variability between hilslopes.

The empirical (or top-down) approach (the subject of this paper) involves (i) making inferences of the storage-discharge relationships, and associated parameters a and b, directly at the catchment scale on the basis of analysis of observed streamflow recession curves in a large number of catchments, followed by (ii) multiple regression analyses of the estimated recession

parameters a and b against measurable climatic and landscape (soils and topography) characteristics.

The streamflow recession curve (Brutsaert and Nieber, 1977) is one of the most widely used catchment runoff signatures, and provides insights into the subsurface flow generation processes (Tague and Grant, 2004). It measures how river flow recedes at the end of a storm event, and is therefore a holistic measure of the catchment's drainage characteristics. For convenience, the recession behavior of the catchment is often expressed in terms of the so-called recession-slope curve, the relationship between the rate of decline rate of flow ($-dQ/dt$) and Q:

$$-\frac{dQ}{dt} = \alpha Q^{\beta} \qquad (2)$$

which is often found to remain invariant and thus represents a unique signature of the catchment response. The coefficient α and exponent β can be directly estimated from observed recession curves by curve fitting, and reflect the net effects of the population of hillslopes (of various sizes and shapes) and the soils that constitute the catchment.

Considerable work has been carried out to derive analytical solutions to the Boussinesq equation governing saturated subsurface drainage from an unconfined homogeneous aquifer into the river below to aid the deciphering of the physical meaning and controls of both recession parameters α and β. Several studies have explored the effects of catchment-scale heterogeneity on the shape of the recession curves. These theoretical studies suggest that the shapes of the recession curves are strongly affected by soil hydraulic conductivity and its vertical and horizontal (downslope) heterogeneity (Rupp and Selker, 2005; Rupp and Selker, 2006; Troch et al., 2008; Harman et al., 2009). Landscape geomorphologic features too can contribute to the shape of the recession curves (Biswal and Marani, 2010; Harman et al., 2009; Lyon and Troch, 2010). However, due to the many simplifying assumptions and lack of data, most of the pioneering studies in this area have been largely theoretical, and only a few went further and validated the equations derived on the basis of the recession curves in real catchments (Harman et al., 2009; Lyon and Troch, 2010).

The storage-discharge (closure) relationship that we are interested in can be derived from the recession-slope curve in a straightforward manner by utilizing the relationship that exists

between parameters a and b of the storage-discharge relationship and the parameters α and β of the recession-slope curve, which can be derived in a straightforward manner by combining equations (1) and (2):

$$a = [\alpha(2-\beta)]^{1/(2-\beta)} \quad (3a)$$

$$b = \frac{1}{2-\beta} \quad (3b)$$

In this study, we explore the nature of the storage-discharge relationship and its controls through empirical analysis of the recession curve data from hundreds of catchments across the continental United States, and their connection to measureable catchment characteristics such as topography, soil properties, and other geomorphologic features.

The theoretical (or bottom-up) approach will follow in the second paper of the series (Ali et al., 2013), which can yield results that are physically consistent, but their applicability in actual catchments is hampered by our inability to fully characterize the heterogeneity of soils (and even some aspects of topography) present in actual catchments, including especially the self-organized heterogeneity that is often present, such as soil catena, and the presence of macro-pores and other preferred pathways, whose effects on flow are difficult to characterize in terms of the Richards equation. On the other hand, empirical relationships extracted from observed recession curves, such as those presented in this paper, are much more realistic in terms of what may emerge at the catchment scale, but are empirical rather than physics-based, which makes them difficult to interpret physically and to extrapolate from gauged to ungauged basins. Success in our quest for physically based closure relations for subsurface flow will come only through a reconciliation of the outcomes of both the empirical (top-down) and theoretical (bottom-up) approaches. This will be pursued in subsequent research, and may be the subject of a future publication.

This paper, which presents the outcomes of the empirical (top-down) approach, begins with a summary of the data (climate and streamflow data, and detailed information on catchment characteristics) presented in Section 2 that also describes the methodology that is used to extract the coefficient and exponent from the recession curves. Section 3 presents the spatial (regional) distribution of the parameters α and β across the continental US, and their interpretation. This is

followed, in Section 4, by a variable selection scheme that is used to define the most important climate and catchment characteristics that determine the observed recession behaviors, along with the validation of the so-derived empirical relationships. Section 5 summarizes the main outcomes of the study, their connection to the results of the modeling work (Ali et al., 2013), and possible avenues towards synthesis.

3.2 Data and Methodology

3.2.1 Data

This study is carried out with the climate and flow data and topographic information taken from the Model Parameter Estimation Experiment (MOPEX) dataset, drainage density data extracted from the National Hydrography Dataset (NHD) (http://nhd.usgs.gov/), and soil properties from the USGS SSURGO dataset (http://soils.usda.gov/survey/geography/ssurgo/). The MOPEX dataset (http://www.nws.noaa.gov/oh/mopex/index.html) provides daily climate and streamflow data from 438 catchments across the continental US, covering a wide range of climate conditions, landscapes, and ecosystems, ranging from very humid environments on the north-west coast (Aridity Index = 0.25) to extremely arid conditions in New Mexico (Aridity Index = 5.5). Aridity Index (AI) is defined as the ratio of mean annual potential evaporation to mean annual precipitation. The MOPEX dataset includes catchments of different drainage areas, ranging from 66 km^2 to 10,328 km^2, consisting of very flat to very steep (10%) hillslopes, permitting the derivation of recession curves for a wide range of catchment conditions. Of the 438 catchments, 428 catchments with longer than 10 years of continuous historical data are used in this study to estimate the recession curve parameters α and β.

Subsequently, a subset of 50 of these MOPEX catchments are selected to generate regional relationships between the recession curve parameters and several measureable climatic and landscape characteristics. These catchments were chosen under the following criteria to minimize the influence from other confounding factors: reasonable number of flow events, minimal impact of regional groundwater and/or snowmelt, minimal human impact and maximum data availability. We avoided the extreme arid catchments in the south-west (e.g., Arizona, Texas) as there tend to be fewer than ten flow events during the record period, and some of the events are too small to perform recession analysis. Mountainous catchments with significant snowmelt

influence (i.e., ID, WY, etc.) were also excluded, since these tend to have just a single big event that occurs each year in late spring or early summer caused by snowmelt (Ye et al., 2012). Likewise, although most MOPEX catchments have limited human influence, considerable human activities such as agriculture are still present in several Mid-western catchments (Wang and Hejazi, 2011). In the presence of artificial water extraction (Hatfield et al., 2009) and tile drainage (Li et al., 2010), the recession parameters derived from data are not representative of the natural storage-discharge relationships. Furthermore, since the soil dataset we used (i.e., SSURGO) has not been extended to fully cover the western states (i.e., WA, CA), in this study, we will focus only on the eastern catchments with sufficient number of flow events in a year and with minimal influence of processes other than subsurface stormflow generation. Figure 3.1 depicts the 50 catchments selected, which are devoid of such obvious data problems. General information on the selected catchments is provided in Table 3.1.

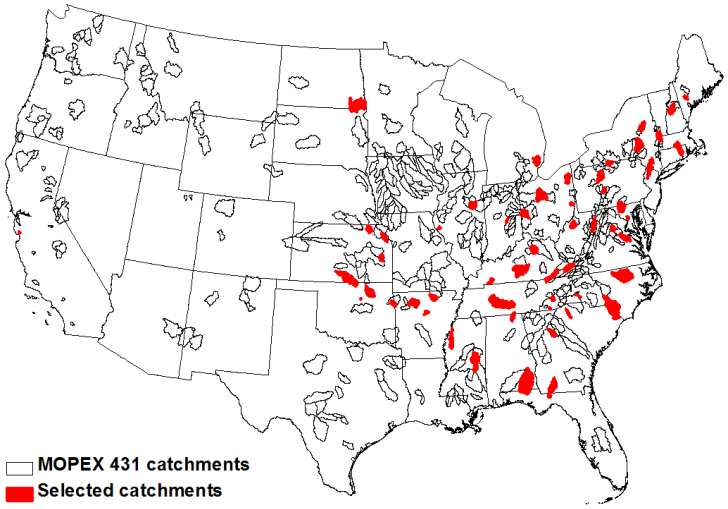

Figure 3.1: Map of the selected catchments

For this purpose the Aridity Index, topographic slope, the mean and standard deviation of saturated hydraulic conductivity at the surface, the vertical (exponential) decay parameter of the saturated hydraulic conductivity, soil porosity, soil depth and drainage density were all estimated for the selected catchments. The drainage density was estimated from the NHD dataset as the ratio of the total channel length within a catchment to the catchment area. Although the MOPEX dataset also provides estimates of saturated hydraulic conductivity, it was an earlier qualitative

estimate based on soil texture, and the resolution was deemed too coarse for this study. Therefore, we used the USGS SSURGO dataset (http://soildatamart.nrcs.usda.gov) to extract the mean and standard deviation of the saturated hydraulic conductivity at the surface and also a vertical exponential decay parameter. The SSURGO dataset is provided by the National Resource Conservation Service (NRCS); it includes both spatial data of the measured map unit, and tabular data of the measurements done within each map unit. Although the coverage of the SSURGO dataset is not as wide as the earlier version of the USGS State Soil Geographic (STATSGO) soils data, we chose to use the SSURGO dataset for this study due to its higher resolution and better data quality. The STATSGO dataset was generated for multi-state, regional, and state level analysis, with the map scale compiled at a scale of 1:250,000, while the SSURGO dataset is compiled at the scales of 1:12,000 and 1:24,000. That is, the resolution of the SSURGO dataset is about 10 times higher than the STASGO dataset (Earls and Dixon, 2005; Bliss et al., 2010). The quality of soil databases is also higher in the SSURGO dataset as the result of the NRCS efforts (Bliss et al., 2010) to provide more precise and detailed spatial and vertical measurements (Anderson et al., 2006). As we will learn from the results, the soil hydraulic properties play a critical role in the subsurface flow generation process, and the SSURGO dataset fits our interest better despite of the more limited coverage.

Table 3.1: Characteristics of the 50 selected catchments

	Min	Mean	Max
α	1.40	2.37	3.84
β	0.99	1.46	1.91
Area(km^2)	66.60	1731.02	9062.40
AI	0.39	0.82	1.5
Slope (degree)	0.41	5.72	22.84
K_s (um/s)	2.5	18.70	74.60
Std. Dev of K_{sat}	1.27	12.13	31.88
Drainage density (km/km^2)	0.04	0.62	1.91
Depth x Porosity (m)	0.18	0.48	0.70
f parameter (m^{-1})	0.11	0.81	2.36

3.2.2 Methodology

3.2.2.1 Data processing

The recession periods in the continuous multi-year hydrographs were extracted by an automatic algorithm developed by Vogel and Kroll (1992). Based on the 3-day moving average of a hydrograph, the falling limb is defined as the segment between each pair of peaks and valleys. To avoid the influence of overland flow, only the late 70% of a falling limb was recorded as a recession period. We adopted Vogel and Kroll's (1992) algorithm for the recession period selection instead of that used by Brutsaert and Nieber (1977), who defined recessions as flow periods when the rainfall ends, because along the east coast of the United States (e.g., NY, VA, MA, etc.) rainfall happens all year round. Given the relatively coarse temporal resolution (daily time scale), it is hard to retrieve recession curves long enough without interruption by subsequent rainfall events to give meaningful regression results. To remove possible noise from small events and fluctuations in big events, only recession periods longer than 10 days were selected, and also recessions with peak flows less than the 10^{th} percentile were excluded. Figure 3.2 shows an example of recession periods identified using our criteria.

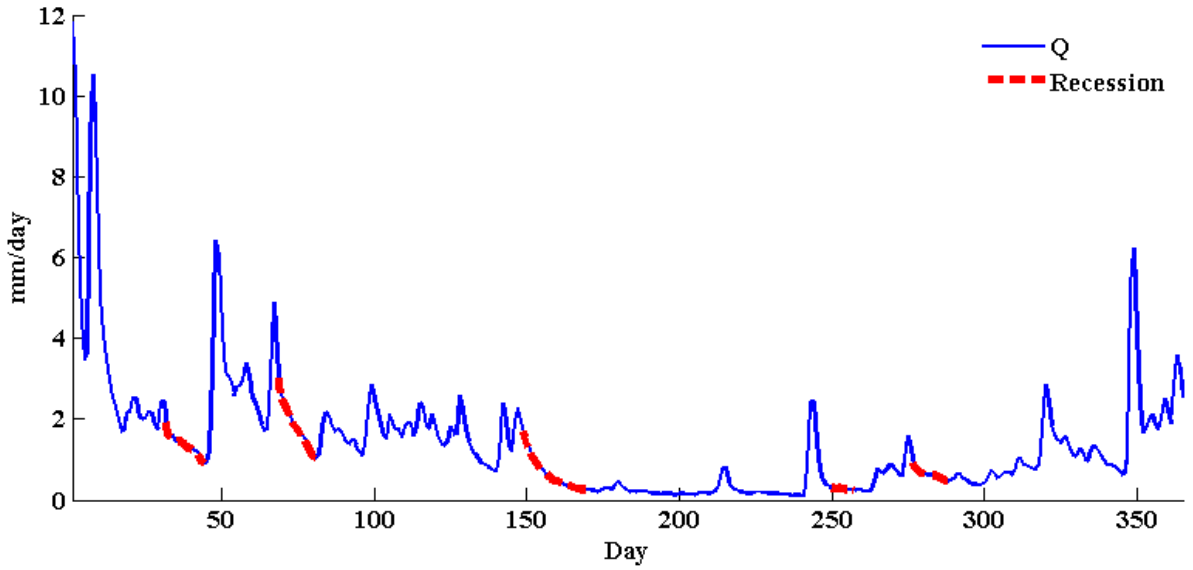

Figure 3.2: Automatic separation of the recession periods. α and β are estimated for the recessions that occur during winter when the ET impact is smallest.

Taking the natural logarithm of equation (2), we then have the linear relationship:

$$\ln(-\frac{dQ}{dt}) = \ln\alpha + \beta \ln Q \qquad (4)$$

This relationship is used to fit the extracted recession curve data as:

$$\ln(Q_{t-1} - Q_t) = \ln\alpha + \beta \ln(\frac{Q_t + Q_{t+1}}{2}) \qquad (5)$$

where t is the tth day of a recession record, Q_{t-1}, Q_t, Q_{t+1} are the flow over three consecutive days. Initial evaluation of α and β values showed significant seasonal variation in several regions, due to the drying effects of evapotranspiration (ET), which is usually highly seasonally dependent. Therefore, as a way to minimize the influence of the unknown ET, in this study we used the α and β values extracted from recessions occurring during winter (December, January and February) only, when ET is deemed the lowest.

The Aridity Index (=PET/P based on mean annual estimates) was calculated from annual precipitation (P) and annual potential evapotranspiration (PET) data from the MOPEX dataset. The same was done for average topographic slope and soil porosity, which are provided in the MOPEX dataset. Drainage density (=L/A) was estimated from the stream length (L) and drainage area (A) extracted from NHD dataset.

The SSURGO data was downloaded as feature dataset by county. For this study, we needed the soil data at the catchment scale in a raster format so as to calculate the standard deviation. A procedure was developed to merge the SSURGO data, clip the data by the catchment boundary, retrieve the soil porosity (ϕ), which can be used to describe the soil water storage capacity when combined with soil depth (ϕd), saturated hydraulic conductivity at the top and bottom layer as well as the vertically averaged value for each map unit, and then convert the data to raster data type. These reconstructed raster data with the average porosity or saturated hydraulic conductivity at the surface were then used to compute the spatial average hydraulic conductivity value and its standard deviation.

We assumed that the saturated hydraulic conductivity decreases exponentially with depth:

$$K_b = K_s \exp(-fd) \qquad (6)$$

where K_s, K_b are the surface and bottom saturated hydraulic conductivity, f is the decay parameter, and d is the soil depth. Each of these parameters is highly variable in space, including the exponential decay parameter, f. In order to obtain a more robust estimate of f at the catchment scale, we estimated spatial (arithmetic) averages of both surface and bottom saturated hydraulic conductivity values using available point values, as well as the spatial average of their vertical mean, and a spatially average depth. Then it can be shown that the vertical decay parameter can be obtained from:

$$f = \frac{\overline{K}_s - \overline{K}_b}{\overline{K}.\overline{d}} \qquad (7)$$

where $\overline{K}_s$ is the spatially averaged surface saturated hydraulic conductivity, $\overline{K}_d$ is the spatially averaged bottom saturated hydraulic conductivity, $\overline{K}$ is the spatial average of the vertical mean saturated hydraulic conductivity, $\overline{d}$ is the spatial average of the surveyed soil depth. Clearly, this is only an approximate estimate of the exponential decay parameter, yet this is the best that can be achieved at such large scale, given the paucity of datasets currently available.

3.2.2.2 Parameter regionalization: variable selection procedure

Several recent studies have attempted to understand how soil properties and topographic and geomorphologic characteristics control subsurface flow generation in a quantitative way (Rupp and Selker, 2006; Troch et al., 2008; Biswal and Marani, 2010). Estimated values of α and β in their original or logarithmic forms were first plotted against all the candidate predictors to derive individual relationships between the predictors and α and β. Although not all the relationships for the recession coefficient and exponent would be statistically significant, they provide information for down-selecting the predictors. In this paper, to determine the most influential factors, we experimented with different forms of the predictor and the response using linear regressions. Both α and β obtained from winter recessions and their natural logarithmic forms were used as the response in the linear regression, while all parameters including AI, slope, drainage density, porosity, soil depth, mean, standard deviation and vertical decay parameter of saturated hydraulic conductivity, and others, and their natural logarithmic forms were used as

candidate predictors. A variable selection scheme was developed to eliminate redundant or insignificant predictors.

Due to the limited sample size, cross validation was employed to improve the reliability of the final selected regression model. That is, 75% of the data were randomly selected as training data used to fit the model and for the variable selection. After the selection, the remaining 25% of the data were used to validate the model selection results (Figure 3.3). This cross-validation was conducted 50 times on average in order to reduce the potential bias in the sample selection (we repeated this three times and obtained similar results). The predictors retained by the model selection criteria and the R^2 of the validation in the test data were recorded each time. Finally, an averaged R^2 over all 50 validation tests is calculated and the frequency for each predictor chosen by the different criteria was also recorded. The predictors that were retained most often in all three methods were considered the most influential factors in predicting α and β derived from the recession curves.

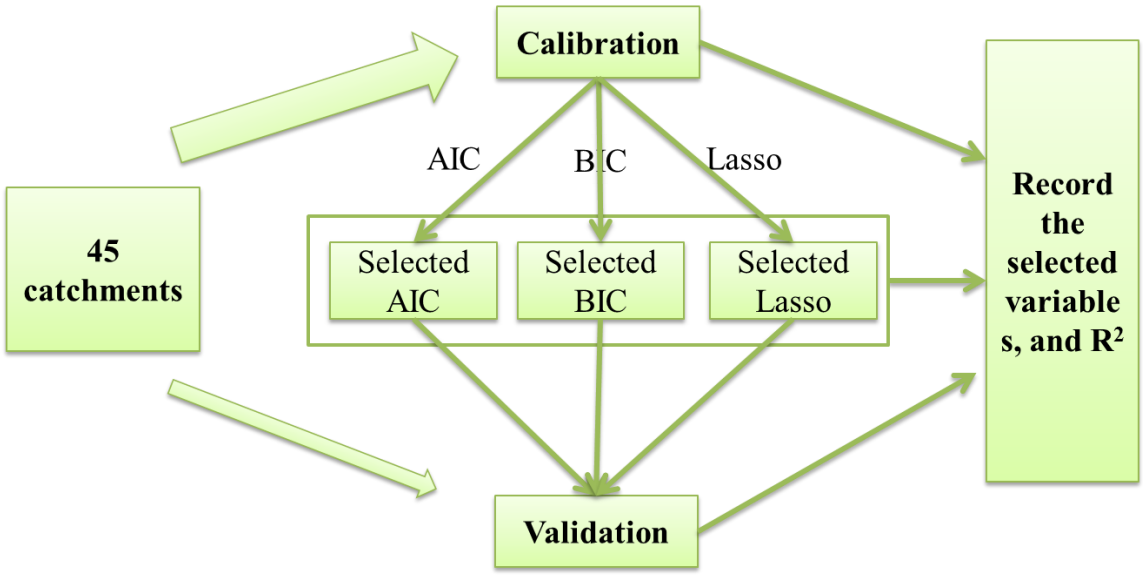

Figure 3.3: Flow chart of the variable selection process

Three statistical criteria were used in the variable selection: the Akaike Information Criterion (AIC), the Bayesian Information Criterion (BIC), and the *least absolute shrinkage and selection operator* (LASSO). The AIC is a statistical metric used in model selection, with a penalty term

for increase in model size (2*k*), to choose the most suitable model with the least information loss (Akaike, 1974). It has also been applied to assess the necessary model complexity to get the required quality of model predictions (Engelhardt et al., 2012). For linear regression models, it can be computed as follows:

$$AIC = -2\ln(\,Likelihood\,) + 2k = n\ln\frac{\sum(\hat{y} - \bar{y})^2}{n} + 2k \qquad (8)$$

where n is the sample size (=50 here) and k is the number of predictors used in each model, $\hat{y}$ is the value of the response (i.e. α or β or their logarithmic forms) predicted by the fitted linear regression model, while $\bar{y}$ is the mean of the sample response. BIC is also a model selection criterion based on the likelihood function (Schwarz, 1978). Like AIC, it also has a penalty term for the increase in model size, but is larger than AIC ($k\ln(n)$):

$$BIC = -2\ln(Likelihood) + k\ln(n) = n\ln\frac{\sum(\hat{y} - \bar{y})^2}{n} + k\ln(n) \qquad (9)$$

Both AIC and BIC select a subset of the candidate predictors. The variables are either retained or removed. This is a discrete process, which often leads to high variances and does not help reduce the error in the full model. The class of methods called shrinkage methods are more continuous and could avoid the high variability in AIC and BIC by estimating the regression coefficients that minimize the penalized residual sum of squares. LASSO is one of the shrinkage methods that do both shrinkage and variable selection by selecting those variables that minimize the following objective function (Hastie et al., 2009):

$$\| y - \hat{y} \|^2 + \lambda \sum | \omega_j | \qquad (10)$$

where $\hat{y}$ is the value of the response (i.e. α, β or their logarithmic forms) predicted by the fitted linear regression model, y is the observed value of the sample response, λ is the coefficient to be optimized, ω_j is the coefficient of each predictors. A large λ will force some of the coefficients to be zero, which is part of the variable selection process. As a result, AIC is more focused on minimizing the prediction error, which favors larger models. BIC, in contrast, tends to select

smaller models as it imposes larger penalty on the model size, while LASSO helps minimize the variance and is more consistent in selecting the models (Hastie et al., 2009). In this study, we tested all three methods, counted the times different predictors were selected by each method in the 50 tests, calculated the frequency they were selected by different methods, and lastly finalized a set of predictors that were more often retained than removed (that is, the frequency each predictor was chosen must be larger than 50%) in all three methods.

3.3 Results

3.3.1 The spatial patterns of α, β

Before we take a closer look at the 50 selected catchments, we look at the regional patterns of the regressed α, β values from the recession curves of all 428 catchments estimated from winter recessions to see if we can gain any insight into what could explain these patterns. These are presented in Figure 3.4. Finding common catchment characteristics with similar ranges of α, β may provide clues about factors that may be relevant.

It is noted that α has a larger range than β, although most of them fall in the interval between 2 to 4. As we can see from the figure, α is generally larger along the eastern and western coasts as well as the upper Midwest where climate is more humid, smaller in catchments in or near the Appalachian Mountain, and is even smaller in the semi-arid and high mountain regions of the west (NM, ID, AZ, etc.). There are some exceptions, e.g., in Texas, where some arid catchments also have large α values: this could be related to uncertainties in the model fitting and selection processes due to the ephemeral streams that limit the number of observations available from the 10 years record used for deriving the recession periods.

Figure 3.4b illustrates the regional pattern of β, which exhibits a more diverse pattern. Roughly there is a decreasing trend in β from the coastal regions towards the interior. Specifically, β is around 2 in the catchments along the east coast except for those in Florida, it drops to values less than 1.5 in catchments in the central US. In the mid-western and western mountainous catchments, as well as in catchments in the arid southern US, β is around 1. Its value again increases to over 1.5 in catchments along the west coast. Looking at this in another way, β is large in humid and steep catchments near the Appalachian mountain as well as along

the western coastal range, but is small in extremely arid catchments in the south (i.e. NM, AZ, TX, etc.) and topographically flat catchments in the Midwest. An exception is that β is small in the coastal mountainous catchments in the West, which are humid as well as steep. This could be caused by poor data quality as those catchments are dominated by a single flow event per year, driven heavily by snowmelt. The significant snowmelt overwhelms the contribution from subsurface flow, leading to unreliable estimates of α and β.

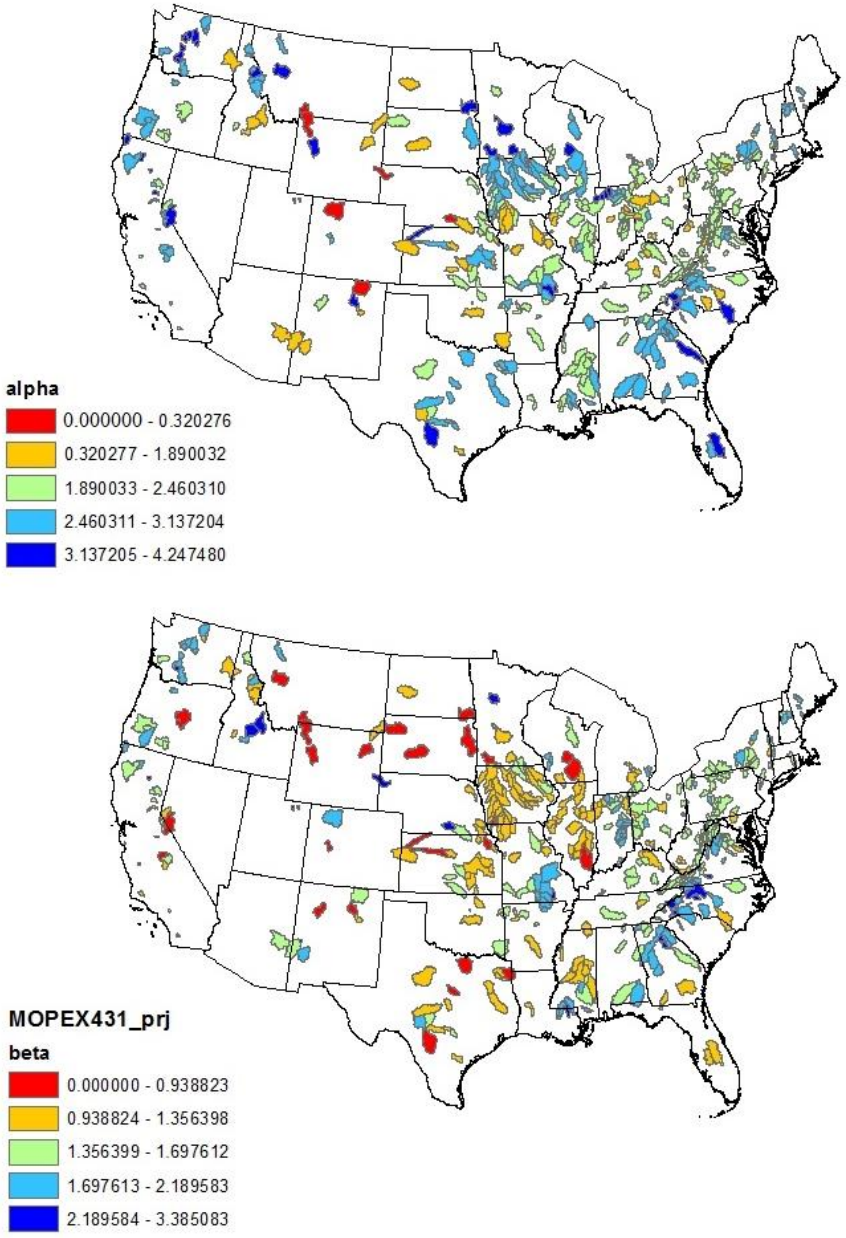

Figure 3.4: Spatial distribution of α and β.

3.3.2 Variable selection results

Figure 3.5 presents the initial scatter plots of possible relationships between α and β and various climatic, geomorphologic and soil hydraulic properties for the 50 selected catchments: aridity index *AI*, the drainage area, topographic slope, θ, drainage density, D_p, soil water storage capacity, ϕd, mean and standard deviation of surface saturated hydraulic conductivity (i.e., *Ks*, σ_{Ks}) and the vertical exponential rate of decay saturated hydraulic conductivity, *f*. Although these candidate variables individually do not explain much of the variances in α, β (i.e., $R^2 < 0.5$), many of them do have significant relationships with α and β (i.e., *p*-value < 1%). As seen from Figures 3.5 and 3.6, the aridity index and topographic slope are closely related to both α and β, while α is also related to drainage density and the mean and standard deviation of surface saturated hydraulic conductivity (K_s, σ_{Ks}).

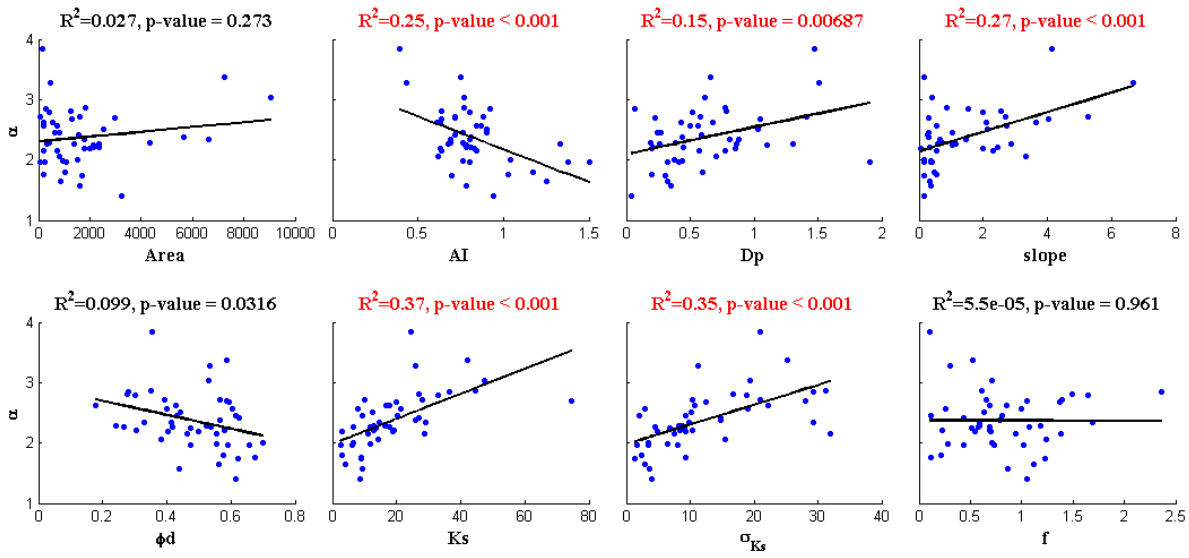

Figure 3.5: Individual scatter plots of each predictor versus α.

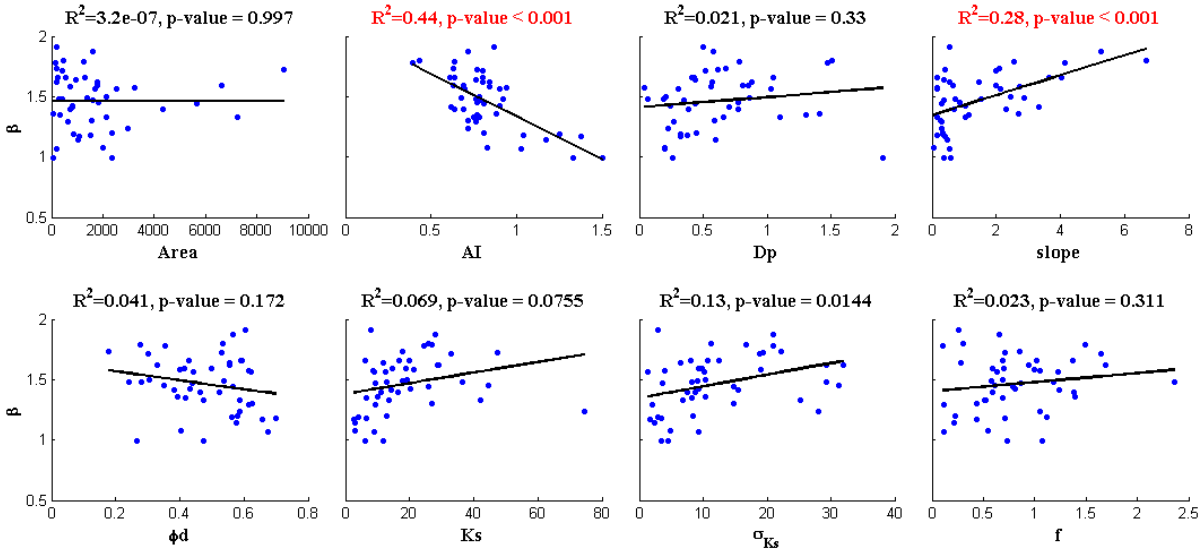

Figure 3.6: Individual scatter plots of each predictor versus β.

In the next step, we determined variables that *together* give a better prediction of α and β. As R^2 always benefits from having more predictors, to avoid over-fitting, a variable selection procedure was carried out to identify the most influential predictors. Figure 3.7 presents the frequency that each variable was selected by the three statistical criteria discussed earlier in Section 2.2.2 for α and β. For α, the variables selected more than half of the time for all three criteria are: D_p, θ, K_s, (ϕd) and f. For β, a smaller number of predictor variables were retained most often in all three methods (AIC, BIC and Lasso), and only AI and f were selected. The resulting regressions are:

$$\alpha = \frac{1.67 D_p^{\,0.06} \exp(0.01\theta + 0.009 K_s)}{(\phi d)^{0.17} f^{0.07}} \tag{11}$$

$$\beta = 2.27 e^{-0.53 AI} f^{0.05} \tag{12}$$

As we can see from both equations, the decay parameter f is found to be important for both α and β; α is also related to other soil and topographic properties while, interestingly, β is also influenced by climatic aridity index (AI) besides the decay parameter f.

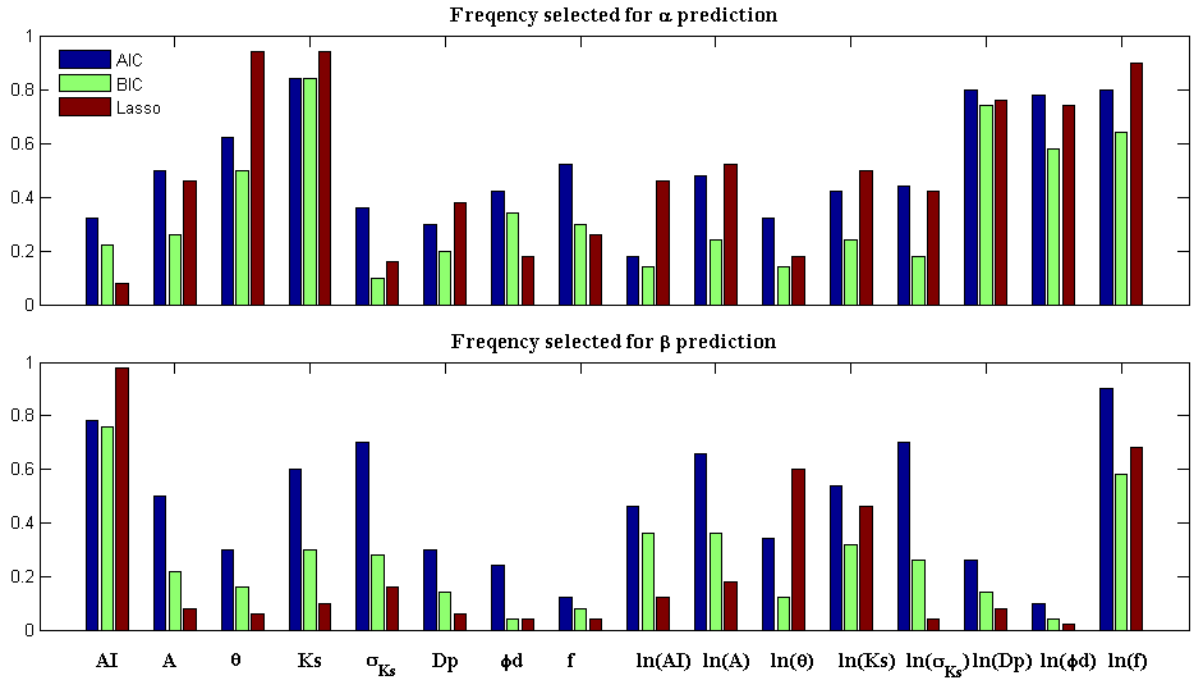

Figure 3.7: Frequency selected for α and β prediction.

Table 3.2 presents the averaged R^2 values over the 50 runs, for the calibration and validation sets for the full models that kept all the candidate variables, and the reduced model with only the selected variables. To reduce the bias due to our relatively small sample size, we randomly selected 75% of the catchments (training dataset) to do the calibration and used the remaining 25% catchments for validation. The model fits the data well for the training set both for the full model and the reduced new model with R^2 values larger than 0.8. Although R^2 drops in the testing dataset used for validation, the reduced model is more accurate than the over-fitted full model with R^2 improved to 68%. The regression obtained for β is also good in the training dataset, with R^2 equal to or larger than 0.75. Although the prediction precision drops in the testing dataset, the reduced model improved R^2 by 80%. One possible reason for R^2 dropping from calibration to validation is the limited sample size, since only 12 catchments were used for validation: the small sample size may add variance to the prediction and decrease R^2 of the validation.

Table 3.2: The averaged R2 of the full model with all the variables, and the new model with only the chosen variables after the selection

		R^2_Full model	R^2_New model
α	Calibration	0.84	0.85
	Validation	0.32	0.54
β	Calibration	0.84	0.75
	Validation	0.27	0.49

3.4 Discussion: Interpretation of the derived functional forms of α, β

The derived functional forms for α and β (Eqs. 11 and 12), though completely empirical, are still consistent with trends suggested by the application of hydraulic theory governing shallow subsurface flow on hillslopes expressed in the form of the Boussinesq equation (Brutsaert and Nieber, 1977; Rupp and Selker, 2005, 2006). Since our work was carried out at catchment scale, and most of the previous analytical derivations were derived for a single aquifer at the hillslope scale, we would not expect similar functional forms for the storage-discharge relationship. However, the variables that are found to be important from our empirical analyses are the same as the variables that appear in these analytical results. For example, in the case of hydraulic theory, the coefficient of the recession-slope curves, α, for a homogeneous aquifer, was found to be a function of the hydraulic conductivity (K_s), average aquifer thickness (d), length of the river network (L), drainage area (A), and porosity(ϕ) (Brutsaert and Lopez, 1998,1999):

$$\alpha = \frac{\psi(\beta)(4K_s d^2 L^2 / A)^{2-\beta}}{(\phi d)A} \qquad (13)$$

where ψ(β) is a polynomial function of β. In subsequent work (Rupp and Selker, 2005) showed that β can be strongly affected by the vertical decrease of the saturated hydraulic conductivity, and showed that $\beta = (2h+1)/(h+1)$, where h is a parameter of the power-law relationship of K_s with depth. This is also the case in the results of our analysis here (i.e., Equations 11 and 12), except that the stream length and drainage area were combined into a drainage density, as was done by Biswal and Marani (2010).

The analytical derivations of Rupp and Selker (2005) through the application of the Boussinesq equation to sloping aquifers highlighted the role of topographic slope, which is also confirmed in the present study. Finally, the study by Rupp and Selker (2005) also highlighted the impact of the vertical decrease of saturated hydraulic conductivity on the exponent β, although in their case they assumed a power law decay in the vertical (as opposed to the exponential decay used here). Rupp and Selker (2005) also showed that the it is the decrease in saturated hydraulic conductivity in the vertical that gives rise to the exponent β being greater than 2.

Our empirical analyses also show that the exponential decay rate of the saturated hydraulic conductivity is one of the two most influential variables governing the magnitude of the exponent β. In fact, the exponential decay parameter f is the only variable that is considered important for both the coefficient, α, and exponent, β. Although the importance of vertical decrease of hydraulic conductivity has been recognized and understood within the broader context of flow convergence (Chapman, 1999; Harman and Sivapalan, 2009), our study has helped to confirm it in many actual catchments. Although the estimate of the f parameter used here is only approximate due to paucity of measurements, its appearance in the regressions still underlines its importance in controlling the shape of the recession curve.

Besides the vertical convergence of water movement controlled in this case by the vertical decay of the hydraulic conductivity, our results also indicate that the recession exponent at the catchment scale is also strongly related to the aridity index (AI). This climate impact is not explicitly included or needed in either the hydraulic theory or heterogeneity theory (Harman et al., 2009; Harman and Sivapalan 2009). Not only was this parameter clearly selected in the reduced models, but the magnitude of the coefficient before it in the functional form for β is at least one order of magnitude larger than that of the hydraulic conductivity decay parameter. This inconsistency with hydraulic or heterogeneity theory is also apparent in the comparison of the expressions for α and β derived here with the equivalent results (not presented here for reasons of brevity) obtained by numerical simulation and up-scaling derived by Ali et al. (2013), in which case only the hydraulic conductivity, its variability in space (both vertical and lateral), and topographic slope were the most important parameters needed for regionalizing the recession curve parameters.

One can attribute two reasons as to why climate in the form of the aridity index, *AI*, has an impact on the shape and magnitude of the recession curve. Firstly, the component variables such as K_s, ϕd, θ, and D_p are all individually and collectively dependent on climate, and this enables it to appear in the empirical regression relationship for β. Secondly, climate aridity impacts differently the actual heterogeneity of both soils and topography that is present in a catchment and that impacts the drainage behavior of the catchment over and above what is captured by the point scale (soils) and hillslope scale measures of soils and topography used in the current study. The first relates to differences between mean properties of many catchments caused by climate differences, whereas the second relates to differences in heterogeneity. But both of these effects are the result of co-evolution of climate, topography and soils, mediated by vegetation, through the erosional and pedogenic processes that contribute to soil formations, but none of them is yet to be captured by extant hydraulic and/or heterogeneity theories. Our empirical results show that β is more strongly related to AI but not α. This may be due to (i) the influence of climate on the vegetation that develops in a given area, and the role of vegetation, through the action of roots in soil development, leading to vertical gradients of soil hydraulic properties, such as the hydraulic conductivity.

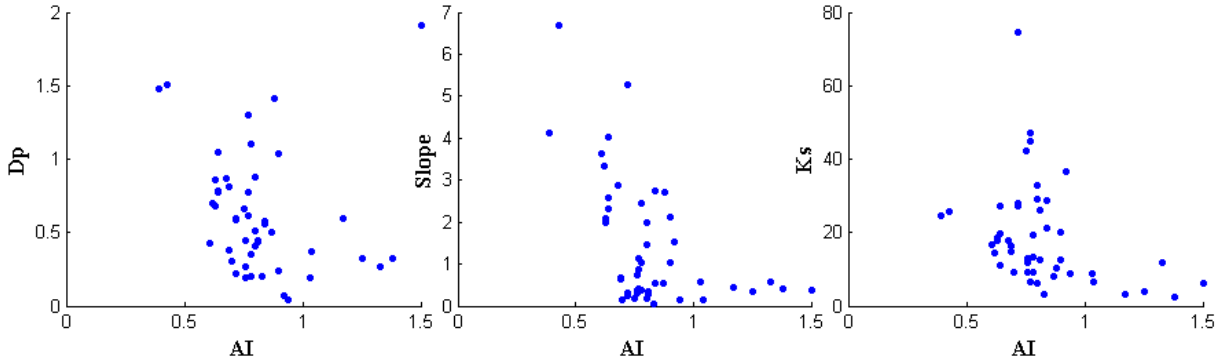

Figure 3.8: Individual scatter plots of each predictor versus *AI*.

There is increasing evidence of such co-evolution in the organized heterogeneity exhibited by many landscape properties. For example, Wang and Wu (2013) found in 185 MOPEX catchments across the continental U.S. that the scaled perennial drainage density decreases monotonically with AI. Likewise, Xu *et al.* (2012) found that in several Australian

catchments the fractions of vegetation cover that are deep rooted perennial or shallow rooted ephemeral show a systematic relationship with AI. In the case of the 50 study catchments used here, we therefore explored possible co-dependence between climate and landscape properties, using the available data, even if these are somewhat limited. Figure 3.8 presents scatter plots of the relationships between topographic slope, drainage density, and saturated surface hydraulic conductivity. They point to some co-dependence, even if not compelling enough for a claim that there is a clear dependence on climate. Nevertheless, given the clear dependence of the β parameter on *AI*, this co-dependence is worthy of more detailed analysis on a larger set of catchments (around the nation and around the world) that have the necessary soils and topographic data available. This is beyond the scope of this study.

3.5 Conclusions

The goal of this study has been to develop an empirically-based parameterization of storage-discharge relations for subsurface stormflow for use in land surface models (LSMs) or catchment-scale rainfall-runoff models. The approach adopted capitalizes on a straightforward relationship between the storage-discharge relations and a catchment's recession curve (or the recession-slope relationship). In this case, the storage-discharge relationship was developed based on inferences from measured catchment streamflow recession curves in several catchments across continental United States, followed by performing multiple regressions of the recession curve parameters against measurable climate, soil and topographic properties. This analysis also helped to identify the climatic and catchment characteristics that control the recession behavior without recourse to extant theory relating to shallow subsurface flow in heterogeneous catchments.

The analyses reported here were carried on 50 selected catchments mostly in the eastern half of the U.S., chosen from the widely available MOPEX dataset. The parameters relating to a power-law type recession-slope curve, a coefficient α and the exponent β, were extracted from observed streamflow hydrographs in all 50 catchments during the winter period in order to minimize the influence of evapotranspiration. Any connection between these two parameters and climatic and landscape properties were explored through initial scatter plots between α, β and these catchment and climate characteristics on an individual basis. This indicated that α is related

to aridity index, drainage density, topographic slope, saturated hydraulic conductivity at the surface and its spatial variance, whereas β was found to be only related to aridity index and topographic slope. None of the properties was sufficient individually to predict the recession curve parameters.

We then applied three different model selection methods to choose variables that would collectively help predict the empirically observed α and β values. This analysis showed that the soil water storage capacity, drainage density, topographic slope, mean saturated hydraulic conductivity at the surface and its vertical decay parameter with depth are essential for predicting α, while the aridity index and the parameter describing vertical decay of saturated hydraulic conductivity are the only variables needed for predicting β. This analysis resulted in statistically significant predictive relationships in terms of the predictor variables for both α and β.

The trends indicated by these empirically derived functional relationships are found to be consistent with corresponding expressions presented in the literature that were derived from extant hydraulic or heterogeneity theory. In this sense, these results are a confirmation of the predictions from existing theories. For example, the importance of the vertical decay of saturated hydraulic conductivity with depth in governing the exponent β is consistent with theoretical predictions and in general confirms the role flow convergence on the nature of subsurface flow recession behavior. Yet, the empirical analyses also, for the first time, revealed the important role of climate, in the form of the aridity index, on the recession curve parameters. There is no explanation for this in existing theories, as also confirmed by the parallel work of Ali et al. (2013), which do not and cannot presently incorporate the effect of climate. We attributed this climate dependence to the role of co-dependence of catchment landscape properties and climate, possibly in the context of their long-term co-evolution.

There remains the question of how to benefit from the regionalized equations derived in this paper for the original goal of the research: develop parameterizations of subsurface stormflow for land surface models. The statistical model derived here has in effect captured the net effects of co-evolution and is therefore useful for extrapolations in the region within which it was derived. Although the statistical model provides important insights into the factors that control the recession curves, due to the limited number of catchments and the relative humid

climate of these catchments, its validity for extrapolation to regions other than the relatively humid eastern U.S. is not clear. The empirical relationship may or may not change when one moves from the relatively humid catchments to more arid ones, since the physical meaning behind the statistical model is still not clear. On the other hand, parameterizations derived on the basis of traditional hydraulic theory (e.g., Ali et al., 2013) also have limitations, because so far they do not include the effects of co-evolution. There is therefore a clear need for a reconciliation of these approaches so that we can derive parameterizations that are based on widely applicable physics, and yet capture the net effects of co-evolution of climate, soils, topography and vegetation. This is beyond the scope of this study, and is left for future research.

3.6 Acknowledgements

This study was supported by the Office of Science of the U.S. Department of Energy as part of the IMPACTS project funded by the Earth System Modeling program to improve hydrologic parameterizations in land surface models for predicting changes in droughts in the future climate. PNNL is operated for DOE by Battelle Memorial Institute under Contract DE-AC05-76RLO1830.

References

Akaike, H. (1974). A new look at the statistical model identification, *IEEE Transactions on Automatic Control,* 19 (6), 716–723, doi:10.1109/TAC.1974.1100705, MR 0423716.

Ali, M., S. Ye, H.-Y Li, M-Y Huang, L.R. Leung, A. Fiori and M. Sivapalan (2013). Subsurface stormflow parameterization for land surface models: Up-scaling from physically based numerical simulations at hillslope scale. Submitted to *J. Hydrol.* (this issue).

Anderson, R.M., V. I. Koren, and S. M. Reed (2006), Using SSURGO Data to improve Sacramento model a priori parameter estimates. *J. Hydrol.*, 320 (1), 103–116.

Beven, K. J., and M. J. Kirkby (1979), Towards a simple, physically based, variable contributing area model of catchment hydrology, *Hydrol. Sci. Bull.*, 24, 43–69.

Beven, K. J., M. J. Kirkby, N. Schofield, and A. F. Tagg (1984), Testing a physically based flood forecasting model (topmodel) for three U.K. catchments. *J. Hydrol.*, 69(1–4), 119–143. DOI: 10.1016/0022-1694(84) 90159-8.

Beven, K. J. (1997), TOPMODEL: a critique, *Hydrol. Process.*, 11, 1069-1085.

Bliss, N. B., S. W. Waltman, and A. C. Neale (2010), Detailed soil information for hydrologic modeling in the conterminous United States, Amer. Geophys. Union, Fall Meeting, San Francisco, 13-17 December 2010, EOS Transactions, Suppl., v. 91: Abstract H43B-1227. Available online at http://www.agu.org/meetings/fm10/waisfm10adv.html

Biswal B., and M. Marani (2010), Geomorphological origin of recession curves, *Geophys. Res. Lett.*, 37, L24403, doi:10.1029/2010GL045415.

Brutsaert, W., and J. L. Nieber (1977), Regionalized drought flow hydrographs from a mature glaciated plateau, *Water Resour. Res.*, 13(3), 637–644.

Brutsaert, W., and J. P. Lopez (1998), Basin-scale geohydrologic drought flow features of riparian aquifers in the southern Great Plains, *Water Resour. Res.*, 34, 2, 233-240.

Brutsaert, W., and J. P. Lopez (1999), Comment on "Basin-scale geohydrologic drought flow features of riparian aquifers in the southern Great Plains" - Reply, *Water Resour. Res.*, 35(3), 911-911.

Chapman, T. G. (1999), A comparison of algorithms for stream flow recession and baseflow separation, *Hydrol. Process.*, 13(5), 701–714.

Earls, J., and B. Dixon (2005), A comparative study of the effects of input resolution on the SWAT model. *Ecol. Environ.*, 12, 213–222.

Eltahir, E. A. B., and P. J. F. Yeh (1999), On the asymmetric response of aquifer water level to floods and droughts in Illinois. *Water Resour. Res.*, 35, 1199–1217.

Engelhardt, I., J. G. De Aguinaga, H. Mikat, C. Schuth, O. Lenz and R. Liedl (2012), Complexity versus simplicity: an example of groundwater model ranking with the Akaike Information Criterion, *Hydrol. Earth Syst. Sci. Discuss.*, 9, 9687-9714, doi:10.5194/hessd-9-9687-2012.

Francini,M., and M. Pacciani (1991), Comparative Analysis of several conceptual rainfall-runoff models, *J. Hydrol.*, 122, 161-219.

Harman, C. J., M. Sivapalan, and P. Kumar (2009), Power law catchment-scale recessions arising from heterogeneous linear small-scale dynamics, *Water Resour. Res.,* 45, W09404, doi:10.1029/2008WR007392.

Harman, C. J., and M. Sivapalan (2009), A similarity framework to assess controls on shallow subsurface flow dynamics in hillslopes, *Water Resour. Res.,* 45, W01417, doi:10.1029/2008WR007067.

Hastie, T., R. Tibshirani, and J. Friedman, (2009), *The Elements of Statistical Learning: Data Mining, Inference and Prediction*. Springer, pp. 61-78.

Hatfield, J.L., L. D. McMullen, and C. S. Jones (2009), Nitrate-nitrogen patterns in the Raccoon River Basin related to agricultural practices, *J. Soil Water Cons.,* 64, 190–199, doi: 10.2489/jswc.64.3.190.

Hou Z., M. Huang, L. R. Leung, G. Lin, D. M. Ricciuto (2012), Sensitivity of surface flux simulations to hydrologic parameters based on an uncertainty quantification framework applied to the Community Land Model, *J. Geophys. Res.*, 117, D15108, doi: 10.1029/2012JD017521.

Huang, M., Z. Hou, L.R. Leung, Y. Ke, Y. Liu, Z. Fang, and Y. Sun (2013), Uncertainty analysis of runoff simulations and parameter identifiability in the Community Land Model – Evidence from MOPEX basins, *J. Hydrometeor.*, doi: http://dx.doi.org/10.1175/JHM-D-12-0138.1

Huang, M., and X. Liang (2006), An assessment of impact of reducing parameters and identification of parameter uncertainties in the VIC-3L model with applications to ungauged basins. *J. Hydrol.,* 320, 37–61.

Huang, M., X. Liang, and L. R. Leung (2008), A generalized subsurface flow parameterization considering subgrid spatial variability of recharge and topography. *J. Hydrometeorol.,* 9(6), 1151-1171.

Koster, R., P. Dirmeyer, Z. Guo, G. Bonan, E. Chan, P. Cox, C.T. Gordon, S. Kanae, E. Kowalczyk, D. Lawrence, P. Liu, C. Lu, S. Malyshev, B. McAvaney, K. Mitchell, D. Mocko, T. Oki, K. Oleson, A. Pitman, Y. C. Sud, C. M. Taylor, D. Verseghy, R. Vasic, Y. Xue, and T. Yamda (2004), Regions of strong coupling between soil moisture and precipitation, *Science,* 305, 1138–1140.

Lawrence, D. M., K. W. Oleson, M. G. Flanner, P. E. Thornton, S. C. Swenson, P. J. Lawrence, X. Zeng, Z. L. Yang, S. Levis, K. Sakaguchi, G. B. Bonan, and A. G. Slater (2011),

Parameterization improvements and functional and structural advances in version 4 of the Community Land Model, *J. Adv. Model. Earth Syst.,* 3, M03001, doi:10.1029/ 2011MS000045.

Li, H, M. Sivapalan, D. Liu and F. Tian (2010), Water and nutrient balances in a large tile-drained agricultural catchment: A distributed modeling study. *Hydrol. Earth Syst. Sci.,* 14, 2259–2275, doi:10.5194/hess-14-2259-2010.

Li, H., M. Huang, M. S. Wigmosta, Y. Ke, A. M. Coleman, L. R. Leung, A. Wang, and D. M. Ricciuto (2011), Evaluating runoff simulations from the Community Land Model 4.0 using observations from flux towers and a mountainous watershed, *J. Geophys. Res.,* 116, D24120, doi:10.1029/2011JD016276.

Liang, X., D. P. Lettenmaier, E. F. Wood, and S. J. Burges (1994), A simple hydrologically based model of land surface water and energy fluxes for general circulation models, *J. Geophys. Res.,* 99, 14, 415-428.

Liang, X., Z. H. Xie, and M. Y. Huang (2003), A new parameterization for surface and groundwater interactions and its impact on water budgets with the variable infiltration capacity (VIC) land surface model, *J. Geophys. Res.,* 108 (D16), 8613, doi:10.1029/2002JD003090.

Lyon, S. W., and P. A. Troch (2010), Development and application of a catchment similarity index for subsurface flow, *Water Resour. Res.,* 46, W03511, doi:10.1029/2009WR008500.

Niu, G.-Y., Z.-L. Yang, R. E. Dickinson, and L. E. Gulden (2005), A simple TOPMODEL-based runoff parameterization (SIMTOP) for use in global climate models, *J. Geophys. Res.,* 110(D21), D21106.

Niu, G.-Y., Z.-L. Yang, R. E. Dickinson, L. E. Gulden, and H. Su (2007), Development of a simple groundwater model for use in climate models and evaluation with Gravity Recovery and Climate Experiment data, *J. Geophys. Res.,* 112(D7), D07103.

Oleson K. W., D. M. Lawrence, G. B. Bonan, M. G. Flanner, E. Kluzek, P. J. Lawrence, S. Levis, et al., (2010), Technical description of version 4.0 of the Community Land Model (CLM), NCAR Technical Note NCAR/TN-478+STR, 257 pp.

Oleson, K.E., D.M. Lawrence, G, Bonan, B. Drewniak, M Huang, C. D. Koven, S. Levis, F. Li, W. J. Riley, Z. M. Subin, S. C. Swenson, P. E. Thornton, A. Bozbiyik, R. Fisher, E. Kluzek, J.-F. Lamarque, P. J. Lawrence, L. R. Leung, S. Muszala, D. M. Ricciuto, W. Sacks, J. Tang, Z.-L. Yang, 2013. Technical Description of version 4.5 of the Community Land Model (CLM), June 2013, National Center for Atmospheric Research, Boulder, CO. http://www.cesm.ucar.edu/models/cesm1.2/clm/CLM45_Tech_Note.pdf.

Ringeval, B., B. Decharme, S. L. Piao, P. Ciais, F. Papa, N. de Noblet-Ducoudré, C. Prigent, P. Friedlingstein, I. Gouttevin, C. Koven, and A. Ducharne (2012), Modelling sub-grid wetland in the ORCHIDEE global land surface model: evaluation against river discharges and remotely sensed data, *Geosci. Model Dev.,* 5(4):941–962, doi:10.5194/gmd-5-941-2012.

Robinson, J. S., and M. Sivapalan (1995) Catchment-scale runoff generation model by aggregation and similarity analyses. *Hydrol. Process.*, 9(5-6), 555–574.

Rodríguez-Iturbe, I., and J. B. Valdés (1979), The geomorphologic structure of hydrologic response, *Water Resour. Res.*, 15(6), 1409–1420, doi:10.1029/WR015i006p01409.

Rupp, D., and J. Selker (2005), Drainage of a horizontal Boussinesq aquifer with a power law hydraulic conductivity profile, *Water Resour. Res.*, 41, W11422, doi:10.1029/2005WR004241.

Rupp, D. E., and J. S. Selker (2006b), On the use of the Boussinesq equation for interpreting recession hydrographs from sloping aquifers, *Water Resour. Res.*, 42, W12421, doi:10.1029/2006WR005080.

Schwarz, G. E. (1978), Estimating the dimension of a model, *Annals of Statistics*, 6 (2), 461–464. doi:10.1214/aos/1176344136

Seneviratne, S. I., T. Corti, E. L. Davin, M. Hirschi, E. B. Jaeger, I. Lehner, B. Orlowsky, A. J. Teuling (2010), Investigating soil moisture-climate interactions in a changing climate: A review, *Earth Sci. Rev.*, 99 (3-4) 125-161.

Tague, C., and G. Grant (2004), A geological framework for interpreting the low-flow regimes of Cascade streams, Willamette River Basin, Oregon, *Water Resour. Res.*, 40, W04303, doi:10.1029/2003WR002629.

Todini, E. (1996), The ARNO rainfall-runoff model. *J. Hydrol.*, 175, 339–382.

Troch, P. A., G. A. Carrillo, I. Heidbüchel, S. Rajagopal, M. Switanek, T. H. M. Volkmann, and M. Yaeger (2008), Dealing with landscape heterogeneity in watershed hydrology: A review of recent progress toward new hydrological theory, *Geogr. Compass*, 2, doi:10.1111/j.1749-8198.2008.00186.x.

Viney N. R., and M. Sivapalan (2004), A framework for scaling of hydrologic conceptualizations based on a disaggregation–aggregation approach. *Hydrol. Process.*, 18(8),1395–1408.

Vogel, R. M., and C. N. Kroll (1992), Regional geohydrologic-geomorphic relationships for the estimation of low-flow statistics, *Water Resour. Res.*, 28(9), 2451– 2458.

Wang, D. and M. Hejazi (2011), Quantifying the relative contribution of the climate and direct human impacts on mean annual streamflow in the contiguous United States, *Water Resour. Res.*, 47, W00J12, doi:10.1029/2010WR010283.

Warrach, K., M. Stieglitz, H. T. Mengelkamp, and E. Raschke (2002), Advantages of a topographically controlled runoff simulation in a Soil-Vegetation-Atmosphere transfer model. *J. Hydrometeorol.*, 3(4), 131-148.

Wang, D., and L. Wu (2012), Similarity between runoff coefficient and perennial stream density in the Budyko framework, *Hydrol. Earth Syst. Sci.*, 17, 315–324, doi:10.5194/hess-17-315-2013 .

Xu, X., D. Yang and M. Sivapalan (2012), Assessing the impact of climate variability on catchment water balance and vegetation cover, *Hydrol. Earth Syst. Sci.*, 16, 43–58.

Ye, S., M. Yaeger, E. Coopersmith, L. Chang, and M. Sivapalan (2012), Exploring the physical controls of regional patterns of Flow Duration Curves, Part 2: Role of seasonality, the regime curve, and associated process controls, *Hydrol. Earth Syst. Sci.*, doi:10.5194/hess-16-1-2012.

Zucker, L. A. and L. C. Brown (1998), Agricultural Drainage:Water Quality Impacts and Subsurface Drainage Studies in the Midwest, Ohio State University Extension Bulletin 871, the Ohio State University, Columbus, USA.

Part II: Nutrient Transport

Chapter 4

Dissolved Nutrient Retention Dynamics in River Networks: A Modeling Investigation of Transient Flows and Scale Effects

Abstract[1]

We have used a dynamic hydrologic network model, coupled with a transient storage zone solute transport model, to simulate dissolved nutrient retention processes during transient flow events at the channel network scale. We explored several scenarios with a combination of rainfall variability, and biological and geomorphic characteristics of the catchment, to understand the dominant factors that control the transport of dissolved nutrients (e.g., nitrate) along channel networks. While much experimental work has focused on studying nutrient retention during base flow periods in headwater streams, our model-based theoretical analyses, for the given parameter combinations used, suggest that high-flow periods can contribute substantially to overall nutrient retention, and that bulk nutrient retention is greater in larger rivers compared to headwaters. The relative efficiencies of nutrient retention during high- and low-flow periods vary due to changes in the relative sizes of the main channel and transient storage zones, as well as due to differences in the relative strengths of the various nutrient retention mechanisms operating in both zones. Our results also indicate that nutrient retention efficiency at all spatial scales of observation has strong dependence on within-year variability of streamflow (e.g., frequency and duration of high and low flows), as well as on the relative magnitudes of the coefficients that govern biogeochemical uptake processes: the more variable the streamflow, the greater the export of nutrients. Despite limitations of the model parameterizations, our results suggest that increased attention must be paid to field observations of the interactions between process hydrology and nutrient transport and reaction processes at a range of scales to assist with extrapolation of understandings and estimates gained from site-specific studies to ungauged basins across gradients in climate, human impacts, and landscape characteristics.

[1]This work has been submitted for publication to Water Resources Research as: Ye, S., T. P. Covino, M. Sivapalan, N. B. Basu, H.-Y. Li, and S.-W. Wang, Dissolved nutrient retention dynamics in river networks: A modeling investigation of transient flows and scale effects. All figures, tables and data were created by Sheng Ye unless otherwise indicated.

4.1 Introduction

The phenomenon of oxygen depletion, or "hypoxia", in receiving waters such as lakes, estuaries and coastal areas is now a worldwide environmental problem. This is partially caused by excess nutrient loading from terrestrial landscapes to aquatic environments that stimulates phytoplankton growth, the decomposition of which leads to depletion of dissolved oxygen. A large hypoxic zone occurs periodically in the northern Gulf of Mexico, where aquatic life is under threat due to nutrient induced eutrophication (Rabalais *et al.,* 2002). Over 98% of the total nitrogen and phosphorous loading to the Gulf of Mexico is sourced to the Mississippi and Atchafalaya Rivers (Dunn, 1996), much of which originates from fertilized agricultural lands in the Mid-west region of the United States. With increased attention to the eutrophication problems in the Gulf of Mexico and the greater Mississippi River Basin, there has been considerable emphasis given to quantifying the sources of nutrients, and the processes associated with the uptake, retention, and/or removal of nutrients within the catchments and sub-catchments (Bencala and Walters, 1983; Dodds *et al.,* 2002; Donner *et al.,* 2002; Mulholland *et al.,* 2002; Alexander *et al.,* 2009; Claessens and Tague, 2009; Claessens *et al.,* 2009). To avoid the confusion it might cause, in this paper we define nutrient retention as the temporary storage of nutrients in biomass (i.e., uptake) and removal as the permanent loss of nutrient from the system (i.e., denitrification). We acknowledge that this retention is not necessarily equal to net loss from the stream system because it does not include contributions from remineralization (Brookshire *et al.,* 2009) or groundwater recharge (Covino *et al.,* 2010b). Brookshire has found that during baseflow periods streams could maintain steady state with equivalent nutrient loss by retention and gain from remineralization and groundwater inputs. However, in the absence of adequate information or data (e.g., denitrification rate, mineralization rate, groundwater concentration) to constrain a more complex representation of the nutrient cycle (e.g., including uptake, denitrification, mineralization), in this paper we limit our model to account for gross retention of inorganic nitrogen. More complex representations that incorporate various components of the nutrient cycle, transport of particulate organic nitrogen, and transport of other nutrients could be accounted for in our model given adequate process parameterizations or field-based evidence to constrain these additional aspects of stream biogeochemistry.

The study of nutrient retention and removal processes within large catchments can be organized into two distinct, but interacting, components: (i) the terrestrial landscape, and (ii) river networks, which are reactive pathways that connect the outputs of terrestrial systems to receiving waters. Both components involve interactions of flow (hydrological) processes with biogeochemical, geomorphological, and ecological processes on land and in the river network, all of which exhibit considerable heterogeneity and process complexity. In order to understand these processes and to use such understanding for management, we need predictive tools (i.e., models) that are based on fundamental theories of flow, transport and reaction across the landscape and in the river network. This paper is aimed at describing the processes and interactions occurring exclusively within the river network and for this reason many details of landscape (hillslope) processes are left out. Previously, there have been several catchment modeling studies that have focused on landscape (hillslope) biogeochemical scale processes (Viney *et al.,* 2000; Li *et al.,* 2010). The work presented here focuses on dissolved nutrients, e.g., nitrate; however, the model can easily be further adapted to handle other solutes. The accompanying papers in this special section by Harman *et al.* (2011), Thompson *et al.* (2011), Guan *et al.* (2011) and Basu et al. (2011) address separately the transport and biogeochemical transformations in several components of the landscape and stream network, such as in the vadose zone, individual stream reaches, and in small catchments. Furthermore, the paper by Basu *et al.* (2011) specifically addresses the effects of intra-annual streamflow variability on nitrate retention at the catchment scale, using a stochastic modeling approach.

The theory of "nutrient spiraling" (Webster and Patten, 1979; Newbold *et al.,* 1982) serves as the foundation for much of the experimental and modeling work being carried out in the area of dissolved nutrient transport in river networks. It describes the coupled hydrological (e.g., advection) and biogeochemical (e.g., uptake) processes that control downstream nutrient transport and the cycling, or "spiraling", of nutrients between inorganic and organic forms (Newbold *et al.,* 1982). Bencala and Walters (1983) proposed the "transient storage" model, which separates the river channel into two interacting compartments: the flowing water column or "main channel" (MC) zone and a more stagnant "transient storage" (TS) zone. The TS zone is a general term that represents any flow path where the velocity is much smaller than that in the MC. Examples include surface water "dead zones" such as pools, off-channel storages such as floodplains, the hyporheic zone, and other flow non-uniformities where the velocity is much

smaller than that in the MC (Stofleth *et al.*, 2008; Stewart *et al.*, 2011). Bencala and Walters' TS model is the basis for the now widely used one-dimensional transport model with inflow and transient storage (OTIS) (Runkel, 1998). The OTIS model uses coupled partial differential equations in time and space (downstream distance) to characterize nutrient transport and transformation in rivers; it can consider transport and retention from both the MC and TS zones, including exchanges between the two. The model is also widely used, in combination with field measurements of solute concentrations and loads, to characterize reach-scale hydrologic and biogeochemical processes and their parameterizations (Runkel, 2007; Böhlke *et al.*, 2009).

The mean distance a nutrient travels downstream before being taken up is defined as the uptake length, S_W [L] (Newbold *et al.*, 1982). The traditional approach to estimating S_W is to perform isotopic tracer or nutrient addition experiments within a stream reach and then plot the decline in nutrient concentration against downstream distance – the negative inverse of the slope (e.g., regression line) of this decline is S_W (Stream Solute Workshop, 1990; Payn *et al.*, 2008; Böhlke *et al.*, 2009; Hall *et al.*, 1998, 2009a). Since S_W is related to hydrologic characteristics (e.g., velocity, depth), an uptake velocity defined as $v_f = (Q/w)/ S_W$ (where, Q [L^3/T] is stream discharge, and w [L] is wetted stream width), which partially accounts for hydrologic influences, is often computed to compare streams of different sizes and flow states (Stream Solute Workshop, 1990). Accordingly, uptake velocity v_f [L/T] reflects biological demand relative to available nutrient concentration (Wollheim *et al.*, 2006).

Previous studies have suggested that transient storage zones play an important role in nutrient retention within river channels (Runkel and Bencala, 1995). They can act as a sink at the beginning of tracer injection experiments and as a source after injection is complete (Bencala and Walters, 1983). It has been hypothesized that an increase in A_{TS}/A_{MC}, the ratio of the cross-sectional area of the TS zone (A_{TS}) to the cross-sectional area of the MC zone (A_{MC}) can promote nutrient uptake (Bencala and Walters, 1983; Mulholland and De Angelis 2000; Paul and Hall, 2002). However, there have been several studies that cast doubt on the existence and possible effects of these linkages (Hall *et al.*, 2002; Ensign and Doyle, 2006). Further work is still needed, at a range of scales, to understand and clarify the relative contributions of retention mechanisms in MC and TS zones.

A majority of nutrient release experiments have been carried out in small headwater streams (Tank *et al.*, 2008) during low flow conditions (Hall *et al.*, 2009b), which may represent times and conditions of high nutrient retention (Peterson *et al.*, 2001; Böhlke *et al.*, 2009). Nutrient release experiments are typically more tractable in small headwater streams than in larger rivers or during times of high discharge (Hall and Tank, 2003; Hall *et al.*, 2009b). However, Hall *et al.*'s (2009b) work in a mountain stream suggested that biological demand for nitrate was much higher than expected during floods and that reach scale nutrient uptake during low flows and spring floods were similar. This can potentially be attributed to the presence of a large hyporheic zone (i.e., increased extent of the hyporheic zone during flood events) relative to the size of the drainage area. Furthermore, recent modeling studies have indicated that in spite of the low efficiency of retention and removal per unit length, larger rivers, with associated longer travel times and larger mass input, can have significant contributions to transport of nutrients throughout the overall network in spite of lower nutrient retention efficiencies (Wollheim *et al.*, 2006; Ensign and Doyle, 2006), the reasons for which are not fully clear. Combined, these results suggest that it is important to understand nutrient retention processes across a range of flow states and stream sizes.

Characterization of biogeochemical processes in streams is typically accomplished through a combination of field experiments and process models (Bencala and Walters, 1983; Runkel, 1998; Claessens and Tague, 2009; Claessens *et al.*, 2009; Covino *et al.*, 2010a). The results of these field experiments are used to estimate model parameters and to understand the factors affecting nutrient transport at the reach scale. To understand how nutrient transport processes evolve in the downstream direction, and how they impact the dynamics in larger rivers, we need catchment network scale models that can accommodate terrestrial loading, transport and transformation along the river channel network. There are several biogeochemical models that are in wide use to predict nutrient transport at different spatial scales (e.g., Smith *et al.*, 1997; Donner *et al.*, 2002; Mulholland *et al.*, 2002, 2008; Seitzinger *et al.*, 2002, Wollheim *et al.*, 2006, 2008; Alexander *et al.*, 2009). Many of these models use observed data to predict nutrient transport as a function of hydrologic variables (i.e., stream depth, travel time). These empirical relationships are then applied at the catchment scale, to obtain annual estimates of nutrient export (Smith *et al.*, 1997; Goolsby *et al.*, 2000). Other models have applied the one-dimensional advection-dispersion equation to capture reach scale nutrient cycling processes for each month,

and have expressed bulk retention k_e as a function of nutrient concentration, flow depth and water temperature (e.g., Alexander *et al*., 2009). Many of these models have assumed steady flow conditions, and although they capture the impact of seasonal variability on nutrient transport, they are unable to make predictions under highly variable flow conditions that occur during flood events, as well as seasonally over the year, or in space (e.g., across the river network), a notable exception being the work by Wollheim *et al.* (2008). The work presented in this paper specifically addresses the problem of characterizing the likely impacts of variable flow dynamics (within-event as well as inter-event) on nutrient retention and export processes, and associated scale effects.

Every catchment possesses unique hydrological, biological, and geomorphic characteristics. These factors, which partially control nutrient transport, may vary both within catchments, as well as between catchments. Without a more complete understanding of the process controls on nutrient transport and transformation and their variability across spatial and temporal scales, it is difficult to develop generalized models and predictions. Furthermore, field experiments have produced contradictory results, and the existence of relationships between the size of the TS zone and nutrient uptake remain inconclusive (e.g., Marti *et al.,* 1997; Ensign and Doyle, 2006). This is partially due to uncertainty regarding retention and/or removal rates in the MC and TS zones, knowledge of the relative sizes of the TS and MC zones, and consequently the relative contributions from the two zones that combine to produce bulk nutrient retention. Lack of resolution of these questions will have significant impacts on our ability to predict nutrient transport at the catchment scale. For example, moving in the downstream direction in a river network, nutrient retention may: be reduced by the increase of both flow depth and flow velocity; potentially increase due to increasing A_{TS}/A_{MC} ratio accompanying the increase in stream size; or remain constant due to the compensating effects of the above two factors.

To address these questions, a comprehensive numerical framework that can accommodate the impact of various process controls (i.e., hydrology, biogeochemistry and geomorphology) on nutrient transport within catchments is needed. Ideally, models of nutrient transport processes at the network scale must be consistent with more widely accepted process representations, such as those represented in the OTIS model, and with field observations. This has been the motivation for the modeling study presented here. A recent review by Helton *et al*. (2011) has highlighted

major weaknesses in the current generation of nitrogen cycling models in river networks in that they: oversimplify catchment hydrology; oversimplify network hydrogeomorphology; incorporate unidirectional uptake of nitrogen rather than cycling in the context of other elements (i.e., stoichiometric constraints); and focus on base-flow or annual mean conditions, ignoring the ecological relevance of seasonal cycles and faster temporal dynamics.

This paper focuses on the last of these, namely, the influence of temporally dynamic hydrology on nutrient export, and particularly we: distinguish between retention during high flow and low flow periods; determine the relative contributions of the TS and MC zones to retention; and, investigate the roles of hydrologic variability (as governed by climate and landscape filtering), network geomorphology, and scaling these dynamics across space and time. We implement a coupled hydrological-solute-transport model to address the following questions:

(1) How much nutrient retention occurs during low flow periods versus during high flow periods, and what are the contributions to retention from the main channel (MC) and the transient storage (TS) zones?
(2) What are the impacts of within-year streamflow variability on the fraction of nitrate removed and delivered at the catchment scales?
(3) How are the answers to the two questions posed above influenced by scale effects (i.e., size of river or contributing catchment area), including how retention rates and their process controls change as one moves from the reach scale to the network scale?

Through implementation of the model across the river network of a ~500km^2 catchment we seek to elucidate catchment scale biogeochemical and hydrological responses, as different from reach scale process representations, and to understand how hydrologic variability interacts with network structure and patterns of hydraulic geometry and solute transport processes, giving rise to these newly emergent properties.

4.2 Methodology

The modeling framework we use here combines a dynamic flow model in a river network, based on the representative elementary watershed (REW) theory of Reggiani *et al.* (1998, 1999, 2001), with a network nutrient transport and retention model based on upscaling of the OTIS model

equations for dissolved nutrients (Bencala and Walters, 1983; Runkel, 1998), with explicit inclusion of the interactions between the MC and TS zones. The focus of the present paper is on the network nitrate (NO_3-N) retention processes; for this reason hillslope processes are somewhat over-simplified and hillslope flow response is simulated with a linear bucket model with an assumed mean residence time. NO_3-N concentrations of hillslope flows are assumed constant in time and space, and yet, since discharge is highly variable, the nitrate load is variable as well. The details of each of the model components are given in Figure 4.1. More advanced versions of these components are elaborated upon in the accompanying papers by Harman *et al*. (2011), Thompson *et al*. (2011), and Guan *et al.* (2011).

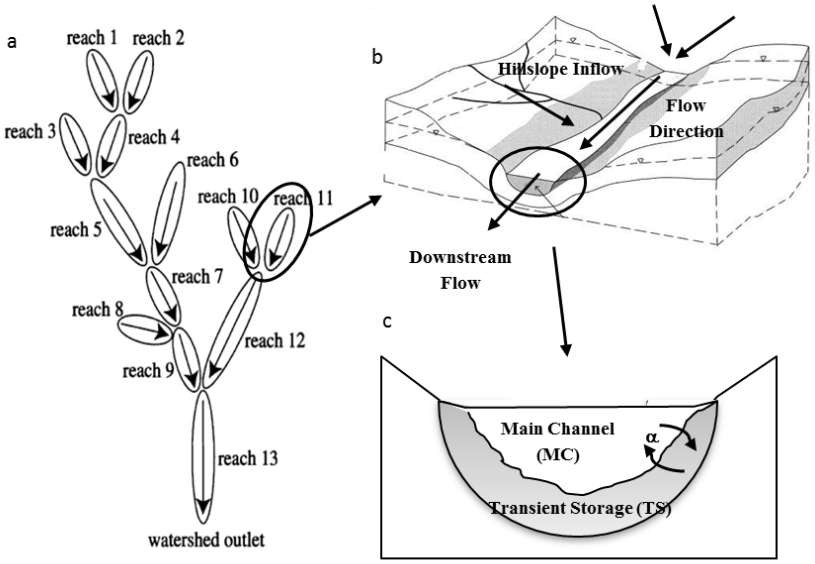

Figure 4.1: Schematic of the coupled hydrological-solute-transport model: (a) Watershed discretization into several REWs organized around the river network; (b) each REW includes a hillslope (landscape element) and a channel reach; (c) two-zone solute transport model that includes the main channel (MC) zone and a transient storage (TS) zone; α is a coefficient that governs nutrient exchange between the MC and TS zones.

4.2.1 Study area

The nominal study area is the Little Vermilion River catchment (Figure 4.2) and the river network is extracted from a DEM for this catchment. This catchment drains a 489 km^2 area across three counties, Vermilion, Champaign and Edgar, and is generally flat with a slope of 1%

or less (Mitchell *et al.*, 2000; Algoazany, 2006). It is a typical agricultural catchment in east-central Illinois that is drained by an extensive network of tile drains. The land use in Little Vermilion is quite intensive. Nearly 90% of the area is planted with a rotation of corn and soybean crops. The dominant soil type in this catchment is silty loam and silty clay loam, with low hydraulic conductivity values.

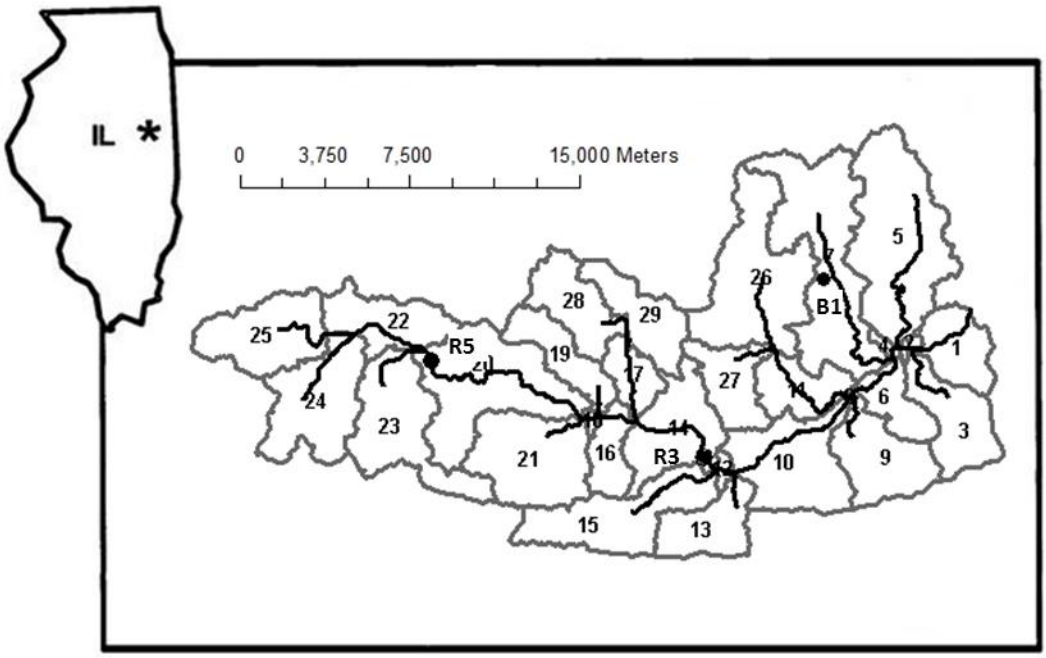

Figure 4.2: Map of the study area, Little Vermilion Basin in east-central Illinois, including the delineation of 29 REW boundaries. Bold line is the river network

4.2.2 Network hydrologic model

The network flow model, based on the REW approach, builds on the balance equations for mass and momentum for a hierarchical river network derived by Reggiani *et al.* (2001). The REW approach disaggregates the whole catchment into a number of sub- catchments (REWs), with the REWs being considered the smallest functional units of the model, with each REW having only one stream reach and being linked to all other REWs via the river network. Tian (2006) developed a numerical model, THREW (TsingHua Representative Elementary Watershed), based on a set of ordinary differential equations (ODEs) of the coupled mass and momentum

balance equations at the REW scale (Li and Sivapalan, 2011), including extensions to incorporate explicit formulations for energy balance applicable to cold regions (Tian *et al.,* 2006).

Since our objective is to explore process controls on nitrate transport in a river network only, we use a simplified version of THREW, where each REW is divided into two sub-regions only: a hillslope region and a channel region (Figure 4.1). We use a simple lumped bucket model to represent the hillslope response to precipitation for REW_i:

$$\frac{dS_h^i}{dt} = PA^i - Q_h^i - ET^i \tag{1}$$

$$Q_h^i = \frac{S_h^i}{\tau_h} \tag{2}$$

$$ET^i = \frac{S_h^i}{\tau_e} \tag{3}$$

where S^i_h is water storage of REW i in the hillslope [L^3], P is the rainfall intensity [$L\ T^{-1}$] and is assumed uniform across the catchment, A^i is the area of REW i [L^2], Q^i_h is flow that enters the channel network directly from the local hillslope area [$L^3\ T^{-1}$], τ_h is the mean residence time with respect to subsurface flow [T], ET^i is the evaporation [$L^3\ T^{-1}$], and τ_e is mean residence time with respect to evapotranspiration [T]. The presence of an extensive network of tile drains leads to the dominance of subsurface drainage while surface runoff is rare (Li *et al.,* 2010). These considerations justify the use of simple conceptual models of the hillslope hydrologic response (Basu *et al.,* 2009), such as the one adopted here.

The water balance equation for the river reach i (associated with REW_i), with inflows from the hillslope and two upstream nodes, can be written as follows:

$$\frac{dS_{MC}^i}{dt} = Q_h^i + \sum Q_{up}^j - Q_{out}^i \tag{4}$$

$$Q_{out}^i = v^i A_{MC}^i \tag{5a}$$

$$Q_{up}^j = v^j A_{MC}^j \tag{5b}$$

where S^i_{MC} is water storage at local reach i [L^3], Q^j_{up} is the inflow from upstream nodes (in a bifurcating network we assume there are at most two upstream reaches) [L^3 T^{-1}], v^j is the velocity at upstream end, for reach j [L T^{-1}], A^j_{MC} is cross-sectional area of the j^{th} upstream reach [L^2], Q^i_{out} is the outflow from reach i [L^3 T^{-1}], and v^i is the velocity at local reach i [L T^{-1}].

The channel cross-sectional area A^i_{MC} is estimated at the beginning of any time step by dividing the water storage (S^i_{MC}) at the end of previous time step by the channel reach length (L^i), while the velocity v^i is estimated through recourse to a reach scale momentum balance equation (i.e., Saint-Venant momentum balance equation).

$$\underbrace{\rho A^i_{MC} L^i \frac{d}{dt} v^i}_{\text{Inertia}} = \underbrace{\rho g A^i_{MC} L^i \sin\gamma^i}_{\text{Gravity}} - \frac{1}{8}\underbrace{\rho P^i L^i \zeta^i v^i \mid v^i \mid}_{\text{Chezy resistance}} \pm \underbrace{\sum_{j\neq i} \frac{1}{4} \rho g h^i (A^i_{MC} + A^j_{MC}) \cos\delta^{ij}}_{\text{Pressure forces exchanged across end sections}} - \frac{1}{2}\underbrace{\rho g h^i A^i_{MC}}_{\text{Pressure forces at catchment outlet}} \quad (6)$$

where, ρ is the density of water [M T^{-3}], A^j_{MC} is cross-sectional area in an upstream or downstream reach j [L^2], L^i is reach length of REW i [L], g is gravitational acceleration [L T^{-2}], $\sin\gamma^j$ is the mean slope of REW i, P^i is average wetted perimeter of local REW i [L], h^i is the mean depth of REW i [L], ζ^i is the Darcy-Weisbach friction coefficient ($\zeta^i = 8g\,(n^i)^2 (R^i)^{-1/3}$, n^i is a roughness coefficient and R^i is the hydraulic radius), and δ^{ij} is the angle of confluence of upstream reach j and local reach i. In Equation 6, when reach j is upstream of reach i, the sign in front of the pressure force term is generally + and is – when reach j is downstream of reach i. The last item in Equation 6 will remain only if the local reach is directly upstream of the outlet. As the influence of the confluence angle on the resulting velocity is very small, we assume it is equal to 1 (unity) and remove it without loss of accuracy. In this paper, for simplicity we ignore the inertia term in the momentum equation and we obtain the simplified equation for velocity as follows:

$$v^i = \frac{1}{n^i} \sqrt{\frac{(R^i)^{1/3}}{P^i L^i} \left(A^i_{MC} L^i \sin\gamma^i \pm \sum_{j\neq i} \frac{1}{4} h^i (A^i_{MC} + A^j_{MC}) - \frac{1}{2} h^i A^i_{MC}\right)} \quad (7)$$

4.2.3 Specification of hydraulic geometry

The size of the TS zone is directly related to the wetted perimeter of the channel, and so to accurately simulate the retention rate in TS, it is necessary to adequately represent the hydraulic geometry of the channel. The hydraulic geometry is also crucial to capture the space-time variations of flow velocity that ultimately determines the water residence time in the river reaches. An extensive survey of at-a-site and downstream hydraulic geometry has been carried out for Illinois streams by Stall and Fok (1968). They obtained best fits between measured top width, flow depth, velocity and cross sectional area as power functions of flow frequency and drainage area for several streams in Illinois. The relations for top width and flow depth extracted from the results of Stall and Fok (1968) are as follows:

$$\ln w^{i}_{\text{top}} = -1.23 + 0.27 \ln A^{i}_{MC} + 0.18 \ln A_d{}^{i} \tag{8a}$$

$$\ln h^{i}_{MC} = 1.23 + 0.73 \ln A^{i}_{MC} - 0.18 \ln A_d{}^{i} \tag{8b}$$

where w^{i}_{top} is the top-width of reach i [L], h^{i}_{MC} is the mean depth of reach i [L], A^{i}_{MC} is the cross-sectional area of reach i [L^2], and $A_d{}^{i}$ is the total contributing (drainage) area for the outlet at reach I [L^2]. We use these regionalized equations to construct the hydraulic geometry across the network of the Little Vermilion River catchment. Previous versions of the THREW model assumed the channel cross-sectional area to be rectangular (Tian, 2006; Li *et al.*, 2010; Li and Sivapalan, 2011). In this paper, in order to better characterize the wetted perimeter and channel flow velocity and solute transformations, especially under low flow conditions, the cross-section was changed from rectangular to trapezoidal. Model predicted magnitudes of flow velocity, both at-a-site and downstream, were tested and successfully verified against the corresponding regionalized estimates of Stall and Fok (1968) (not included here for reasons of brevity).

4.2.4 Network model of solute transport

The solute transport model is derived from the One-Dimensional Transport with Inflow and Storage model (OTIS) applicable to a single reach (Bencala and Walters, 1983; Runkel, 1998).

$$\frac{\partial C_{MC}}{\partial t} = -\frac{Q}{A_{MC}}\frac{\partial C_{MC}}{\partial x} + \frac{1}{A_{MC}}\frac{\partial}{\partial x}(A_{MC} D \frac{\partial C_{MC}}{\partial x}) + \frac{q_L}{A_{MC}}(C_L - C_{MC}) + \alpha(C_{TS} - C_{MC}) - k_c C_{MC} \quad (9a)$$

Advection; Dispersion; Lateral flux; Nutrient exchange; Uptake from MC

$$\frac{dC_{TS}}{dt} = \alpha \frac{A_{MC}}{A_{TS}}(C_{MC} - C_{TS}) - k_s C_{TS} \quad (9b)$$

Nutrient exchange; Uptake from TS

where C_{MC} is nitrate concentration within the MC [M L^{-3}], C_{TS} is concentration within the transient storage zone [M L^{-3}], C_L is the concentration of lateral inflow [M L^{-3}], A_{MC} is the cross section area of MC [L^2], A_{TS} is cross section area of TS zone [L^2], x is longitudinal distance [L], D is dispersion coefficient [L^2 T^{-1}], α is the exchange rate between the main channel and transient storage [T^{-1}], q_L is lateral inflow rate [L^3 T^{-1} L^{-1}], and k_c and k_s are the uptake rate coefficients for reactive solutes from the MC and the TS zones, respectively [T^{-1}]. This model considers nutrient advection and dispersion in the MC, but in the TS zone solutes are assumed well mixed and the flow velocity is slow enough not to account for flows in the longitudinal direction. The nutrient exchanges between the MC and TS zones are assumed to be proportional to the concentration gradient between the two compartments.

In the current study we seek to investigate nutrient transport at the network scale, across stream types and sizes, and during both low flow and high flow periods. Accordingly, we upscale the above model to the network scale, assuming that the effects of hydrodynamic dispersion are small and negligible compared to network dispersion (also known as geomorphologic dispersion) (see Robinson *et al.,* 1995 for a justification of this assumption), and the nutrient retention in the MC zone is a function of water storage and the average of the upstream inflow concentrations and the local concentration. Upscaling of the OTIS biogeochemistry equations (Equations 9a,b) to the network scale then leads to the following two coupled governing equations for a stream reach belonging to REW *i* (each reach is considered as individual segment to which Equations 9a,b are applied):

$$\frac{d(S^i_{MC}C^i_{MC})}{dt}$$

$$= \underbrace{Q^i_h C^i_h}_{\text{Hillslope input}} + \underbrace{\sum(Q^j_{up}C^j_{MC})}_{\text{Upstream inputs}} - \underbrace{Q_{out}{}^i C^i_{MC}}_{\text{Output}} - \underbrace{\alpha S^i_{MC}(C^i_{MC} - C^i_{TS})}_{\text{Nutrient exchange}} - \underbrace{k_c \frac{(C^i_{MC} + \sum C^j_{MC}/2)}{2} S^i_{MC}}_{\text{Water Column \& Benthic Uptake}} \quad (10a)$$

$$\frac{d(S^i_{TS}C^i_{TS})}{dt} = \underbrace{\alpha \frac{A_{MC}}{A_{TS}} S^i_{TS}(C^i_{MC} - C^i_{TS})}_{\text{Nutrient exchange}} - \underbrace{k_s C^i_{TS} S^i_{TS}}_{\text{Uptake from TS}} \quad (10b)$$

where C^i_{MC} is the concentration in the local channel [M L^{-3}], C^i_{TS} is the concentration within the transient storage zone [M L^{-3}], C^j_{MC} is the concentration in the upstream reach j [M L^{-3}], α is the exchange rate between the MC and TS zones [T^{-1}], S^i_{TS} is the volume of water in the TS zone [L^3] ($S^i_{TS} = L^i \; P^i \; h_{TS}{}^i$, L^i is the length of the reach, P^i is the wetted perimeter, and $h_{TS}{}^i$ is the depth of TS zone, which is assumed constant), and k_s is the uptake rate coefficient from TS zone [T^{-1}].

In this paper the model is implemented with k_c assumed to vary with flow depth, as $k_c = v_c/h$ (where v_c is the uptake velocity in MC [L T^{-1}], in analogy with the relationship often assumed between the first order retention rate and uptake velocity of the *combined system*: $k_e = v_f/h$). In the base experiment, decreasing k_c as a function of flow depth, h, assumes that uptake/removal on benthic biofilms dominates MC retention. There is a possibility that pelagic uptake could increase in the downstream direction, in which case the k_c would not decrease with increasing depth; however in the absence of empirical evidence on pelagic uptake, we decided not to include this scenario here. Detailed theoretical and field investigations to quantify this impact could be important for future study. The uptake velocity in MC (v_c) and uptake coefficient in TS (k_s) are assumed to follow first order kinetics (as in Wollheim *et al.*, 2006). Since the goal here is to examine the impact of hydrologic variability on nutrient retention and because limited data are available for the scaling of MC and TS uptake metrics from headwater to higher order reaches v_c and k_s are set at constant values across the catchment. As data evidence and process formulations advance, these aspects can be improved in subsequent versions of the model.

4.2.5 Climate and nitrate inputs

In the research that is reported in this paper, the coupled model is driven by stochastic precipitation inputs that are generated by a stochastic event rainfall model developed by Robinson and Sivapalan (1997). In order to explore the effects of flow variability on net retention, we constructed three different rainfall scenarios (consisting of 10-year long synthetic time series), and simulated the coupled hydrological and nutrient transport processes within the stream network under each scenario. For illustration we have denoted these as Climates 1, 2 and 3: Climate 1 (low variability), Climate 2 (intermediate), and Climate 3 (high variability). The rainfall series are a function of storm duration, t_r, inter-storm period, t_b, and mean rainfall intensity, p. The storm duration, t_r and inter-storm period, t_b are assumed to follow exponential probability density distributions, and their mean values vary sinusoidally with time of year ($t = T+A.\sin[2\pi/(\xi- \xi_r)/ \omega]$, where t represents the mean value for the exponential distribution (for t_r or t_b) for a given time period within the year, T is the corresponding annual average value (annual mean of t_r, t_b), A is the amplitude of the seasonal variation, ω is the total number of time units in a year (here 8760 hours per year), ξ is the time within the year, and ξ_r is the seasonal phase shift); the precipitation intensity (p) is statistically dependent on t_r, its conditional distribution (given t_r) follows a gamma distribution, as the parameters of this gamma distribution are also a function of t_r, the mean p of the gamma distribution also varies sinusoidally like t_r and t_b. All three climates share the same seasonality (the amplitude, A and the phase shift ξ_r), in which rainfall occurs during the spring and fall seasons and similar annual precipitation (~1000 mm per year) but distinct annually averaged storm duration, t_r inter-storm period, t_b and rainfall density, p. The details of the model are given in Robinson and Sivapalan (1997).

The annual mean value of these characteristics of rainfall inputs are presented in Table 4.1 for the three climates. There has been no attempt to match any of these climatic inputs, including annual rainfall and potential evaporation totals, their intra-annual variability and the statistical characteristics of storm events to climatic conditions prevailing in the Little Vermilion River catchment. All simulations used a hillslope residence time, τ_h, of 100 hours, and evaporation time scale, τ_e, of 100 hours. Figure 4.3 presents, as illustration, the time series of

precipitation inputs for Climate 2. Except when the focus of the analysis is on comparisons between different climate scenarios, most of the results presented in subsequent sections relate to Climate 2, with the mean annual water balances as follows: ET/P = 0.50, Q/P = 0.50, Q_b/Q = 0.22 (P, ET, Q and Q_b are, respectively, annual precipitation, evaporation, total runoff, and baseflow). These are not meant to be exact reproductions of the water balance of the Little Vermilion River catchment; nevertheless, they are representative of well-drained agricultural basins in much of Mid-western United States.

Table 4.1: Effects of hydrological variability and geomorphologic and biogeochemical factors on nitrate net retention rates during high and low flows

	Climate 1			Climate 2			Climate 3		
Mean t_r (hr)	34			34			15		
Mean t_b (hr)	76			186			227		
Mean p (mm/hr)	0.4			0.8			2.0		
Mean CV(Q) of headwater streams	2.08			3.01			3.44		
CV(Q) of outlet stream	2.01			2.92			3.32		
	Whole year	During high flows	During low flows	Whole year	During high flows	During low flows	Whole year	During high flows	During low flows
k_e when k_c decreases, TS depth constant(/hr)	0.0135	0.012	0.0217	0.0116	0.0103	0.0185	0.0112	0.0101	0.0185
k_e when k_c decreases , TS depth increases downstream(/hr)	0.0214	0.0202	0.0326	0.0179	0.017	0.0267	0.017	0.0163	0.0263

Nitrate concentrations of hillslope contributions to the river channels are kept constant in space and time at a notional value of 15 *mg* NO_3-N/*l* during both flood events and baseflow periods, which is the mean concentration of observed tile drain data in Little Vermilion catchment. Low temporal variability in nitrate concentrations relative to that of water discharge

in intensively managed agricultural catchments (i.e., chemostatic export) has been discussed in recent papers (Basu *et al.*, 2010; Thompson *et al.*, 2011; Guan *et al.*, 2011).

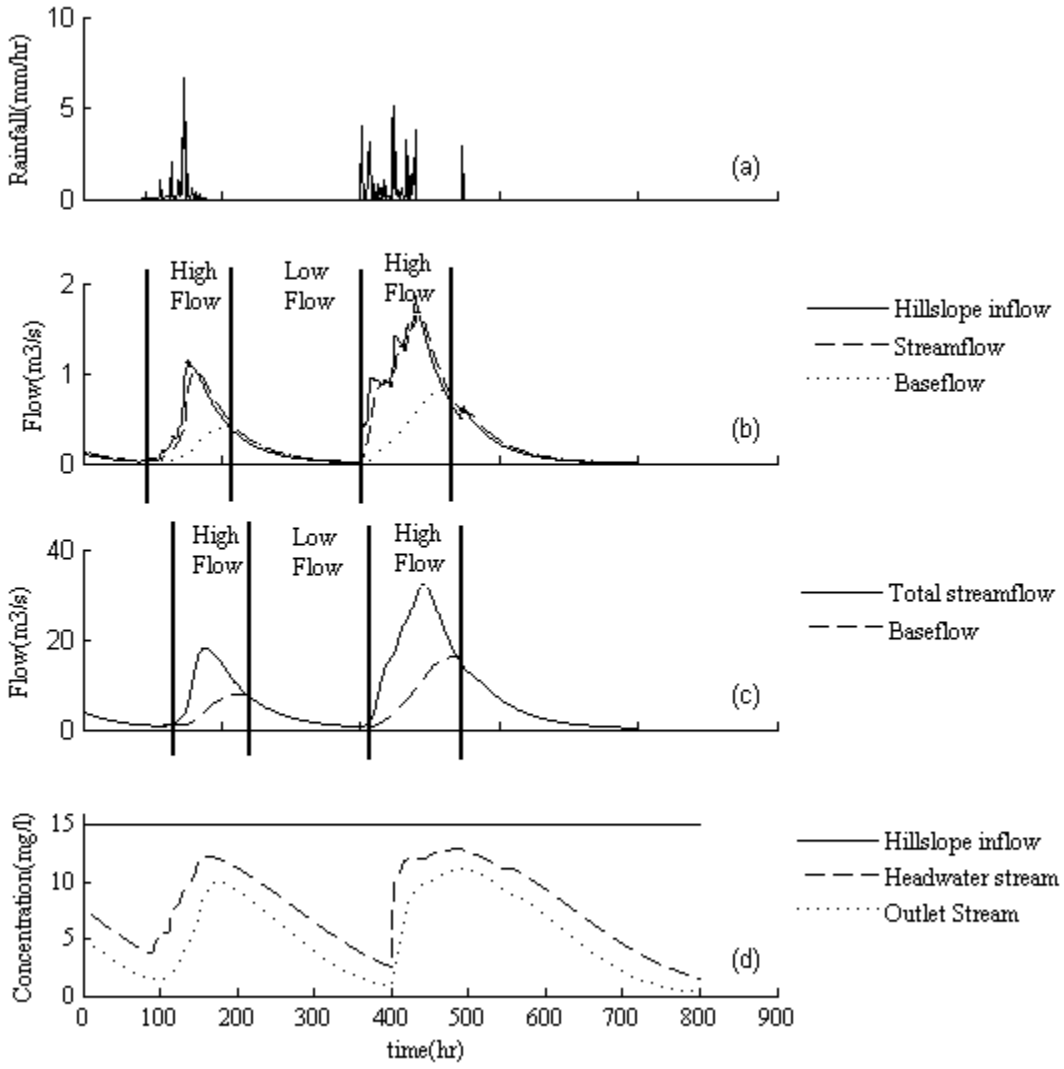

Figure 4.3: Schematic describing typical time series of rainfall, hillslope inflows and sreamflows and nutrient concentrations for Climate 2 (see Table 4.2): (a) rainfall event patterns - intensity=0.8mm/hr, tr=34hr, tb=186hr; (b) hillslope inflows and streamflow for a headwater stream; (c) streamflow at the catchment outlet, and illustration of flow separation into high flow and low flow periods; (d) nutrient concentration of hillslope input (assumed constant at 15 mg NO3-N/l), and for a 1st order REW and at the catchment outlet.

Parameters associated with the solute transport processes within the coupled model are also assumed to remain constant in space and time. Our assumed first-order kinetic model precludes any dependence on background nitrate concentrations (O'Brien *et al.*, 2007; Covino *et al.*, 2010b) and dependence on other environmental variables such as temperature are also ignored for the present. The parameter values are notional literature values chosen from a survey of field measurements, as shown in Table 4.2 (Runkel, 2000; De Smedt *et al.*, 2005; Hall *et al.*, 2009b; Stewart *et al.*, 2011). Default values of the nutrient uptake parameters used in this study are: v_c = 0.002 m hr^{-1}, k_s=0.2 hr^{-1} and α = 0.1 hr^{-1}. According to Stewart *et al.* (2011), the ratio of the size of the hyporheic TS zone to that of MC is 0.35, which is an average value for the Ipswich River network in Massachusetts. In this paper, in the default case, the thickness of the TS zone is held constant throughout the network at a value of 0.06 m; for a typical first order reach this produces a mean A_{TS}/A_{MC} = 0.35, which is consistent with Stewart *et al.* (2011).

Table 4.2: The literature sources for the parameter values chosen

Parameter	***Value in base experiment***	***Sources***
v_c	0.002 m/hr	0.001 - 1.07 (Hall *et al.*, 2009a)*[1]
α	0.1/hr	0.036 – 3.6 (De Smedt *et al.*, 2005)
k_s	0.2/hr	0.01 – 7.2 (Runkel, 2000)
TS depth constant	thickness=0.06m	makes A_{TS}/A_{MC}~0.35 for a 1st order REW
TS depth increases downstream	A_{TS}/A_{MC}=0.35	(Stewart *et al.*, 2010)

*1 These only refer to the uptake velocity of the whole stream v_f; the range of values for v_c used n this paper are smaller.

In this paper, we explore the effects of MC contributions as opposed to TS dominance of uptake and retention processes. As part of the sensitivity analysis presented later in the paper, we will also consider two scenarios in which MC and TS contributions are roughly equivalent and where the MC contribution is larger than TS through the use of larger v_c values and smaller k_s values. Each scenario is simulated for a 10-year period, and the initial nutrient storages in MC and TS are assumed to be zero (i.e., there is no nutrient stored at the beginning of the simulation). These sensitivity analyses are carried out to verify that the extent of emergent scaling effects

extracted from the simulations are not fundamentally altered by the range of parameter values used here.

4.3 Results

With the use of the coupled hydrological-solute-transport model we explore the richness of variability of nutrient retention process in space and time. In the time domain, we characterize the within-year variability by partitioning the year into event-driven high flow and subsequent low flow periods. In the space domain we partition the river reach into two zones: the main channel (MC) and the transient storage (TS). We begin the analysis in first order catchments (REWs), and systematically extend the analysis of the above partitioning, in a nested manner, to all higher order catchments, including the highest order catchment at the outlet.

Figure 4.3 illustrates the manner in which we partition the year into high flow and low flow periods. It presents the synthetic time series of precipitation for Climate 2, and the corresponding model predicted hillslope inflows (at a constant concentration of 15 *mg/l*), and streamflows and nitrate concentrations for a first order stream (REW 24), and for the stream at the catchment outlet. We use the baseflow separation algorithm of Lyne and Hollick (1979) to partition the time series of flows in all river reaches, into separate event-associated high flow periods and subsequent low flow periods, as shown in Figure 4.3. This allows us to estimate the magnitudes of nitrate loading (inputs), retention and export separately during event (high flow) and inter-event (low flow) periods, for all streams of all orders, and also at the catchment /network scale by aggregating the estimates for all streams that lie within each nested catchment. We repeat the same analyses to estimate the separate contributions to retention by the MC and TS zones. The results are presented next.

4.3.1 Breakdown into high flow and low flow periods, and between MC and TS zones

Figure 4.4 presents the partitioning of the total nitrate inputs between high flow and low flow periods (in this and all subsequent cases the results are annual averages based on 10-year long simulations). In the case of the MC zone, the inputs are loadings from the hillslopes. In the case of the TS zone the inputs are exchanges from the MC zone, which are governed by differences in nutrient concentrations between the two zones. Because the nutrient concentration of hillslope

inflows is constant, loading into the MC during high flows is larger (~3 times) than during low flow periods (Figure 4.4). Regardless of the simplifying assumption of constant concentration of hillslope inflows, the result in terms of loading is consistent with previous research that also has indicated large magnitudes of nutrient loading during high flow periods (Royer *et al.*, 2006). On the other hand, in the case of the TS the differences between high and low flow periods is much less, since the effect of the concentration gradients is modulated by differences in residence time.

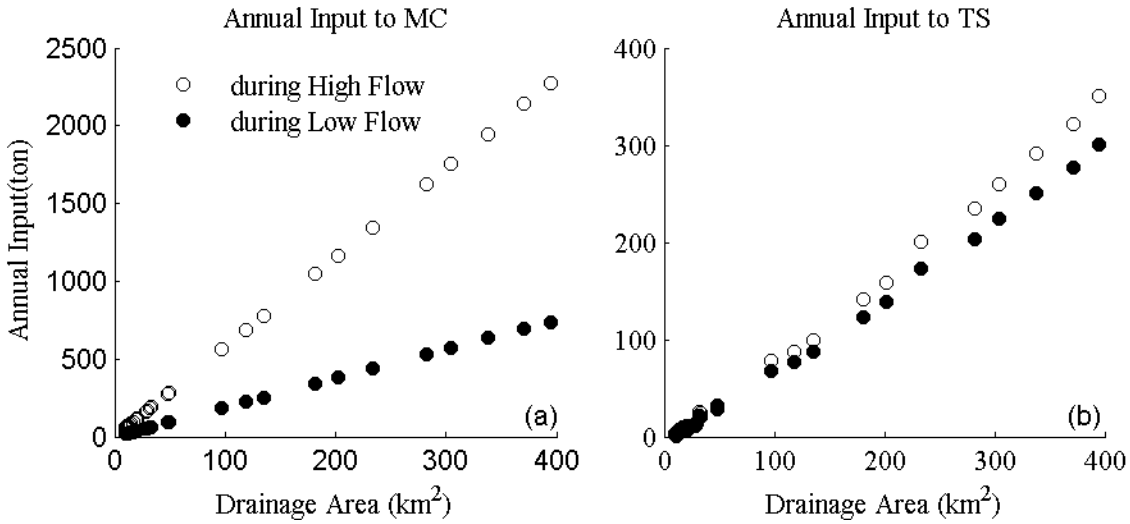

Figure 4.4: (a) Hillslope inputs into the MC zone as a function of drainage area, separately during high flow and low flow periods, respectively; (b) exchange of nitrate from the MC zone into the TS zone, separately during high flow and low flow periods, respectively, as a function of catchment size.

We next present the corresponding results for bulk retention during high flow and low flow periods separately for the MC and TS zones, as well as for the combined system (see Figure 4.5). We define the fractional retention as the ratio of nitrate retained in a certain zone during a certain period versus the total retention that occurs in both MC and TS zones through the year. For example, $f_{h\text{-}MC}$ is the percentage of nitrate retained in MC during high flow versus the total retention in both MC and TS zones annually. The calculation of the fractional retention during high flow and low flow periods is as follows:

$$f_{h-MC} = \frac{\sum_i \int_{T_h} k_c C^i_{MC}(t) S^i_{MC}(t) dt}{\sum_i \int_T (k_c C^i_{MC}(t) S^i_{MC}(t) + k_s C^i_{TS}(t) S^i_{TS}(t)) dt} \qquad (11a)$$

$$f_{l-MC} = \frac{\sum_i \int_{T_l} k_c C^i_{MC}(t) S^i_{MC}(t) dt}{\sum_i \int_T (k_c C^i_{MC}(t) S^i_{MC}(t) + k_s C^i_{TS}(t) S^i_{TS}(t)) dt} \qquad (11b)$$

where $f_{h\text{-}MC}$ is the fractional retention in MC during high flow, $f_{l\text{-}MC}$ is the fractional retention in MC during low flow period, T_h is the duration of high flow period [T], T_l is the duration of low flow period [T], and T is the total simulation period [T].

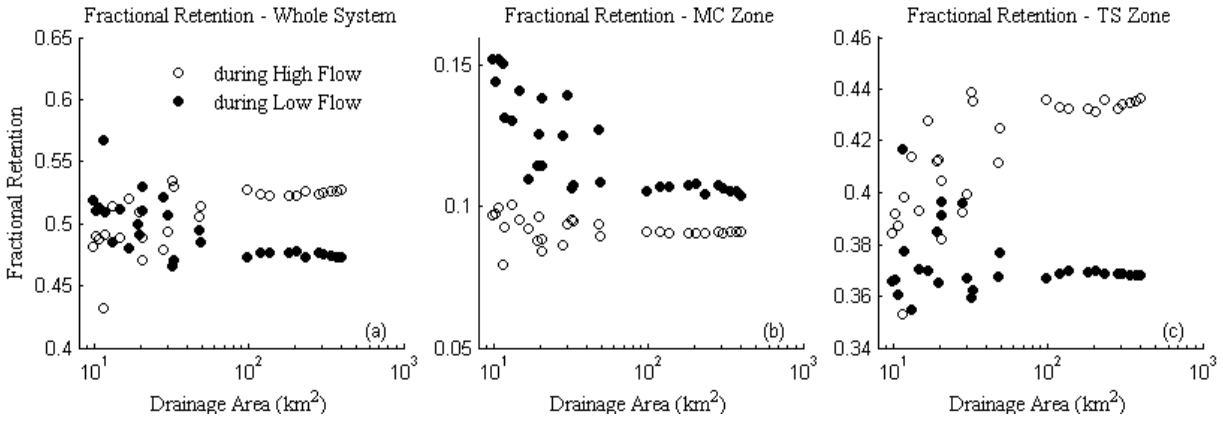

Figure 4.5: Fraction of retention separately during high flow and low flow periods, respectively, as a function of drainage area: (a) from the combined system (MC and TS zones together); (b) from the MC zone only; and (c) from the TS zone only.

The results for fractions retained presented in Figure 4.5 indicate that even though the bulk loadings from hillslopes are vastly different during the two flow periods (e.g., 3.5 times larger during high flows, as shown in Figure 4.4), the magnitudes of the fractions retained are much closer in all three cases (certainly not 3.5 times different); the respective fractions (i.e., fractions of the total amounts of retention that occurred during the two periods) fall in the range 0.4-0.6. The retention fraction in the MC zone in the range 0.08-0.15 is much smaller than in the TS zone (in the range 0.35-0.45). We also find that in the case of the MC zone, the fraction

retained during high flow periods is low (0.1) and remains invariant with drainage area, whereas the fraction retained during low periods decreases with increasing drainage area. The situation is reversed in the TS zone: the fraction retained during high flows increases with increasing catchment area in the TS zone and remains invariant with drainage area during low flow periods. These trends are similar to trends presented by Wollheim *et al.* (2008). In all three cases, despite the sharp discrepancies in hillslope loading between high flows and low flows, the differences in the actual retention are much smaller.

This compensation in fractional retention could be related to the retention efficiency: it may be higher during low flows, and lower during high flows. We will now look at the corresponding results for retention efficiency in more detail. The retention efficiency is defined as the ratio between the nitrate retained in MC or TS zone during high or low flow period and the total nitrate load from the hillslope during the high or low flow period. Figure 4.6 presents the estimated retention efficiencies at the catchment scale separately for the MC and TS zones, as well as for the combined system. The calculation of the retention efficiency in the MC zone is as follows:

$$Eff_{h-MC} = \frac{\sum_i \int_{T_h} k_c C^i_{MC}(t) S^i_{MC}(t) dt}{\sum_i \int_{T_h} C^i_h(t) Q^i_h(t) dt} \qquad (12a)$$

$$Eff_{l-MC} = \frac{\sum_i \int_{T_l} k_c C^i_{MC}(t) S^i_{MC}(t) dt}{\sum_i \int_{T_l} C^i_h(t) Q^i_h(t) dt} \qquad (12b)$$

where $Eff_{h\text{-}MC}$ is the retention efficiency within MC during high flow periods, $Eff_{l\text{-}MC}$ is the retention efficiency within MC during low flow periods. The method for the calculation of retention efficiencies in the TS zone is similar. Figure 4.6 demonstrates that the retention efficiency during low flows is about three times higher than during high flows, in all three cases (whole system, as well as separately in the MC and TS zones), consistent with previous research that has noted that nitrate retention is most efficient during low flow periods (Alexander *et al.*, 2009). In all cases, the retention efficiency at the catchment scale is shown to increase with

increasing drainage area. These results indicate that although the nitrate loading from hillslopes during high flows is over three times higher than during low flows (see Figure 4.4), the much smaller retention efficiencies during high flows (i.e., about a third of that during low flow) nearly compensates for the differences in hillslope loadings giving rise to somewhat equivalent values for fractional retention during high and low flow periods, as shown in Figure 4.5 above.

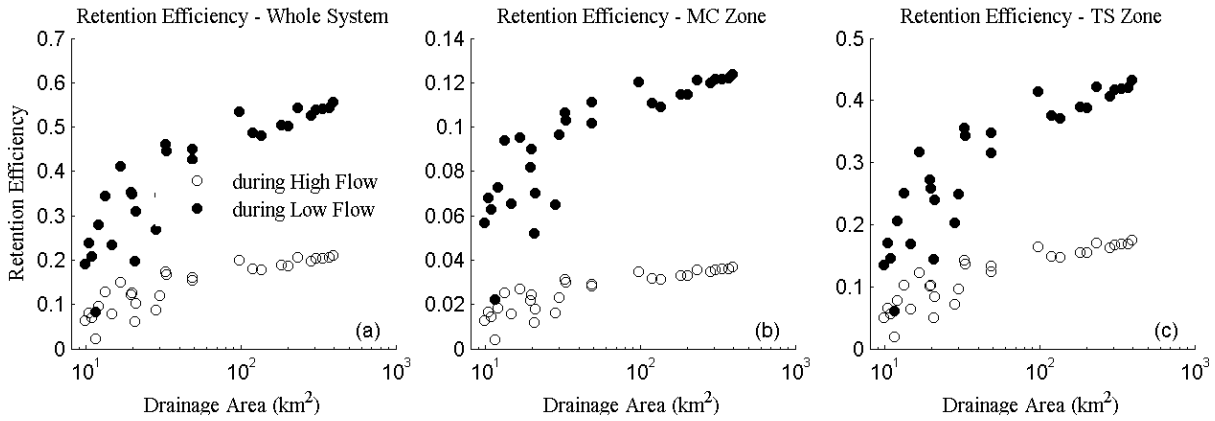

Figure 4.6: Retention efficiency estimated separately during high flow and low flow periods, respectively, as a function of drainage area: (a) from the combined system (MC and TS zones together); (b) from the MC zone only; and (c) from the TS zone only.

We further investigate the differences between the two sets of retention efficiencies, and if these can be explained by recourse to estimates of three different timescales: residence time in the main channel (τ_{MC}), nitrate reaction time in the MC zone (SRT-MC) and in the TS zone (SRT-TS). Following Stewart *et al.* (2011) and Botter *et al.* (2010), as a first attempt, we define these timescales for each REW as follows (using previous notation):

$$\tau_{MC} = L/v \tag{13a}$$

$$\text{SRT-MC} = h/v_c \tag{13b}$$

$$\text{SRT-TS} = \frac{A_{MC}/A_{TS} + k_s/\alpha}{k_s} \tag{13c}$$

The corresponding timescales at the network scale are defined as follows:

$$T^i = \tau^i w^i + \sum T^j w^j \quad (14a)$$

where $$w^i = A^i / A_d^i \quad (14b)$$

and $$w^j = A_d^j / A_d^i \quad (14c)$$

where T^i is the total time within REW i, T^j is the total time within all upstream REWs j, τ^i is the time within each reach (which can be either τ_{MC}, SRT-MC or SRT-TS as per Equations 13a,b,c), w^i is the weight for each component (which is related to the respective areas of the REWs), A^i is the area of REW i, A_d^i is the drainage area of current REW i, and A_d^j is the drainage area of the upstream reach j. We would expect the respective ratios of water residence time to solute reaction time (Damkohler number (Da), Ocampo *et al.*, 2006) to provide a first order indication of the efficiency of retention in both the MC and TS zones. Since the water exchange between MC and TS is assumed small enough to ignore in the paper, water residence time related to nutrient uptake in the TS zone is therefore assumed to be the same as in MC (τ).

For the reason of brevity, we will not show detailed results of the network scale residence times or the reaction times (calculated from Equation 14) here. The trends in these numerical results are that the residence time during low flows is larger than during high flows for all catchment sizes, while the reaction times in the MC zone, SRT-MC, and in the TS zone, SRT-TS, show an opposite trend in that the reaction times are much larger during high flows than during low flows. This suggests larger ratios of residence times to reaction times (i.e., the Damkohler number Da), i.e.,, higher efficiencies during low flow periods than during high flow periods. The shorter reaction time in TS zone than in the MC zone leads to a larger Damkohler number in TS zone, i.e., higher (roughly 2 to 4 times) retention efficiency in the TS zone than in the MC zone (Figure 4.6). This explains the much larger fractional retention by TS than by MC zone shown in Figure 4.5 (about 4.5 times greater during high flow and 2.5 times during low flow).

4.3.2 Effects of within-year hydrologic variability on retention efficiency

The results presented so far indicate significant differences between the loadings and retention efficiencies between high and low flow periods, including the relative contributions of the MC and TS zones to the overall nitrate retention processes. One can therefore foresee that intra-

annual streamflow variability, i.e., the strength of fluctuations of streamflows between high flows and low flows, can significantly impact net retention and overall retention efficiency at the catchment (space) scale and annual timescale. In order to assess the net effect of within-year hydrologic variability we constructed three different rainfall scenarios and implemented the coupled model under each of these scenarios in Monte Carlo fashion. Summary statistics for the rainfall inputs and for the resulting streamflows are presented in Table 4.1, where we quantified the intra-annual variability of flows in terms of the coefficient of variation, *CV(Q)*. The concentrations of nitrate inflows from hillslopes are still maintained at 15 NO_3-N*mg/l* throughout the year.

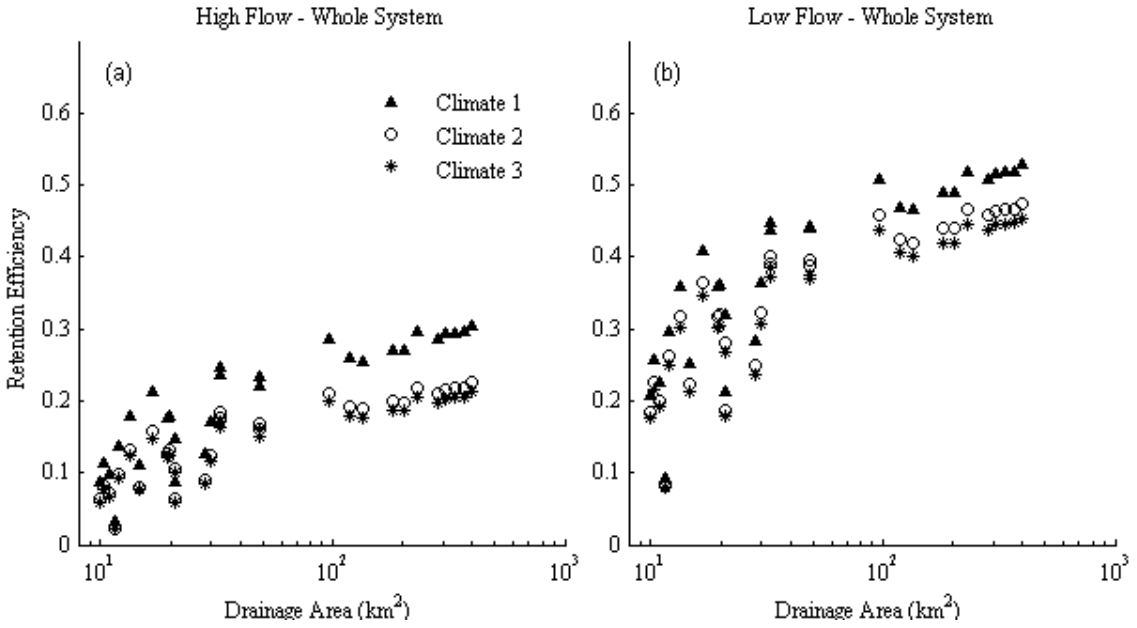

Figure 4.7: Catchment scale retention efficiencies as a function of drainage area for Climate 1 (p=0.4mm/hr, t_r=34hr, t_b =76hr), Climate 2 (p=0.8mm/hr, t_r=34hr, t_b=186hr) and Climate 3 (p=2.0mm/hr, t_r=15hr, t_b =227hr) for the whole system (MC and TS): (a) High Flow Periods, (b) Low Flow Periods.

Figure 4.7 presents the variation of retention efficiencies (nitrate retained during high/low flow periods in MC/TS zone as percentage of total loading during those periods) as a function of catchment size for the three different climates considered (note that retention efficiency is the ratio of retention to net loading from the hillslopes). The results for the whole system (i.e., MC and TS zones together) indicate that the increase of hydrologic variability, as represented in the

three climate scenarios, with Climate 3 being most variable, leads to a reduction of retention efficiencies in the combined system, during high flow periods.

4.3.3 Scale effects: relative roles of biogeochemical and geomorphologic factors

So far we have explored the partitioning of retention fractions between high flow and low flow periods, and the breakdown of the contributions of the MC and TS zones to total retention. The analyses have revealed that ultimately these can be explained in terms of retention efficiencies and a competition between residence times and reaction times. Along the way, we also discovered that the richness of distribution of bulk uptakes and retention efficiencies also systematically change with increasing catchment size.

The default parameterizations that we have adopted in the simulations so far have assumed that the thickness of the TS zone is constant across the entire network. In view of the demonstrated importance of the TS zone, what impact does this assumption have on the scaling behavior of nutrient retention? Similarly, we have assumed that the uptake rate in the MC zone is equal to $k_c=v_c/h$. By making this assumption, we are ensuring that the nutrient retention in the MC zone becomes less efficient as we move from headwater streams to the much deeper, higher order streams. Although the plankton in the water column also contributes to the nutrient retention, given the relatively shallower water column and shorter residence time available for uptake, it is relatively minor compared to the benthic uptake. Therefore in this paper we will focus on the impact of the TS depth. These are important questions because there is as of yet very little empirical evidence for these rather strong assumptions: whether the thickness of the TS zone remains constant downstream or increases with the increase in the spatial scale. In order to generate insights into their relative effects on the predicted scaling behavior, we carried out a new set of simulations where we allowed the thickness of the TS zone to increase in the downstream direction, in such a way as to maintain a constant A_{TS}/A_{MC} ratio at a value of 0.35 (Briggs *et al.* 2010).

Figure 4.8 presents a comparison of two events (approximately 25 days) in the 10-year long time series of retention rates from the MC and TS zones, corresponding to Climate 2, and

for two different scenarios: (a) thickness of TS remains constant across the network, (b) thickness of TS increases in downstream direction (A_{TS}/A_{MC} is held constant at 0.35) while in both scenarios, v_c is held constant at 0.002 m hr^{-1}. This part of the model sensitivity analyses with respect to the size of the TS zone is summarized in the top half of Table 4.3. The results are presented for a headwater stream and for the stream at the catchment outlet. The results indicate that, for varying k_c ($k_c=v_c/h$, v_c=constant), increase of A_{TS} in the downstream direction leads to much higher retention from the TS zone with increasing catchment size: the retention rate at the outlet stream increases from around 7 kg/hr to 12kg/hr when A_{TS} becomes larger in the downstream direction (Figure 4.8b and d) while the retention rate in MC does not change.

Table 4.3: Summary of different scenarios simulated in sensitivity analyses involving combinations of climate, geomorphology and biogeochemistry

		Climate 1	**Climate 2**	**Climate 3**
Impact of TS depth	**TS depth constant**	Low streamflow variability, TS depth constant with TS dominance	Intermediate streamflow variability, TS depth constant with TS dominance (base experiment)	High streamflow variability, TS depth constant with TS dominance
	TS depth increases downstream	Low streamflow variability, TS depth constant with TS dominance	Intermediate streamflow variability, TS depth constant with TS dominance	High streamflow variability, TS depth constant with TS dominance
Impact of v_c, k_s	**TS dominant (v_c =0.002m/hr, k_s =0.2/hr)**		Intermediate streamflow variability, TS depth constant with TS dominance (base experiment)	
	MC, TS equivalent (v_c =0.002m/hr, k_s =0.05/hr)		Intermediate streamflow variability, TS depth constant with equivalent MC, TS dominance	
	MC dominant (v_c =0.02m/hr, k_s =0.2/hr)		Intermediate streamflow variability, TS depth constant with MC dominance	

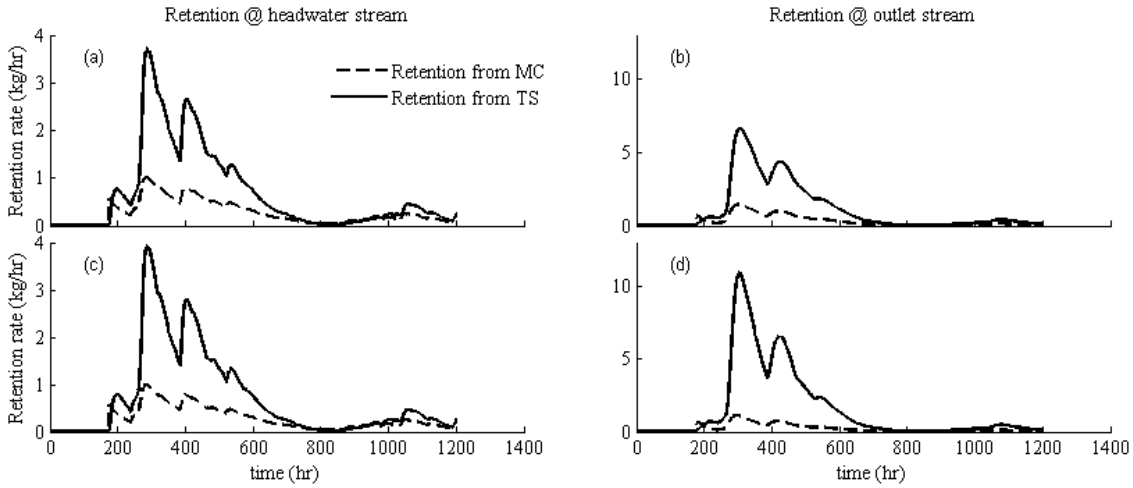

Figure 4.8: Schematic describing retention rates (from MC and TS zones) for two parameter combinations: Case 1 (a, b) – v_c maintained constant at 0.002m/hr, thickness of the TS zone maintained constant; Case 2 (c, d) – v_c maintained constant at 0.002m/hr, thickness of the TS zone increases in the downstream direction, with the ratio A_{TS}/A_{MC} maintained constant at 0.35: (a),(c) retention rates for a headwater stream; (b), (d) retention rates for the higher order stream at the outlet.

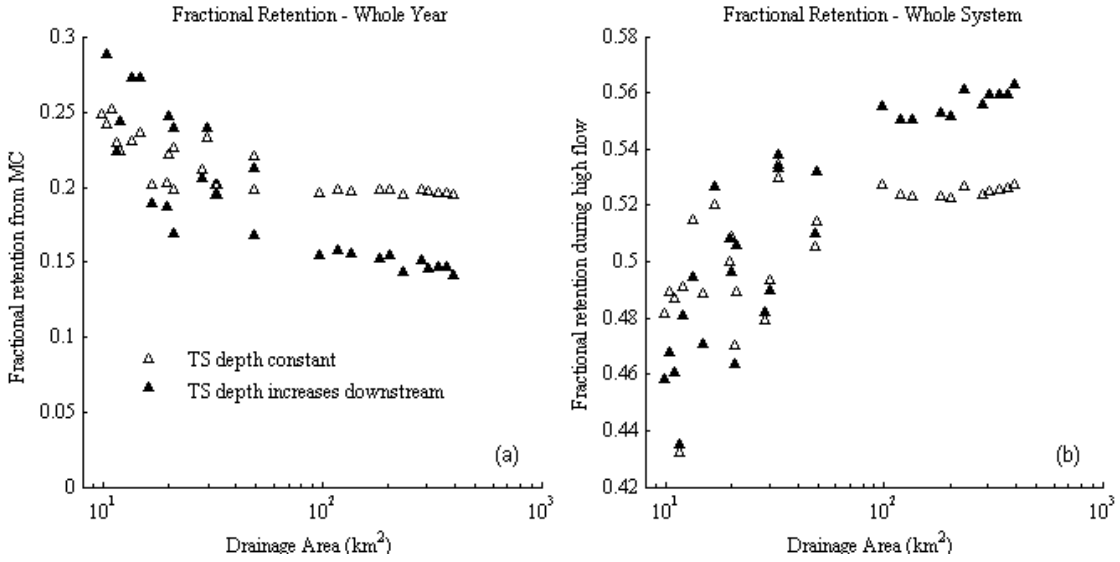

Figure 4.9: (a) Fractional retention from the MC zone over the whole year, (b) fractional retention during high flows over the combined system (MC and TS zones together), both as functions of drainage area. These results are presented two scenarios of A_{TS}/A_{MC} ratio: (i) A_{TS} constant, and (ii) A_{TS} increases downstream (A_{TS}/A_{MC}=0.35).

Figure 4.9 summarizes the results of this sensitivity analyses (i.e., with respect to the size of the TS zone, as summarized in the top half of Table 4.3) in terms of (1) the fraction contributed to total retention (over the whole year) by the MC zone, and (2) the fractional retention from the combined (MC and TS) system during high flow periods. The results in Figure 4.9a indicate that the fractional retention contributed by the MC zone is much less when the size of the TS zone is allowed to increase in the downstream direction. Figure 4.9b presents the corresponding results for the fractional retention during high flows for the combined system. When k_c decreases downstream, the assumption of variable TS size makes a bigger contribution to the fraction retained during high flows

4.4 Discussion of results

The results presented have demonstrated that there are substantial differences between nutrient retention rates during high flow and low flow periods. The differences are due to (i) variability in hillslope water and nitrate inputs, leading to differences in flow depth, velocity and nutrient concentration, and (ii) the differing roles and contributions from the MC and TS zones, leading to differences in retention efficiencies. Similar differences are observed between the contribution from MC and TS, which can be related to the parameters chosen in the simulations and the assumptions about the scaling affect arising from the parameters chosen (v_c and k_s). In the following we seek generalizable insights based on the use of the model, and manipulation of model predictions: reaction times (governed by both the solute transport properties, flow depth and the relative sizes of the MC and TS zones, which are indirectly affected by variable flow depths).

4.4.1 Effects of hydrologic variability: bulk parameterization based on timescales

In Figure 4.7 we demonstrated that within-year hydrologic variability can have a significant impact on net retention at the catchment scale, especially during high flow periods. In particular, increasing variability leads to decreasing retention efficiency. This can be attributed to faster velocities and hence shorter residence times, provided the reaction times remain relatively invariant.

The effect of hydrologic variability and the connection to residence times is illustrated in Figure 4.10. In this figure we first express the strength of retention for all three climate scenarios in terms of a catchment scale delivery ratio *DR* (1-Retention Efficiency), the percentage of nutrient exported. The delivery ratio *DR* estimated for the three climates is then presented as a function of residence time in the river network τ_{MC}, (in a semi-log plot), for the whole year as well as for the high flow and low flow periods. The results indicate that (i) there is an almost exponential relationship between *DR* and τ_{MC} (as reflected in the straight lines in the semi-log plots), and (ii) the slopes of the lines tend to decrease with increasing hydrologic variability, for all flow periods (Figure 4.10). This confirms that the first order control of *DR* (and hence the retention efficiency) is the residence time distribution. We then fitted the empirical *DR* vs τ_{MC} relationship to the following function: $DR = \exp(-k_e \tau_{MC})$, and estimated k_e, which can be deemed as a first-order rate coefficient k_e at the catchment scale, and can be seen as a net measure of nutrient retention. Estimated values of k_e for the three climates, during high and low flow periods, are presented in Table 4.1 and indicate that estimated k_e values decrease with increasing streamflow variability, and increases with the increment in TS zone size.

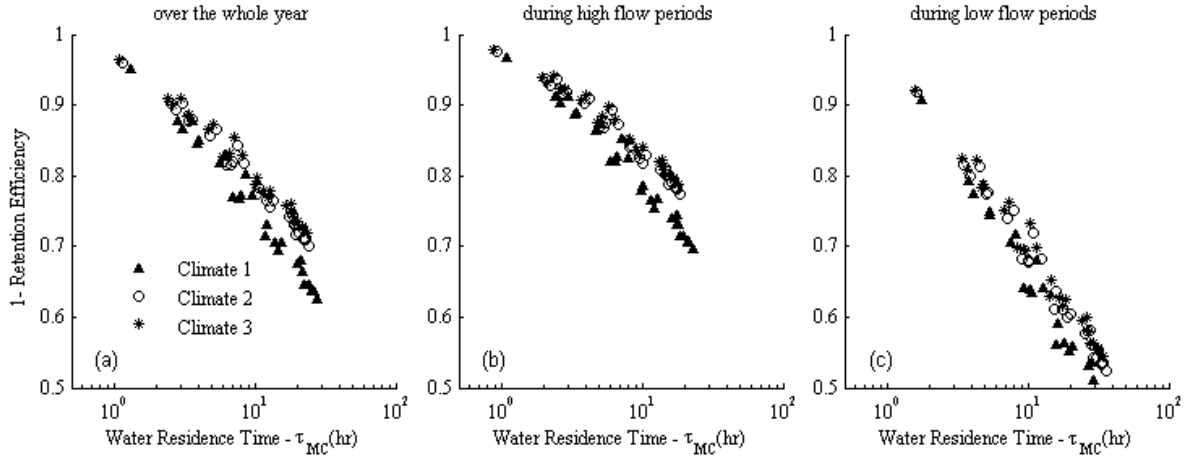

Figure 4.10: Catchment scale delivery ratio 1- Retention Efficiency as a function of weighted residence time τ_{MC} (as a surrogate for drainage area) for Climate 1 (p=0.4mm/hr, t_r=34hr, t_b =76hr), Climate 2 (p=0.8mm/hr, t_r=34hr, t_b=186hr) and Climate 3 (p=2.0mm/hr, t_r=15hr, t_b =227hr: (a) for the whole year; (b) during high flow periods; (c) during low flow periods.

4.4.2 Scaling effect: relative roles of nutrient uptake and geomorphologic factors

The results presented so far have demonstrated the importance of the ratio between water residence time and solute reaction time. Two factors that play important roles in governing the estimates of both residence and reaction times are the flow condition in the stream, and the relative magnitudes of the nutrient uptake parameters k_c and k_s, and how they change in time and space (across the river network). Flow state determines (a) velocity v, which governs residence time τ_{MC}, (b) flow depth h, which in combination with k_c governs reaction time in the MC zone, SRT-MC, and (c) the ratio A_{TS}/A_{MC}, with both A_{MC} and A_{TS} changing with the magnitude of flow, which together with k_c and k_s determines reaction time in the TS zone, SRT-TS.

Because of the paucity of consistent empirical data across diverse field experiments, we made several assumptions in the parameterizations chosen for the base experiment: (i) that the TS retention is more dominant than MC, through adoption of v_c =0.002m/hr and k_s =0.2/hr; (ii) that the benthic uptake and retention is dominant over pelagic uptake, by setting the retention rate in the MC to decrease with flow depth ($k_c = v_c / h$); (iii) that the TS depth is constant from headwater to outlet, by setting the TS depth to be constant at 0.06m. These assumptions are critical to understanding and interpreting the model results presented in Figures 4.8 and 4.9, and summarized in terms of the effective rate coefficient k_e in Table 4.1, since they are likely to impact the results of the base experiment and the effects of the three climate scenarios chosen.

In order to generate insights into these effects, we carried out sensitivity analyses with the model under a new set of scenarios, where (i) TS is the major contributor; (ii) the contributions from TS and MC are roughly equivalent; (iii) the retention from MC is more dominant. The combinations of parameter values chosen for each of these scenarios are presented in the bottom half of Table 4.3. Figure 4.11 presents the impacts of various combinations of v_c and k_s in terms of (1) the fraction contributed to total retention (over the whole year) by the MC zone and (2) the fractional retention from the combined (MC and TS) system during high flow periods. The results in Figure 4.11a indicate that with a smaller k_s or a larger v_c, the fractional retention from MC will increase equally across the entire network. Figure 4.11b presents the corresponding results for the fractional retention during high flows for the combined system. The combination with largest v_c and k_s values contributes to higher uptake and removal during high flow periods.

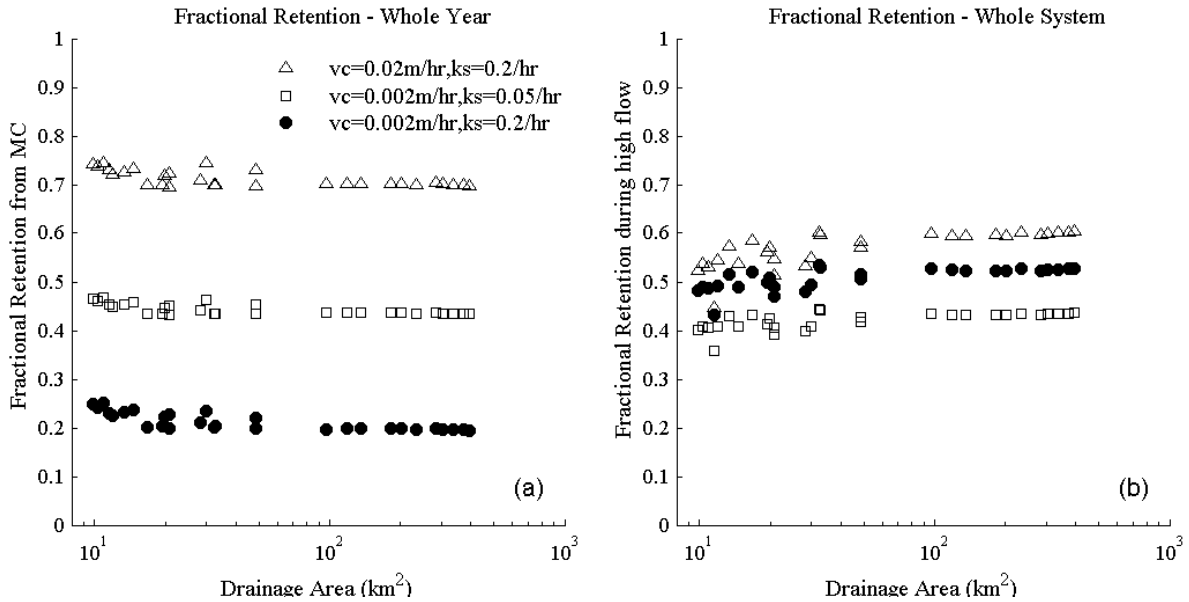

Figure 4.11: The three combinations of v_c and k_s impact on (a) Fractional retention from the MC zone over the whole year, (b) fractional retention during high flows over the combined system (MC and TS zones together), both as functions of drainage area. These results are presented for three different combinations of k_s and v_c: (i) MC dominant, v_c =0.02m/hr and k_s=0.2/hr, (ii) MC and TS are equivalent, v_c=0.002m/hr and k_s=0.05/hr, (iii) TS dominant, v_c =0.002m/hr and k_s=0.2/hr

The sensitivity analysis with respect to the combination of v_c and k_s values (Figure 4.11) demonstrates that although the magnitudes of contributions from MC and TS change with the different parameter combinations adopted, and the contribution of TS decreases with the retention rate in TS (k_s), the resulting change is uniform from headwater streams to the outlet. That is, the scaling effect of the MC and TS contributions remains, and so does the impact of hydrologic variability on the retention efficiencies during high flow and low flow periods in the MC and TS zones (details not presented here for brevity).

The sensitivity analysis with respect to the TS thickness indicates that the scaling effect of the contribution of MC can be amplified or attenuated by the TS zone thickness. For streams where benthic uptake is dominant, increasing TS zone thickness in the downstream direction adds further to the decrease in the fractional retention from the MC zone from headwater streams to the catchment outlet. These results suggest that, when considering nutrient retention at the catchment scale, especially when they include large rivers, the scaling of TS thickness in the downstream direction can be more important than the actual retention rate. Further experiments

and modeling need to be done to parameterize the effects of both the morphology and the biogeochemistry of the transient storage zone.

4.5 Conclusions

One of the main conclusions from this numerical modeling study is that, within the limitations of the model (for example, the assumption of first order kinetics), retention of dissolved nutrients during high flow periods can indeed be significant, and should not be ignored. For the parameter combinations used in this study, the total mass retained during high flows constitutes ~50% of the total annual retention. This is in spite of the much lower retention efficiencies during high flows compared to during low flow periods. This can be attributed to much larger loading during high flows, which overwhelms the reduced retention efficiency, and leads to an overall higher retention of total N mass in the system. This difference in nutrient load is quite significant in the MC zone but is much smaller in the TS zone since the residence time helps modulate the concentration gradients to limit the nutrient access to TS zone. While previous studies have focused primarily on the decrease in the nutrient retention efficiency during storm events, we showed for the first time that despite the reduced efficiency total mass retention is greater than during baseflow. This result is similar to the findings of Ensign *et al.* (2006) who noted strong ammonium retention during storm events in a coastal agricultural stream in North Carolina. This observation calls for increased focus on understanding nutrient dynamics during storm events.

Moreover, an important consequence of the retention during high flow periods is that the nature of within-year variability of streamflows can have a significant impact on the bulk retention, delivery ratio and retention efficiency. This is due to the differences between the rates of retention and the dominant retention mechanisms as streamflows change over the range from low to high flows. Our model simulations demonstrated that intra-annual streamflow variability does have a significant impact on retention rates at all scales: the more variable the streamflow is, compared to mean discharge, the less nitrate is retained in the channel network (i.e., greater export). A first order uptake rate estimated at the scale of the whole 3rd order network, k_e, was seen to decrease with increased streamflow variability. While the importance of intra-annual variability has already been highlighted in previous studies (i.e., Wollheim *et al.* 2008*;* Botter *et al*. 2010), and in particular the companion paper by Basu *et al.* (2011), the results presented in

this paper for the first time quantify this effect by systematically simulating precipitation events of different frequencies and intensities. Climate change is forecast to alter the rainfall frequencies and intensities more severely than the mean values, contributing to increased within-year variability, which can translate to a reduction in nutrient removal efficiencies, thus exacerbating critical concerns about increased N export. Consequently, further investigations into the effect of the intra-annual rainfall variability on nutrient retention are critical.

Finally, the contributions of high flow periods to total annual bulk retention is further enhanced in large rivers, even as the efficiency of retention decreases from headwater to higher order streams, and to large rivers. This too can be explained through recourse to the increase of loading in larger rivers compared to headwater streams. We have demonstrated in this study for the first time that despite reduced efficiency in nutrient retention with river size, the total mass retention is greater in larger rivers thus necessitating increased focus on understanding nutrient dynamics in larger rivers. Further experiments focusing on nutrient spiraling in larger rivers are therefore critically needed (e.g., Tank *et al.*, 2008).

Clearly, there is considerable room for the model we presented here to be substantially improved. A recent review paper has highlighted key areas in which the current generation of nitrate cycling models at the river network scale needs to be advanced (Helton *et al.*, 2011). There is currently insufficient information and understanding to adequately constrain parameterizations (i.e. functional forms) of the various processes. For example, not much is known about the relative contributions of benthic and pelagic uptake, or the partitioning of retention between the TS and MC zones, their dependence on flow and environmental conditions (e.g., temperature, turbidity, nutrient concentrations, see: Covino *et al.*, 2010b), and how these processes scale across stream networks and flow states. Similarly, the conceptual approach we have adopted to simulate the effects of the TS zone is highly restrictive, and poses problems towards its parameterization. These call for further detailed field investigations in large rivers, during both low and high flow events.

We recognize that modeling gross retention of dissolved nitrogen in a stream network is simplistic, and processes like mineralization, groundwater inputs or the role of particulate nitrogen could also be important. A pseudo-steady state (inputs = outputs) during baseflow has

been observed in four southeastern small streams (Brookshire *et al.*, 2009), where uptake was compensated by remineralization and groundwater inputs. However, because of lack of adequate information (i.e. mineralization rates of N, concentration of groundwater recharge or concentrations of PON); here we have focused primarily on gross nitrogen retention. Gross nutrient retention has commonly been measured during baseflow periods in small streams, and very few studies have explored the effect of within-year streamflow variations on this metric as a function of spatial scale of observation. However, the model we presented here can be extended to study the questions on particulate vs. dissolved, organic vs. inorganic nitrogen, and gross nitrogen retention vs. mineralization in stream ecosystems in future studies. Given the importance of the impact of nutrient concentration on uptake, more field measurements quantifying the relationship between nutrient concentration and uptake within a single stream system at different catchment scales (e.g., Earl *et al.*, 2006; Covino *et al.*, 2010a; Covino *et al.*, 2010b) will be crucial for improving the ability of numerical models to simulate nutrient uptake over a range of nutrient concentrations. Finally, here we have chosen a simple bucket model to represent the hillslope contributions, where we arbitrarily assumed a constant concentration of hillslope inputs, which is clearly not realistic. A more sophisticated hillslope model with both hydrologic and biogeochemical components is needed, and is crucial to investigating the effects of land use changes on nutrient export. Clearly, these extensions are beyond the scope of the present modeling study, and are left for future research.

4.6 Acknowledgments

Work on this paper commenced during the Summer Institute organized at the University of British Columbia (UBC) during June-July 2009 as part of the NSF-funded project: *Water Cycle Dynamics in a Changing Environment: Advancing Hydrologic Science through Synthesis* (NSF Grant EAR-0636043, M. Sivapalan, PI). Thanks also due to Marwan Hassan and the Department of Geography of UBC for hosting the Summer Institute and for providing outstanding facilities. Work on the paper was also partially supported by NSF-Project: *Using Empirical and Modeling Approaches to Quantify the Importance of Nutrient Spiraling in Rivers* (Grant DEB-0922118, Jennifer Tank, PI).

References

Alexander, R. B., J. K. Böhlke, E. W. Boyer, M. B. David, J. W. Harvey, P. J. Mulholland, S.P. Seitzinger, C. R. Tobias, C. Tonitto, and W. M. Wollheim (2009), Dynamic modeling of nitrogen losses in river networks unravels the coupled effects of hydrological and biogeochemical processes, *Biogeochemistry, 93*, 91-116.

Algoazany, A. S. (2006), *Long-term Effects of Agricultural Chemicals and Management Practices on Water Quality in a Subsurface Drained Watershed*, PhD thesis, University of Illinois at Urbana-Champaign.

Basu, N. B., P. S. C. Rao, H. Winzeler, S. Kumar, P. Owens, and V. Merwade (2009), Parsimonious modeling of hydrologic responses in engineered watersheds: Structural heterogeneity versus functional homogeneity, *Water Resour. Res.*, 46 W04501, doi:10.1029/2009WR007803.

Basu, N. B., P. S. C. Rao, S. E. Thompson, N. V. Loukinova, S. D. Donner, S. Ye, and M. Sivapalan (2011), Spatiotemporal averaging of in-stream solute removal dynamics, *Water Resour. Res*., 47, W00J06, doi:10.1029/2010WR010196.

Bencala, K. E., and R. A. Walters (1983), Simulation of solute transport in a mountain pool-and riffle stream: a transient storage model, *Water Resour. Res., 19(3)*, 718-724.

Böhlke, J. K. , R. C. Antweiler, J. W. Harvey, A. E. Laursen, L. K. Smith, R. L. Smith, and M. A. Voytek (2009), Multi-scale measurements and modeling of denitrification in streams with varying flow and nitrate concentration in the upper Mississippi River basin, USA, *Biogeochemistry,* 93, 117–141.

Botter, G., N. B. Basu, S. Zanardo, P. S. C. Rao, and A. Rinaldo (2010), Stochastic modeling of nutrient losses in streams: Interactions of climatic, hydrologic, and biogeochemical controls, *Water Resour. Res*., 46, W08509, doi:10.1029/2009WR008758.

Briggs, M. A., M. N. Gooseff, B. J. Peterson, K. Morkeski, W. M. Wollheim, and C. S. Hopkinson (2010), Surface and hyporheic transient storage dynamics throughout a coastal stream network, *Water Resour. Res.*, 46, W06516, doi:10.1029/2009WR008222.

Brookshire, E. N. J., H. M. Valett, S. Gerber (2009), Maintenance of terrestrial nutrient loss signatures during in-stream transport, *Ecology*, 90, 293-299.

Claessens, L. and C. L. Tague (2009), Transport-based method for estimating in-stream nitrogen uptake at ambient concentration from nutrient addition experiments, *Limnol. Oceanogr.: Methods, 7,* 811-822.

Claessens, L., C. L. Tague, P. M. Groffman and J. M. Melack (2009), Longitudinal assessment of the effect of concentration on stream N uptake rates in an urbanizing watershed, *Biogeochemistry,* doi: 10.1007/s10533-009-9376-y.

Covino, T. P., B. L. McGlynn and R. A. McNamara (2010a), Tracer Additions for Spiraling Curve Characterization (TASCC): Quantifying stream nutrient uptake kinetics from ambient to saturation, *Limnology and Oceanography: Methods*, 8: 484 – 498.

Covino, T.P., B.L. McGlynn, and M.A. Baker (2010b), Separating physical and biological nutrient retention and quantifying uptake kinetics from ambient to saturation in successive mountain stream reaches, *Journal of Geophysical Research – Biogeosciences*, 115, G04010, doi: 10.1029/2009JG001263.

De Smedt, F., W. Brevis, and P. Debels (2005), Analytical solution for solute transport resulting from instantaneous injection in streams with transient storage, *J. Hydrol.*, 315, 25-39.

Dodds, W. K., A. J. Lopez, W. B. Bowden, S. Gregory, N. B. Grimm, S. K. Hamilton, A. E. Hershey, E. Marti, W. H. McDowell, J. L, Meyer, D. Morrall, P. J. Mulholland, B. J. Peterson, J. L. Tank, H. M. Valett, J. R. Webster and W. M. Wollheim (2002), N uptake as a function of concentration in streams, *J. N. Am. Benthol. Soc., 21(2)*, 206-220.

Donner, S. D., M. T. Coe, J. D. Lenters, T. E. Twine and J. A. Foley (2002), Modeling the impact of hydrological changes on nitrate transport in the Mississippi river basin from 1955 to 1994, *Global Biogeochemical Cycles, 16(3),* 1043, 10.1029/2001GB001396.

Dunn, D. D. (1996), Trends in nutrient inflows to the Gulf of Mexico from streams draining the conterminous United States 1972-1993. *US Geol. Surv., Water-Res. Invest. Rep.,* 96-4113. Austin, TX: US Geol. Surv. 60 pp.

Earl, S. R., H. M. Valett, and J. R. Webster (2006), Nitrogen saturation in stream ecosystems, Ecology, 87(12), 3140-3151.

Ensign, S. H. and M. W. Doyle (2006), Nutrient spiraling in streams and river networks, *J. Geophys. Res., 111*, G04009, doi:10.1029/2005JG000114.

Ensign, S.H., S. K. McMillan, S. P. Thompson, and M. F. Piehler (2006), Nitrogen and Phosphorus Attenuation within the Stream Network of a Coastal, Agricultural Watershed, *J. Environ. Qual.*, 35, 1237-1247.

Goolsby, D. A., W. A. Battaglin, B. T. Aulenbach, and R. P. Hooper (2000), Nitrogen flux and sources in the Mississippi River Basin, *Sci. Total Environ.*, 248, 75– 86.

Guan, K., S. E. Thompson, C. J. Harman, N. B. Basu, P. S. C. Rao, M. Sivapalan, A. I. Packman and P. K. Kalita (2011), Spatiotemporal scaling of hydrological and agrochemical export dynamics in a tile-drained Midwestern watershed. *Water Resour. Res.,* 47, W00J02, doi:10.1029/2010WR009997.

Hall, R. O., B. J. Peterson and J. L. Meyer (1998), Testing a nitrogencycling model of a forest stream by using a nitrogen-15 tracer addition, *Ecosystems*, 1, 283– 298.

Hall, R. O. Jr., E. S. Bernhardt and G. E. Likens (2002), Relating nutrient uptake with transient storage in forested mountain streams, *Limnol. Oceanogr., 47(1),* 255-265.

Hall, R. O. Jr. and J. Tank (2003), Ecosystem metabolism controls nitrogen uptake in streams in Grand Teton National Park, Wyoming, *Limnol. Oceanogr., 48(3),* 1120-1128.

Hall, R. O. Jr., J. L. Tank, D. J. Sobota, P. J. Mulholland, J. M. O'Brien, W. K. Dodds, J. R. Webster, H. M. Valett, G. C. Poole, B. J. Peterson, J. L. Meyer, W. H. McDowell, S. L. Johnson, S. K. Hamilton, N. B. Grimm, S. V. Gregory, C. N. Dahm, L. W. Cooper, L. R. Ashkenas, S. M. Thomas, R. W. Sheibley, J. D. Potter, B. R. Niederlehner, L. T. Johnson, A. M. Helton, C. M. Crenshaw, A. J. Burgin, M. J. Bernot, J. J. Beaulieu, and C. P. Arango (2009a), Nitrate removal in stream ecosystems measured by ^{15}N addition experiments: Total uptake, *Limnol. Oceanogr., 54(3),* 653-665, 2009a.

Hall, R. O. Jr, M. A. Baker, C. D. Arp, and B. J. Koch (2009b), Hydrologic control of nitrogen removal, storage, and export in a mountain stream, *Limnol. Oceanogr., 54(6),* 2128-2142.

Harman, C. J., P. S. C. Rao, N. B. Basu, G. S. McGrath, P. Kumar and M. Sivapalan (2011). Climate, soil and vegetation controls on the temporal variability of vadose zone transport. *Water Resour. Res.* 47, W00J13, doi:10.1029/2010WR010194.

Helton, A. M., G. C. Poole, J. L. Meyer, W. M Wollheim, B. J. Peterson, P. J. Mulholland5, E. S. Bernhardt, J. A. Stanford, C. Arango, L. R Ashkenas, L. W. Cooper, W. K Dodds, S. V. Gregory, R. O. Hall Jr, S. K Hamilton, S. L. Johnson, W. H. McDowell, J. D. Potter, J. L Tank, S. M. Thomas, H. M. Valett, J. R. Webster, and L. Zeglin (2011), Thinking outside the channel: modeling nitrogen cycling in networked river ecosystems. *Front. Ecol. Environ.*, 9(4): 229–238, doi:10.1890/080211.

Li, H. and M. Sivapalan (2011), Effect of spatial heterogeneity of runoff generation mechanisms on the scaling behavior of event runoff responses in a natural river basin. *Water Resour. Res.*, 47, W00H08, doi:10.1029/2010WR009712.

Li, H, M. Sivapalan, D. Liu and F. Tian (2010), Water and nutrient balances in a large tile-drained agricultural catchment: A distributed modeling study. *Hydrol. Earth Syst. Sci.*, 14, 2259–2275, doi:10.5194/hess-14-2259-2010.

Lyne, V. and M. H. Hollick (1979), Stochastic time-variable rainfall-runoff modelling. In: *Proc. Hydrology and Water Resources Symposium*, Perth, pp. 89-92, Inst. of Engrs. Australia.

Marti, E., N. B. Grimm and S. G. Fisher (1997), Pre- and postflood retention efficiency of nitrogen in a Sonoran Desert stream. *J. N. Am. Benthol. Soc. 16,* 805–819.

Mitchell, J. K., G. F. McIsaac, S. E. Walker, and M. C. Hirschi (2000), Nitrate in river and subsurface drainage flows from an east central Illinois watershed, *Transactions of the ASAE*, 43(2), 337-342.

Mulholland, P. J., and D. L. DeAngelis (2000), Effect of surface/subsurface exchange on nutrient dynamics and nutrient spiraling in streams, pp. 149-166. In: J. B. Jones, Jr. and P. J. Mulholland (eds.), *Streams and Ground Waters*. Academic Press, San Diego, CA.

Mulholland, P. J., J. L. Tank, J. R. Webster, W. B. Bowden, W. K. Dodds, S. V. Gregory, N. B. Grimm, S. K. Hamilton, S. L. Johnson, E. Marti, W. H. McDowell, J. L. Merriam, J. L. Meyer, B. J. Peterson, H. M. Valett and W. M. Wollheim (2002), Can uptake length in stream be determined by nutrient addition experiments? Results from an inter-biome comparison study, *J. N. Am. Benthol. Soc., 21(4)*, 504-560.

Mulholland, P. J., A. M. Helton, G. C. Poole, R. O. Hall, S. K. Hamilton, B. J. Peterson, J. L. Tank, L. R. Ashkenas, L. W. Cooper, C. N. Dahm, W. K. Dodds, S. E. G. Findlay, S. V. Gregory, N. B. Grimm, S. L. Johnson, W. H. McDowell, J. L. Meyer, H. M. Valett, J. R. Webster, C. P. Arango, J. J. Beaulieu, M. J. Bernot, A. J. Burgin, C. L. Crenshaw, L. T. Johnson, B. R. Niederlehner, J. M. O'Brien, J. D. Potter, R. W. Sheibley, D. J. Sobota and S. M. Thomas (2008), Stream denitrification across biomes and its response to anthropogenic nitrate loading. *Nature, 452,* 202–205.

Newbold, J. D., P. J. Mulholland, J. W. Elwood and R. V. O'Neill (1982), Organic-carbon spiraling in stream ecosystems, *Oikos, 38,* 266– 272.

O'Brien, J. M., W. K. Dodds, K. C. Wilson, J. N. Murdock, and J. Eichmiller (2007), The saturation of N cycling in Central Plains streams: 15N experiments across abroad gradient of nitrate concentrations, *Biogeochemistry*, 84, 31-49, doi: 10.1007/s10533-007-9073-7.

Ocampo, C. J, C. E. Oldham and M. Sivapalan (2006), Nitrate attenuation in agricultural catchments: Shifting balances between transport and reaction. *Water Resour. Res.,* 42, W01408, doi: 10.1029/2004WR003773.

Paul, M. J. and R. O. Hall (2002), Particle transport and transient storage along a stream size gradient in the Hubbard Brook Experimental Forest. *J. N. Am. Benthol. Soc.*, 21(2):195-205.

Payn, R.A., M. N. Gooseff, D. A. Benson, O. A. Cirpka, J. A. Zarnetske, W. B. Bowden, J. P. McNamara and J. H. Bradford (2008), Comparison of instantaneous and constant-rate tracer experiments through non-parametric analysis of residence time distributions, *Water Resour. Res.*, 44, doi:10.1029/2007WR006274.

Peterson, B. J., W. M. Wollheim, P. J. Mulholland, J. R. Webster, J. L. Meyer, J. L. Tank, E. Marti, W. B. Bowden, H. M. Valett, A. E. Hershey, W. H. McDowell, W. K. Dodds, S. K. Hamilton, S. Gregory, D. D. Morrall (2001), Control of nitrogen export from watersheds by headwater streams, *Science, 292(5514)*, 86–90.

Rabalais, N. N., R. E. Turner and W. J. Wiseman, Jr. (2002), Gulf of Mexico hypoxia, aka "the dead zone", *Annu. Rev. Ecol. Syst., 33,* 235-263.

Reggiani, P., M. Sivapalan and S.M. Hassanizadeh (1998), A unifying framework for catchment thermodynamics: balance equations for mass, momentum, energy and entropy, and the second law of thermodynamics, *Adv. Water Resour.*, **22**, 367–398.

Reggiani, P., S. M. Hassanizadeh and M. Sivapalan (1999), A unifying framework for watershed thermodynamics: constitutive relationships. *Adv. Water Resour.*, 23, 15-39.

Reggiani, P., M. Sivapalan, S.M. Hassanizadeh and W. G. Gray (2001), Coupled equations for mass and momentum balance in a bifurcating stream channel network: theoretical derivation and computational experiments, *Proc. Roy. Soc., Ser. A. Math. Phys. Engng. Sci.*, **457**, 157–189.

Robinson, J. S. and M. Sivapalan (1997), Temporal scales and hydrological regimes: Implications for flood frequency scaling. *Water Resour. Res.*, 33, 12, 2981-2999.

Robinson, J. S., M. Sivapalan and J. D. Snell (1995), On the relative roles of hillslope processes, channel routing and network geomorphology in the hydrological response of natural catchments. *Water Resour. Res.*, 31(12), 3089-3101.

Royer, T. V., M. B. David and L. E. Gentry (2006), Timing of riverine export of nitrate and phosphorus from agricultural watersheds in Illinois: Implications for reducing nutrient loading to the Mississippi River. *Environmental Science and Technology,* 40*:* 4126–4131.

Runkel, R. L. and K. E. Bencala (1995), *Transport of Reacting Solutes in Rivers and Streams*, Chapter 5: in V. P. Singh (editor), *Environmental Hydrology*, Kluwer Academic Publishers, Dordrecht, The Netherlands, p. 137-164, 1995.

Runkel, R. L. (1998), *One Dimensional Transport with Inflow and Storage (OTIS): A Solute Transport Model for Streams and Rivers*. U.S. Geological Survey Water Resources Investigation Report No. 98–4018, http://co.water.usgs.gov/otis.

Runkel, R. L. (2000), Using OTIS to model solute transport in streams and rivers, U.S. Geol. Surv. Fact Sheet, FS-138-99, 4 pp.

Runkel, R. L. (2007), Toward a transport-based analysis of nutrient spiraling and uptake in streams. *Limnol. Oceanogr.: Methods*, *5*, 50–62, 2007.

Seitzinger, S. P., R. V. Styles, E. W. Boyer, R. B. Alexander, G. Billen, R. W. Howarth, B. Mayer and N. V. Breemen (2002), Nitrogen retention in rivers: model development and application to watersheds in the northeastern U.S.A., *Biogeochemistry, 57/58*: 199–237, 2002.

Smith, R. A., G. E. Schwarz and R. B. Alexander (1997), Regional interpretation of water quality monitoring data, *Water Resour. Res., 33 (12)*, 2781-2798.

Stall, J. B. and Y. S. Fok (1968), Hydraulic Geometry of Illinois Streams, Illinois State Water Survey Report CR-92.

Stewart, R. J., W. M. Wollheim, M. N. Gooseff, M. A. Briggs, J. M. Jacobs, B. J. Peterson and C. S. Hopkinson (2011), Separation of river network-scale nitrogen removal among main channel and two transient storage compartments, *Water Resour. Res.*, 47, W00J10, doi:10.1029/2010WR009896.

Stofleth, J. M., F. D. Shields Jr, and G. A. Fox (2008), Hyporheic and total transient storage in small, sand-bed streams, *Hydrol. Process.* 22, 1885-1894.

Stream Solute Workshop (1990), Concepts and methods for assessing solute dynamics in stream ecosystems, *J. N. Am. Benthol. Soc., 9(2)*, 95-119, 1990.

Tank, J. L., E. J. Rosi-Marshall, M. A. Baker and R. O. Hall, Jr. (2008), Are rivers just big streams? A pulse method to quantify nitrogen demand in a large river, *Ecology, 89(10)*, 2935-2945.

Thompson, S. E., N. B. Basu, J. Lascurain Jr., A. Aubeneau, and P. S. C. Rao (2011), Relative dominance of hydrologic versus biogeochemical factors on solute export across impact gradients. *Water Resour. Res.*, 47, W00J05, doi:10.1029/2010WR009605.

Tian, F. (2006), *Study on Thermodynamic Watershed Hydrological Model (THModel)*. Ph.D. thesis, Department of Hydraulic Engineering, Tsinghua University, Beijing, China, 168pp.

Tian, F., H. Hu, Z. Lei and M. Sivapalan (2006), Extension of the representative elementary watershed approach for cold regions via explicit treatment of energy related processes. *Hydrol. Earth Syst. Sci.*, 10, 619-644.

Viney, N. R., M. Sivapalan and D. E. Deeley (2000), A conceptual model of nutrient mobilisation and transport applicable at large catchment scales. *J. Hydrol.*, 240(1-2), 23-44.

Webster, J. R., B. C. Patten (1979), Effects of watershed perturbation on stream potassium and calcium dynamics, *Ecol. Monogr.*, 49, 51–72

Wollheim, W. M., C. J. Vörösmarty, B. J. Peterson, S. P. Seitzinger, C. S. Hopkinson (2006), Relationship between river size and nutrient removal, *Geophys. Res. Lett., 33*, L06410, doi:10.1029/2006GL025845.

Wollheim, W. M., B. J. Peterson, S. M. Thomas, C. H. Hopkinson and C. J. Vorosmarty (2008), Dynamics of N removal over annual time periods in a suburban river network, *J. Geophys. Res. -Biogeosciences*, 113, G03038.

Chapter 5

Scale Effects of Dissolved Nutrient Retention in River Networks: A Comparative Modeling Investigation

Abstract[1]

The river network is the most important connector of terrestrial ecosystems to the oceans and other receiving waters across spatial gradients. Water, sediments and nutrients are transported, cycled and altered by coupled hydrological, erosional and biogeochemical processes occurring in river networks. Our understanding of dissolved nutrient spiraling processes is limited in big rivers (>2000L/s) due to the difficulty and costs in doing empirical measurements at all scales across the river network. Coupled dynamic hydrologic and biogeochemical models at the network scale may be a way to generate hypotheses and where possible to make needed predictions. In this chapter we modify the coupled hydrologic and biogeochemical process model used previously in Chapter 4 with field measurements in small rivers as well as big rivers to simulate the nutrient spiraling at the network scale, and to gain understanding of the role of big rivers. The biogeochemical processes in the model are described based on empirical regressions between the uptake rates and hydrological and biological characteristics derived from field measurements in 15 Western and Midwestern catchments with different turbidity and land uses. The coupled model is then applied to the 15 catchments to explore nutrient uptake patterns within catchments, between catchments, and across three different solutes. The model simulations suggest that big rivers are not pipes, that they contribute more to nutrient uptake given their share of stream length. The differences between catchments can be attributed to differences in nutrient input loads and the uptake lengths. A regression tree model applied to understand the dominant controls of nutrient transport in the river network for each solute indicates that ammonium uptake is dominated by land use and the biotic metabolism while nitrate retention is mainly influenced by human impacts, in the form of land use, and ammonium is preferred by the microbes and algae rather than nitrate. Different from the two compounds of nitrogen, phosphate retention is dominated by turbidity, which may be because of the role of sediment sorption. With future quantification of the transient storage size and uptake rates in the future, this model framework could be used to estimate pelagic, benthic, and transient storage

uptake components of the total uptake separately to assess the hydrologic, biologic and geomorphologic controls on nutrient spiraling across catchments and solutes.

[1]Material in this chapter work is planned to be submitted for publication to the *Water Resources Research* (or other) journal. All figures, tables and data presented here were created by Sheng Ye, unless otherwise indicated.

5.1 Introduction

Due to increasing human activities such as urbanization and fertilizer application for agricultural use since the beginning of the 20th century, nitrogen and phosphorus inputs to aquatic systems worldwide have increased significantly (Bouwman et al., 2005; Seitzinger et al., 2005; Mulholland et al., 2008). These excessive nutrients have led to severe degradation of fresh water and coastal ecosystems, causing growth of blue-green algae, reduction of dissolved oxygen, increasing aquatic organism mortality, and decreasing species diversity. In this way they have caused damage to entire aquatic ecosystems (OECD, 1982), reduced water quality of coastal areas, and destroyed coastal environments through hypoxia, as is the case in the Gulf of Mexico (Alexander, et al., 2000; Rabalais et al., 2002). As the critical link between the terrestrial and coastal ecosystems, the river network plays an important role in nutrient transport and transformation. Despite the large fraction of nutrient transformation and removal occurring in the landscape itself, studies show that a large amount of nutrients can also be retained and removed by the aquatic system associated with the river network itself (Alexander et al., 2000; Bernhardt et al., 2005). In other words, the river system does not simply deliver nutrient from the landscape all the way to the ocean (i.e., in the form of "pipes" or conduits), but it also acts as a significant nutrient sink through processes such as plant uptake, bacteria-mediated denitrification and sediment sorption during the transport to the ocean (Billen et al., 1991).

Given the importance of the riverine aquatic system for nutrient retention, extensive research has been carried out in this area to understand how nitrogen and phosphorus are transformed and transported in streams/rivers, through both empirical field measurements (Dodds et al., 2002; Tank et al., 2008; Claessens and Tague, 2009; Claessens et al., 2009; Hall et al., 2009) and model simulations (Donner *et al.*, 2002; Seitzinger et al., 2002; Wollheim et al., 2008a; Alexander et al., 2009; Aguilera et al., 2013). Many of the field measurements have been conducted in small headwaters (Ensign and Doyle, 2006; Tank et al., 2008) since nutrient removal rate is believed to be high in small headwater streams due to the shallow flow depths that normally prevail there and also because headwater streams generally make up a larger fraction of the total stream length in a river basin than do "big rivers" (Alexander et al., 2000; Peterson et al., 2001). However, recent simulation studies have found that despite their relatively

small fraction of the total stream length in a river basin, the big river contribution to total nutrient uptake can be considerably more than would be commensurate with their fraction of total stream length. In the 16 eastern catchments studied by Seitzinger et al. (2002), the 1st to 4th order streams, which constituted 90% of the total stream length, yet accounted for only half of the total nutrient retention while the 5th and higher order streams retained the other half of the nutrient uptake within the small 10% of the total stream length that they occupied. Other simulation based studies have also indicated that large rivers could have considerable impact on nutrient retention in river basins as a whole due to the effect of increases in both biological activity (Wollheim et al., 2006) and nutrient inputs with increasing stream size (Mulholland et al., 2008; Ye et al., 2012).

If the big rivers can no longer be considered as "pipes" that merely serve as conduits (i.e., transporters) of nutrient transport, then the nutrient spiraling that occurs within the river system consisting of the hierarchical network of inter-connected stream reaches of various sizes deserve much more attention than they have attracted before. To better understand the role of big rivers, we would of course need more empirical data from field measurements carried out in streams of all sizes, but especially in big rivers, while respecting their position in the stream network. However, most previous experiments in this area have been carried out in small headwater streams during low flow periods with discharges less than 1000L/s, indeed mostly less than 200L/s (Tank et al., 2008). Although several recent empirical studies are now giving more attention to studying big rivers (Tank et al., 2008), there is still not much published data available for the community to use towards the development of more universal theories applicable across all scales (Aguilera et al., 2013). Most previous observations have been made at the outlet of a single segment of the river, and there have been relatively few experiments conducted across the entire river network, from headwater to downstream outlet all at once (Seitzinger et al., 2002), probably because it is expensive and time consuming to measure the nutrient spiraling processes continuously and in space-time across the entire stream network (Helton et al., 2011). Given these measurement difficulties, river network models of nutrient transport and transformation may be a suitable alternative tool to upscale the mechanisms found at the reach scale to the observations at basin scale (Aguilera et al., 2013) and extrapolate the measured uptake parameters at both scales to the whole river network. Such models could also be used to further study the impact of network scale heterogeneity in lateral nutrient input

concentration, temporal hydrologic variability, and in-stream nutrient saturation, on nutrient retention mechanisms across the river network (Wollheim et al., 2008a, b).

Several different models have been developed to quantify nutrient uptake during transport in river networks (Smith et al. 1997; Alexander et al. 2000, 2009; Seitzinger et al., 2002; Wollheim 2006, 2008a). Most of these models are parameterized on the basis of previous suite of measurements made at small streams only (i.e., LINX II dataset Mulholland et al., 2008, 2009; Hall et al., 2009) through developing multiple regression relationships. The potential problems with this approach are: 1) due to the lack of big river nutrient uptake data, it is hard to validate results simulated by simple extrapolation of the regressions using data from small streams to big rivers – even if the results were calibrated we may still obtain apparently right results for the wrong reasons; and, 2) there may be a significant variability in the regression relationships governing nutrient uptake among different catchments – especially when the magnitude of nutrient input grows with river size, this discrepancy between specific catchments to what is predicted by the regression line could be magnified by the increasing magnitude of nutrient inputs. Model simulations could be improved if we could develop a relatively universal model framework that could scale up from the reach scale to network scale with sufficient knowledge of nutrient uptake mechanisms across all scales (including small streams and big rivers), parameterized by measurements at the outlet to account for the local characteristics of nutrient retention (Marti et al., 2004; Dodds et al., 2006; Tank et al., 2008; Aguilera et al., 2013). This is the motivation for the present work: this work is supported by nutrient uptake data collected during sustained field experiments in 15 big rivers across the United States, supplementing the previous dataset assembled in a large number of small streams (called here as the meta-data), which has been the subject of several previous modeling studies.

The work presented here is aimed at developing a modeling framework that up-scales the reach scale measurements to the catchment scale by empirical relationships of nutrient uptake characteristic and the hydrologic and biogeochemical characteristics of the river network across scales. This is done by adjusting the relationship obtained using measured data (including meta-data, as well as new data in 15 big rivers) and parameterize the model for these 15 specific catchments. The goals of the work are to: 1) develop a model that utilizes both the meta-data and new field measurements in big rivers to describe nutrient uptake processes at catchment scale; 2)

examine the spatial distribution of nutrient uptake within a single catchment, including quantifying the distribution as a function of river size, i.e., small streams vs. big rivers; 3) characterize the variation of the spatial patterns of nutrient uptake across several study catchments and across three different solutes; and 4) explore likely physical controls for the estimated within-catchment and between-catchment patterns of nutrient removals.

5.2 Methodology

5.2.1 Model Structure

The coupled network flow and nutrient transport model presented here is a further extension of the model used previously by Ye et al. (2012; also Chapter 4 of this dissertation). The flow part of the model is based on the REW approach developed by Reggiani et al. (2001): the whole catchment is divided into a number of sub-catchments (REWs), each REW, as the smallest functional unit, includes one stream reach and is connected to upstream and downstream reaches/REWs via the river network. Tian et al. (2006) implemented a numerical model of flow in the river network, THREW (TsingHua Representative Elementary Catchment) based on the REW concepts, which was later used in a distributed runoff modeling investigation by Li and Sivapalan (2011). The model we use here is a simplified version of the original THREW model, while keeping the main mass and momentum balance equations for flow in the river network from the THREW model.

The flow model has several advantages compared to models presently in use for flow and nutrient transport at network scale: (i) it is physically based at the scale of constituent stream reaches, (ii) it can easily be applied to simulate dynamic flow conditions, not just steady state, and (iii) it is computationally efficient, and hence can easily be applied to large networks over long timescales. The mass balance equations for each component stream reach are as follows:

$$\frac{dS^i}{dt} = Q_l^i + \sum Q_{up}^j - Q_{out}^i \qquad (1)$$

$$Q_{out}^i = v^i A^i \qquad (2a)$$

$$Q_{up}^j = v^j A^j \qquad (2b)$$

where S^i is water storage at local reach i [L^3], Q^i_l is the lateral inflow [L^3 T^{-1}], Q^j_{up} is the inflow from upstream nodes [L^3 T^{-1}], v^j is the velocity at upstream end, for reach j [L T^{-1}], A^j is cross-sectional area of the j^{th} upstream reach [L^2] (=S^j/L, where L is the reach length), Q^i_{out} is the outflow from reach i [L^3 T^{-1}], and v^i is the velocity at local reach i [L T^{-1}]. Velocity v^i is estimated by the reach scale momentum balance equation (i.e., Saint-Venant momentum balance equation).

$$v^i = \frac{1}{n^i}\sqrt{\frac{(R^i)^{1/3}}{P^i L^i}\left(A^i_{MC} L^i \sin\gamma^i \pm \sum_{j\neq i}\frac{1}{4}h^i(A^i_{MC}+A^j_{MC}) - \frac{1}{2}h^i A^i_{MC}\right)} \qquad (3)$$

where n^i is roughness coefficient of local REW i, R^i is the hydraulic radius P^i is average wetted perimeter, $\sin\gamma^j$ is the mean slope of REW i, and h^i is the mean depth of REW i [L]. Detailed derivation of these equations and an explanation of the assumptions behind them can be found in Tian et al. (2006) and Ye et al. (2012).

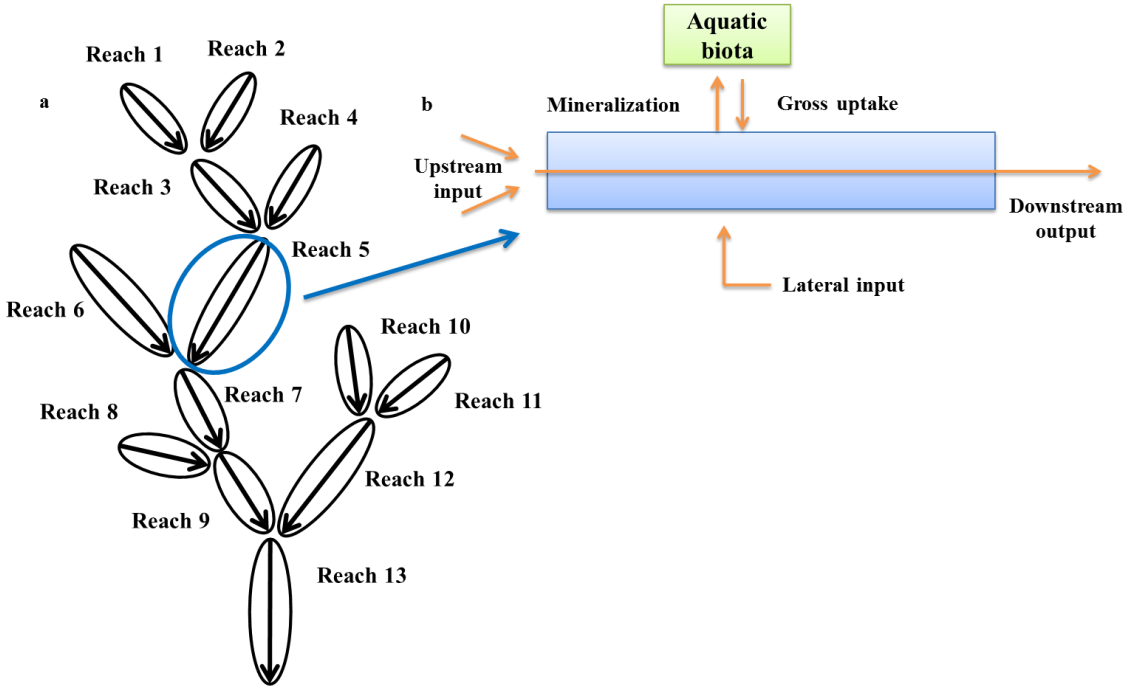

Figure 5.1: Schematic of the solute transport model coupled with hydrological dynamics: (a) Catchment discretization into many representative elementary catchments (REWs) distributed around the river network; (b) each REW includes a channel reach receiving water and dissolved nutrient from lateral inflow

Note that, different from Ye et al. (2012), due to the lack of reliable hydraulic geometry information for the 15 study catchments reported here (see later), the shape of the channel is assumed to be rectangular and the channel width is estimated from DEMs available for these catchments, and then rescaled through conditioning with the measured width at the catchment outlet. A schematic description of the sub-catchment delineation for a typical catchment and the flow routing across the river network is presented in Figure 5.1.

The nutrient part of the model, expressed in terms of the mass balance equation for nutrient transport and transformation, also at the scale of an individual stream reach in the river network, is as follows:

$$\frac{d(S^i C^i)}{dt} = Q_l^i C_l^i + \sum (\mathrm{Q}_{up}^j \mathrm{C}_{up}^j) - Q_{out}^i \mathrm{C}^i - N_{tu}^i + N_{\min}^i \qquad (4)$$

$$N_{tu}^i = R^i (Q_{iout}^i C^i) \qquad (5)$$

$$N_{\min}^i = \beta N_{tu}^i \qquad (6)$$

where C^i is the solute concentration (i.e., NH_4, NO_3, or PO_4) at the local reach [ML^{-3}], C^i_l is the solute concentration of lateral inflow [ML^{-3}], C^j_{up} is the solute concentration of the upstream reach j [ML^{-3}], N^i_{tu} is gross retention in the water column [MT^{-1}], N^i_{min} is the mineralization component returning to the water column [MT^{-1}]. Mineralization is estimated as a fraction of the total nutrient retention, represented as a constant β. Based on LINX I data set (Peterson et al., 2001), β is set to 0.185 for NH_4, 0.034 for NO_3 (Laura Johnson, personal communication) and 0.045 for PO_4 (Mulholland et al., 1985). The term R is the fraction of the nutrient in the water column that would be retained [-], and is estimated as follows (Wollheim et al., 2006):

$$R^i = 1 - \exp(-\frac{L^i}{S_w^i}) \qquad (7)$$

where S_w^i is the uptake length at the local reach i. This formulation is identical to two alternative formulations that have been proposed in the literature, given by:

$$R^i = 1 - \exp(-\frac{v_f^i}{H_L^i}) \qquad (8a)$$

$$R^i = 1 - \exp(-\frac{L^i}{v^i} k^i) \qquad (8b)$$

In Equation 8(a) proposed by Wollheim et al. (2006), H_L [LT^{-1}] is the hydraulic load defined as $H_L = Q/(wL)$, and v_f [LT^{-1}] is vertical uptake velocity defined as $v_f = Q/(wS_w)$, where w is the width of the channel [L] and Q is discharge [L^3 T^{-1}]. In Equation 8(b) used by Ye et al. (2012; also Chapter 4 of this dissertation), k (T^{-1}) is an uptake rate k (T^{-1}), defined as the ratio of flow velocity (LT^{-1}) over the uptake length S_w [L], i.e., $k=v/S_w$, which makes L^i/v^i a residence time in reach i. Clearly Equations 7, 8(a) and 8(b) represent equivalent formulations.

However, in this chapter we will use the formulation in Equation (7) because it uses uptake length S_w, which is obtained by direct measurement in the field (both in the case of the LINX I dataset as well as in the "big river" experiments), as in this way we avoid the rounding errors that would be introduced during the conversion from one formulation to another. Also, the nutrient uptake metrics measured in the 15 big rivers refer to overall "bulk" uptake, instead of separate main channel and transient storage components (as was done by Ye et al., 2012, Chapter 4). At present we do not have the data support to separate the total uptake into separate main channel and transient storage contributions.

We also include a mineralization component here, estimated as a percentage of the total uptake, where the percentage is borrowed from the previous studies in the literature. Theoretically the measured uptake is the net uptake, i.e., total uptake minus mineralization. However, since the duration of the field experiments is too short for solutes retained by the biota during the experiments to be mineralized back into the water column, the only amount of nutrients mineralized is from previous uptake, which is much smaller compared to the nutrients added and retained during the experiments. Therefore, we can ignore the nutrient mineralization during the experiments and consider the measured uptake length is approximately related to total net uptake, which means we need to reintroduce a mineralization component to account for nutrients mineralized from uptake prior to the experiments.

5.2.2 Study catchments

To develop the relationship between nutrient uptake and catchment characteristics across scales, big river measurements are needed to fill the lack of knowledge in rivers with discharges larger

than 2000L/s. Five Midwestern rivers and ten Western rivers across the United States, spanning a gradient of nutrient enrichment, biological activity and turbidity were selected by the Big River Team (Tank et al., 2008). These are the catchments that will be used in the comparative modeling investigation presented in this paper. Figure 5.2 presents a map showing the locations of the 15 big rivers. The Midwestern rivers are relatively nutrient enriched with high percentage of agricultural land use, while the ten Western rivers (five arid and five mountainous) have relatively low nutrient concentrations (except for the Colorado River), covering a wide range of sediment concentrations and turbidity.

The model was set up in each of these 15 catchments. The 15 rivers can be grouped into three classes based on their climate and land use characteristics: the five Midwest rivers (Muskegon, Tippecanoe, White, Manistee, and St. Joseph) with high nutrient concentrations due to intense agricultural land use, five mountain west rivers (Salmon, Snake, Buffalo, Seedskadee and Henry's Folk) with relatively low nutrient concentration level and high forest cover, and five arid west rivers (Bear, Colorado, Ouray, Green, North Platte) having an arid climate. The 10 western catchments are part of the Great Divide Basin. The uptake lengths and concentrations for ammonium, nitrate, soluble reactive phosphorus measured at the outlets of these catchments by the Big River Team were used for the model development and calibration, as discussed in Section 2.2. Note that, due to the presence of a reservoir along the river network, we did not include the Bear Lake in the Bear River catchment in the model simulations, as the model is not yet capable of lake or reservoir simulation. Bear Lake is one small tributary of the Bear River, and also given the small influence of lakes and reservoirs on nutrient retention (Seitzinger et al., 2002), removing the lake from further consideration is deemed acceptable for the purpose of this study.

5.2.3 Model set up and parameterization

To apply the model in real world catchments, we need the lateral inflow discharge (Q_l) and concentration (C_l) as inputs to set up the model, and then the parameterization of the local uptake length for each solute in each stream reach in the river network (S_w). Below is a brief description of how these issues are handled in this study.

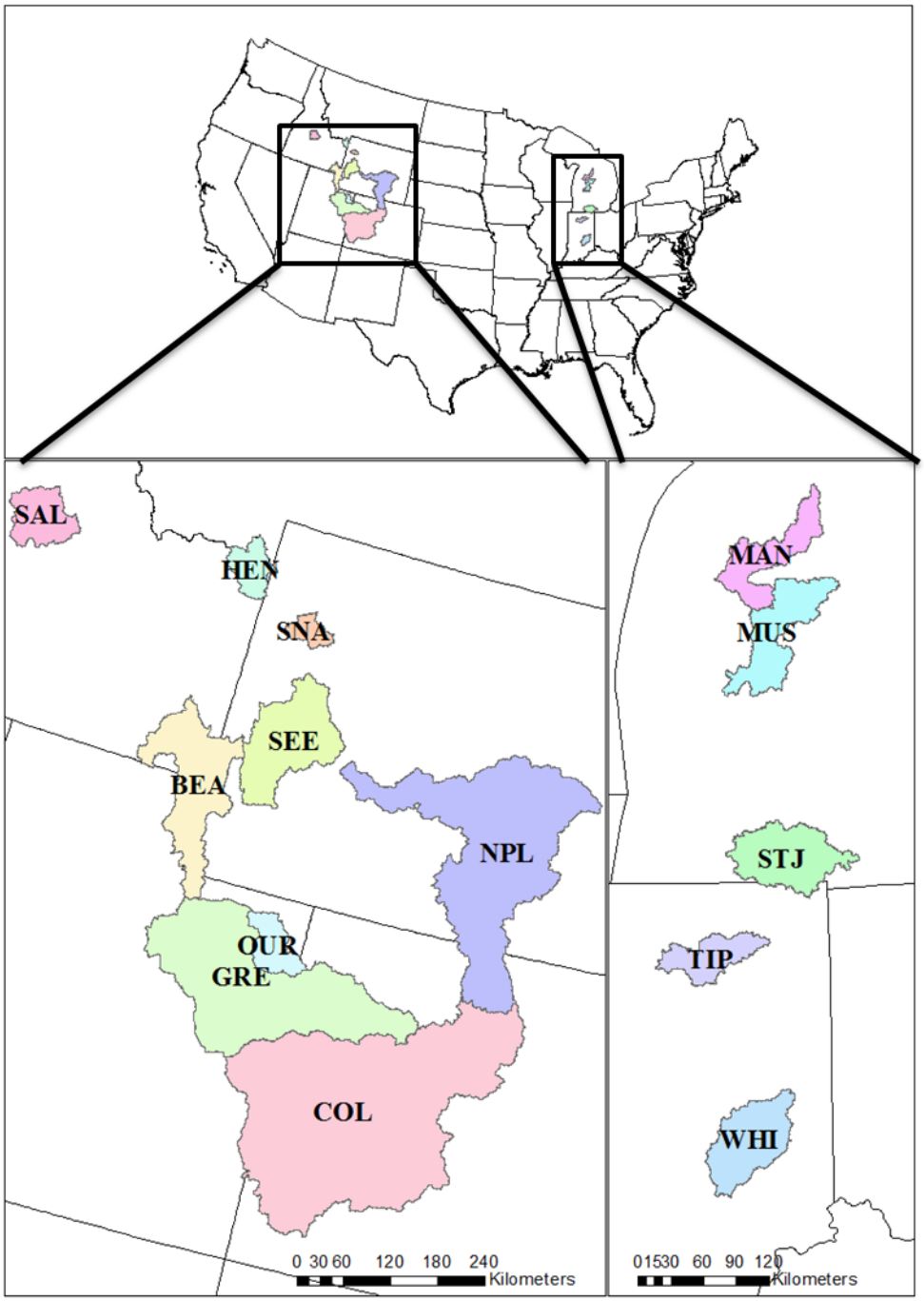

Figure 5.2: Map of the 15 big rivers: five mountain west rivers: Salmon River, ID (SAL); Henry's Folk, ID (HEN); Snake River, WY (SNA); Buffalo River, WY (BUF); Seedskadee River, WY (SEE); five arid west rivers: Bear River, UT (BEA); Green River, UT (GRE); Ouray River, UT (OUR); Colorado River, CO (COL); North Platte River, WY (NPL); and five Midwest rivers: Manistee River, MI (MAN); St. Joseph River, MI (STJ); Muskegon River, MI (MUS); Tippecanoe River, IN (TIP); and White River, IN (WHI).

Inputs: Lateral inflow and concentration

Fifteen (15) minute flow data were collected from the USGS gauges at the outlet of each catchment near where the field experiments were conducted during the summer when the uptake length was measured, as part of the "big river" experiments. Since the experiments were conducted during the low flow period, the temporal variability of flow was very low and for simplicity in the model it was assumed to be at steady state during the measurements. An average value was then calculated from the three month, 15 minute flow data, normalized by the drainage area, which is then used as lateral inflow, assuming that it is homogeneous across the catchment. For each sub-catchment (REW), the lateral inputs were estimated after multiplying the estimated lateral inflow per unit area by the individual area of each REW.

Due to the lack of data on lateral inflow concentrations, and also since the aim of this paper is to understand how nutrients are retained in the river network, as a simplification we assumed a homogeneous and constant (in time) nutrient concentration of the lateral inflow. With the input of the lateral water inflows and nutrient concentrations, the model can then simulate the concentrations everywhere in the network, including at the catchment outlet, which we can then be compared against concentrations measured at the outlet. This provides the ability to adjust (i.e., calibrate) the lateral inflow concentration everywhere in the catchment such that model simulated concentration at the outlet matches the measured one. In addition, we collected nutrient concentrations from several USGS groundwater sites located within the study catchments and, as a check, compared these against the calibrated lateral concentrations. The comparisons indicated (Appendix Table A.1) that the calibrated lateral inflow concentrations for the three solutes (NH_4, NO_3 and PO_4) in most of the Western rivers fell within the range of USGS observations. The calibrated values were however found to be larger than the USGS groundwater measurements in the Mid-western Rivers, especially for NO_3. One likely reason could be the intense anthropogenic activities within these catchments: much of the nutrients in these river systems may come from surface or near-surface flows caused by fertilizer application in tile drained landscapes. Either way, the comparison gave us confidence in the calibrated lateral flow concentrations assumed in the model: they are within the reasonable range.

Parameterization: S_w

Uptake length (S_w) is defined as the distance that a solute will travel in the downstream direction in the river before it is removed from the water column. However, we only have measurements of S_w at one point for the whole river (i.e., the outlet), whereas to model the nutrient uptake in the entire river network, we need the S_w for each segment of the network.

Therefore, we need a scaling approach to estimate the S_w for each reach based on the measured S_w at the outlet. Based on previous experience, we know that S_w is closely related to the flow (Tank et al., 2008) as well as the concentration (Mulholland et al, 2008; Alexander et al., 2009). Here we adapted the scaling approach presented in Hall et al. (2013): we perform a multiple linear regression analysis of the relationship between uptake length (S_w) and the flow condition (Q/w) as well as the concentration level (C), in the form of $\log Sw = \alpha_1 + \alpha_2 \log(Q/w) + \alpha_3 \log C$. In this study, we combine the previous meta-data used in Hall et al. (2013), and add to it the new data obtained during the "big river" experiments on the 15 rivers. To obtain the regression relationship we used the same algorithm adopted by Hall et al. (2013), and obtained separate scaling relationship for the three solutes (NH_4, NO_3, PO_4) as follows:

NH_4: $$\log S_w^{\,i} = 2.18 + 0.79 \log(Q^i / w^i) + 0.32 \log C^i \qquad (9a)$$

NO_3: $$\log S_w^{\,i} = 2.52 + 0.52 \log(Q^i / w^i) + 0.27 \log C^i \qquad (9b)$$

PO_4: $$\log S_w^{\,i} = 2.46 + 0.98 \log(Q^i / w^i) + 0.13 \log C^i \qquad (9c)$$

where Q^i is the flow discharge at local reach i, w^i is the width of reach i, C^i is the solute concentration at reach i as mentioned before. The statistics of the three regressions can be found in table 5.1:

Table 5.1: The sample size n, R^2 for the three regressions

Solutes	Sample size (n)	R^2
NH_4	159	0.70
NO_3	208	0.3
PO_4	124	0.68

However, the observations from the 15 big river catchments indicated large variations between the rivers, the difference between the actual S_w and the predicted S_w was found to be more than an order of magnitude in some catchments. To accommodate the variations between the big rivers, we rescaled the predicted S_w: assumed the relationship between S_w and the flow condition (Q/w) and concentration level (C) are the same across scales and the various catchments, that is, the two coefficients α_2 and α_3 are universal for all catchments, whereas the intercept (α_1) which indicates the specific biological demand in each catchment, and for this reason was allowed to vary from river to river based on the characteristics of the benthic and pelagic biota. Based on the S_w, Q/w and concentrations measured at the outlet, we can then back-calculate the α_1 value for each river. For example, take the S_w of NH_4 in Buffalo River: the measured S_w is14868 m, the concentration is 5μg/L, and Q/w is 32.67m^2/min, now substitute these into Equation 9a: log(14868) = α_1+ 0.79log(32.67) + 0.32log(5), this way we get α_1=2.75. We then rescale the S_w for each solute in each river to get a specific scaling relationship of S_w over the flow condition (Q/w) and concentration level (C).

In the model, we applied three different scenarios to explore how different the nutrient uptake length would be: 1) the S_w predicted by the equation presented in Hall et al. (2013) with only the small stream data from previous meta-analysis (i.e., meta-data); 2) the S_w predicted by Equation 9 with both the small stream data and the 15 big river data (meta-data + big rivers); 3) and the rescaled S_w from Equation 9 as we described above (empirically re-scaled). As the rescaled S_w is based on the measured S_w, for the brevity of the paper, we will use the rescaled S_w to stand for the actual observed S_w in the paper, and use the "universal regressions" to refer to the S_w predicted by equation presented in Hall et al. (2013) with only the small stream data from previous meta-analysis and by Equation 9.

5.2.4 Regression tree model

The Big River Team collected not only uptake metrics but also many parameters that may be helpful to characterize the study catchments, such as land use information, metabolism and biologic activity. One of the objectives of this study is to characterize the differences in nutrient uptake rates between the catchments and attribute these differences to aspects of the climate and landscape characteristics, including biogeochemical factors. To achieve this, in this study we

propose to use a regression tree model to explore the relationship between the simulated reach scale daily net uptake rates (gross retention – mineralization) per kilometer and a suite of potential physical characteristics.

Regression tree is a nonlinear predictive model. It is constructed by recursively partitioning the available data set into two subsets. It begins with the whole data space, progresses along in steps, and stops based on the adopted stopping rule (Breiman et al., 1984). The terminal cells are considered as leaves and assigned an average value of the predicted variable. Each time the data space is divided into two child nodes (t_R, t_L), we aim to maximize the deduction of residual sum of squares (RSS) between the parent nodes and the sum of child nodes $\Phi(t)$:

$$\Phi(t) = RSS(t) - (RSS(t_R) + RSS(t_L)) \qquad (10)$$

$$RSS(t) = \sum (y_i - y_{avg})^2 \qquad (11)$$

where $\Phi(t)$ is the target function, the deduction of residual sum of squares we want to maximize, RSS(t) is the residual sum of squares of the total data set, $RSS(t_R)$ is the residual sum of squares of the right tree node, and $RSS(t_L)$ is the residual sum of squares of the left tree node, y_i is the ith value of the predict array, here it is the daily net uptake per kilometer for ith river, and y_{avg} is the mean of all the predict variables, here it is the mean daily net uptake per kilometer for all the rivers belong to the subset.

The tree model is helpful when there are several candidate influential variables which are also inter-correlated and there is a big difference among the samples, in which case a global model such as linear regression, may not work for all the samples. Since we have many candidate catchment characteristics we think may be related to the nutrient uptake, and the biologic characteristics are related in a complex way, the regression tree model suits our purpose well.

5.3 Results

5.3.1 Uptake length

The first set of results relate to the scaling of the uptake length, S_w, on the basis of Equation 9, using the LINX I meta-data for small streams through combination with the "big river" data. Figure 5.3 presents the uptake lengths for the three solutes in all 15 catchments estimated in three different ways: (1) the equation presented in Hall et al. (2013) with only the small stream data from previous meta-analysis (labeled *meta-data*); Equation 9 with the use of both the small stream data (i.e., meta-data) and the data from big rivers (labeled *meta data + big rivers*); and the rescaled S_w from Equation 9 using the method described in Section 5.2.3 (i.e., empirically re-scaled). For some of the catchments, the results are left blank because the S_w there could not be measured.

As can be seen from Figure 5.3, the variation of empirically re-scaled S_w among the catchments is larger than the variation of S_w predicted by the two universal regressions with meta-data only and using meta-data plus big river data. This suggests that the biologic characteristics in these catchments (i.e., as inferred from the intercepts in the $S_w/(Q/w)$ versus concentration relationships) are highly variable, and hence it is necessary to treat each river individually to account for their unique characteristics. Generally, the empirically re-scaled S_w is larger than the S_w predicted by meta-data or meta-data plus big river data in most of the catchments, except for a few catchments where they are smaller: e.g., *Sw* of NH_4 at Snake and Green Rivers; S_w of NO_3 at St. Joseph River; and S_w of PO_4 at St. Joseph, Muskegon, Seedskadee and Ouray Rivers. But the differences between the empirically rescaled S_w and the S_w estimated from regression using the meta-data only or the meta-data plus big river data are not consistent across the different solutes. For example, in Muskegon River the rescaled S_w for NH_4 is one magnitude larger than S_w predicted by the two universal regressions, but the rescaled S_w for PO_4 is only half the S_w predicted by the two universal regressions. Given the difference in the uptake mechanisms of nitrogen and phosphorus, it is reasonable to infer that the controlling catchment characteristics for different solutes could be different. We will explore this in Section 5.4.3.

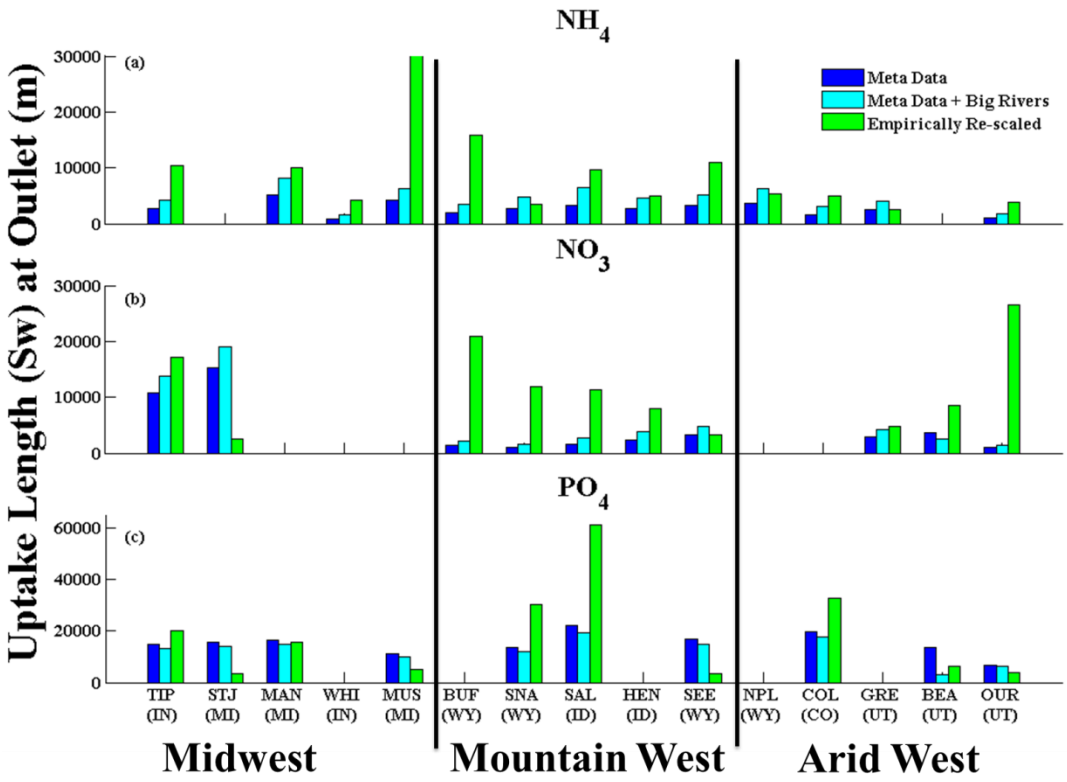

Figure 5.3: Comparison of the uptake length predicted by small streams regression of Q/w and concentration (blue), small streams + big river regression (cyan) and empirically re-scaled small streams + big river regression by measured data (green) (a) NH_4; (b) NO_3; (c) PO_4

5.3.2 Model simulation results

We applied the three sets of rescaled S_w estimates from Equation 9 to all the 15 rivers, accounting for both between-catchment and within-catchment variations of the S_w, along with the lateral inflow calculated from USGS flow observations at the outlet and the lateral inflow concentrations calibrated to match the observed concentrations at the outlet (each time based on the rescaled S_w). Selected results are presented in Figure 5.4. For each of the solutes, based on the uptake length (S_w) shown in Figure 5.3, we selected two representative catchments to present in Figure 5.4: one catchment has the measured uptake length (S_w) close to the S_w predicted by the regression relations of Hall et al. (2013) and Equation 9; the other catchments have the measured uptake length (S_w) either much larger or much smaller than the S_w predicted by the regression

equations from Hall et al. (2013) and Equation 9, leading to very different nutrient uptake behaviors: different concentrations, net uptake and catchment scale total percentage of removal.

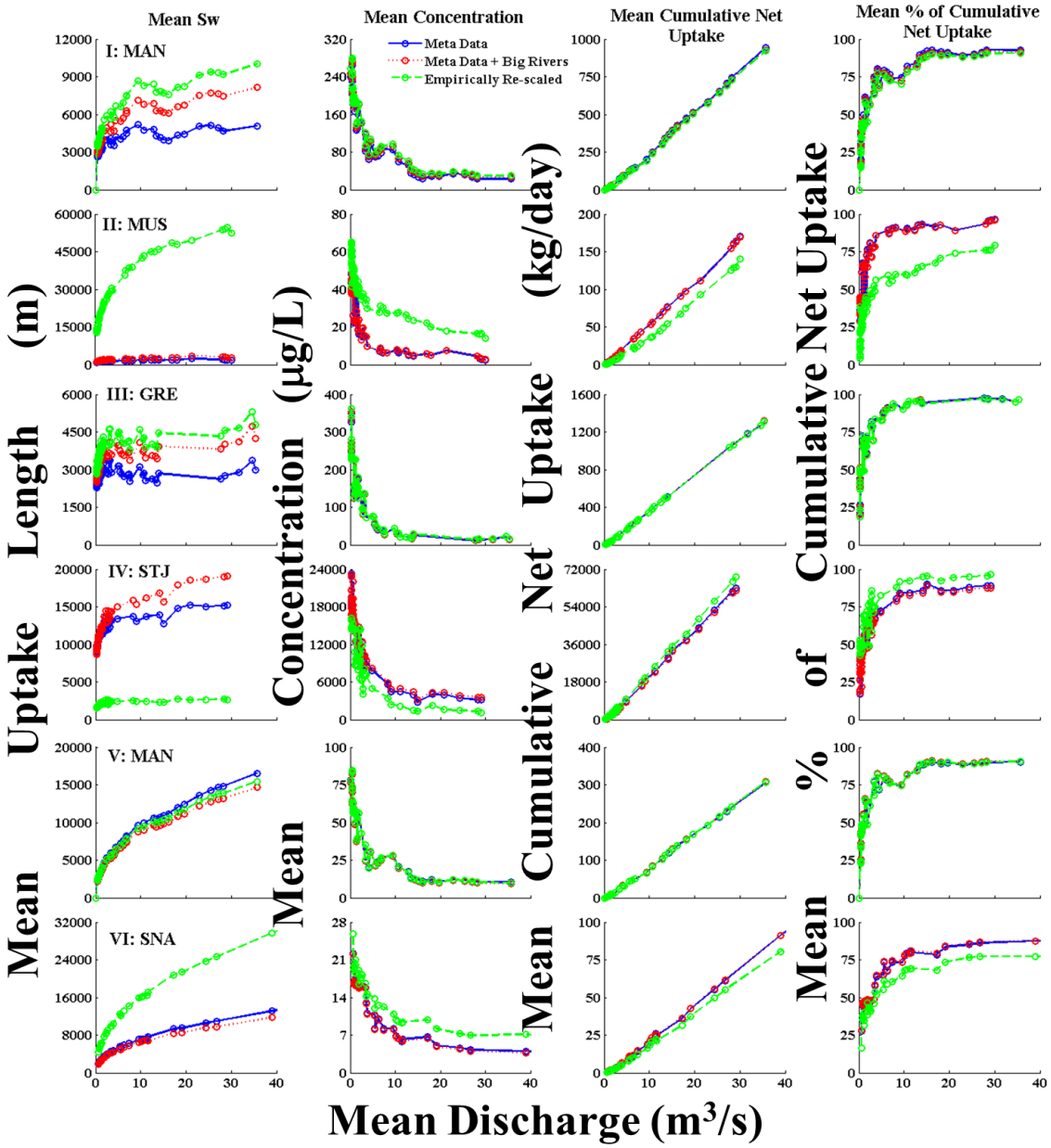

Figure 5.4: (a) Mean uptake length (Sw) ; (b) mean concentration; (c) mean cumulative net uptake; (d) mean cumulative percentage of net uptake for each solute at catchments predicted by Sw from meta data (blue), meta data plus big river observations (red) as well as re-scaled empirical Sw (green): (I) NH_4 at Manistee; (II) NH_4 at Muskegon; (III) NO_3 at Green; (IV) NO_3 at St. Joseph; (V) PO_4 at Manistee; (VI) PO_4 at Snake.

As we can see from Figure 5.4, the differences between the S_w predicted by a combination of the regression relationship of Hall et al. (2013) and by Equation 9 are small across the various catchments: the resulting nutrient uptake behavior characteristics are almost the same (i.e. concentration, daily net uptake, cumulative removal portion, etc.). While the nutrient transport in rivers are not only different from catchment to catchment, they are also different in terms of the biological activities with variable divergence from the average regression relationship of S_w over flow condition (Q/w) and concentration, i.e., in terms of the difference between the rescaled S_w and the S_w calculated from Hall et al. (2013) and Equation 9. For example, uptake behaviors estimated using the rescaled S_w of NH_4 (Figure 5.4I) and PO_4 (Figure 5.4V) at Manistee River, NO_3 at Green River (Figure 5.4III) are close to the uptake behaviors estimated using the *Sw* predicted from the meta-data or the meta-data + big river data. They are also quite different from each other: the rescaled S_w of NH_4 at Muskegon River is one magnitude larger the S_w estimated from the meta-data or the meta-data + big river data, leading to much higher concentration, one magnitude smaller daily net uptake as well as nearly 20% smaller in terms of the total percentage of ammonium that is retained in the water column by the whole catchment (Figure 5.4II). The rescaled values of S_w of NO_3 at St. Joseph River is much smaller than that S_w predicted from the meta-data or the meta-data + big river data, resulting in the concentration that is nearly one third of the concentration simulated by the other two universal regressions and almost three times the daily net uptake and total nitrate estimated by the two universal regressions (Figure 5.4IV). The rescaled S_w of PO_4 at Snake River is about twice that of the S_w estimated by the two universal regressions. As in the case of NH_4 at Muskegon River, this leads to a higher concentration across the catchment and much smaller daily net uptake and total removal from the water column (Figure 5.4VI). These results indicate that, given the big variations that the big rivers exhibit compared to the estimated from the universal regressions, it is necessary to measure solute uptake metrics for each river individually.

5.4 Discussion of results

Once the network model calibration is completed, the model results can be mined to gain considerable insights into the nutrient uptake processes across the network, including variations as a function of scale, as well as differences between the 15 “big river” study catchments. The results of these diagnostic analyses are organized into three groups: (1) scaling behavior within

each catchment, with a particular focus on differences between big rivers and small streams, (2) differences of network scale variations between different catchments, and (3) differences of uptake behavior between the three solutes: NO_3, PO_4 and NH_4, and their physical controls. The results of these analyses are presented next.

5.4.1 Comparison within catchment: big rivers vs. small streams

We first look at the nutrient transport patterns within a single catchment, and the effect of scale. Despite the variability among catchments and among solutes, there is one trend that is consistent in the model predictions: big rivers are not just pipes. Their contribution to nutrient retention in the whole river network is significant. This is illustrated next in detail.

If big rivers are mere pipes, then we would expect an exponentially increasing uptake length with increased flow in the downstream direction. If the S_w increases in the downstream direction, then nutrient concentration would likewise increase in the downstream direction: this is because nutrients will continue to come into the river network with the lateral inflow, and with increasing S_w, less of the nutrient would be removed from the water column. As a result, daily net uptake would stabilize downstream due to the low retention efficiency with increasing size of rivers and the cumulative uptake of the total input would decrease. In the event, the model simulations produced completely different results. After the rapid downstream increase from headwater to lower order reaches, the uptake length (S_w) tended to stabilize in bigger rivers (Figure 5.4, 1st column), which is consistent with the findings of Hall et al. (2013) with the use of a simple scaling approach based on meta-data of many small streams (Hall et al., 2013). According to Tank et al. (2008), if S_w increases exponentially with flow, that would mean hydrologic control is dominant; on the other hand, if it declines at turn points, then this allows biologic control to takes over in big rivers. Our simulation results indicate that more probably, in big rivers, biologic demand increases just as hydrologic influence increases, balancing out each other and creating a more stable S_w, suggesting that perhaps a dynamic equilibrium may be reached as a result. As we look at the nutrient uptake results, instead of increasing, we see stable concentrations downstream after the initial quick decline (Figure 5.4, 2nd column). Also the daily net uptake keeps increasing linearly with flow, and the increment does not decline downstream

(Figure 5.3, 3rd column); and the cumulative uptake of the total input tends to stabilize after the rapid increase in small order streams.

To quantify the big river contributions to nutrient retention, we divided the stream reaches within the river networks into two groups: small streams with mean flow less than 2000 L/s and big rivers with mean flow larger than 2000L/s. Note that 2000L/s is chosen here as the threshold because it is the natural break-point we have inferred from the meta-analysis of previous measurements (Tank et al., 2008). This also happens to be where traditional stream analysis techniques could be used and beyond which streams are not wade-able. Figure 5.5 presents the partitioning between small streams and big rivers of both total flow length and total daily net uptake for each solute in each of the 15 study catchments. Note the daily net uptake is based on the empirically re-scaled S_w.

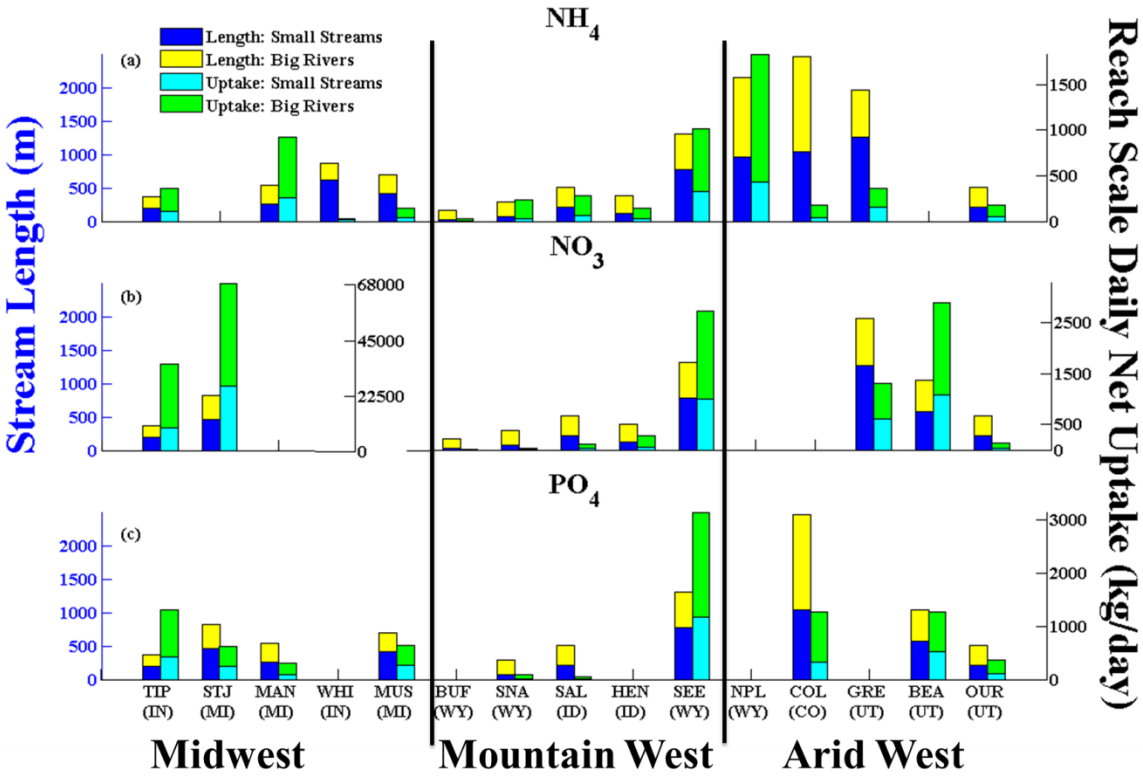

Figure 5.5: Partition of the stream length and reach scale daily net uptake between small streams (Q<2000L/s) and big rivers (Q>2000L/s) for each solute (a) NH_4; (b) NO_3; (c) PO_4

Looking at flow length first (the left bar), we can see that total stream length varies between catchments, mostly related to the drainage area of the catchments (as per Hack's law). Similar to flow length, daily net uptake also varies a lot between catchments. However, it is not necessarily proportional to stream length: large catchments with longer stream lengths could yet have relatively small daily net uptake (i.e. NH_4 in Colorado River) whereas medium sized catchments may retain much more nutrients (i.e. NO_3 in Midwestern Rivers). This is because daily net uptake is not only related to stream length, but could also be influenced by the uptake length and the magnitude of nutrient inputs. For example, the low NH_4 uptake in Colorado River could be related to the relatively low lateral inflow concentration while the low NH_4 uptake in Muskegon River is probably because of the extremely large uptake length (> 50,000m), and the high NO_3 uptake in the two Midwestern Rivers could be attributed to the high lateral inflow concentration (>10000 μg/L) arising from high agricultural land use.

Figure 5.5 also indicates that the combination of all big rivers in a stream network could make a significant contribution to the total daily net uptake (the green portion of the right bar can be quite long, even longer than the cyan portion). In this case, as in Figure 5.5, stream reaches are divided into small reaches and big rivers using a flow break-point of 2000L/s. To look at the partition between small streams and big rivers, the information in Figure 5.5 is now re-presented in Figure 5.6 in terms of percentages. In Figure 5.6, the left bar presents the fraction of stream reaches that can be considered as small streams (Q<2000L/s) and the fraction that would be classified as big rivers (Q>2000L/s).

As can be seen in Figure 5.6, the partitioning of total stream length and total nutrient uptake between small streams (Q<2000L/s) and big rivers (Q>2000L/s) do vary a lot from catchment to catchment. Despite the between-catchment differences, the big river (green) fraction of total nutrient uptake is larger than the small stream (yellow) fraction, and the fraction of nutrient retained in big rivers is larger than the corresponding fraction of total stream length in all 15 study catchments and for all three solutes. This suggests that the larger contribution of the big rivers to total nutrient uptake is not because of the longer travel distance. In other words, big rivers do not perform as pipes, in that they contribute more than their share of the total flow length.

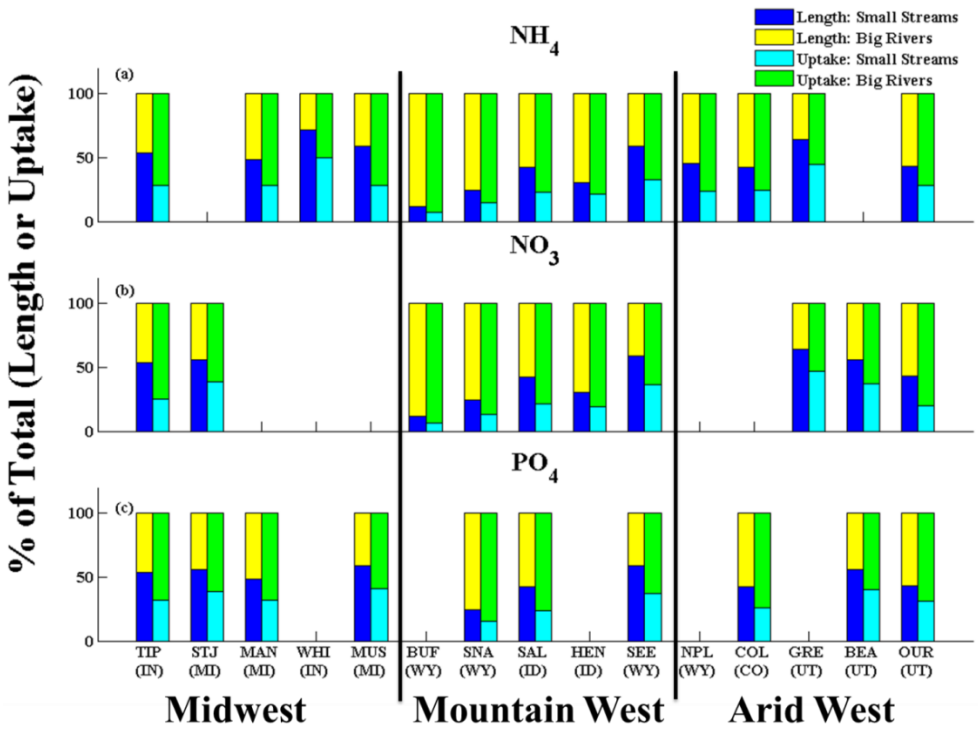

Figure 5.6: Percentage partition between small streams and big rivers for stream length and net uptake (a) NH_4; (b) NO_3; (c) PO_4. The blue portion represents small stream (Q<2000L/s) length as percentage of the total stream length, while the yellow portion refers to big river (Q>2000L/s) length as percentage of the total stream length. The cyan portion is the contribution of small stream nutrient uptake as percentage of the total nutrient uptake, while the green portion the percent of nutrient that is retained by big rivers.

5.4.2 Comparison across catchments

The results in Figure 5.6 showed that big rivers uptake a larger fraction of nutrients compared to their share of the total stream length. In spite of that common the results in Figure 5.6 also showed considerable variability between the catchments. For example, the partitioning of total stream length between small streams and big rivers are different (i.e. the small stream share of stream length is much smaller in the Mountain West catchments than in the Mid-west and Arid West catchments); partitioning of total nutrient uptake also varies from catchment to catchment. To better interpret and visualize how the reach-scale nutrient uptake varies spatially within each catchment and between catchments, we divided the uptake by the reach length. Figures 5.7 to 5.9 present the daily net uptake per kilometer of each reach across the 15 catchments for all three solutes: NH_4, NO_3 and PO_4, respectively.

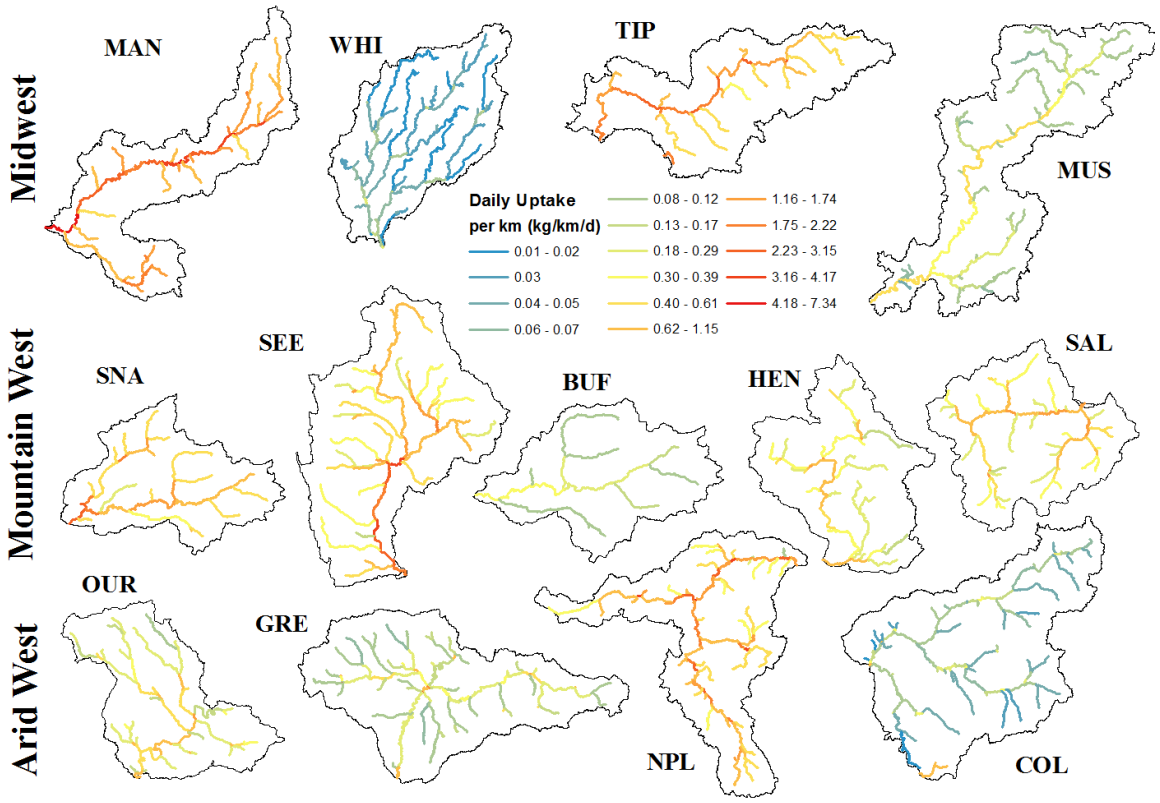

Figure 5.7: Map of reach scale daily net uptake per km for NH_4 at each catchment, the stream segments are colored by the reach scale daily net uptake per km, from high to low, they are colored from dark blue to red.

Figure 5.7 shows the daily net uptake of ammonium (NH_4) per kilometer of each reach. As we saw in Figure 5.6, the mainstreams, which are clearly big rivers, are highlighted by a warmer color, that is, the mainstreams uptake more ammonium per kilometer. Generally, the higher the stream order, the more the nutrient per kilometer the reach retains. This spatial distribution is consistent across catchments. Between the catchments, the per-kilometer-uptake is not uniform; the between-catchment variability could be attributed to input concentration and uptake capability (S_w). The uptake-per-kilometer is lowest on average in White River and Colorado River (the color tends to be blue or green); this is probably because of the limited source of ammonium in these western rivers where the inflow concentration is between 20 to 30μg/L and the concentration at the outlet is around 1μg/L. Uptake-per-kilometer is highest in the Manistee, Tippecanoe and Seedskadee Rivers, due to the relatively small S_w and larger lateral

inputs (lateral inflow concentration > 150μg/L, outlet concentration > 10μg/L). The high inflow concentration is probably related to higher fertilizer application in these agricultural catchments. Although the concentration in Muskegon is as high as in the other Midwest catchments, the uptake length (S_w) is much larger, leading to a medium level uptake-per-kilometer.

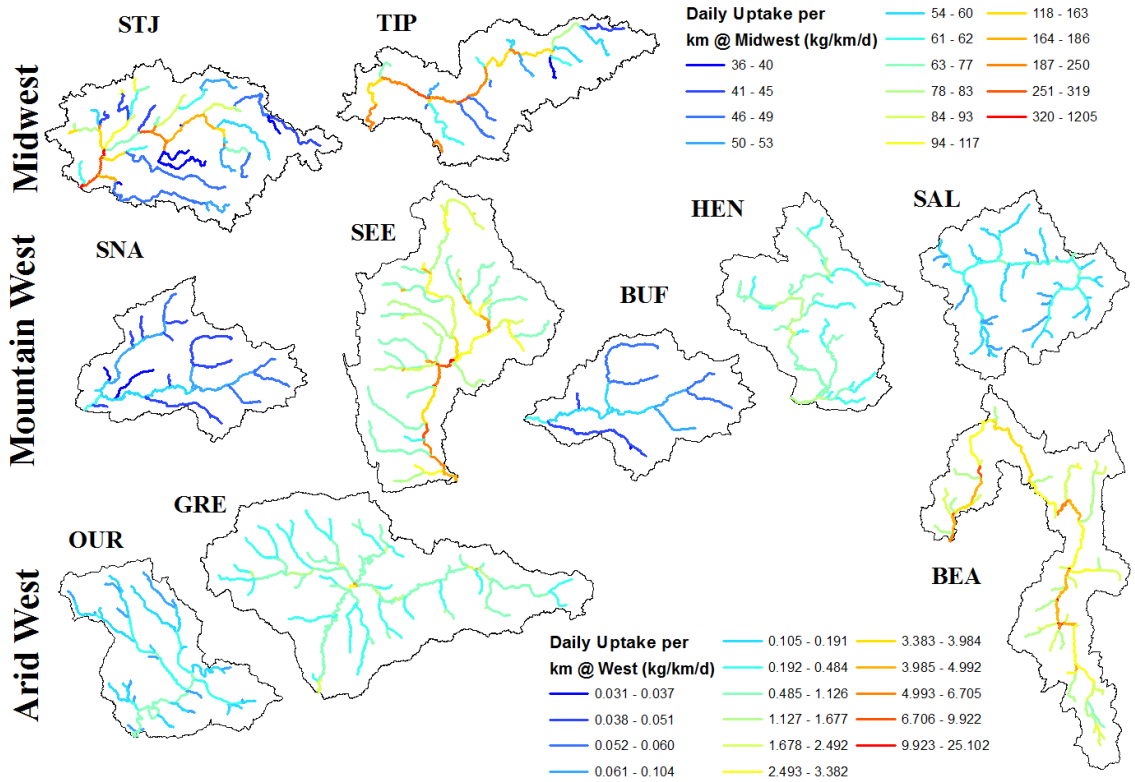

Figure 5.8: Map of reach scale daily net uptake per km for NO_3 at each catchment, the stream segments are colored by the reach scale daily net uptake per km, from high to low, they are colored from dark blue to red.

Figure 5.8 presents the amount of nitrate (NO_3) retained in each reach per day per kilometer. As is the case with ammonium, the mainstreams stand out with a warmer color, suggesting larger amount of uptake per kilometer compared to the small tributaries. The variability between catchments in term of daily net uptake per kilometer is on average much larger than in the case of ammonium. We can see two scales in these figures, with the uptake rates in Midwest Rivers being nearly two orders of magnitude larger than in the western rivers. The large uptake (per km) in largely agricultural Midwest Rivers is mostly due to the high nitrate input sourcing (lateral inflow concentration > 10000μg/L) from fertilizer application. In the West,

the uptake (per km) is much smaller, though still with considerable variability. It is higher in Bear and Seedskadee Rivers due to the relative high lateral inflow concentrations (> 500μg/L) compared to the other West rivers, and lower in Buffalo and Snake because of the low inflow concentrations (around 10μg/L) and relatively large S_w (> 10000m), the concentration in Salmon is also low, but due to the smaller S_w, the uptake per km is larger than in Buffalo and Snake.

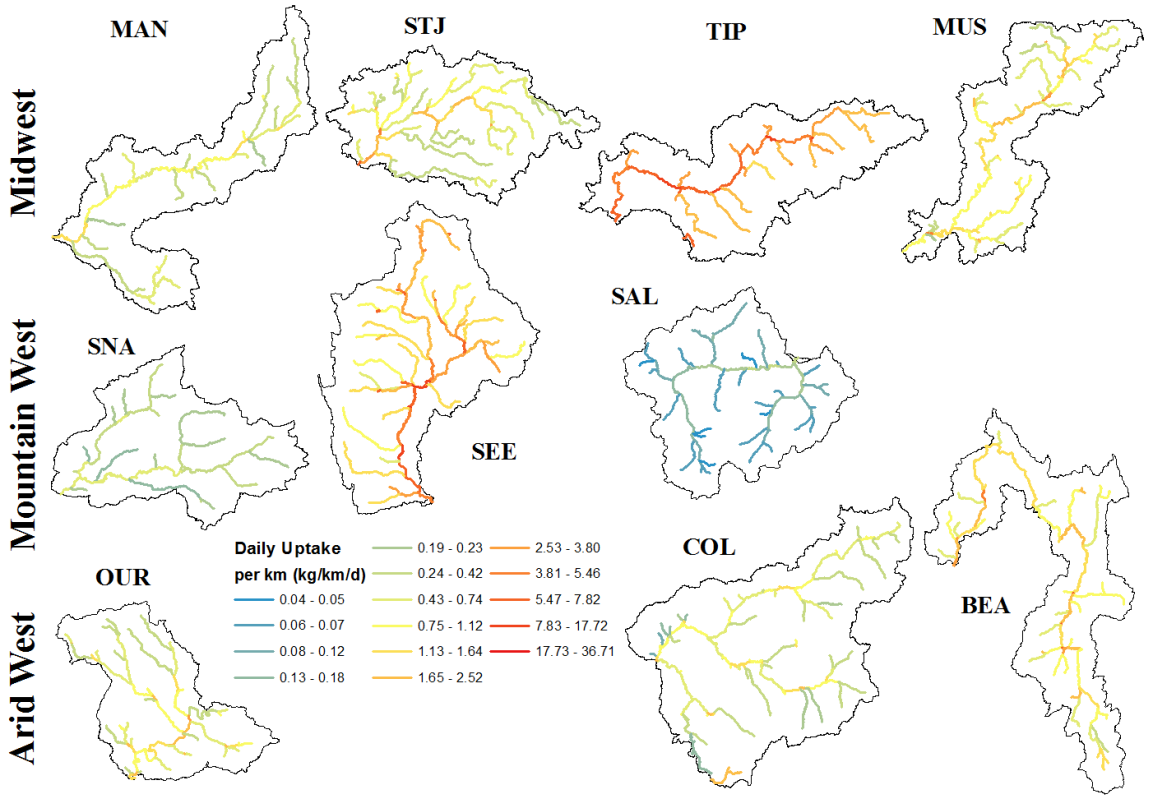

Figure 5.9: Map of reach scale daily net uptake per km for PO_4 at each catchment, the stream segments are colored by the reach scale daily net uptake per km, from high to low, they are colored from dark blue to red.

Finally, Figure 5.9 displays the daily net uptake of phosphate (PO_4) per kilometer for each reach in all 15 catchments. Consistent with the within-catchment spatial patterns seen in Figures 5.7 and 5.8 for ammonium and nitrate, the big mainstream rivers remove more phosphate per kilometer. The variability between catchments is larger than in the case of ammonium but much smaller than that of nitrate. The daily net uptake per kilometer is lowest in Salmon and Snake Rivers because of the low input concentrations (< 40μg/L) and relatively large S_w (> 25000m). The daily net uptake (per km) is highest in Tippecanoe, Seedskadee and Bear Rivers

due to the combined impact of the high input concentrations (the lateral inflow concentration > 500 μg/L) and relatively shorter S_w (< 6000m).

5.4.3 Comparison across solutes: the controlling factors

Apart from the differences between the catchments the nutrient uptake behavior also exhibits differences between different solutes, as already seen in Figures 5.7, 5.8 and 5.9. For example, we already saw that Muskegon has a medium per-kilometer net ammonium uptake compared to other catchments, but a relatively high per-kilometer net uptake of phosphate (nitrate data is not available). On the other hand, in Ouray, the per kilometer net uptake of is relatively low for nitrate, and relatively high for ammonium and phosphate. For some of the Mountain West Rivers (Snake, Buffalo, Henry's Fork and Salmon), per kilometer net uptake is relatively high for ammonium but relatively low for nitrate and phosphate.

From the comparison of all 15 catchments, we have already seen that these differences could be attributed to differences in inflow concentration and in uptake length. The medium per kilometer net uptake in Muskegon for ammonium is most likely due to the combined effect of high inflows and larger uptake lengths, while the low per kilometer net uptake of nitrate in Ouray is probably caused by the larger uptake length. If we want to correctly estimate the variability of net uptake between catchments and between solutes, it is necessary to understand the factors controlling the nutrient uptake, including whether these are different between the three different solutes.

To address the issue of physical controls of nutrient uptake, we applied the regression tree model presented in Section 5.2.4 to analyze the key controlling factors for all three solutes. Among all the catchment parameters we put together, 22 variables were selected as candidate variables to be used as inputs to the regression tree model. These include total catchment area, land use (the actual and percentage of developed land, forest, agricultural, wetland, native land and agricultural plus developed land), turbidity, total suspended sediment (TSS), measures of metabolism (mean gross primary production (GPP) and mean ecosystem respiration (ER)), dissolved inorganic nitrogen (DIN), biotic activity (seston chlorophyll a, benthic chlorophyll a, seston ash-free dry mass (AFDM), and benthic AFDM)).

Figure 5.10 presents the most dominant factors controlling the daily net uptake for NH_4, NO_3 and PO_4. For ammonium, the controlling factors are land use type (area fractions of wetland and forest) and mean GPP, which is consistent with the findings of Hall et al. (2013). The first split is wetland percentage: the smaller the wetland occupation, the larger the daily net uptake; within the left branch, the larger the GPP, the larger the daily net uptake. For nitrate, land use pattern is the only dominant factor: the smaller the forest land use, the higher the daily net uptake. This is consistent with what we have found previously, for nitrate, where the impact of the amount of lateral input is overwhelming. On the other hand, turbidity is apparently the most important factor in the case of phosphate uptake: the higher the turbidity, the larger the daily net uptake. This close correlation with turbidity is probably because of sediment sorption, which is the hypothesized mechanism of phosphorus removal from the water column.

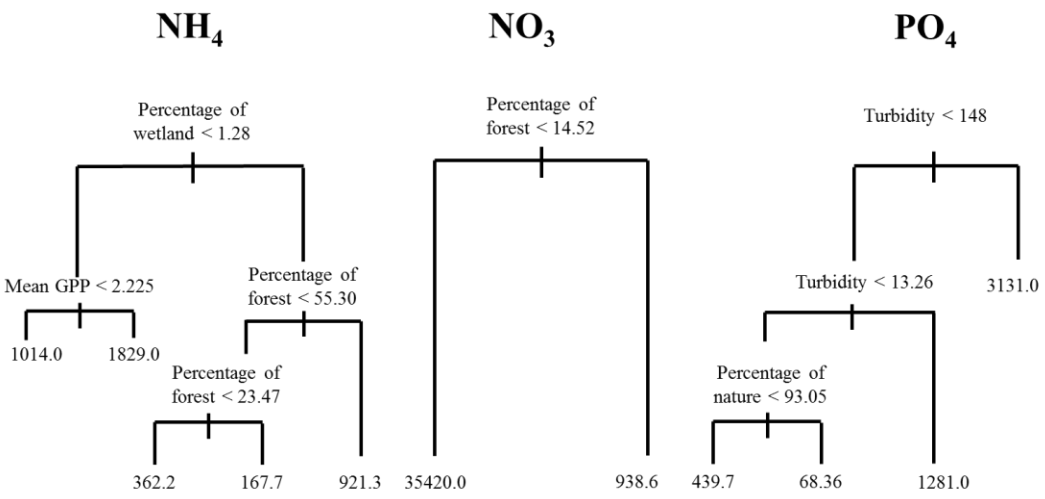

Figure 5.10: Regression tree of the dominant factors for reach scale daily net uptake of (a) NH_4; (b) NO_3; (c) PO_4.

Figure 5.11 shows the most dominant factors controlling, this time daily net *uptake per kilometer* for NH_4, NO_3 and PO_4. More variables are needed to predict the daily net uptake-per-kilometer for NH_4, such as mean ER and benthic chlorophyll a, whereas forest cover remains still the only controlling factor for nitrate. This finding is consistent with the hypothesis that algae and microbes prefer ammonium to nitrate, and also nitrate is bio-geochemically leaky,

especially when human impact is significant. For phosphate, besides turbidity, mean ER is also influential when considering the uptake per kilometer.

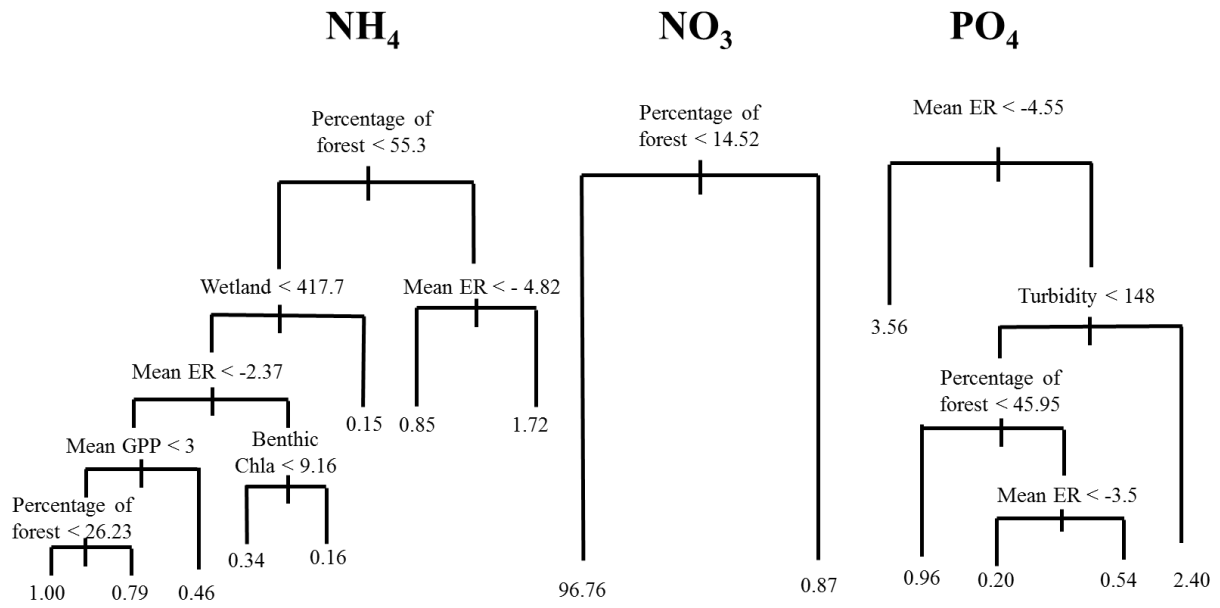

Figure 5.11: Regression tree of the dominant factors for reach scale daily net uptake per km of (a) NH_4; (b) NO_3; (c) PO_4.

5.5 Conclusions

This chapter presented a model-based exploration of scale effects on bulk removal for three different types of dissolved nutrients in river networks, with a particular focus on the relative contributions of small streams and big rivers to bulk removal, and the underlying physical controls. For this purpose we have utilized an improved version of the coupled network scale hydrological and biogeochemical model used by Ye et al. (2012, Chapter 4 of this dissertation). The major improvement has been in the area of parameterization of nutrient removal: in this study we have used empirical relationships derived from field measurements, both from small streams (meta-data from several previous studies) and also from 15 large rivers, which were carried out as part of this study. Observations from 15 big rivers spanning across gradients of land use, turbidity and biological activity, in combination with the meta-data on small streams,

permitted us to generate model parameters across the entire stream network, from headwater streams all the way to big rivers at the outlet of the catchments.

Despite large variations between big rivers, we found similar trends that clearly indicated that big rivers are not mere pipes. The model results showed that, consistent with several previous studies, the uptake from big rivers is as large as, even larger than, that from small streams. In fact, big rivers uptake a larger fraction of nutrients relative to their fraction of total stream length. In addition, maps of daily net uptake per kilometer suggest that for each kilometer, big rivers are still more active in terms of nutrient uptake than small streams. Big rivers contribute a larger amount of nutrient per kilometer than tributaries due to the much larger nutrient source from lateral inflow as well as the leftover amounts from upstream.

The comparison of nutrient uptake metrics between the 15 big river catchments indicated that the differences are most likely due to differences in lateral input nutrient loads and/or the nutrient uptake length. The lateral inflow nutrient concentration is usually determined by land use patterns while the uptake length could be influenced by many factors, e.g., in-stream biologic metabolism activity, flow dynamics. Regression tree analysis to explore dominant controls on net uptake indicated that removal of the three solutes, i.e., nitrate, ammonium and phosphate, from the water column happened by different mechanisms. Ammonium uptake is dominated by biotic metabolism as well as land use, which is related to the amount of ammonium source. Uptake of nitrate, being more biogeochemically leaky, is more related to land use which contributes to abundance of lateral input. On the other hand, phosphate retention is dominated by turbidity, presumably due to the role of sediment sorption.

The results from this study have several implications for catchment management aimed at contributing to reduction of eutrophication of receiving waters, such as for example the hypoxia in the Gulf of Mexico. Evidence that big rivers are not mere pipes, but with significant capability to remove nutrients, in relation to headwater streams, means that more attention should be paid in the future to maintain and enhance this capability of big rivers. Some of the ways that this can be done include naturalization of streams and rivers, allowing them to meander: these efforts help to lengthen travel distances, increase residence time and thus enhance biological uptake. Other actions include setting up vegetated riparian corridors that enhance biological demand.

Furthermore, customized approaches can be developed for rivers with different excessive nutrients. For rivers with high phosphorus flux, approaches to increases flow dynamics would be more efficient whereas for rivers with high nitrate flux, land use management could be more crucial.

There is considerable room for further improvement of the model used in this study. Currently, the model simulates bulk uptake only. Model realism would advance considerably if the bulk uptake could be separated into its pelagic, benthic and transient storage components. This will require targeted field measurements aimed at quantifying the separate contributions of pelagic, benthic and transient storage zone uptake to the total nutrient uptake. This will help make better predictions for the right reasons, and also help explain the physical factors that control uptake of different nutrients. The hydrological part of the model is sophisticated enough to simulate dynamics of flow at event scale, and therefore there is potential for an enhanced version of the model to be used to simulate the nutrient uptake processes during different flow conditions, and to study the role of temporal variability, including seasonal variability, on nutrient removal processes. In terms of spatial variability, the model will benefit from future field experiments designed to collect a set of uptake rate parameters (v_f, S_w, etc.) within the same river network from headwaters all the way down to the outlet.

5.6 Acknowledgements

The experimental data of the 15 rivers were measured by the Big River Team, and this research was supported by the NSF Grant: *Using Empirical and Modeling Approaches to Quantify the Importance of Nutrient Spiraling in Rivers* (DEB-0922118, Jennifer Tank, PI). We thank Jennifer Tank, Michelle Baker, Emma Rosi-Marshall, Robert Hall, and A J Reisinger, members of the Big River Team, for not only providing the extensive dataset collected during their big river experiments, but also for assisting with the data analysis, modeling and model diagnostics presented in this chapter.

References

Alexander, R. B., R. A. Smith, and G. E. Schwarz, (2000), Effect of stream channel size on the delivery of nitrogen to the Gulf of Mexico, *Nature*, 403, 758– 761.

Alexander, R. B., J. K. Böhlke, E. W. Boyer, M. B. David, J. W. Harvey, P. J. Mulholland, S.P. Seitzinger, C. R. Tobias, C. Tonitto, and W. M. Wollheim (2009), Dynamic modeling of nitrogen losses in river networks unravels the coupled effects of hydrological and biogeochemical processes, *Biogeochemistry, 93*, 91-116.

Aguilera, R., R. Marce´, and S. Sabater (2013), Modeling nutrient retention at the watershed scale: Does small stream research apply to the whole river network?, *J. Geophys. Res. Biogeosci.*, 118, 728–740, doi:10.1002/jgrg.20062.

Bernhardt, E. S., G. E. Likens, R. O. Hall, D. C. Buso, S. G. Fisher, T. M. Burton, J. L. Meyer, W. H. McDowell, M. S. Mayer, W. B. Bowden, S. E. G. Findlay, K. H. Macneale, R. S. Stelzer and W. H. Lowe, (2005), Can't see the forest for the stream? The capacity of instream processing to modify terrestrial nitrogen exports, *BioScience*, 52, 219 – 230, doi :10.1641/0006-3568(2005)055 [0219:ACSTFF]2.0.CO;2.

Billen G., C. Lancelot and M. Meybeck (1991) N, P and Si retention along the aquatic continuum from land to ocean. In: Mantoura RFC, Martin JM & Wollast R (Eds) Ocean Margin Processes in Global Change (pp 19–44). *Dahlem Workshop Reports*, Wiley

Bouwman, A. F., G. Van Drecht, J. M. Knoop, A. H. Beusen, C. R. Meinardi (2005), Exploring changes in river nitrogen export to the world's oceans. *Glob. Biogeochem. Cycles* 19, GB1002, doi:10.1029/2004GB002314 (2005).

Breiman, L., J. H. Friedman, R. Olshen, C. J. Stone (1984), Classification and Regression Trees, Wadsworth International Group, Belmont, California.

Claessens, L. and C. L. Tague (2009), Transport-based method for estimating in-stream nitrogen uptake at ambient concentration from nutrient addition experiments, *Limnol. Oceanogr.: Methods, 7*, 811-822.

Claessens, L., C. L. Tague, P. M. Groffman and J. M. Melack (2009), Longitudinal assessment of the effect of concentration on stream N uptake rates in an urbanizing watershed, *Biogeochemistry*, doi: 10.1007/s10533-009-9376-y.

Dodds, W. K., A. J. Lopez, W. B. Bowden, S. Gregory, N. B. Grimm, S. K. Hamilton, A. E. Hershey, E. Marti, W. H. McDowell, J. L, Meyer, D. Morrall, P. J. Mulholland, B. J. Peterson, J. L. Tank, H. M. Valett, J. R. Webster and W. M. Wollheim (2002), N uptake as a function of concentration in streams, *J. N. Am. Benthol. Soc., 21(2)*, 206-220.

Dodds, W. K. (2006), Nutrients and the 'dead zone': the link between nutrient ratios and dissolved oxygen in the northern Gulf of Mexico. *Frontiers in Ecology and the Environment* 4: 211 – 217.

Donner, S. D., M. T. Coe, J. D. Lenters, T. E. Twine and J. A. Foley (2002), Modeling the impact of hydrological changes on nitrate transport in the Mississippi river basin from 1955 to 1994, *Global Biogeochemical Cycles, 16(3)*, 1043, 10.1029/2001GB001396.

Ensign, S. H. and M. W. Doyle (2006), Nutrient spiraling in streams and river networks, *J. Geophys. Res., 111*, G04009, doi:10.1029/2005JG000114.

Hall, R. O. Jr., J. L. Tank, D. J. Sobota, P. J. Mulholland, J. M. O'Brien, W. K. Dodds, J. R. Webster, H. M. Valett, G. C. Poole, B. J. Peterson, J. L. Meyer, W. H. McDowell, S. L. Johnson, S. K. Hamilton, N. B. Grimm, S. V. Gregory, C. N. Dahm, L. W. Cooper, L. R. Ashkenas, S. M. Thomas, R. W. Sheibley, J. D. Potter, B. R. Niederlehner, L. T. Johnson, A. M. Helton, C. M. Crenshaw, A. J. Burgin, M. J. Bernot, J. J. Beaulieu, and C. P. Arango (2009), Nitrate removal in stream ecosystems measured by ^{15}N addition experiments: Total uptake, *Limnol. Oceanogr., 54(3)*, 653-665, 2009a.

Hall, R. O., M. A. Baker, E. J. Rosi-Marshall, and J. L. Tank (2013), Solute specific scaling of inorganic nitrogen and phosphorus uptake in streams, *Biogeosciences Discuss*., 10, 6671-6693.

Helton, A. M., G. C. Poole, J. L. Meyer, W. M Wollheim, B. J. Peterson, P. J. Mulholland5, E. S. Bernhardt, J. A. Stanford, C. Arango, L. R Ashkenas, L. W. Cooper, W. K Dodds, S. V. Gregory, R. O. Hall Jr, S. K Hamilton, S. L. Johnson, W. H. McDowell, J. D. Potter, J. L Tank, S. M. Thomas, H. M. Valett, J. R. Webster, and L. Zeglin (2011), Thinking outside the channel: modeling nitrogen cycling in networked river ecosystems. *Front. Ecol. Environ.*, 9(4): 229–238, doi:10.1890/080211.

Li, H, M. Sivapalan, D. Liu and F. Tian (2010), Water and nutrient balances in a large tile-drained agricultural catchment: A distributed modeling study. *Hydrol. Earth Syst. Sci.*, 14, 2259–2275, doi:10.5194/hess-14-2259-2010.

Mart í E., J. Aumatell, L. God é, M. Poch, and F. Sabater (2004), Nutrient retention efficiency in streams receiving inputs from wastewater treatment plants, *J. Environ. Qual.*, 33, 285–293.

Mulholland, P. J., J. D. Newbold, J. W. Elwood, and L. A. Ferren (1985), Phosphorus spiraling in a woodland stream： seasonal variations, *Ecology*, 66(3), 1012-1023.

Mulholland, P. J., and D. L. DeAngelis (2000), Effect of surface/subsurface exchange on nutrient dynamics and nutrient spiraling in streams, pp. 149-166. In: J. B. Jones, Jr. and P. J. Mulholland (eds.), *Streams and Ground Waters*. Academic Press, San Diego, CA.

Mulholland, P. J., A. M. Helton, G. C. Poole, R. O. Hall, S. K. Hamilton, B. J. Peterson, J. L. Tank, L. R. Ashkenas, L. W. Cooper, C. N. Dahm, W. K. Dodds, S. E. G. Findlay, S. V. Gregory, N. B. Grimm, S. L. Johnson, W. H. McDowell, J. L. Meyer, H. M. Valett, J. R. Webster, C. P. Arango, J. J. Beaulieu, M. J. Bernot, A. J. Burgin, C. L. Crenshaw, L. T. Johnson, B. R. Niederlehner, J. M. O'Brien, J. D. Potter, R. W. Sheibley, D. J. Sobota and S. M. Thomas (2008), Stream denitrification across biomes and its response to anthropogenic nitrate loading. *Nature*, *452*, 202–205.

Mulholland, P. J., R. O. Hall, D. J. Sobota, W. K. Dodds, S. E. G. Findlay, N. B. Grimm, S. K. Hamilton, W. H. Mcdowell, J. M. O. Brien, J. L. Tank, L. R. Ashkenas, L. W. Cooper, C. N. Dahm, S. V. Gregory, S. L. Johnson, J. L. Meyer, B. J. Peterson, G. C. Poole, H. M. Valett, J. R. Webster, C. P. Arango, J. J. Beaulieu, M. J. Bernot, A. J. Burgin, C. M. L. Crenshaw, A. M. Helton, L. T. Johnson, B. R. Niederlehner, J. D. Potter, R. W. Sheibley, and S. M. Thomas (2009), Nitrate removal in stream ecosystems measured by 15N addition experiments : Denitrification. *Limnol. Oceanogr.*, 54:666–680.

OECD. (1982). Eutrophication of Waters: Monitoring, Assessment and Control. OECD: Paris.

Peterson, B. J., W. M. Wollheim, P. J. Mulholland, J. R. Webster, J. L. Meyer, J. L. Tank, E. Marti, W. B. Bowden, H. M. Valett, A. E. Hershey, W. H. McDowell, W. K. Dodds, S. K. Hamilton, S. Gregory, D. D. Morrall (2001), Control of nitrogen export from watersheds by headwater streams, *Science*, *292(5514)*, 86–90.

Rabalais, N. N., R. E. Turner and W. J. Wiseman, Jr. (2002), Gulf of Mexico hypoxia, aka "the dead zone", *Annu. Rev. Ecol. Syst., 33*, 235-263.

Reggiani, P., M. Sivapalan, S.M. Hassanizadeh and W. G. Gray (2001), Coupled equations for mass and momentum balance in a bifurcating stream channel network: theoretical derivation and computational experiments, *Proc. Roy. Soc., Ser. A. Math. Phys. Engng. Sci.*, 457, 157–189.

Seitzinger, S. P., R. V. Styles, E. W. Boyer, R. B. Alexander, G. Billen, R. W. Howarth, B. Mayer and N. V. Breemen (2002), Nitrogen retention in rivers: model development and application to watersheds in the northeastern U.S.A., *Biogeochemistry, 57/58*: 199–237, 2002.

Seitzinger, S. P., J. A. Harrison, E. Dumont, A. H. W. Beusen, and A. F. Bouwman (2005), Sources and delivery of carbon, nitrogen, and phosphorus to the coastal zone: An overview of Global Nutrient Export from Watersheds (NEWS) models and their application, *Global Biogeochem. Cycles*, 19, GB4S01, doi:10.1029/2005GB002606.

Smith, R. A., G. E. Schwarz and R. B. Alexander (1997), Regional interpretation of water quality monitoring data, *Water Resour. Res., 33 (12)*, 2781-2798.

Tank, J. L., E. J. Rosi-Marshall, M. A. Baker and R. O. Hall, Jr. (2008), Are rivers just big streams? A pulse method to quantify nitrogen demand in a large river, *Ecology, 89(10)*, 2935-2945.

Tian, F., H. Hu, Z. Lei and M. Sivapalan (2006), Extension of the representative elementary watershed approach for cold regions via explicit treatment of energy related processes. *Hydrol. Earth Syst. Sci.*, 10, 619-644.

Wollheim, W. M., C. J. Vörösmarty, B. J. Peterson, S. P. Seitzinger, C. S. Hopkinson (2006), Relationship between river size and nutrient removal, *Geophys. Res. Lett., 33*, L06410, doi:10.1029/2006GL025845.

Wollheim, W. M., C. J. Vörösmarty, B. J. Peterson, S. P. Seitzinger, C. S. Hopkinson (2006), Relationship between river size and nutrient removal, *Geophys. Res. Lett., 33,* L06410, doi:10.1029/2006GL025845.

Wollheim, W. M., B. J. Peterson, S. M. Thomas, C. H. Hopkinson and C. J. Vörösmarty (2008a), Dynamics of N removal over annual time periods in a suburban river network, *J. Geophys. Res. -Biogeosciences,* 113, G03038.

Wollheim, W. M., C. J. Vörösmarty, A. F. Bouwman, P. Green, J. Harrison, E. Linder, B. J. Peterson, S. P. Seitzinger, and J. P. M. Syvitski (2008b), Global N removal by freshwater aquatic systems using a spatially distributed, within-basin approach, *Global Biogeochem. Cycles,* 22, GB2026, doi:10.1029/2007GB002963.

Ye, S., T. P. Covino, M. Sivapalan, N. B. Basu, H.-Y. Li, and S.-W. Wang (2012), Dissolved nutrient retention dynamics in river networks: A modeling investigation of transient flows and scale effects, *Water Resour. Res.,* 48, W00J17, doi:10.1029/2011WR010508.

Chapter 6

Modeling Dissolved Nutrient Retention Dynamics in River Networks: Prediction of Transient Flow Effects with Improved Empirically Derived Parameterizations

Abstract

As the corridors linking the hillslope, lakes and the oceans, river networks play an important role in nutrient transport and transformation from the terrestrial landscape to the estuaries and coastal seas. Much of our previous understanding of the nutrient spiraling process in river networks has been based on measurements that are limited to headwaters, and during low flow periods with minimal hydrologic variability. Such measurements have now been extended to big rivers as well, given the growing attention to their potentially large contribution to nutrient uptake in the whole river system. However, partly due to technical constraints, most of these experiments are still being carried out during low flow periods; the effects of temporal hydrologic variability are still not being able to be considered. In Chapter 4, we have showed the potential influence of within-year hydrologic variability on nutrient retention efficiency at the annual time scale based on theoretical modeling analysis carried out in a hypothetical river network. In this Chapter, we revisit this issue with the model developed in Chapter 5 that was based on empirical measurements. This coupled hydrologic and biogeochemical process model is applied to a small agricultural catchment in eastern Illinois to study nitrate transport and transformation processes. The uptake metric is calibrated based on a six-year observation of nitrate concentrations at one tile drainage station and two river stations. Three different climate scenarios with increasing within-year hydrologic variability (same as used in Chapter 4) are applied to the catchment. The results suggest that even in a nitrate-enriched catchment such as this, the river is not just a pipe, i.e., the nutrient uptake mechanisms in the river system can still reduce nutrient concentrations significantly. The model simulations also confirmed the finding in Chapter 4 that nutrient retention efficiency at all spatial scales of observation has a strong dependence on within-year variability of streamflow: the more variable the streamflow, the greater the export of nutrients.

6.1 Introduction

Eutrophication has become one of the most critical environmental problems affecting aquatic ecosystems across the U.S. (Bricker et al., 1999) causing irregular rapid propagation of algae, reducing dissolved oxygen, increasing aquatic organism mortality and decreasing species diversity (OECD, 1982). The excessive nutrients (mainly nitrogen and phosphorus) that contribute to the degradation of water quality in rivers, lakes and estuaries are mainly derived from fertilizers applied to agricultural lands and the sewage water from urban areas (Turner and Rabalais, 1994; Vitousek, 1997; Peterson et al., 2001). Before we can design best management practices to overcome water quality problems, we need to understand nutrient transformation and transport mechanisms in these aquatic ecosystems, and how they are inter-connected (Howarth et al., 2002; Ensign and Doyle, 2006).

As the corridors that link the hillslopes, lakes and the oceans, as well as function as important nutrient sinks, streams and rivers have attracted considerable attention recently from researchers and practitioners (Bencala and Walters, 1983; Dunn, 1996; Fisher et al., 1998; Dodds et al., 2002; Donner et al., 2002; Mulholland et al., 2002, 2008). Nutrient (usually nitrate, ammonium, and phosphate) uptake metrics (such as uptake length S_w, uptake velocity v_f, areal uptake rate U) have been measured in several locations across the continental United States (Bencala and Walters, 1983; Runkel, 1998; Claessens and Tague, 2009; Claessens *et al.*, 2009; Hall et al., 1998, 2002, 2003, 2009a). Synthesis studies conducted on these measured uptake data indicate significant regression relationships between the uptake metrics and discharge (Alexander et al., 2000; Tank et al., 2008; Helton et al., 2011; Hall et al., 2013), e.g., the larger the discharge, the larger the uptake length (S_w). A similar relationship has also been found for nutrient uptake length with nutrient concentrations in streamflow; the nutrient uptake mechanism exhibits the characteristic of saturation (Mulholland et al., 2008; Hall et al., 2013): the higher the concentration level, the larger the uptake length (S_w).

Because of the negative relationship between discharge and nutrient uptake, many previous studies have focused on headwaters or small streams and during low flow periods, since these are considered as the most efficient nutrient sinks (Peterson et al., 2001). Modeling results at the river network scale have indicated that the exclusive focus on small streams may limit our

understanding of nutrient transport and transformation at larger scales, since big rivers do not just function as pipes, i.e., they are not mere conduits for flow and nutrient transport. They are major critical zones for nutrient uptake, and due to the disproportional increase in nutrient input with increasing size of rivers from lateral flows, they tend to be responsible for more nutrient retention than small streams (Seitzinger et al., 2002; Ensign and Doyle, 2006; Wolheim et al., 2006; Mulholland et al., 2008; Ye et al., 2012). This projected importance of big rivers for nutrient uptake at river network scale has inspired many new field measurements in big rivers to help understand the up-scaling of nutrient retention from small streams to big rivers (Tank et al., 2008; Hall et al., 2013).

Measurements in big rivers also tend to be conducted in summer during low flow periods because of the difficulty to measure nutrient retention during fluctuating flows (Doyle 2005). The principles of injection techniques that are widely used to measure nutrient retention rates are not applicable to variable flow conditions due to the dilution of injection solutions. However, the results of continuous numerical modeling carried out over longer (i.e., annual) periods have clearly highlighted the importance of high flow periods for nutrient uptake, since it is during these periods that most of the nutrients are exported from the terrestrial landscapes into rivers (Meyer and Likens, 1979; Jones et al., 1996; Doyle 2005). This is particularly true for phosphate, which usually enters the rivers with sediments in absorbed form, since these sediments usually enter the river network with overland flow during big flow events rather than with baseflow. Observations have suggested that even during the high flow periods, small streams do not necessarily behave as pipes; significant amount of nutrients could still be removed from the water column due to the exchange with the hyporheic zone (Hall et al., 2009b). Model simulations also indicate that, similar to the impact of big rivers, the high nutrient loading during high flows could compensate for the lower removal efficiency and make the high flow periods relatively more important than low flow periods when considering total annual nutrient uptake (Böhlke et al., 2009). Therefore, the understanding of uptake processes gained during low flow periods is not sufficient to construct the long term patterns of nutrient dynamics (Fisher et al., 2004).

Due to the technical difficulties with nutrient retention measurements during variable flows, the use of coupled river network models of hydrologic dynamics and nutrient uptake

mechanisms has become an alternative approach to explore nutrient retention dynamics (Doyle 2005). This model should be able to upscale the processes from the reach scale to the network scale with consideration of both the hydrologic and the biologic controls at the local scale. Many river network models have been developed to study the impact of hydrologic variability on nutrient retention processes over annual time periods (Doyle 2005; Wolheim et al., 2008; Botter et al., 2010; Aguilera et al., 2013). These theoretical studies have indicated that nutrient uptake rate is related to the frequency of rainfall events, catchment residence time, catchment shape, nutrient concentration level and the strength of local biological activity (Wolheim et al., 2008; Botter et al., 2010). The large load of nutrients during high flows could compensate for the lower removal efficiency, giving rise to the fact that instead of low flows, the modal discharge is the most representative discharge in nutrient retention studies and should be given more attention (Doyle, 2005). However, most of the models presented are either too theoretical (Botter et al., 2010) or are not validated in real catchments due to the absence of the empirical data from big rivers (Doyle 2005; Wolheim et al., 2008; Aguilera et al., 2013).

Here we present a coupled river network model that is developed from both the published small stream data as well as the big river data from the Big River Team (Tank et al., 2009) to up-scale from headwater streams to big rivers and is parameterized using empirical measurements from small and big streams, as shown in Ye et al. (2014; Chapter 5). We then apply this model to a catchment in East Illinois where we calibrate and validate the parameters in the model with long-term nitrate concentration measurements at two gauges located along the river network. Three climate scenarios with different rainfall frequencies are introduced to the catchment to study the impact of hydrologic variability on the nutrient transformation and transport processes across the river network, and how this impact changes from headwater to big rivers downstream. With this understanding we can then separate the biologic and hydrologic contributions to the variability of nutrient uptake mechanisms across the year.

6.2 Methodology

6.2.1 Study area and data availability

The study area is the Little Vermillion River (Figure 1), located in east-central Illinois. The river network is extracted from the DEM with 30m resolution. The total drainage area of this

catchment is 489 km^2 with nearly 90% of the land put to agricultural use. The dominant soil type is silty loam and silty clay loam, with low saturated hydraulic conductivities. The topographic gradient is also very gentle, with the surface slope in this catchment being around 1% or less (Mitchell *et al.*, 2000; Algoazany, 2006). To drain out the water for corn and soybean planting, extensive tile drains have been introduced in the past: studies have shown that tile drainage could contribute over 80% of the annual runoff in this region (Li et al., 2010).

Hydrological, biogeochemical and management data had been collected from 1991 to 2000. There are in total two river stations, four subsurface stations and four surface stations to monitor flow, sediment and variable nutrient concentrations. For the study here, we used rainfall data and flow and nitrate data from one subsurface station (tile drain station B) and two river stations from 1993 to 1999, which is the period of overlap for the three stations. Rainfall data is spatially averaged at a daily time step, the temporal resolution for flow data is daily as well, while nitrate concentrations were measured at a frequency close to bi-weekly. Daily potential evaporation data from the contiguous MOPEX catchment is used for the evaporation calculation.

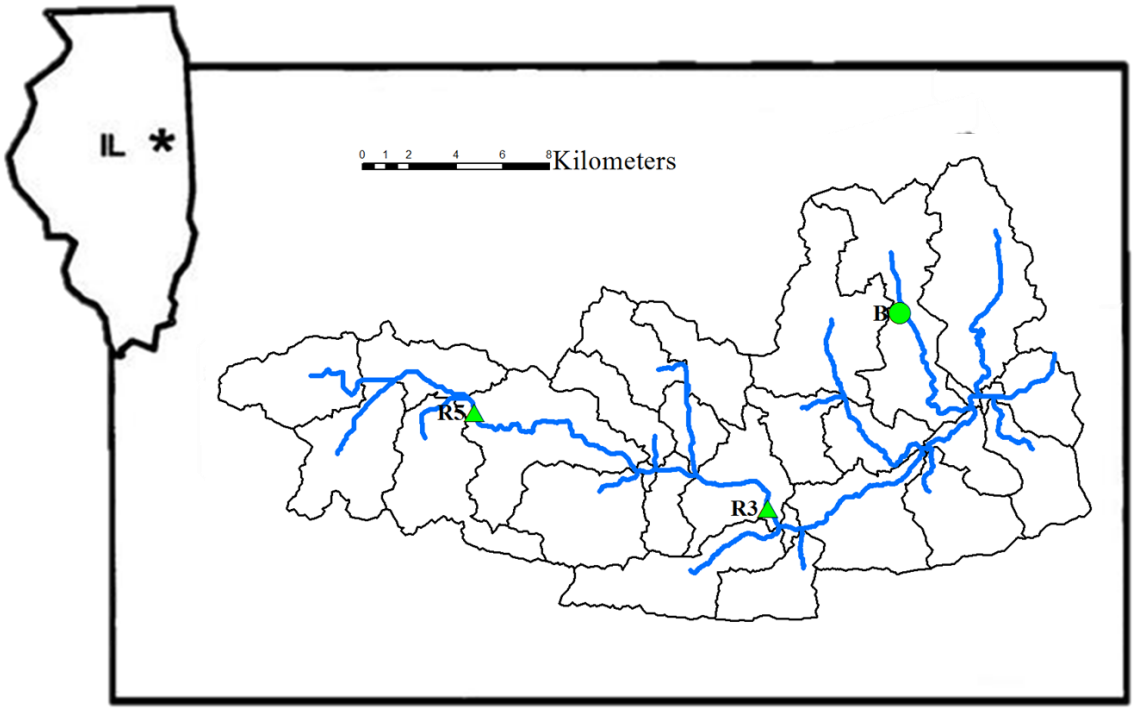

Figure 6.1: Map of the study area, Little Vermilion Basin in east-central Illinois, including the delineation of 29 REW boundaries. Blue bold line is the river network, the green circle is the tile drain station and the green triangles are the river stations.

6.2.2 Model structure

Figure 2 presents the schematic diagram of the coupled river network model that is used here. Based on the representative elementary watershed (REW) concept (Reggiani et al., 2001), the catchment is divided into 29 sub- catchments (REWs). Each REW has one hillslope component and one stream reach, which is connected with upstream and downstream as part of the river network. The water balance equation at the hillslope is as follows:

$$\frac{dS_h^i}{dt} = P^i - Q_s^i - Q_{tile}^i - ET^i \qquad (1)$$

where S^i_h is the local hillslope water storage at REW i [L^3], P^i is the spatial averaged daily rainfall [L^3 T^{-1}], $Q^i_s = S^i_h - S_c$ is the saturation excess surface flow [L^3 T^{-1}], S_c is a constant that refers to the soil water capacity [L^3], $Q^i_{tile} = (S^i_h - S_{tile})/T_{tile}$ is the tile drainage [L^3 T^{-1}], S_{tile} is the threshold for initiation of tile drainage [L^3], T_{tile} is the characteristic time for tile drainage [T], and $ET^i = PET\ (S^i_h/S_e)$ is evaporation over the REW i [L^3 T^{-1}], PET is the observed potential evaporation [L^3 T^{-1}] and S_e is deemed as the evaporation storage (a parameter of the model). Since we are focused on the impact of hydrologic variability on nutrient retention, nutrient storage in the soil is not modeled. A constant concentration level will be used for both the surface flow and tile drainage so as to exclude other influences such as coupling between lateral flow and nutrient concentration, so that we can focus on the hydrologic impact.

The river network part presented here is adapted from the model developed in Ye et al. (2014; Chapter 5). The mass balance equations for water are as follows:

$$\frac{dS^i}{dt} = Q_s^i + Q_{tile}^i + \sum Q_{up}^j - Q_{out}^i \qquad (2)$$

where S^i is water storage at local reach i [L^3], $Q^j_{up} = v^j A^j$ is the inflow from upstream nodes [L^3 T^{-1}], v^j is the velocity at upstream end, for reach j [L T^{-1}], A^j is cross-sectional area of the j^{th} upstream reach [L^2] (=S^j/L, where L is the reach length), $Q^i_{out} = v^i A^i$ is the outflow from reach i [L^3 T^{-1}], v^i is the velocity at local reach i [L T^{-1}] and A^i is cross-sectional area of local reach i [L^2]. Velocity v^i is estimated by reach scale momentum balance equation (i.e., Saint-Venant momentum balance equation).

$$v^i = \frac{1}{n^i}\sqrt{\frac{(R^i)^{1/3}}{P^i L^i}(A^i_{MC} L^i \sin\gamma^i \pm \sum_{j\neq i}\frac{1}{4}h^i(A^i_{MC} + A^j_{MC}) - \frac{1}{2}h^i A^i_{MC})} \quad (3)$$

where n^i is roughness coefficient of local REW i, R^i is the hydraulic radius P^i is average wetted perimeter, $\sin\gamma^j$ is the mean slope of REW i, and h^i is the mean depth of REW i [L]. Detailed derivation and explanation can be found in Tian et al. (2006) and Ye et al. (2012).

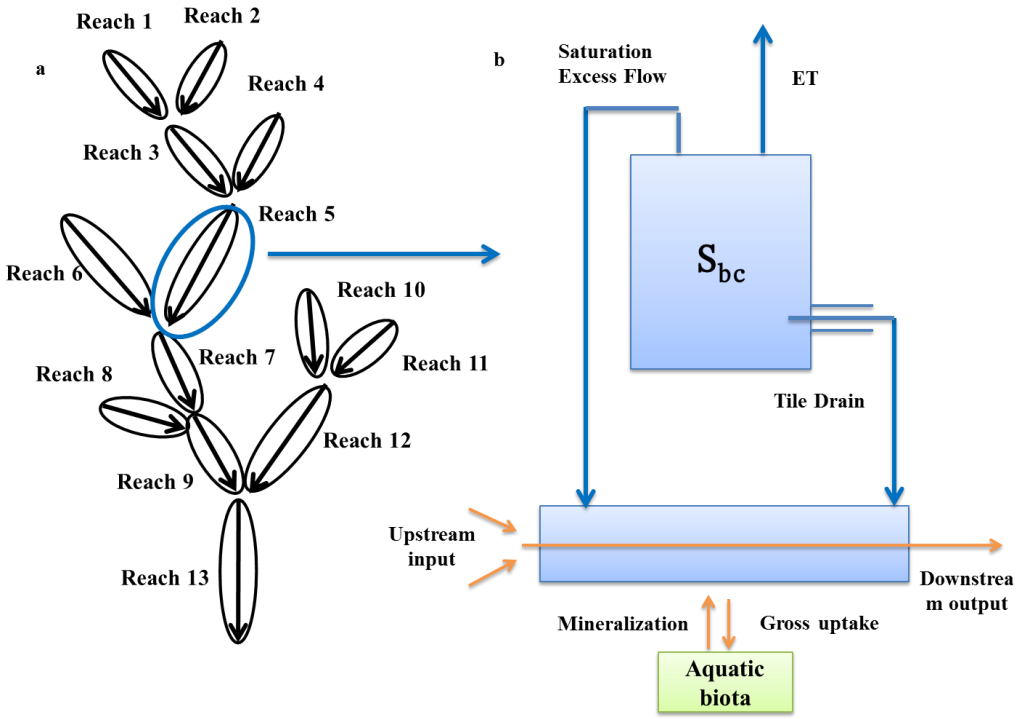

Figure 6.2: Schematic of the solute transport model coupled with hydrological dynamics: (a) Watershed discretization into many representative elementary watersheds (REWs) distributed around the river network; (b) each REW includes a hillslope component producing saturation excess flow and tile drainage and a channel reach receiving water and dissolved nitrate from hillslope.

The mass balance equation for nutrient transformation and transport in the river network is as follows:

$$\frac{d(S^i C^i)}{dt} = (Q^i_s + Q^i_{tile})C^i_l + \sum(Q^j_{up} C^j_{up}) - Q^i_{out} C^i - N^i_{tu} + N^i_{\min} \quad (4)$$

where C^i is the nitrate concentration (NO_3) at the local reach i [ML^{-3}], C^i_l is the solute concentration of lateral inflow [ML^{-3}], C^j_{up} is the solute concentration of the upstream reach j [ML^{-3}], $N^i_{min}=\beta N^i_{tu}$ is mineralization returning to the water column [$M T^{-1}$], β is the estimated fraction of mineralization out of total nutrient retention. Based on the LINX I data set, β is set to 0.034 for NO_3 (Johnson et al., 2013). $N^i_{tu} = R^i (S^i C^i)$ is gross retention in the water column [$M T^{-1}$], and R^i is the fraction of the nutrient in the water column that would be retained [-], which is calculated as follows (Wolheim et al., 2006):

$$R^i = 1 - \exp(-\frac{L^i}{S^i_w}) \quad (5)$$

where L^i is the length of the local reach i [L] and $S_w{}^i$ is the uptake length at the local reach i and is calculated by the following regression relationship that was developed from previous data in small streams and recently measured data from15 big rivers (see Ye et al., 2014; also, Chapter 5):

$$\log S^i_w = \gamma + 0.52 \log(Q^i / w^i) + 0.27 \log C^i \quad (6)$$

where Q^i is the discharge at local reach i, w^i is the width of the reach i, C^i is the solute concentration in reach i as mentioned earlier and γ is a constant representing the strength of local biological activity that will be calibrated using observed nitrate data (please refer to Ye et al., 2014; also, Chapter 5, for detailed explanation of the development of this regression).

6.2.3 Model calibration and validation

There are five parameters in the model that need calibration, four in the hillslope flow component, soil water capacity (S_c), threshold for tile drainage occurrence (S_{tile}), the characteristic time for tile drainage (T_{tile}) and evaporation storage (S_e), and one in the river network nitrate component, the intercept in the uptake length estimation (γ) (see Equation 6). The calibrations were conducted in two stages: firstly the intercept (γ) in the S_w estimation and secondly, parameters of the hillslope flow component.

Calibration of the intersect (γ) in S_w regression

In Ye et al. (2014; Chapter 5), the intercept in the uptake length (S_w) estimation regression was calculated using measured uptake length (S_w) at the outlet of the catchment. However, none of the nitrate uptake metrics was directly measured in the Little Vermillion River. Fortunately, however, we have the nitrate concentration at one tile drainage station and also in two river stations, and in this way S_w can be estimated through model calibration. Here, we temporarily dropped the hillslope flow component, and replaced the hillslope inflow (saturation excess flow and tile drainage) by the measured tile drainage from one subsurface station B (Figure 1). The observed tile drainage was normalized by the drainage area and then applied to all the REWs, assuming homogeneity of hillslope lateral inflow right across the network. The flow and nitrate measurements at river station R5: with one-third of total drainage area was used for calibration and the observations at river station R3 located in the middle of the catchment were used for validation. The overlap period of the three stations (subsurface station B, river station R5 and R3) dated from July 1993 to the end of 1999. The latter half year of 1993 was considered as a warm-up period of the simulation and the results from 1994 to 1999 were counted for calibration and validation.

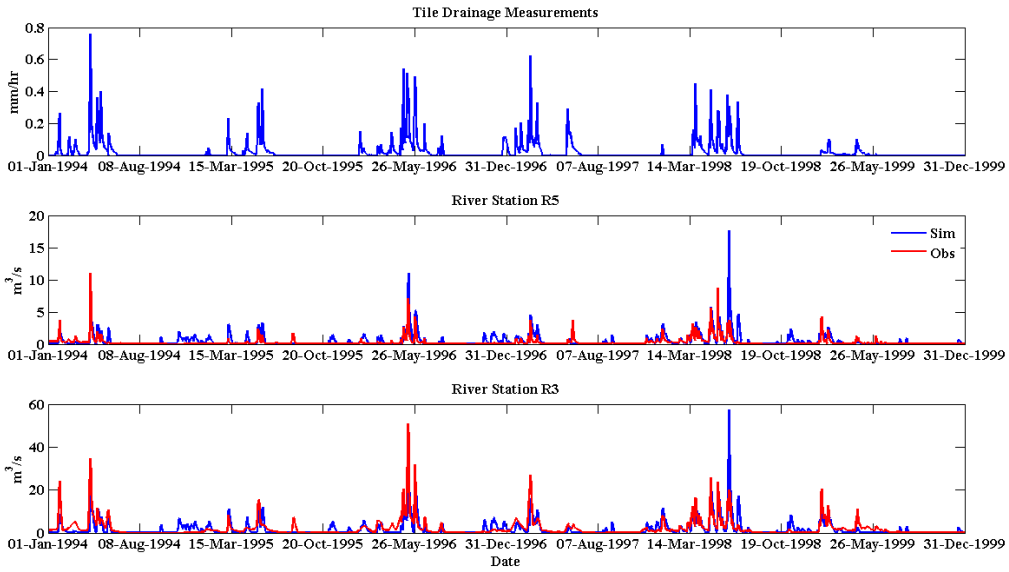

Figure 6.3: Time series data from Jan 1st, 1994 to Dec 31st, 1999 of (a) observed tile drain data at subsurface station B; (b) model simulated (blue) and observed (red) flow data at river station R5; (c) model simulated (blue) and observed (red) flow data at river station R3.

Figure 3 shows the measured discharge data from a tile drain at subsurface station B and the comparison between model simulated flow and observed discharge at river station R5 and R3. As we can see, the model simulation captures nearly all of the flow events quite well except for the flow peak in the middle of 1998. This underestimation of peak flow is because of the smaller tile drain observation (Figure 3a). One possible reason could be that the distribution of tile drains may not be as homogeneous as we assumed, and that there may be larger flows in other hillslope segments.

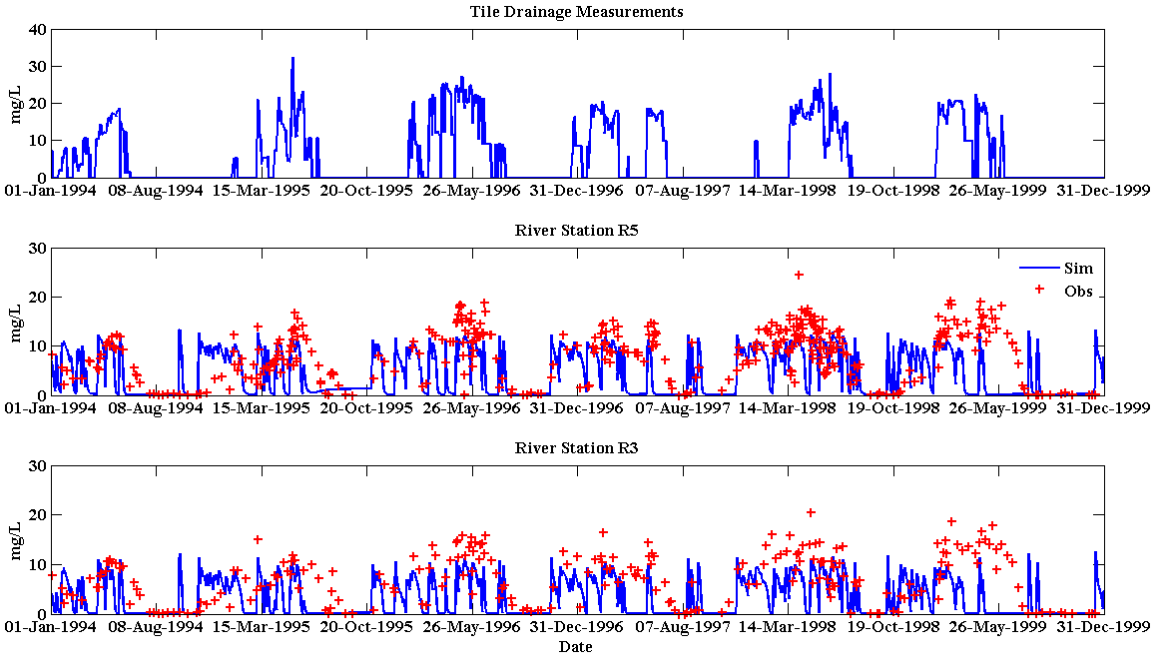

Figure 6.4: Time series data from Jan 1st, 1994 to Dec 31st, 1999 of (a) observed nitrate concentration data at subsurface station B; (b) model simulated (blue) and observed (red) nitrate concentration at river station R5; (c) model simulated (blue) and observed (red) nitrate concentration at river station R3.

Figure 4 presents the measured nitrate concentrations at subsurface station B that were used as inputs to the river network model as well as the model simulated and observed nitrate concentrations at river stations R5 and R3. Although the model simulations did not capture the annual cycle in the nitrate concentration fully, it managed to get the order of magnitude right as well as the decrease in nitrate concentrations from hillslope to reaches further downstream. The discrepancies in the annual cycle are most probably related to the absence of such a cycle in the

tile drain stations. The other possibility could be measurement errors during low flows: when the flow is lower than 1 m^3/s at the two river stations, observed nitrate concentrations may not be reliable. Still, this performance is deemed sufficient for the goals of our study.

Calibration of the hillslope flow component

In the second stage, we added back the hillslope flow component and applied the measured rainfall and potential evaporation as inputs to the hillslope component. As in the case of the first stage calibration, we ran the model from July 1993 to the end of 1999 and used the half year of 1993 as warm-up period and considered the results from 1994 to 1999. We calibrated the four parameters, i.e., soil water capacity (S_c), threshold for tile drainage occurrence (S_{tile}), the characteristic time for tile drainage (T_{tile}) and the evaporation storage (S_e), at subsurface station B and validated it at river stations R5 and R3.

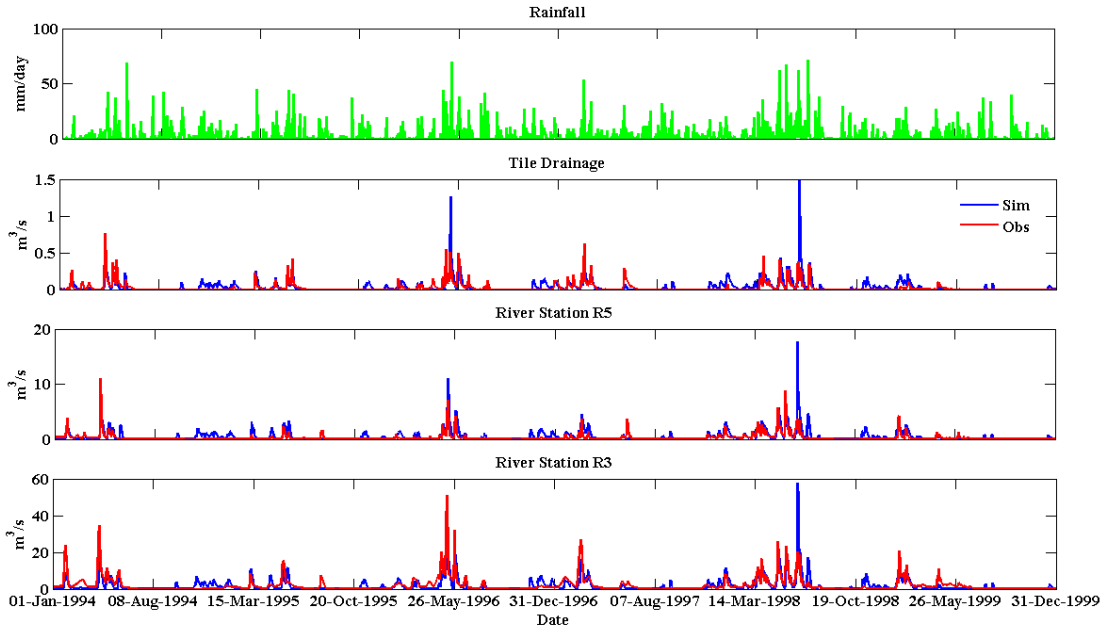

Figure 6.5: Time series data from Jan 1st, 1994 to Dec 31st, 1999 of (a) measured spatial averaged rainfall (b) model simulated (blue) and observed tile drainage (red) data at subsurface station B; (c) model simulated (blue) and observed (red) flow data at river station R5; (d) model simulated (blue) and observed (red) flow data at river station R3.

As we can see from Figure 5, the model successfully captured the individual flow events and reproduced the dry period in flow from summer to winter despite the many rainfall events. The

Nash-Sutcliffe coefficients at the two river stations are larger than 0.5, suggesting a sufficiently good fit to the observed flows.

6.2.4 Climate scenarios

To explore the impact of hydrological variability on nutrient retention, we applied three 10-year long synthetic rainfall series to the catchment and used the hillslope flow component to generate hillslope inflows to the river network. The three synthetic rainfall series were generated by a stochastic event rainfall model developed by Robinson and Sivapalan (1997). They are calculated based on three characteristics: storm duration (t_r), inter-storm period (t_b), and mean rainfall intensity (p), all of which are random. Storm duration, t_r and inter-storm period, t_b are assumed to follow exponential probability density distributions, and their mean values are assumed to vary sinusoidally with time of the year. The precipitation intensity (p) is statistically dependent on t_r, and its conditional distribution (given t_r) follows a gamma distribution: since the parameters of this gamma distribution are also a function of t_r, the mean p of the gamma distribution also varies sinusoidally, similar to t_r and t_b. The three climates share similar annual precipitation (around 1000 mm per year, which is the average for this region) and seasonality, in which rainfall comes during the spring and fall seasons, but different mean storm duration (t_r), inter-storm period (t_b), and rainfall density (p) to construct distinct hydro-climates. As we go from Climate 1 to Climate 3, within-year variability increases. The annual mean characteristics of the rainfall inputs and the coefficient of variation (CV) of streamflows are presented in Table 6.1 for the three climates. Figure 6 is an example of the flow and concentration variations under Climate 2. The high flows and low flows are separated based by the baseflow separation algorithm of Lyne and Hollick (1979):

$$Q_b(t) = aQ_b(t-1) + \frac{1-a}{2}(Q(t) + Q(t-1)) \qquad (7)$$

where $Q_b(t)$ is the baseflow at time t, $Q(t)$ is the streamflow at time t, and α is a constant.

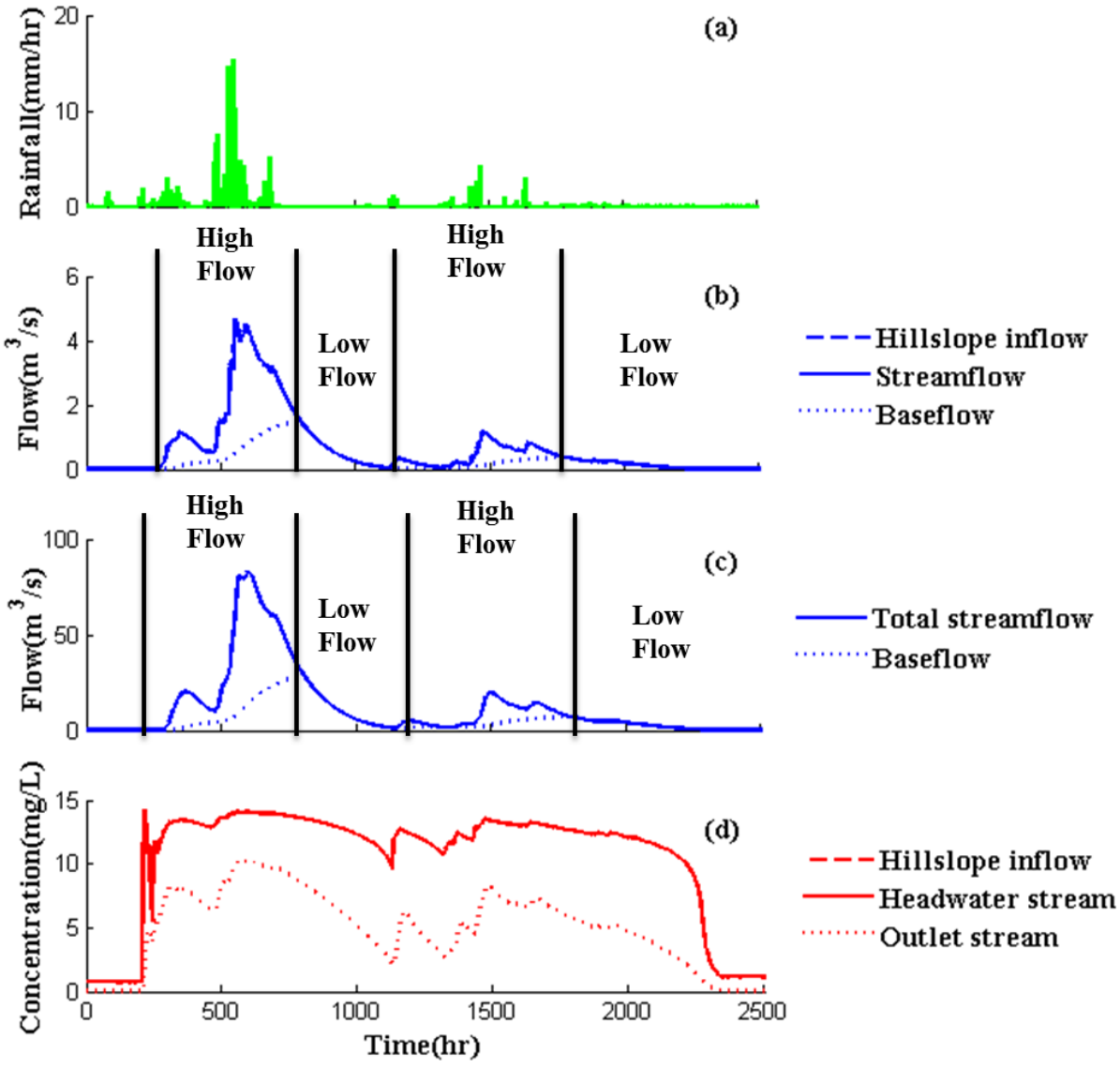

Figure 6.6: Schematic describing typical time series of rainfall, hillslope inflows and streamflows and nutrient concentrations for Climate 1 (see Table 6.2): (a) rainfall event patterns - intensity=0.4mm/hr, t_r=34hr, t_b=76hr; (b) hillslope inflows and streamflow for a headwater stream; (c) streamflow at the catchment outlet, and illustration of flow separation into high flow and low flow periods; (d) nutrient concentration of hillslope input (assumed constant at 15 mg NO3-N/l), and for a 1st order REW and at the catchment outlet.

Nitrate concentrations of the hillslope flow contributions to the river channels are kept constant in space and time, during both flood events and baseflow periods, at a notional value of

15 *mg* NO_3-N/*l*, which is the mean concentration of observed tile drain data in the Little Vermilion catchment. Low temporal variability in nitrate concentrations relative to that of water discharge in intensively managed agricultural catchments (i.e., chemostatic export) has been discussed in recent papers (Basu *et al.,* 2010; Thompson *et al.,* 2011; Guan *et al.,* 2011).

Table 6.1: Effects of hydrological variability and geomorphologic and biogeochemical factors on nitrate net retention rates during high and low flows

	Climate 1	Climate 2	Climate 3
Mean t_r (hr)	34	15	34
Mean t_b (hr)	76	227	186
Mean p (mm/hr)	0.4	2.0	0.8
Mean CV(Q) of headwater reaches	3.02	4.04	4.98
CV(Q) of outlet reach	3.00	4.00	4.96

6.3 Results

6.3.1 The impact of biological uptake

Comparing the intercept for uptake length (S_w) we obtained by calibration with the intercepts found in Ye et al. (2014; Chapter 5) based on the measured uptake length in big rivers, we can see the S_w in Little Vermilion is larger than the estimated S_w values from both small streams and the "Big River" data for most of the rivers presented in Ye et al. (2014; Chapter 5). Therefore we will first study the impact of biological uptake, to find out how influential the nutrient uptake is in a nitrate-enriched agricultural catchment such as Little Vermillion.

Figure 7 presents the comparison between observed nitrate concentrations and the model simulated concentrations under two scenarios: one without any biological uptake, the other with nitrate uptake calculated from the calibrated uptake length. That is, in the first scenario, the reduction of nitrate concentration from tile drainage station to the river station is only caused by

dilution, while the decrease in concentration in the second scenario is due to both dilution and uptake.

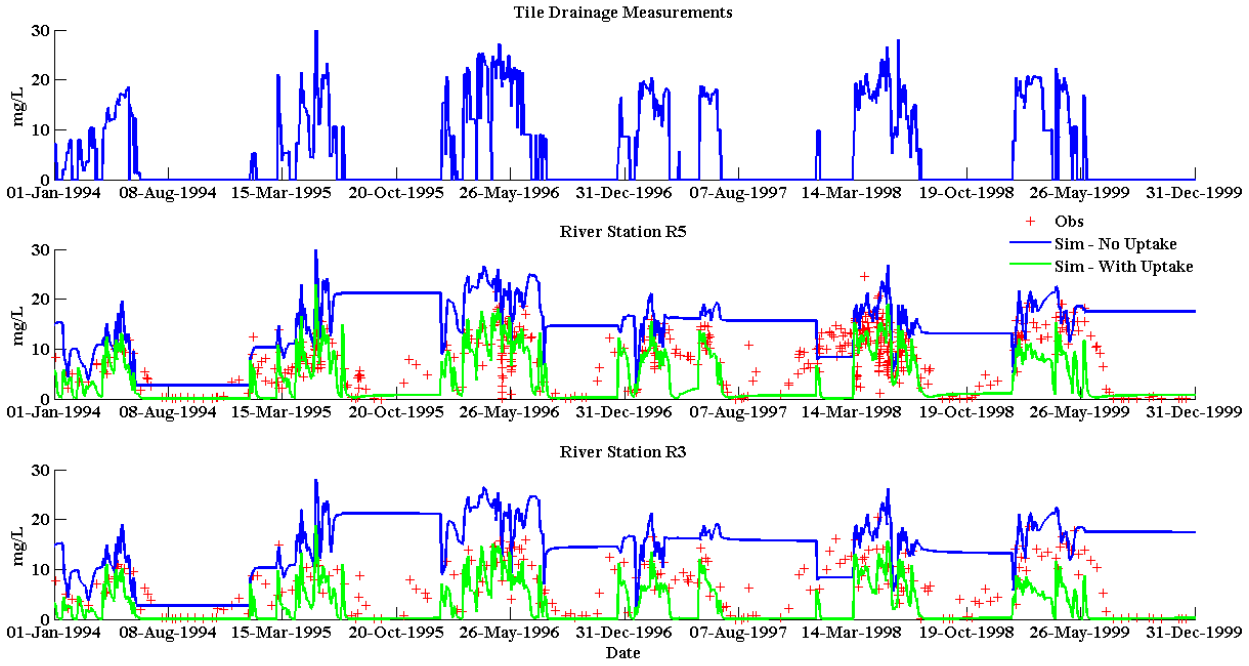

Figure 6.7: Time series data from Jan 1st, 1994 to Dec 31st, 1999 of (a) measured nitrate concentration at one tile drainage station (b) measured nitrate concentration (red plus symbol) and model simulated concentration with (green line) and without (blue line) uptake at river station R5; (c) measured nitrate concentration (red plus symbol) and model simulated concentration with (green line) and without (blue line) uptake at river station R3.

Comparing the nitrate concentration at the tile drainage station that is used as hillslope input with the model simulated concentration at the two river stations in the first "no uptake" scenario, we can see that although the concentration drops slightly due to dilution, the change is not very significant and the simulated concentrations at the river stations is still much higher than observed concentrations. The concentrations are particularly high between flow events. Although there is no nitrate input from the tile drain (hillslope/lateral inflow) during low flows, the concentration is still high at the river stations since there is no uptake; since dilution is limited during such low flows, the concentration remains as high as it is at the end of previous flow events. We then look at the simulated concentration for the two scenarios: overall, the

concentrations are lower when there is biological uptake included. Specifically, the difference in concentration is smallest during flow peaks; and largest during low flow periods. This is understandable: during the flow peaks the uptake length is larger, leading to smaller uptake rate, and the velocity is larger, causing shorter residence time, therefore the percentage of nitrate that can be removed from the river channel is smaller, and *vice versa*. This is consistent with what we found in Ye et al. (2012; Chapter 4): the nutrient (here it is nitrate) retention efficiency is lower during high flows and higher during low flow periods.

6.3.2 High flow vs. low flow periods

Hydrologic variability is the result of the frequency of flow events. Before we explore the impact of variability, we first look at the difference between high flows and low flows, i.e., the difference between flow events and within flow events. Figure 8 presents the mean annual input, net uptake retention efficiency and the partitioning between high flows and low flows under Climate 1 for REWs along the river network. As we can see, the mean annual nitrate input from the hillslopes during high flow periods is about twice the mean annual nitrate input during low flow periods. This difference between the two flow periods is attenuated in the annual net uptake: nitrate input during high flow periods is only about 50% larger than the amount of nitrate retained during low flow periods.

Based on the total input and net uptake, we can estimate the retention efficiency (Eff_h, Eff_l) and the contribution of nitrate uptake (f_h, f_l) for high flow and low flow periods:

$$Eff_h = \frac{\sum_i \int_{Th} (N_{tu}^i(t) - N_{\min}^i(t))dt}{\sum_i \int_{Th} (Q_s^i(t) + Q_{tile}^i(t))C_l dt} \quad (8)$$

$$f_h = \frac{\sum_i \int_{Th} (N_{tu}^i(t) - N_{\min}^i(t))dt}{\sum_i \int_{Th+Tl} (N_{tu}^i(t) - N_{\min}^i(t))dt} \quad (9)$$

where the retention efficiency (Eff_h, Eff_l) is calculated as the fraction of net uptake to total input during high flow periods (Th) or low flow periods (Tl) and the contributions of both periods (f_h, f_l)

are calculated as the fractions of nitrate retained during high flow (*Th*) and low flow (*Tl*) periods to the total net uptake.

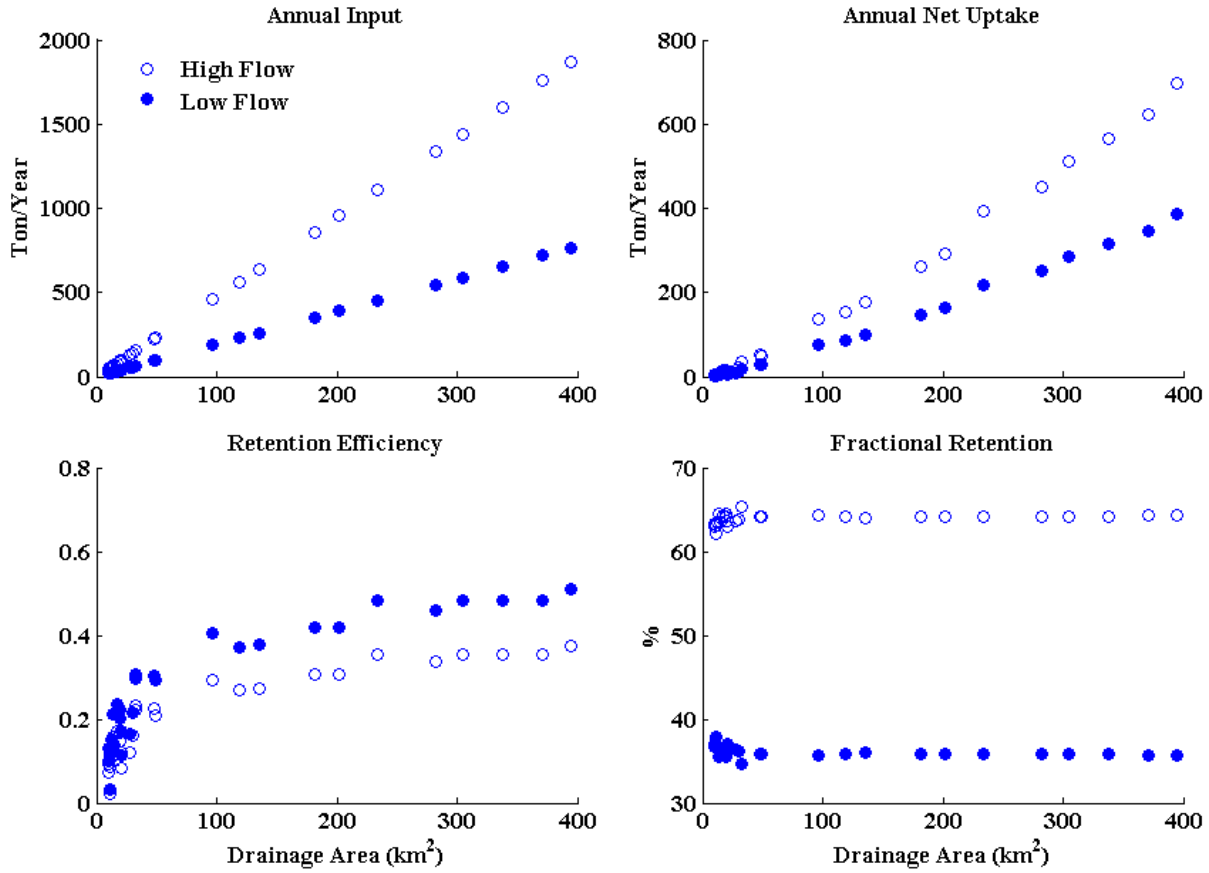

Figure 6.8: Comparison between the high flow period and low flow period of (a) annual input; (b) annual net uptake; (c) annual retention efficiency; and (d) the fractional retention of each period.

As we expected, the retention efficiency during high flows is much smaller, i.e., only a quarter of the efficiency obtained during low flows (Figure 6.8c). The overall mean retention efficiency for the whole catchment during high flows is around 0.4 while the efficiency during low flows is about 0.55. However, the contribution of nitrate retention during high flow periods should not be underestimated by the relatively small retention efficiency. Due to the much larger nitrate inputs during high flow periods, the nitrate retained during high flow period is more than that during low flow periods and this difference increases downstream. Overall, for the whole catchment, high flows contributed over 65% of the total nitrate uptake while the low flows

periods made up 35% of the total retention. Consistent with previous literature, due to the larger nitrate inflows from the terrestrial landscape, the high flow periods are important in the construction of annual nutrient budgets (Doyle 2005; Ye et al., 2012).

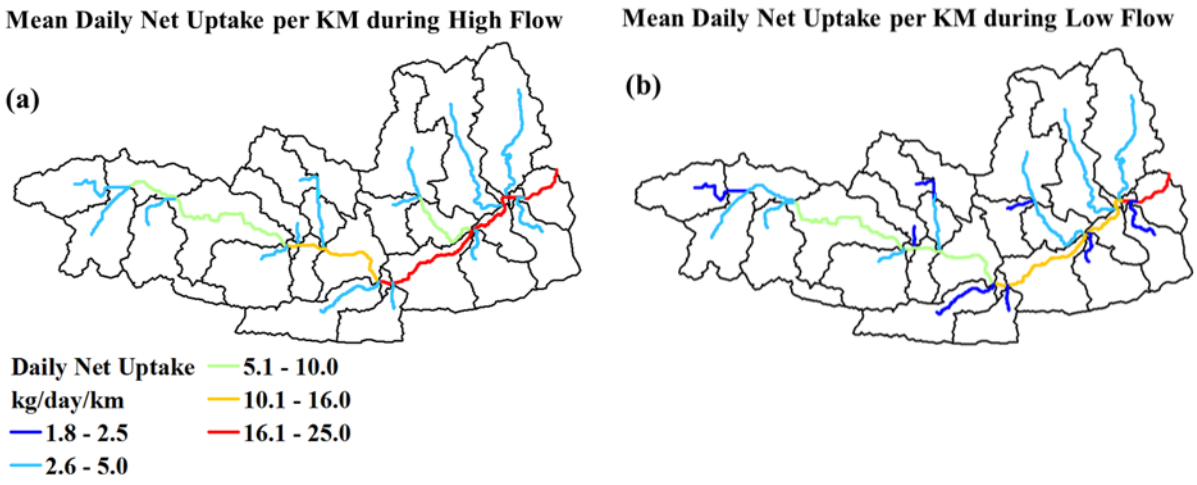

Figure 6.9: Map of the reach scale mean daily net uptake per kilometer (a) during high flow; (b) during low flow.

Figure 6.9 displays the daily average net uptake per kilometer for each reach during high flows and low flows. The amount of nitrate that is removed from the water column in one kilometer increases from headwaters to the outlet: the higher the stream order, the closer the reach is to the outlet, the more nitrate uptake occurs per kilometer. This trend is consistent during high flows as well as low flows. Comparing the two maps, we can see that more nitrate is retained in each reach during the high flow than low flow periods, and this increment in uptake per kilometer is larger in the main stems of the rivers than in headwaters.

6.3.3 Impact of hydrologic variability

We next applied the three climate scenarios to the catchment. Figure 10 shows the mean annual input, net uptake, retention efficiency and fractional retention during high flow and low flow periods under the three different climates. As we can see, most nitrate was exported into the river network under Climate 2, the one with medium variability, while nitrate input to the river network is least under Climate 1 that has the smallest variability (Figure 10a). That is, Climate 2 generates more runoff than the other two climates. This trend remains when we look at the mean

annual net uptake during low flow periods. But it is not seen in the high flow periods, where the nitrate retained from the water column is highest under lowest variability (Climate 1) and lowest under highest variability (Climate 3) (Figure 10b). As a result of these two factors, retention efficiency decreases with hydrologic variability: it is highest under Climate 1 and lowest under Climate 3, with highest variability occurring during both high flow and low flow periods, although the difference between the two climates with higher variability is small during low flow periods (Figure 10c). This is consistent with the theoretical results we found in Ye et al. (2012; Chapter 4). The partitioning of nitrate uptake between high and low flow periods does not follow the climate variability trend: high flow contributes more uptake under Climate 1 with lowest variability, but retains least nitrate from water column during Climate 2 with medium variability.

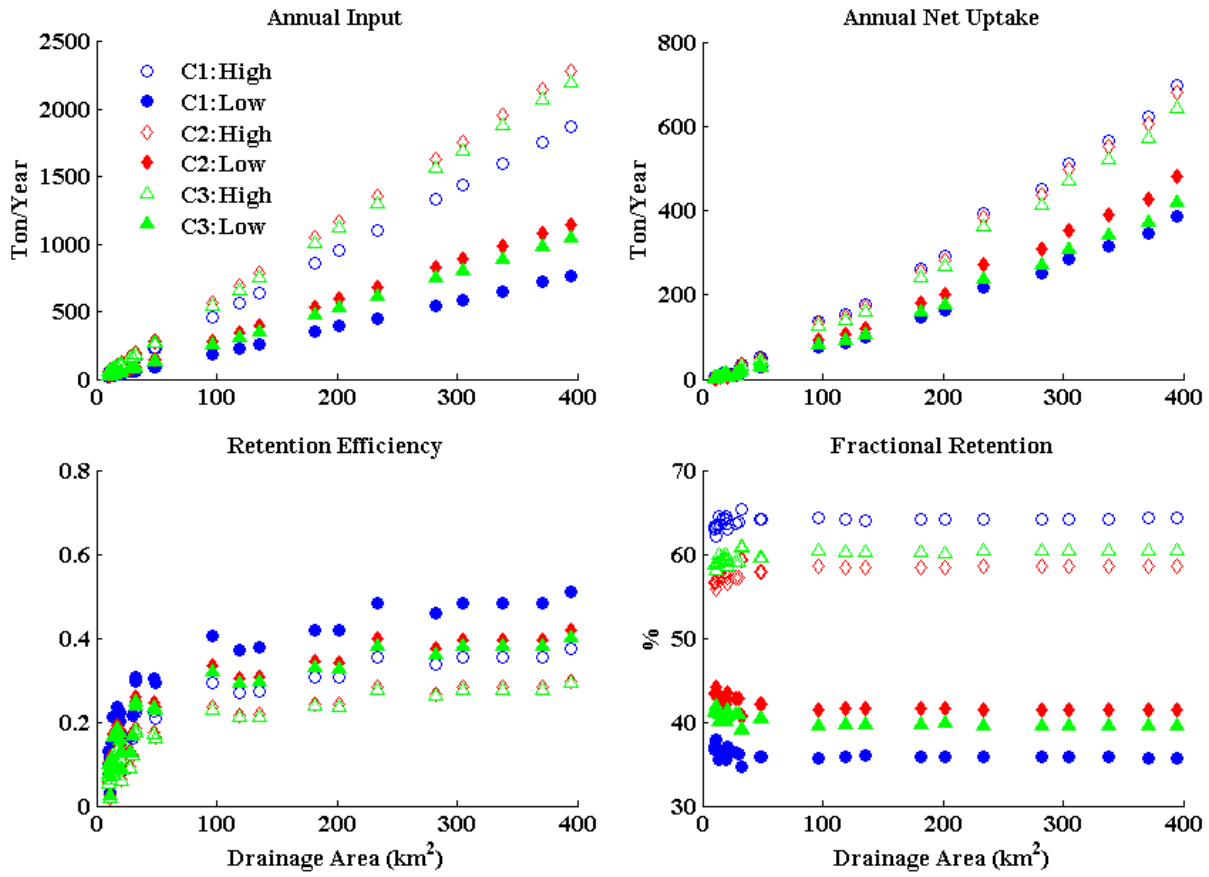

Figure 6.10: Comparison between the high flow period and low flow period for the three climate scenarios of (a) annual input; (b) annual net uptake; (c) annual retention efficiency; and (d) the fractional retention of each period.

6.4 Discussion and conclusions

In this chapter, we applied the coupled hydrologic and biogeochemical river network model developed in Ye et al. (2014; Chapter 5) to the Little Vermillion catchment with an addition of a hillslope flow component to convert the rainfall into hillslope runoff for the study of the impact of hydrologic variability on nutrient retention. Many models have been developed at river network scale. Some are theoretical models without empirical data support (Botter et al., 2010; Ye et al., 2012), and others, due to the lack of big river measurements, are just simple extrapolations of understanding gained from small streams, which may underestimate the variability among rivers (Doyle 2005; Wolheim et al., 2006). The model presented in Ye et al. (2014; Chapter 5) is a combination of the theoretical approach but in combination with empirical observations of both small streams and big rivers, but it was applied during low flow periods only. In this chapter we incorporated this model with a simple hillslope bucket model to estimate the hillslope inflows to the river network and ran it for 10 years to study how the nitrate retention dynamics change with hydrologic conditions.

These preliminary results obtained in this study suggest that rivers do not function as mere transport corridors during either low flow periods or high flow periods. The comparison between the two scenarios (with and without uptake) showed that without uptake, the reduction of nitrate concentration in the river stations due to dilution is much smaller than the decrease caused by uptake. The difference between the two scenarios is larger during low flow periods and smaller at flow peaks, as the retention efficiency is low during flow events and high during low flows. However, even though the efficiency is low during events, it is still considerable, and with the much larger amount of nitrate transported during events, the amount of nitrate retained during high flows is in fact larger than that removed during low flow periods. This difference increases with river size: the higher the stream order is, the more important high flow retention is.

We also applied three climates of different hydrologic variability to the model, although the actual amount of nitrate that enters into the river or is removed from the water column varies, the trend we found in Ye et al. (2012; Chapter 4) with the theoretical model still stands: the overall retention efficiency decreases with variability of flow. The more variable the flow is, the less efficient the river network can be, and this is not necessarily related to the nitrate input.

What is presented in this chapter is just a preliminary application of the model developed in Ye et al. (2014; Chapter 5); more substantial analysis could be done under this model framework. Other more climate scenarios can be applied to the model to explore more fully the impact of climate on the nutrient transformation and transport in river networks. For example, what impact does seasonality and the timing of rainfall events have on nutrient uptake, and how could the intensity and event durations influence the retention mechanisms? We could also test the hypothesis proposed in Doyle (2005) regarding the hydrologic regime that would be the most productive in terms of nutrient retention and how would it vary with river sizes or climates. The mechanism of benthic and pelagic uptake could also be studied separately provided there is more empirical support towards their parameterizations.

References

Aguilera, R., R. Marce ´, and S. Sabater (2013), Modeling nutrient retention at the watershed scale: Does small stream research apply to the whole river network?, *J. Geophys. Res. Biogeosci.*, 118, 728–740, doi:10.1002/jgrg.20062.

Alexander, R. B., R. A. Smith, and G. E. Schwarz, (2000), Effect of stream channel size on the delivery of nitrogen to the Gulf of Mexico, *Nature*, 403, 758– 761.

Algoazany, A. S. (2006), *Long-term Effects of Agricultural Chemicals and Management Practices on Water Quality in a Subsurface Drained Watershed*, PhD thesis, University of Illinois at Urbana-Champaign.

Bencala, K. E., and R. A. Walters (1983), Simulation of solute transport in a mountain pool-and riffle stream: a transient storage model, *Water Resour. Res., 19(3)*, 718-724.

Böhlke, J. K. , R. C. Antweiler, J. W. Harvey, A. E. Laursen, L. K. Smith, R. L. Smith, and M. A. Voytek (2009), Multi-scale measurements and modeling of denitrification in streams with varying flow and nitrate concentration in the upper Mississippi River basin, USA, *Biogeochemistry*, 93, 117–141.

Botter, G., N. B. Basu, S. Zanardo, P. S. C. Rao, and A. Rinaldo (2010), Stochastic modeling of nutrient losses in streams: Interactions of climatic, hydrologic, and biogeochemical controls, Water Resour. Res., 46, W08509, doi:10.1029/2009WR008758.

Bricker, S. B., C. G. Clement, D. E. Pirhalla, S. P. Orlando, and D. R. G. Farrow (1999), National estuarine eutrophication assessment: Effects of nutrient enrichment in the nation's estuaries, report, 71 pp., NOAA, Silver Spring, Md.

Claessens, L. and C. L. Tague (2009), Transport-based method for estimating in-stream nitrogen uptake at ambient concentration from nutrient addition experiments, *Limnol. Oceanogr.: Methods, 7,* 811-822.

Claessens, L., C. L. Tague, P. M. Groffman and J. M. Melack (2009), Longitudinal assessment of the effect of concentration on stream N uptake rates in an urbanizing watershed, *Biogeochemistry,* doi: 10.1007/s10533-009-9376-y.

Dodds, W. K., A. J. Lopez, W. B. Bowden, S. Gregory, N. B. Grimm, S. K. Hamilton, A. E. Hershey, E. Marti, W. H. McDowell, J. L, Meyer, D. Morrall, P. J. Mulholland, B. J. Peterson, J. L. Tank, H. M. Valett, J. R. Webster and W. M. Wollheim (2002), N uptake as a function of concentration in streams, *J. N. Am. Benthol. Soc., 21(2)*, 206-220.

Donner, S. D., M. T. Coe, J. D. Lenters, T. E. Twine and J. A. Foley (2002), Modeling the impact of hydrological changes on nitrate transport in the Mississippi river basin from 1955 to 1994, *Global Biogeochemical Cycles, 16(3),* 1043, 10.1029/2001GB001396.

Doyle, M. W. (2005), Incorporating hydrologic variability into nutrient spiraling, *J. Geophys. Res.*, 110, G01003,doi:10.1029/2005JG000015.

Dunn, D. D. (1996), Trends in nutrient inflows to the Gulf of Mexico from streams draining the conterminous United States 1972-1993. *US Geol. Surv., Water-Res. Invest. Rep.,* 96-4113. Austin, TX: US Geol. Surv. 60 pp.

Ensign, S. H. and M. W. Doyle (2006), Nutrient spiraling in streams and river networks, *J. Geophys. Res.*, *111*, G04009, doi:10.1029/2005JG000114.

Fisher, S. G., N. B. Grimm, E. Marti, R. M. Holmes, and J. B. Jones (1998), Material spiraling in stream corridors: A telescoping ecosystem model, Ecosystems, 1, 19– 34.

Fisher, S. G., R. A. Sponseller, and J. B. Heffernan (2004), Horizons in stream biogeochemistry: Flowpaths to progress, *Ecology*, 85, 2369– 2379.

Hall, R. O., B. J. Peterson and J. L. Meyer (1998), Testing a nitrogen cycling model of a forest stream by using a nitrogen-15 tracer addition, *Ecosystems*, 1, 283– 298.

Hall, R. O. Jr., E. S. Bernhardt and G. E. Likens (2002), Relating nutrient uptake with transient storage in forested mountain streams, *Limnol. Oceanogr., 47(1),* 255-265.

Hall, R. O. Jr. and J. Tank (2003), Ecosystem metabolism controls nitrogen uptake in streams in Grand Teton National Park, Wyoming, *Limnol. Oceanogr., 48(3),* 1120-1128.

Hall, R. O. Jr., J. L. Tank, D. J. Sobota, P. J. Mulholland, J. M. O'Brien, W. K. Dodds, J. R. Webster, H. M. Valett, G. C. Poole, B. J. Peterson, J. L. Meyer, W. H. McDowell, S. L. Johnson, S. K. Hamilton, N. B. Grimm, S. V. Gregory, C. N. Dahm, L. W. Cooper, L. R. Ashkenas, S. M. Thomas, R. W. Sheibley, J. D. Potter, B. R. Niederlehner, L. T. Johnson, A. M. Helton, C. M. Crenshaw, A. J. Burgin, M. J. Bernot, J. J. Beaulieu, and C. P. Arango (2009a), Nitrate removal in stream ecosystems measured by ^{15}N addition experiments: Total uptake, *Limnol. Oceanogr., 54(3),* 653-665, 2009a.

Hall, R. O. Jr, M. A. Baker, C. D. Arp, and B. J. Koch (2009b), Hydrologic control of nitrogen removal, storage, and export in a mountain stream, *Limnol. Oceanogr., 54(6),* 2128-2142.

Hall, R. O., M. A. Baker, E. J. Rosi-Marshall, and J. L. Tank (2013), Solute specific scaling of inorganic nitrogen and phosphorus uptake in streams, *Biogeosciences Discuss*., 10, 6671-6693.

Howarth, R., R. Marino, and D. Scavia (2002), Nutrient pollution in coastal waters: Priority topics for an integrated national research program for the United States, report, U.S. Dep. of Commerce, NOAA, Silver Spring, Md.

Jones, J. B., S. G. Fisher, and N. B. Grimm (1996), A long-term perspective of dissolved organic carbon transport in Sycamore Creek, Arizona, *Hydrobiologia*, 317, 183– 188.

Li, H, M. Sivapalan, D. Liu and F. Tian (2010), Water and nutrient balances in a large tile-drained agricultural catchment: A distributed modeling study. *Hydrol. Earth Syst. Sci.*, 14, 2259–2275, doi:10.5194/hess-14-2259-2010.

Meyer, J. L., and G. E. Likens (1979), Transport and transformation of phosphorus in a forest stream ecosystem, *Ecology*, 60, 1255–1269.

Mitchell, J. K., G. F. McIsaac, S. E. Walker, and M. C. Hirschi (2000), Nitrate in river and subsurface drainage flows from an east central Illinois watershed, *Transactions of the ASAE*, 43(2), 337-342.

Mulholland, P. J., J. L. Tank, J. R. Webster, W. B. Bowden, W. K. Dodds, S. V. Gregory, N. B. Grimm, S. K. Hamilton, S. L. Johnson, E. Marti, W. H. McDowell, J. L. Merriam, J. L. Meyer, B. J. Peterson, H. M. Valett and W. M. Wollheim (2002), Can uptake length in stream be determined by nutrient addition experiments? Results from an inter-biome comparison study, *J. N. Am. Benthol. Soc., 21(4)*, 504-560.

Mulholland, P. J., A. M. Helton, G. C. Poole, R. O. Hall, S. K. Hamilton, B. J. Peterson, J. L. Tank, L. R. Ashkenas, L. W. Cooper, C. N. Dahm, W. K. Dodds, S. E. G. Findlay, S. V. Gregory, N. B. Grimm, S. L. Johnson, W. H. McDowell, J. L. Meyer, H. M. Valett, J. R. Webster, C. P. Arango, J. J. Beaulieu, M. J. Bernot, A. J. Burgin, C. L. Crenshaw, L. T. Johnson, B. R. Niederlehner, J. M. O'Brien, J. D. Potter, R. W. Sheibley, D. J. Sobota and S. M. Thomas (2008), Stream denitrification across biomes and its response to anthropogenic nitrate loading. *Nature, 452,* 202–205.

OECD. (1982). Eutrophication of Waters: Monitoring, Assessment and Control. OECD: Paris.

Peterson, B. J., W. M. Wollheim, P. J. Mulholland, J. R. Webster, J. L. Meyer, J. L. Tank, E. Marti, W. B. Bowden, H. M. Valett, A. E. Hershey, W. H. McDowell, W. K. Dodds, S. K. Hamilton, S. Gregory, D. D. Morrall (2001), Control of nitrogen export from watersheds by headwater streams, *Science*, *292(5514)*, 86–90.

Reggiani, P., M. Sivapalan, S.M. Hassanizadeh and W. G. Gray (2001), Coupled equations for mass and momentum balance in a bifurcating stream channel network: theoretical derivation and computational experiments, *Proc. Roy. Soc., Ser. A. Math. Phys. Engng. Sci.*, **457**, 157–189.

Runkel, R. L. (1998), *One Dimensional Transport with Inflow and Storage (OTIS): A Solute Transport Model for Streams and Rivers*. U.S. Geological Survey Water Resources Investigation Report No. 98–4018, http://co.water.usgs.gov/otis.

Seitzinger, S. P., R. V. Styles, E. W. Boyer, R. B. Alexander, G. Billen, R. W. Howarth, B. Mayer and N. V. Breemen (2002), Nitrogen retention in rivers: model development and application to watersheds in the northeastern U.S.A., *Biogeochemistry, 57/58*: 199–237, 2002.

Tank, J. L., E. J. Rosi-Marshall, M. A. Baker and R. O. Hall, Jr. (2008), Are rivers just big streams? A pulse method to quantify nitrogen demand in a large river, *Ecology, 89(10),* 2935-2945.

Tian, F., H. Hu, Z. Lei and M. Sivapalan (2006), Extension of the representative elementary watershed approach for cold regions via explicit treatment of energy related processes. *Hydrol. Earth Syst. Sci.,* 10, 619-644.

Turner, R. E. and N. N. Rabalais (1994), Coastal eutrophication near the Mississippi river delta, *Nature*, 368, 619-621.

Vitousek, P. M., J. D. Aber, R. W. Howarth, G. E. Likens, P. A. Matson, D. W. Schindler, W. H. Schlesinger and D. G. Tilman (1997), Human alteration of the flobal nitrogen cycle: sources and consequences, *Ecol. Appl.* 7, 737-750.

Wollheim, W. M., C. J. Vörösmarty, B. J. Peterson, S. P. Seitzinger, C. S. Hopkinson (2006), Relationship between river size and nutrient removal, *Geophys. Res. Lett., 33*, L06410, doi:10.1029/2006GL025845.

Wollheim, W. M., B. J. Peterson, S. M. Thomas, C. H. Hopkinson and C. J. Vörösmarty (2008), Dynamics of N removal over annual time periods in a suburban river network, *J. Geophys. Res. -Biogeosciences*, 113, G03038.

Ye, S., T. P. Covino, M. Sivapalan, N. B. Basu, H.-Y. Li, and S.-W. Wang (2012), Dissolved nutrient retention dynamics in river networks: A modeling investigation of transient flows and scale effects, *Water Resour. Res.*, 48, W00J17, doi:10.1029/2011WR010508 (Chapter 4 of this dissertation).

Ye, S., M. Sivapalan, J. L. Tank, M. A. Baker, E. J. Rosi-Marshall, R. O. Hall and A. J. Reisinger (2014), Scale effects of dissolved nutrient retention in river networks: A comparative modeling investigation. Paper in preparation, to be submitted to *Water Resources Research* (Chapter 5 of this dissertation).

Chapter 7

Conclusions

7.1 Major findings of the dissertation

This dissertation was carried out under the guidance of the proposed study framework to explore the factors contributing to hypoxia issue in the Gulf of Mexico caused by excessive nutrient export from the terrestrial landscape. Under this study framework, through a combination of top-down and bottom-up approaches, we studied the mechanisms of nutrient transformation and transport in river networks and how the characteristics of climate influence the nutrient retention in river networks through their influence on hydrologic processes. As introduced in the introduction chapter, we studied these topics from Chapter 2 to Chapter 6, approaching them from two directions: the downward approach that starts from the generation and model-based interpretation of the patterns generated through data analyses, and the upward approach based on the use of theoretical process based models. The exploration is carried out in two parts to respond to the two major objectives raised in Chapter 1: firstly how the climate casts its impact on hydrologic processes, and secondly how nutrient retention changes with changes of hydrologic variability inherited from climate.

This framework was first applied towards the exploration of the dominant hydrologic processes across the continental US. After the analysis of patterns of rainfall and runoff regime curves around the country, a two-stage bucket model was developed and then continually improved with the addition of runoff generation processes that were hypothesized as being essential to catchments with certain characteristics based on the comparison of the shapes of the predicted and observed regime curves. This comparative exploration on the dominant flow generation mechanisms in 197 catchments across a gradient of climates indicated that the seasonality in the climate could have significant influence on the hydrology at catchment scale: the more variable and humid the climate is, the fewer the flow generation processes necessary in capture the first order hydrology.

We then zoom into one widely studied flow generation mechanism: the baseflow generation, to discover the factors controlling the associated storage-discharge relationship, with the view to developing empirical parameterizations for land surface models. Catchment characteristics from 50 eastern catchments (climate, topography, soil, etc.) were extracted and analyzed to study their spatial patterns and their correlation with the coefficient and exponent of the recession slope curve, which can be used to generate the storage-discharge relationship. The statistical analysis demonstrated the dominance of the soil properties such as the vertical decay of hydrologic conductivity on the subsurface flow parameterization. The analysis also highlighted the impact of climate aridity, which has not been considered in previous theoretical deductions. Not only did this result highlight the climate control of parameterization of hydrologic processes, but also showed the importance of a combination of the pattern based empirical analysis and model based theoretical interpretations: for example, the climate impact on the subsurface flow generation is usually overlooked in the derivations based on hydraulic theories alone.

With the understanding gained of the influence of climate variability on the hydrology, we then developed a river network model to study the effects of temporal hydrologic variability inherited from climate on nutrient retention in rivers. The theoretical results produced through modeling pointed out the importance of nutrient spiraling during high flows and their contributions to the annual nutrient budget despite the low uptake efficiency during such high flow events. This significant contribution to nutrient retention during high flows emphasized the impact of hydrologic variability on nutrient transport, i.e., annual nutrient removal efficiency changes with different combinations of the frequency of high flows and low flows. Model simulations showed that the overall retention efficiency would decrease with the increase of the temporal hydrologic variability.

Guided by the synthesis framework combining both data analysis and model interpretation, we then cooperated with stream ecologists to improve our theoretical model based on the patterns seen from the measurements in several “big rivers” combined with previous observations collected from the literature. We replaced the nutrient uptake parameters or metrics with new estimates obtained as functions of flow and concentration level, based on relationships we extracted from the empirical observations. The new coupled hydrology-biogeochemistry

model, with parameters derived from empirical observations, was then applied to the 15 study catchments drainging the 15 big rivers to discover scale effects on nutrient retention. The model simulations suggested that the big rivers can no longer be considered as “pipes”, in that they contribute more to nutrient uptake compared to their share of total stream length. The differences we saw between the 15 catchments were attributed to differences in nutrient input loads and the uptake lengths, while the differences among three different solutes (nitrate, ammonium and phosphate) were show to be due to their distinct biological demand (i.e. ammonium is preferred than nitrate) and transport mechanisms (i.e. phosphate is closely related to the sediment transport).

Finally, to complete the understanding of the impact of climate variability on the nutrient retention, we revisited the catchments studied in Chapter 4 with the new model that had been improved through empirical relationships. A hillslope hydrologic model was incorporated into the new model developed in Chapter 5 to receive the climate forcing and filter it to generate the hillslope inflow to the river network. Three different climates were applied to the new model. The new results, which were consistent with the results presented in Chapter 4, reiterate the importance of hydrologic variability on the nutrient retention.

To conclude, we can see the important influence of climate in hydrological processes: the complexity of hydrologic processes increases with the seasonality in climate, while the controlling factors of the flow generation mechanisms are modified by aridity during the long-term co-evolution of landscape with the climate. Consequently, the variability in climate, transmitted through the temporal organization of flow events, also affects the nutrient uptake efficiency. These understandings could be helpful to customize the regulation of nutrient export to the river systems based on local climate and the hydrologic regime, river size, and land use pattern. For example, given the inverse relationship between the hydrologic variability and the nutrient retention efficiency, avoiding fertilizer application during big events could help increase nutrient reduction in the network. The importance of big rivers in nutrient retention also confirms the importance of the adoption of best management practices even in downstream parts of the river basin. The extension of big river travel distance through meandering or floodplain inundation could lead to more nutrient uptake as well.

7.2 Future work

The work presented in this dissertation is an example to show how the framework proposed in the introductory chapter could be implemented to explore research questions related to the natural system, particularly in water related realms. More efforts could be invested to further understand the nutrient retention in detail in both the hydrology part and the biogeochemistry part.

Let us start from the biogeochemical question that is most closely related to our overarching objective: how is nutrient removed from the water column in river channels? In Chapter 5, we developed a coupled river network model to describe the nutrient uptake based on measurements from small streams and 15 big rivers. However, the relationship we embedded in the model is 1) a simple up-scaling from the measurements at the outlet from a range of stream sizes, without the use of actual data along the river network within the catchment; 2) only valid during low flows when all the measurements took place –more observations during high flow periods are necessary to verify the extension from low flows to high flows; 3) a lumped regression relationship that estimates the overall gross nutrient uptake in the water column without separation into its component processes: i.e. how much is retained by the biota in the water column, near the bed or within the transient storage zone.

We upscaled the nutrient retention rate from the reach scale to the catchment scale based on the data obtained across several catchments instead of within catchments. This relationship could be more reliable if we can have it verified by data collected along the river network. Besides, studies have shown the importance of transient storage (i.e. floodplain) on nutrient uptake during flow events. That is, the empirical relationship between uptake length and flow and concentration level we developed in Chapter 5 may not prevail when the flow is higher than the bankfull discharge, which could lead to a nonlinear increase in the transient storage volume. More observations are needed to verify or modify the estimates of the uptake length during high flow events. Furthermore, to develop a process based model for deeper understanding, separation of the different uptake mechanisms is also essential. For example, given the emphasis on the role of transient storage on nutrient uptake during high flows, it is necessary to separate its

contribution from the pelagic or benthic uptake and to identify the factors contolling the nutrient uptake in each case.

As demonstrated in Chapter 6, the hydrologic variability inherited from climate does have a significant impact on the nutrient retention efficiency in the river network at the annual scale. The hillslope hydrologic model presented there also indicated that the hillslope is not just a linear filter as we have seen from previous studies and in Chapter 2 and 3. To explore the climate impact on the nutrient uptake, more studies are needed on how hillslope converts rainfall into runoff and how the mechanism varies from place to place due to the distinct climatic, topographic, geomorphic, and pedologic properties. We have shown that a simple model can also be used to interpret catchment characteristics when combined with the information learned from the observed patterns. Since the goal in that study was to capture the first order temporal variability impact of climate, the model results were calibrated based on the regime curve. For the study of the nutrient retention in the long term, we need to simulate the runoff at event scale, that is, to calibrate on the time series of flow data. In this way we can see how the temporal organization of rainfall and flow events affect nutrient uptake processes, not only the impact of the frequency, magnitude, and duration but also timing. For instance, the rainfall event occurring right after fertilizer application could flush out more nutrients into the river than one occurring long after the application. This understanding could help us find the best time of fertilizer application to ensure sufficient crop growth and yet minimize nutrient losses.

The simple model we developed in Chapter 2 failed in arid catchments or Midwestern catchments with significant anthropogenic activities. More sophisticated models are needed to simulate the hydrologic processes in arid regions as well as in human impaired regions. Not only can the comparative modeling approach be applied to the whole country, it can also be implemented within one big region with limited climatic differences, i.e. the arid region or northeastern mountainous area, to study in detail how dominant flow generation processes would change with landscape characteristics. This way, we can focus on a small amount of variables and study processes in more depth.

For the study of nutrient retention, it is also important to identify different flow pathways: flow running through areas with different nutrient concentration could lead to large variations in

the amount of nutrient that eventually enters river channels. For example, due to the sorption to the sediment, dissolved phosphorus usually enters streams with surface flow which normally occurs during big rainfall events as infiltration excess runoff or rainfall after a long wet period as saturation excess flows. In agricultural catchments, subsurface flow close to the surface immediately after fertilizer application brings in the largest amount of nitrogen, while in pristine catchments groundwater recharge from aquifers draining through fractured rocks with high nitrogen content may be the biggest nitrogen source.

Not only the flow pathways from the terrestrial landscape to the aquatic system, but also the flow pathways within the river network, governed by river morphology, play an influential role in nutrient uptake. Channel sinuosity could help increase the nutrient uptake by extending the travel time; while channel slope would have opposite impact by reducing the nutrient residence time; and bedrock geology could also influence the nutrient retention through turbidity and sediment supply.

Chapter 3 is an example of the application of the adopted study framework to understand one specific flow generation mechanism: subsurface stormflow generation as a function of soil water storage. The empirical analysis indicated an interesting relationship between climate aridity and the coefficient and exponent in the recession curves. Synthesis between the empirical results and theoretical derivation suggested that climate probably is not just forcing to the terrestrial hydrology but also involved in the formation of hydrology through the co-evolution of catchment properties.

This concept of co-evolution not only can help us acquire the big picture regarding how catchments evolved to the present state, and predict the processes occurring now with the understanding of the connection within each component and the notion of catchment evolution. If we could find out how catchment hydrology changed from the original state defined by local geology to the current status through the modification by climate, vegetation and the feedback between them, then we would be able to predict what kind of hydrology may develop for each catchment given its basic geology and long-term climate history. This is a difficult question, but the framework we presented here could be a useful tool for exploration of such fundamental questions Similar to the neuroscientists' research about human brain functioning, starting from

the basic reflex and hot spots in the brain under specific stimulations, we can look at the change of catchment hydrology and the sensitivity analysis among catchments with a range of variability in one dominant factor by comparative studies of the patterns obtained or models developed for these catchments.

Finally, as a significant extension of this research, we want to know the amount of nutrients is exported into the aquatic ecosystem annually. To be able to estimate the nutrient yield, a terrestrial nutrient cycling model should be developed, which has a much closer relationship with vegetation and can benefit more from the concept of co-evolution of climate-soil-vegetation and how this loop will impact the water and nutrient distribution and storage in the landscape. The framework we applied here could be used to guide our exploration in a changing world and help us manage nature to maximize both the anthropogenic and ecological interests.

Appendix

Table A.1: Calibrated lateral inflow concentration & the measured concentration at outlet

	Calibrated lateral NH4	Measured NH4@ outlet	USGS Groundwater data			Calibrated lateral NO3	Measured NO3@ outlet	USGS Groundwater data			Calibrated lateral PO4	Measured PO4@ outlet	USGS Groundwater data		
			Range	n	Median			Range	n	Median			Range	n	Median
Muskegon	68	14	[0, 20]	6	20	--	330	[580,1800]	6	920	257	9	[0,31]	4	31
St. Joseph	--	32	[20,440]	18	80	28,200	1100	[69,21000]	16	11450	258	11	[0,123]	11	61
Tippecanoe	182	15	--	--	--	18,020	1850	--	--	--	665	67	23	1	--
White	21	1	[0,735]	64	680	--	1650	[0,11900]	64	1870	--	60	[0,20]	64	11
Manistee	330	30	[20,30]	2	25	--	120	[0,9100]	28	1100	110	10	[0,31]	2	31
Snake	70	5	[0,50]	15	30	7	1	[1450,9300]	15	6530	31	3	[160,1900]	15	440
Salmon	61	5	[40,330]	8	300	24	2	[40,403]	8	403	15	4	[20,430]	8	400
Henry's	36	3	[30,866]	2	448	70	6	[20,1400]	4	235	--	16	[4,60]	4	10
Buffalo	20	5	--	--	--	11	3	--	--	--	--	44	--	--	--
Seedskadee	270	14	--	--	--	708	19	15000	1	--	810	22	80	1	--
Green	122	5	[10,6650]	25	225	444	15	[0,33400]	76	180	--	21	[10,2390]	66	40
Ouray	58	2	[20,240]	9	35	48	7	[50,33400]	19	279	122	3	[10,50]	11	50
North Platte	273	5	40	10	40	--	20	[42,187]	10	91	--	20	[0,31]	10	25
Bear	--	12	[10,2950]	7	50	1870	49	[10,15000]	13	6690	810	18	[10,790]	7	20
Colorado	31	1	[20,171]	68	80	--	697	[40,13700]	137	2810	227	12	[10,26]	63	14